NASA CONTRACTOR REPORT

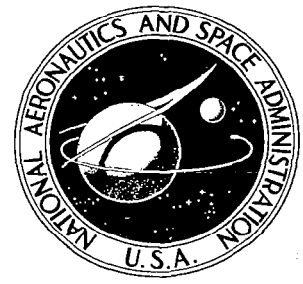

NASA CR-754

AN EXPERIMENTAL STUDY OF PRESSURE DISTRIBUTION CURVES APPLICABLE TO PNEUMATIC TIRES

by S. K. Clark

Prepared by
UNIVERSITY OF MICHIGAN
Ann Arbor, Mich.
for

NATIONAL AERONAUTICS AND SPACE ADMINISTRATION • WASHINGTON, D. C. • MAY 1967

NASA CR-754

AN EXPERIMENTAL STUDY OF PRESSURE DISTRIBUTION CURVES APPLICABLE TO PNEUMATIC TIRES

By S. K. Clark

Prepared under Grant No. NsG-344 by
UNIVERSITY OF MICHIGAN
Ann Arbor, Mich.

for

NATIONAL AERONAUTICS AND SPACE ADMINISTRATION

For sale by the Clearinghouse for Federal Scientific and Technical Information
Springfield, Virginia 22151 – CFSTI price $3.00

TABLE OF CONTENTS

LIST OF ILLUSTRATIONS

LIST OF ILLUSTRATIONS (Concluded)

NOMENCLATURE

English Letters

a = Shell outside radius, in.

b = Shell width, in.

E = Shell modulus of elasticity, psi

I = Shell cross-sectional moment of inertia, $in.^4$

k_f = Foundation modulus, lb/cu in.

k_s = Surface modulus, lb/cu in.

Greek Letters

Π_1 = Dimensionless number $k_f a^4 b/EI$

Π_2 = Dimensionless number k_s/k_f

I. FOREWORD

Motion of a pneumatic tire in the plane of its wheel may be approximated by treating the tire as a cylindrical shell supported by an inflation pressure as well as an elastic foundation, where the tread region is taken to be the shell and the elastic support, or foundation, is considered to be provided by the sidewalls stiffened by air pressure. So far, work with this model has assumed that the shell (carcass) was in contact with a frictionless flat plane. This is the equivalent of running a tire without a tread against the roadway, so that the carcass itself actually bears against the road surface. It has not yet been possible to introduce the tire tread into the equations of motion describing such a model, and to simultaneously retain mathematical simplicity.

A consequence of the absence of a tread in such model studies is the question of discontinuous shear forces at the forward and trailing edges of the contact patch in this two-dimensional tire representation. This point was previously discussed in Ref. 1, but from a purely speculative and theoretical point of view. On the one hand, it seems almost physically unreal that concentrated forces could exist at the forward or trailing edges of a contact patch, yet theory predicts that such is indeed the case. Since the solutions from the equations of motion involving only bending, or even the equations involving both bending and shear deformation, cannot be completely matched at the forward and trailing edges of a contact patch, shear discontinuity is predicted at these points. One is forced to admit that this theoretical framework is known to be correct in a number of other ways, and that somehow these shear discontinuities

must be examined.

Discussions by the Tire and Suspension Systems Research Group concerning this point eventually led us to conclude that the only way to resolve this difficulty was to carry out an experimental program designed to measure typical pressure distribution curves over a range of cylindrical shell model parameters, so that the actual role of the shear discontinuities could be effectively ascertained. For that reason, the experimental program described in this report was initiated.

II. SUMMARY

The object of this experimental work was to identify the various factors which make up and influence the total pressure distribution of a pneumatic tire in the fore-and-aft direction. By implication these same factors cause variations in pressure across the width in a real tire. These factors have been identified as follows:

(a) The basic source of the pressure distribution is the inflation pressure inside the tire. Its effect is uniform throughout the contact area, and equal in magnitude to the inflation pressure.

(b) A secondary source of pressure distribution is bending of the tire carcass in the tread region. This is associated with a parabolic-appearing pressure distribution component having a maximum value at the centerline of the contact area and dropping to zero at the ends of the contact area.

(c) Concentrated forces, appearing as sharp pressure distribution "spikes," occur at the forward and aft ends of the contact patch. These are directly proportional to the bending rigidity of the carcass structure in the tread region, and are associated with the so-called shear discontinuity of the carcass.

(d) The outer covering, or tread of the tire is considerably softer than the carcass structure itself. Its role in the formation of the overall pressure distribution is to attenuate, or diffuse, the sharp pressure distribution spikes set up due to shear effects.

(e) Large tire deflections tend to cause some buckling of the carcass near the center of the contact patch. This reduces pressure near the center

and increases it at the edges of the patch area. This effect is not nearly as concentrated as the shear effect discussed in paragraph (c), but is of the same general form.

These different components of the total pressure distribution effect are illustrated qualitatively in the sketches shown.

From these general conclusions it is possible to explain why certain pressure distribution curves look as they do. For example, pneumatic tire constructions involving high bending stiffness of the carcass and tread in the tread region tend to exhibit rather sharp pressure distribution spikes at the leading and trailing edges of the contact patch, associated with the shear discontinuities previously discussed. The addition of a soft tread tends to reduce or sometimes even eliminate these pressure distribution spikes.

INDIVIDUAL COMPONENTS

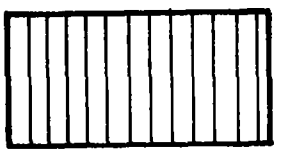

Inflation Pressure Effect (Membrane)

Bending Effect

Shear Effect

COMBINATION EFFECT
INFLATION PLUS BENDING
PLUS DEFLECTION

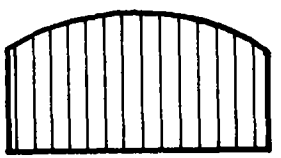

Inflation Pressure Plus Bending for Small Deflections

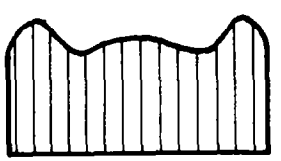

Inflation Pressure Plus Bending for Large Deflections

COMBINATION EFFECT
INFLATION PLUS BENDING
PLUS SHEAR PLUS TREAD

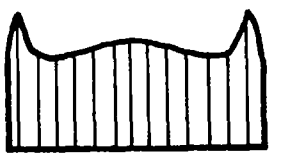

Inflation Pressure Plus Bending Plus Shear With No Tread

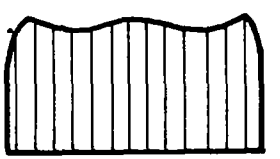

Inflation Pressure Plus Bending Plus Shear With Soft Tread

III. BASIC STRUCTURAL FORM

This report describes an experimental program designed to measure the pressure distribution curves on two-dimensional models representative of the action of a pneumatic tire loaded vertically in its plane. As background for this, extensive work on the cylindrical shell on an elastic foundation has previously been carried out by this group, showing that such a cylindrical model represents most of the characteristics of a pneumatic tire deformed in its plane.[1-3] In order to fabricate models similar to such a shell on an elastic foundation, it was decided to dispense with the internal pressure characteristics of the shell, since these would be relatively hard to obtain in the two-dimensional models to be used here. Generally speaking, it was decided to form models around some central rigid hub by first using a relatively soft material in annular form to represent an elastic foundation. Wrapped around this, and forming an outer surface, would be a harder material exhibiting bending stiffness, in the form of a ring. The entire structure is designed to be two dimensional, and for that reason the ring is made of a sheet material of the same width as the elastic foundation. A sketch of such a structure is shown in Figure 1.

In addition to the basic structure shown in Figure 1, it was desired to examine the role of normal compliance on the shape of the pressure distribution curves. For that purpose, various coatings were applied to the outer surface of the cylinder shown in Figure 1 so as to obtain different values of the normal stiffness, corresponding roughly to the role of the

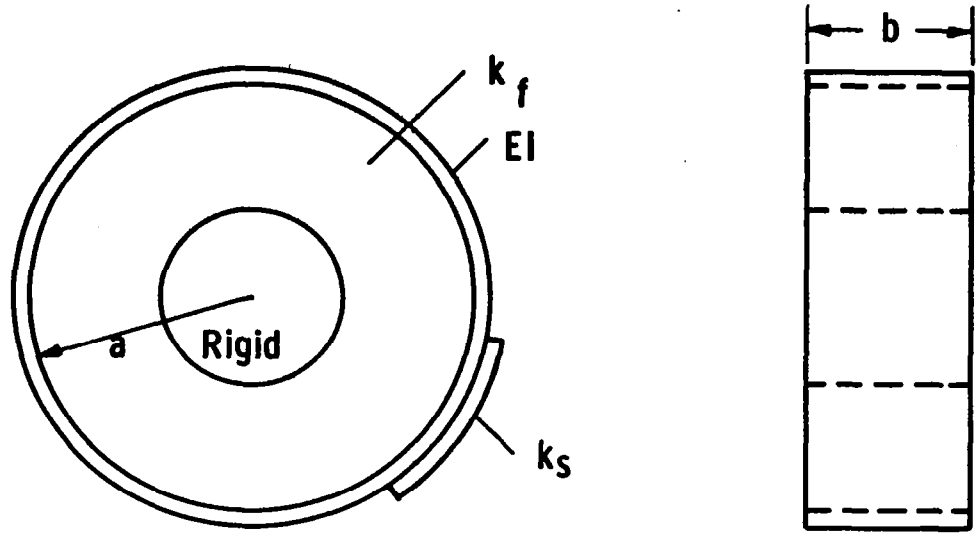

Figure 1. Shell model geometry.

tread in a real pneumatic tire. Such a soft coating is shown over a portion of the periphery of the cylinder in Figure 1, and the normal stiffness of this surface is denoted by the symbol k_s.

Both the quantities k_s and k_f appearing in Figure 1 are representative of the foundation stiffness and have the units of pressure per unit deflection.

Conventional techniques of dimensional analysis show that two dimensionless factors are sufficient to describe the characteristics of the model shown in Figure 1. These have been given the symbols Π_1 and Π_2. The expressions for these are given in Eqs. (1) and (2).

$$\Pi_1 = \frac{k_f a^4 b}{EI} \tag{1}$$

$$\Pi_2 = \frac{k_s}{k_f} \tag{2}$$

Basically Π_1 describes the structural configuration of the cylindrical shell and its elastic foundation. Its value is representative of the relative roles of the foundation modulus and bending stiffness of the cylindrical shell, acting as a band. The cylindrical shell effectively models the carcass and tread region of a tire. For high values of the bending stiffness of the carcass and tread region, the quantity Π_1 will take on small values. On the other hand, for cases where the carcass and tread region have relatively small bending stiffness but the side walls contribute a large amount of elastic support, the dimensionless quantity Π_1 will become large.

There is a certain degree of arbitrariness in the definition of dimensionless constants, but the form given in Eq. (1) for Π_1 is physically representative since it includes both the width as well as the radius of the cylindrical shell. However, it should be noted that the pressure distribution will be independent of width itself. The reason for including the width term in Eq. (1) is seen by noting that the entire bending stiffness of the shell EI appears in the denominator of Eq. (1), so that for a uniform structure a width term will also appear there. In this case, the dimensionless constant Π_1 becomes independent of width.

The second dimensionless constant Π_2 is somewhat simpler to interpret, since it merely represents the ratio of surface normal stiffness, or elastic foundation constant, to the elastic foundation constant of the cylindrical shell support material. It is representative physically of the stiffness of the tread in a real pneumatic tire, compared to the carcass wall stiffness.

For values of the surface foundation constant k_s which are high, such as would be the case if one were dealing with an uncoated metallic surface as will be described later on, then the dimensionless factor Π_2 becomes a large number. On the other hand, if the surface were coated by a relatively thick piece of soft rubber, and if the elastic foundation were relatively stiff, then the dimensionless constant Π_2 would be small.

The complete range of structures possible with the model shown in Figure 1 is describable by the two dimensionless constants Π_1 and Π_2. Note that the radius of the hub does not enter into this description since it influences the value of k_f used in describing the structure.

IV. MODELS AND EXPERIMENTAL APPARATUS

Models were constructed along the general lines illustrated in Figure 1 by using solid aluminum hubs about which one formed the shell on the elastic foundation. In most cases this was done by first forming an outer ring representing the shell itself, and then casting the annular space between the hub and ring full of some castable rubber-like material. A number of models were manufactured, and those used for the pressure distribution curves presented in this report are described in Table I.

TABLE I

MODEL STRUCTURAL PARAMETERS

Model No.	a, in.	k_f, lb/in.^{3}	EI, lb-in.^{2}	b, in.	Π_1	Elastic Foundation Material	Shell Material
1	3.875	27.0	4.0	0.875	1.325×10^3	Foam Rubber	Steel Cord Timing Belt
4	5.99	215.0	21.45	1.0	1.292×10^5	Silastic	Phosphor Bronze Strip
5	6.0	215.0	0.327	1.0	8.52×10^5	Silastic	Cellulose Acetate
6	6.0	143.5	63.2	1.0	2.95×10^3	Silastic	Delrin
7	6.0	215.0	5.55	1.0	4.95×10^4	Silastic	Phosphor Bronze Strip
8	5.0	200.0	0.0	0.75	∞	Silastic	None
9	6.0	215.0	1437.0	1.0	194.0	Silastic	Phosphor Bronze Strip

As may be seen from Table I, many of the models were constructed using a phosphor bronze outer surface or shell accompanied by a castable silastic or silicone rubber as the elastic foundation. In two cases various plastics were used for the outer shell, while in one case an ordinary steel cord timing belt was utilized. The latter model was not completely satisfactory since it was extremely difficult to accurately measure the bending stiffness of the nonhomogeneous belt.

All models were tested with no external covering on the bands as well as with certain standard coverings applied to each of them in turn. These standard coverings were softer than the band itself and thus tended to reduce the values Π_2 associated with the bare shell in contact with the frictionless plane. The values of Π_2 associated with both the plain and coated coverings are given in Table II for the two coatings used, one of these being a thin sheet of rather hard rubber while the second was a considerably thicker sheet of softer rubber material.

TABLE II

MODEL SURFACE PARAMETERS

Model No.	Π_2		
	No Coating	1/16 In. Hard Rubber Sheet	1/4 In. Soft Rubber Sheet
1	172.5	81.5	24.1
4	5.77×10^6	19.3	3.03
5	1.14×10^5	19.3	3.03
6	4.35×10^4	29.0	4.55
7	4.21×10^6	19.3	3.03
8	---	--	--
9	8.6×10^5	19.3	3.03

By using the original shell surface as well as the two types of coatings, a rather wide spread in the dimensionless factor Π_2 can be obtained. Examination of the pressure distribution curves which are presented later in this report will show that this spread in the factor Π_2 was sufficient to cause the pressure distribution curves to change radically in all cases. The photographs of the models are given in Figures 2 and 3.

Most of the difficulties associated with carrying out accurate pressure distribution measurements were found in this case to be associated with low mechanical impedance of the pressure transducers used in some of the early experimental systems. Several attempts were made to utilize strain gage instrumented transducers to measure the pressure distribution under models described here. This was generally not satisfactory, since in the case of the models using phosphor bronze shells the mechanical impedance of the pressure measuring devices was invariably lower than the mechanical impedance of the shell surface itself. This caused a considerable bridging action across the small diameter pressure transducer button or blade used in some of the early experimental constructions. This is illustrated in Figure 4, where a cross section of a typical pressure transducer blade in shown, along with a close up in Figure 5 of the typical bridging action observed when the pressure transducer does not possess sufficiently high mechanical resistance.

After several unsuccessful attempts to utilize strain gage transducers of various kinds, it was finally concluded that the contact pressure between the extremely stiff materials used in the shell models and the rigid steel plate could only be obtained accurately with a pressure transducer whose mechan-

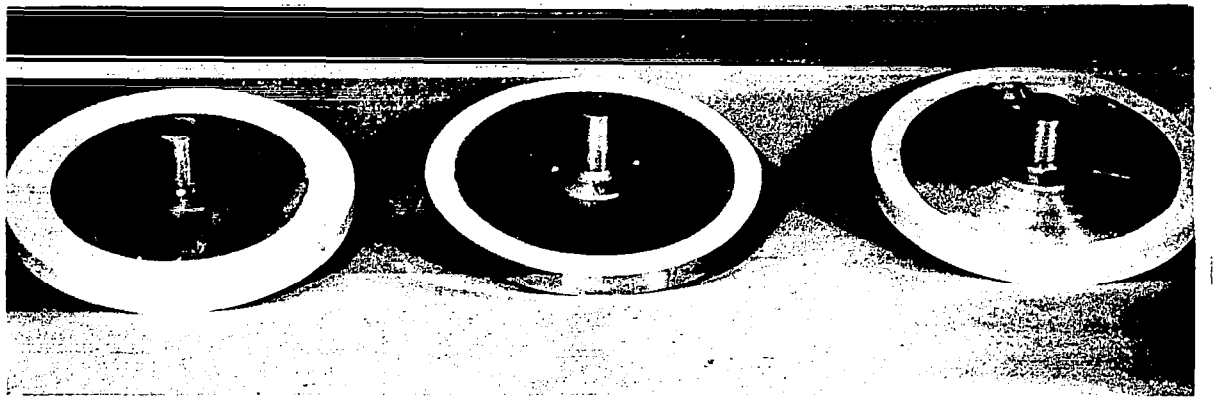

Figure 2. Overall view of test models.

Figure 3. Detailed view of shell and elastic support.

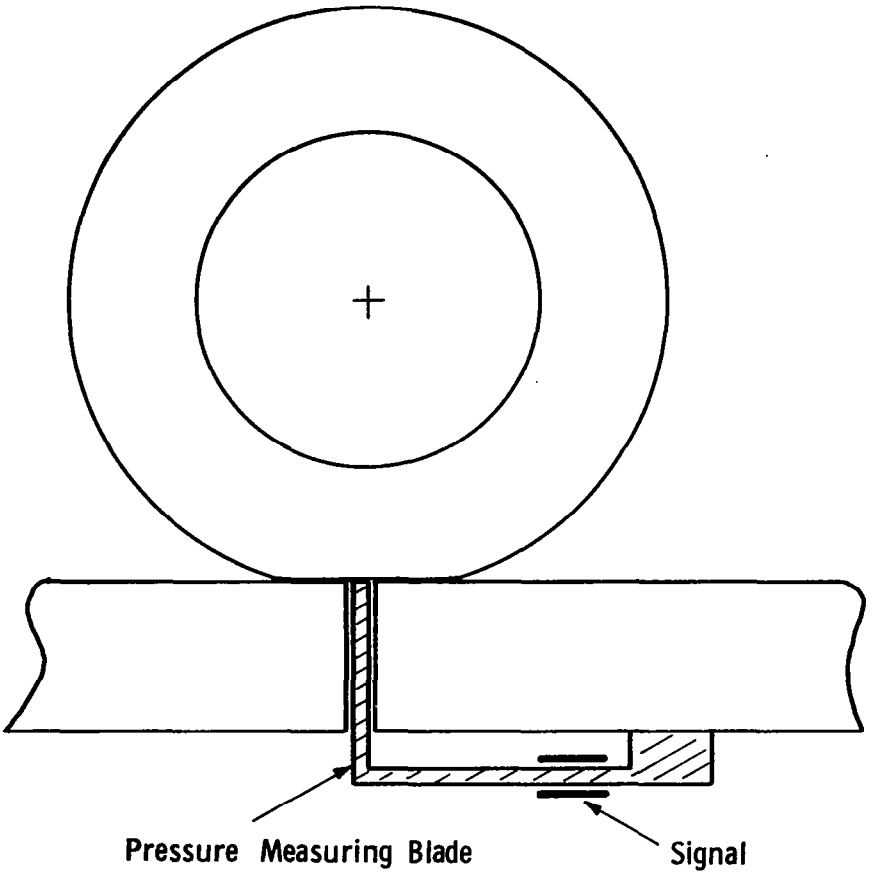

Figure 4. Cross section of pressure measuring area.

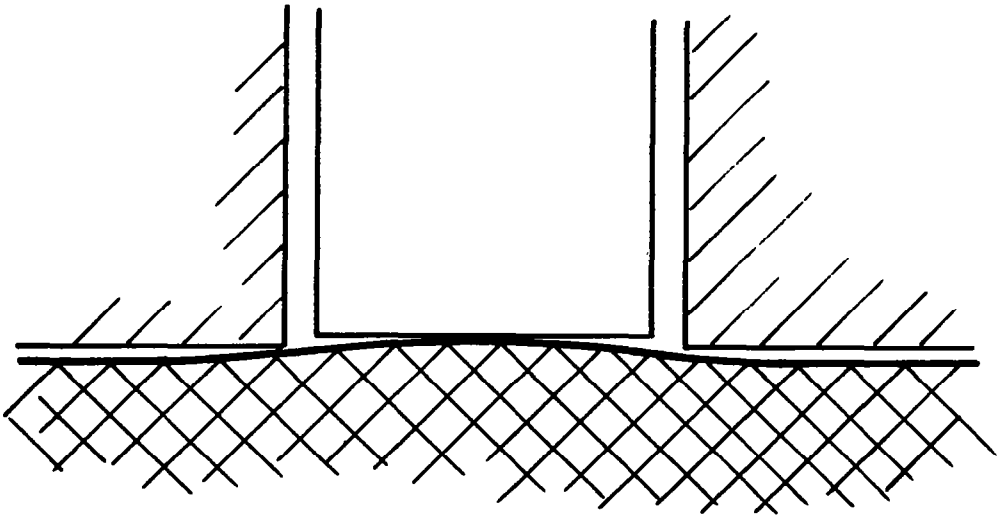

Figure 5. Detailed view of probable "bridging" action across pressure transducer.

ical impedance was a whole order of magnitude higher than that of the stiff shell materials. For this reason, a piezoelectric crystal pressure transducer was obtained and imbedded in an extremely rigid flat steel surface. A circular disc forming the head of this transducer was set flush with the surface in order to measure contact pressure. This is shown in Figure 6, while the transducer holder itself is shown in Figure 7.

A number of tests run with the piezoelectric crystal pressure transducer show that it is extremely well suited for this particular purpose, since the deformation exhibted by it during pressure distribution work are so small as to be negligible compared with corresponding deflections of the elastically-supported cylindrical shell. Extremely sharp pressure pulses may be obtained as shown in the subsequent data.

After a number of unsuccessful attempts to utilize a moving pressure transducer underneath a rotating wheel, the mechanical arrangement shown in Figure 8 was finally adopted. Here, the pressure transducer and associated flat surface are held fixed, while the entire wheel structure is carried on a yoke which is caused to move along the flat plane by means of a hydraulic cylinder fed by a small pump and oil reservoir. This is, of course, reversible so that the wheel may be rolled back and forth over the pressure transducer. Finally, the entire structure is mounted in the head of an Instron testing machine so that the appropriate loads may be applied between the test wheel and the flat surface. This mechanical system is illustrated in Figures 8 and 9.

The output from the pressure transducer was fed through an ordinary

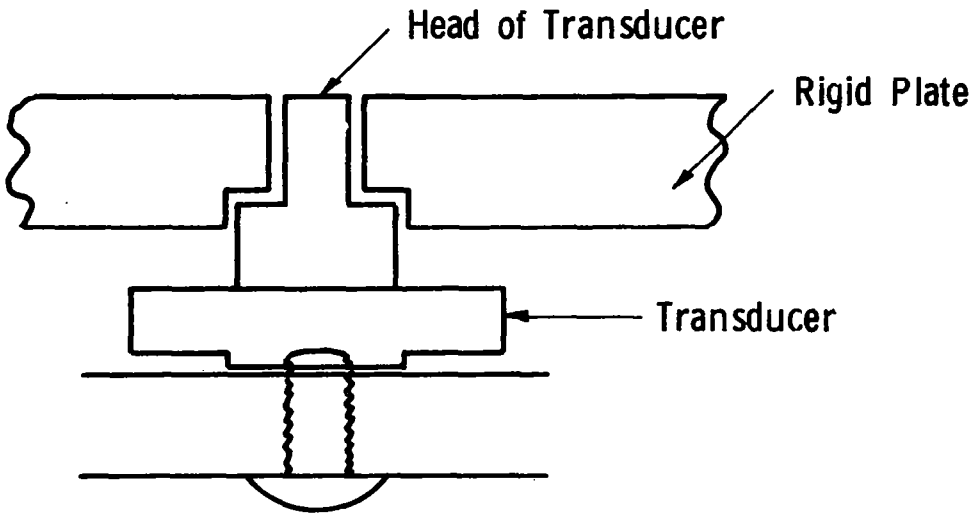

Figure 6. Overall view of pressure measuring plate.

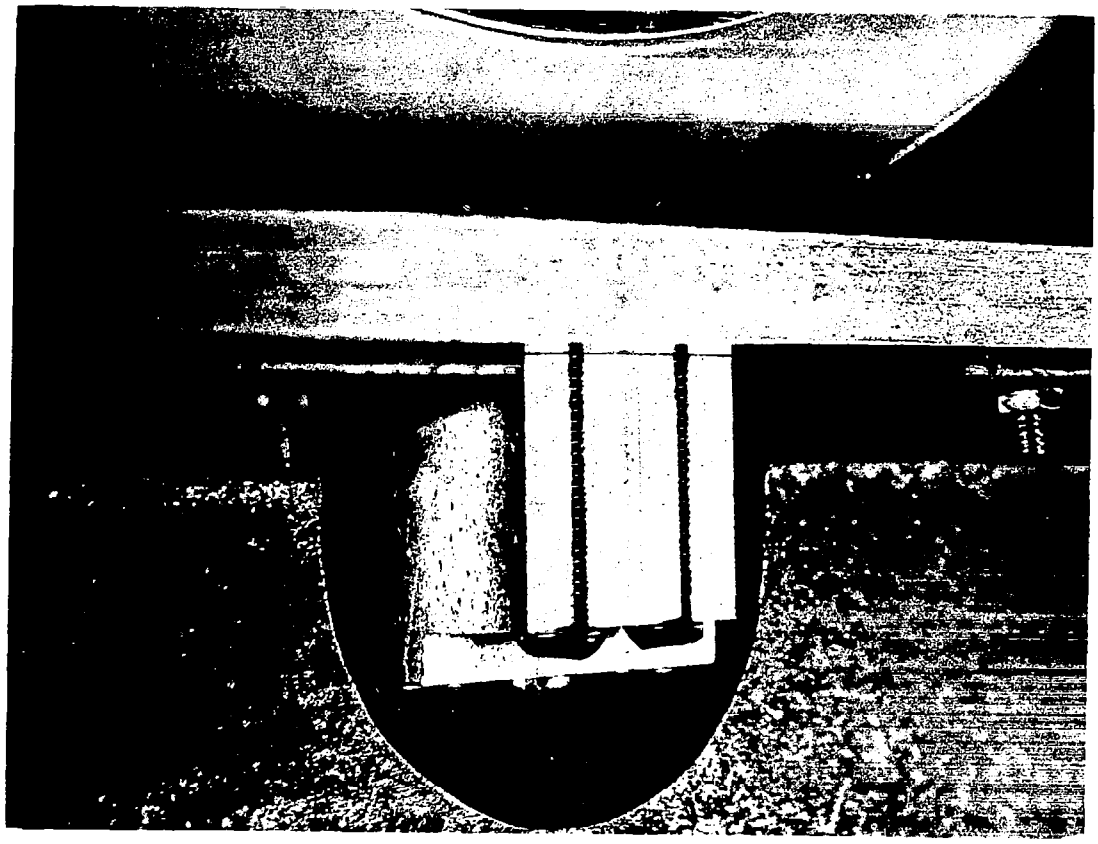

Figure 7. Transducer holder.

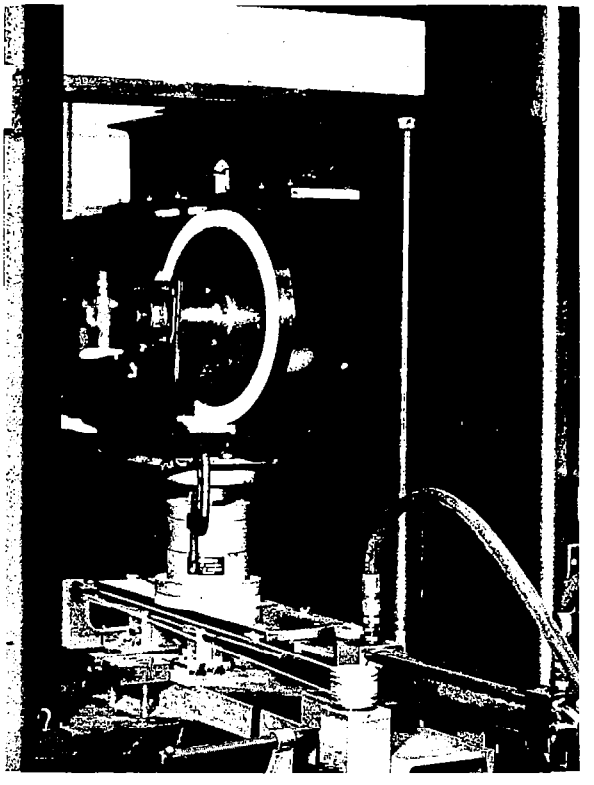

Figure 8. Test arrangement of Instron testing machine.

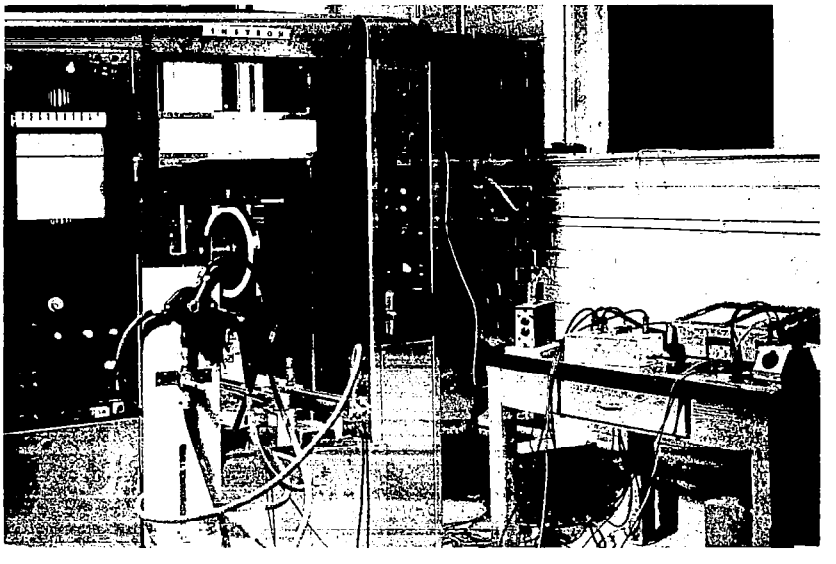

Figure 9. Test arrangement of Instron testing machine.

Kistler charge amplifier and from there into the y-axis of an x-y recorder. The x-axis of the x-y recorder was set to record position of the hydraulic cylinder carrying the yoke and wheel by means of a rotary potentiometer driven by a cord attached to the slide of the tranversing yoke mechanism. This may also be seen in Figures 8 and 9. By this means, the x-y plotter gave a direct record of pressure versus position as the wheel moved across the instrumented measuring plane.

V. PRESSURE DISTRIBUTION CURVES

Pressure distribution curves were obtained for a number of different deflections of each of the models describes in Tables I and II. The deflections were expressed in dimensionless form, as fractional values of the outside radius a of the shell model. Letting the symbol δ represent deflection, and "a" the shell radius, values of deflection were chosen such that:

$$\frac{\delta}{a} = 0.005,\ 0.010,\ 0.015,\ 0.02,\ 0.025,\ 0.030$$

In a typical pressure distribution determination, the deflection of the shell against the flat plane was measured starting from a condition when the shell just contacted the plane, up to the desired value. At that point, vertical displacement of the shell with respect to the plane was held fixed while the shell was rolled across the pressure transducer buried flush with the flat plane. As may be seen from the photographs of Figures 8 and 9, this plane was ground from the flat surface of an I-beam.

The pressure distribution curves obtained from such measurements were recorded on Cartesian coordinate graph paper by means of an x-y recorder, as previously described. A number of recordings had previously been made with each of these models so it was possible to rely on a single trace for each particular test condition, since earlier test runs had shown the pressure distribution curves to be quite reproducible. Slight differences exist between the pressure distribution curves when the wheel travels in the opposite directions, but these were mirror images of one another due to geometric irreg-

ularities in the construction of the model, and due to friction.

The pressure distribution curves are too complex to describe by any simple technique. As previously discussed, they are composed of a portion associated with the ordinary bending rigidity and elastic foundation stiffness of the shell, a second portion associated with shear discontinuities at the forward and leading edges of the contact patch, and a third portion due to the normal compliance of the entire structure. This latter factor tends to cause the shear discontinuity forces and the beam-on-elastic foundation pressure distributions to diffuse together and form a somewhat more regular figure. This factor of normal compliance is well represented by the second dimensionless term Π_2 as given by Eq. (2).

The complexity of the form of the pressure distribution curves, coupled with the large number of tests performed, make it rather difficult to summarize the pressure distribution results in a precise way. Two approximate methods have been chosen to accomplish this. In the first, covered in this section, typical pressure distribution curves illustrating various important features of pressure distribution are presented and discussed, while in a later chapter on analysis of the data is carried out.

One typical form of pressure distribution curve takes place when the normal compliance Π_2 is rather small, particularly when the value Π_1 is also small. A typical curve of this type is shown in Figure 10, which illustrates a shape which is almost parabolic in nature. This is the type of curve which might be expected from a structure in which the bending rigidity played a very small part in the overall picture. This is confirmed by a special set

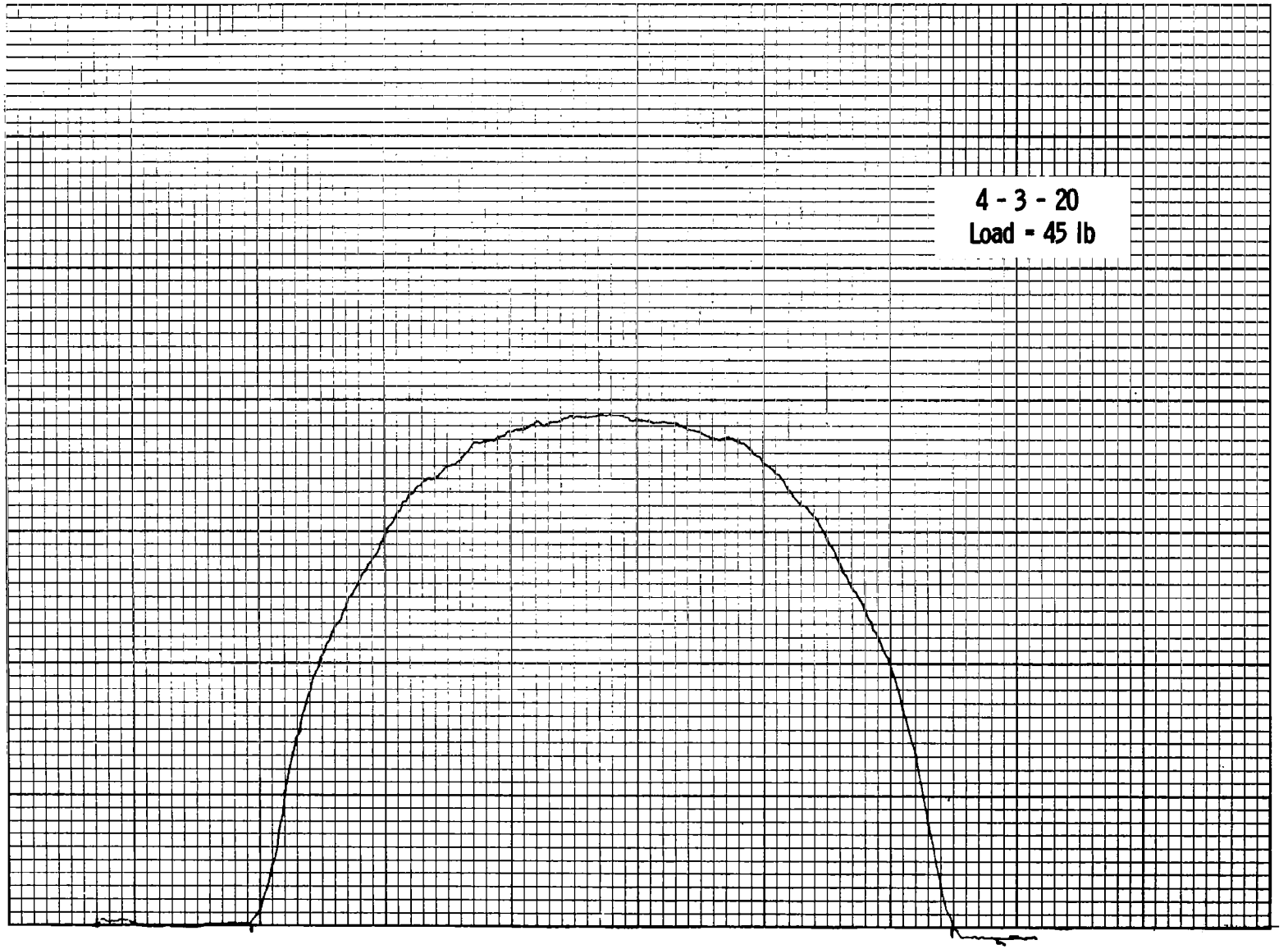

Figure 10. Pressure distribution curve.

of tests on Model No. 8, which was constructed of a pure annular silastic ring without any bending rigidity or shell structure whatsoever. A typical pressure distribution curve from that series of tests in given in Figure 11, which is seen to be very similar to Figure 10. From these, it may be concluded that extremely low values of normal compliance can result in essentially parabolic pressure distribution curves down the length of the contact patch, these curves taking on a form similar to the form observed when no bending enters into the problem. Similar conclusions have been reported by Spengos.[4]

A second general type of curve occurs at the opposite extreme where the factor Π_2 is very large and the bending stiffness is simultaneously high so that Π_1 becomes small. Here an extreme case of the presence of shear discontinuities exists and it may be seen from Figure 12 that typical curves exhibit very marked pressure spikes at the forward and leading edges of the contact patch. A similar curve taken from a different model is also shown in Figure 13.

Variations of the two basic forms of pressure distribution curves previously discussed are primarily controlled by the dimensionless factor Π_2, which is a measure of the compliance or softness normal to the shell. In a real tire, this would be a measure of the softness or stiffness of the tread attached to the carcass, taking into account both the tread material and the thickness of the tread itself. For example, intermediate values of Π_2 coupled with appropriate values of Π_1, can yield curves which are clearly intermediate in form between the two types just discussed. One of these is illustrated in Figure 14.

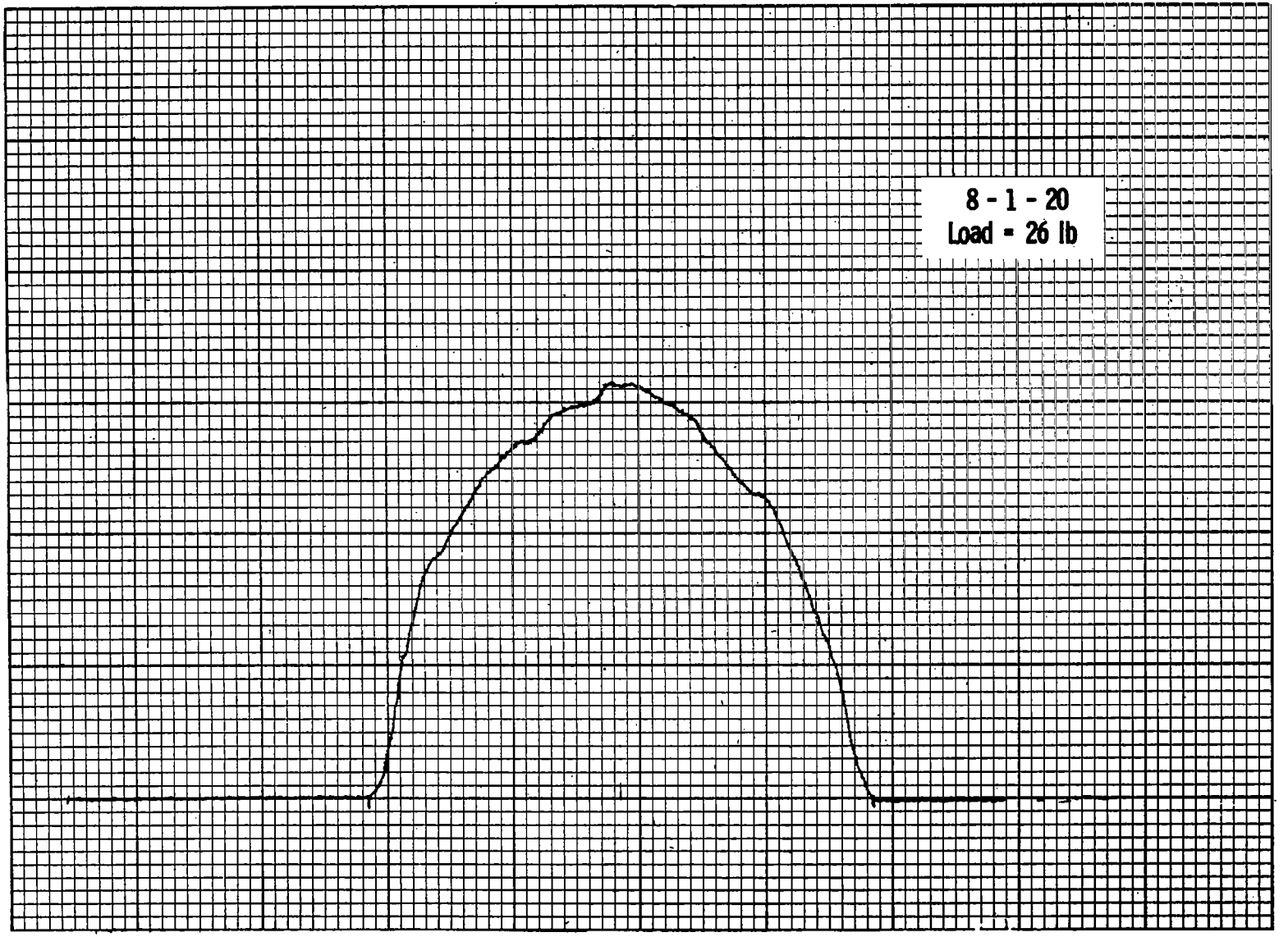

Figure 11. Pressure distribution curve.

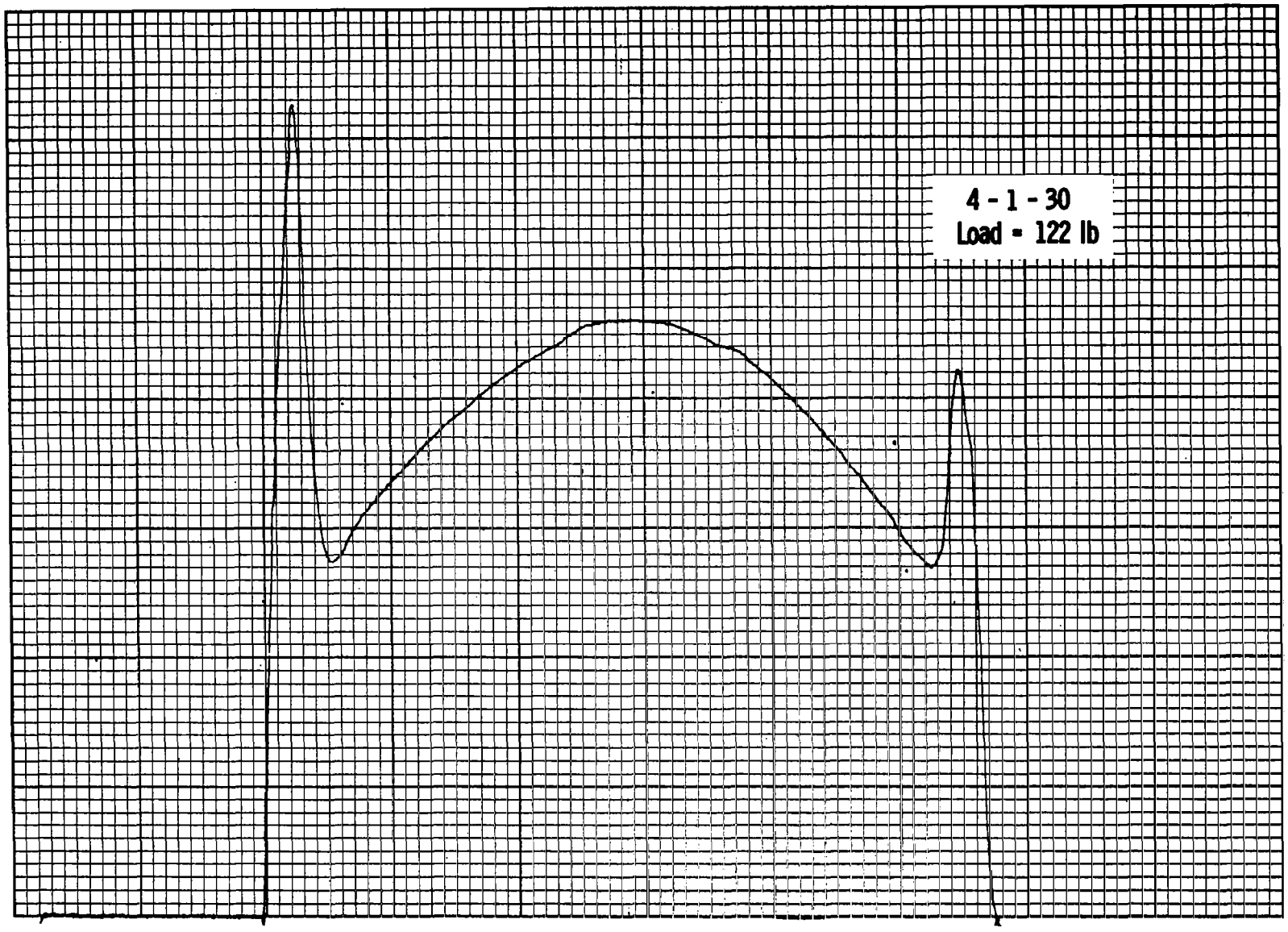

Figure 12. Pressure distribution curve.

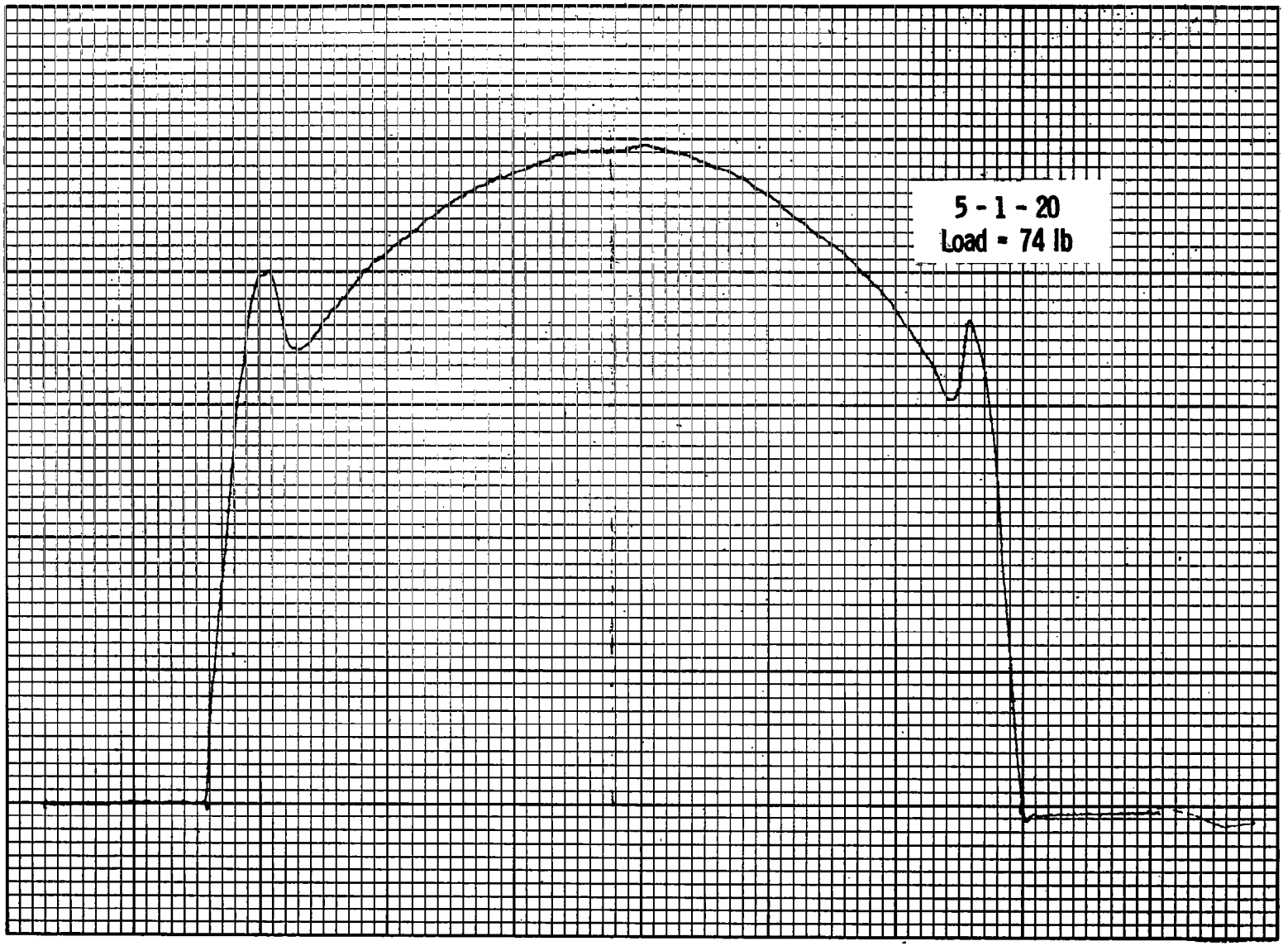

Figure 13. Pressure distribution curve.

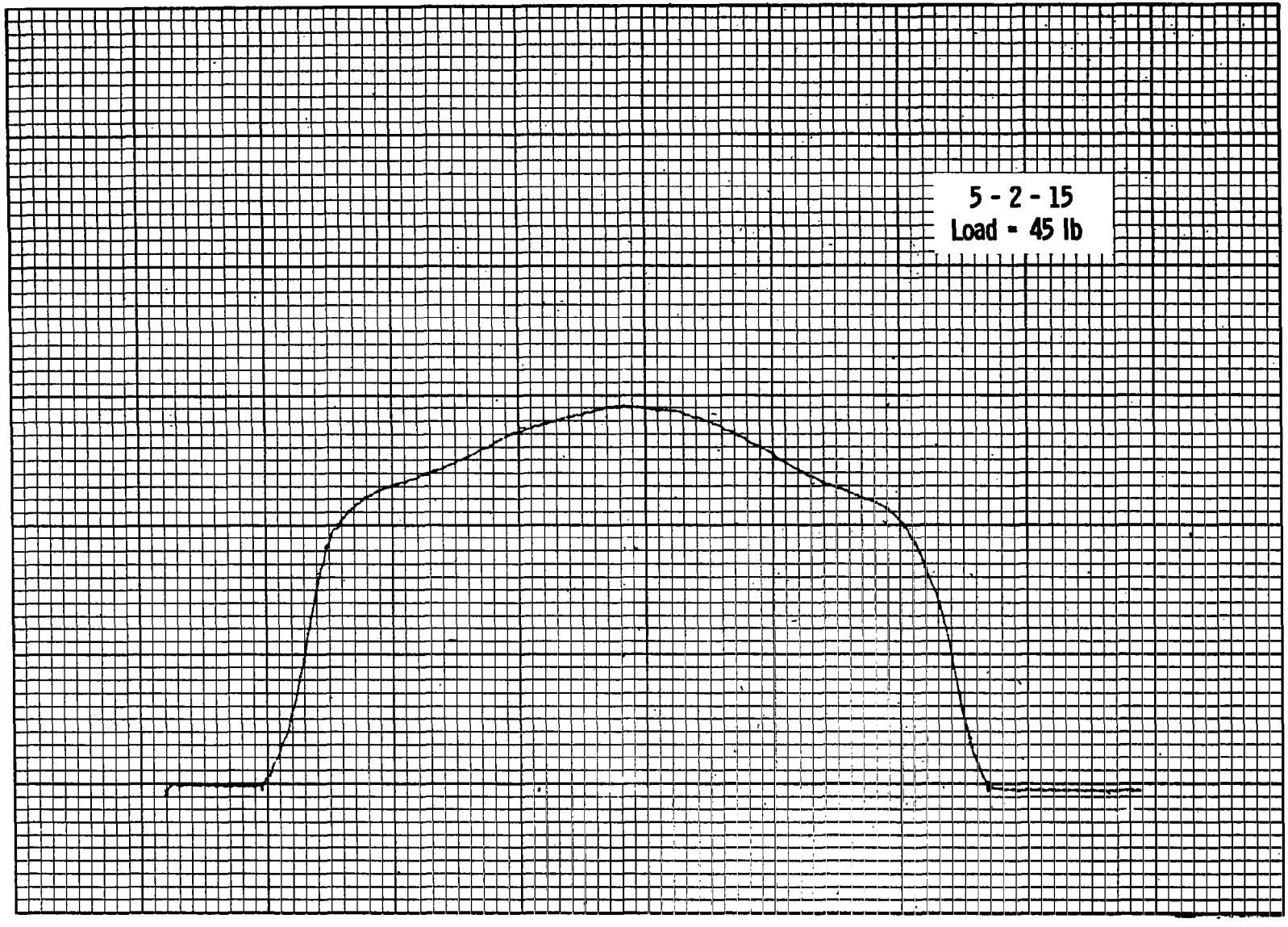

Figure 14. Pressure distribution curve.

An additional factor is the influence of deflection on the pressure distribution curves themselves. Increasingly large deflections can cause increasing shear discontinuities at the forward and leading edges of the contact patch, coupled with a tendency toward higher pressure conditions at these points. Figures 15 and 16 show the same model wheel with the same surface coating, so that both Π_1 and Π_2 are identical, for two different dimensionless deflections, δ/a, the second curve representing the larger value of δ/a. It is seen that increasing the deflection is sufficient to change the basic form of the pressure distribution curve from one which is essentially parabolic into one which exhibits maximum pressures near the forward and leading edges contact patch.

From a study of these curves, it is clear that if one wishes to obtain a parabalic pressure distribution curve, or one close to parabolic, then on a real pneumatic tire one should attempt to provide a deep soft tread. On the other hand, if one wishes to induce high pressure spikes near the forward and leading edges of the contact patch then one should use a thin hard tread and a carcass which is relatively stiff in bending. One can further accentuate this by running the tire at somewhat larger deflections. Compromise pressure distribution curves which are close to uniform can be obtained by interplaying these two factors. In general this would seem to indicate that aircraft tires probably operate under a set of conditions conducive to pressure distribution spikes at forward and aft edges of the contact patch, while automotive tires tend to be more nearly of the nature which exhibit essentially parabolic pressure distribution curves. It should be emphasized that this comment pertains

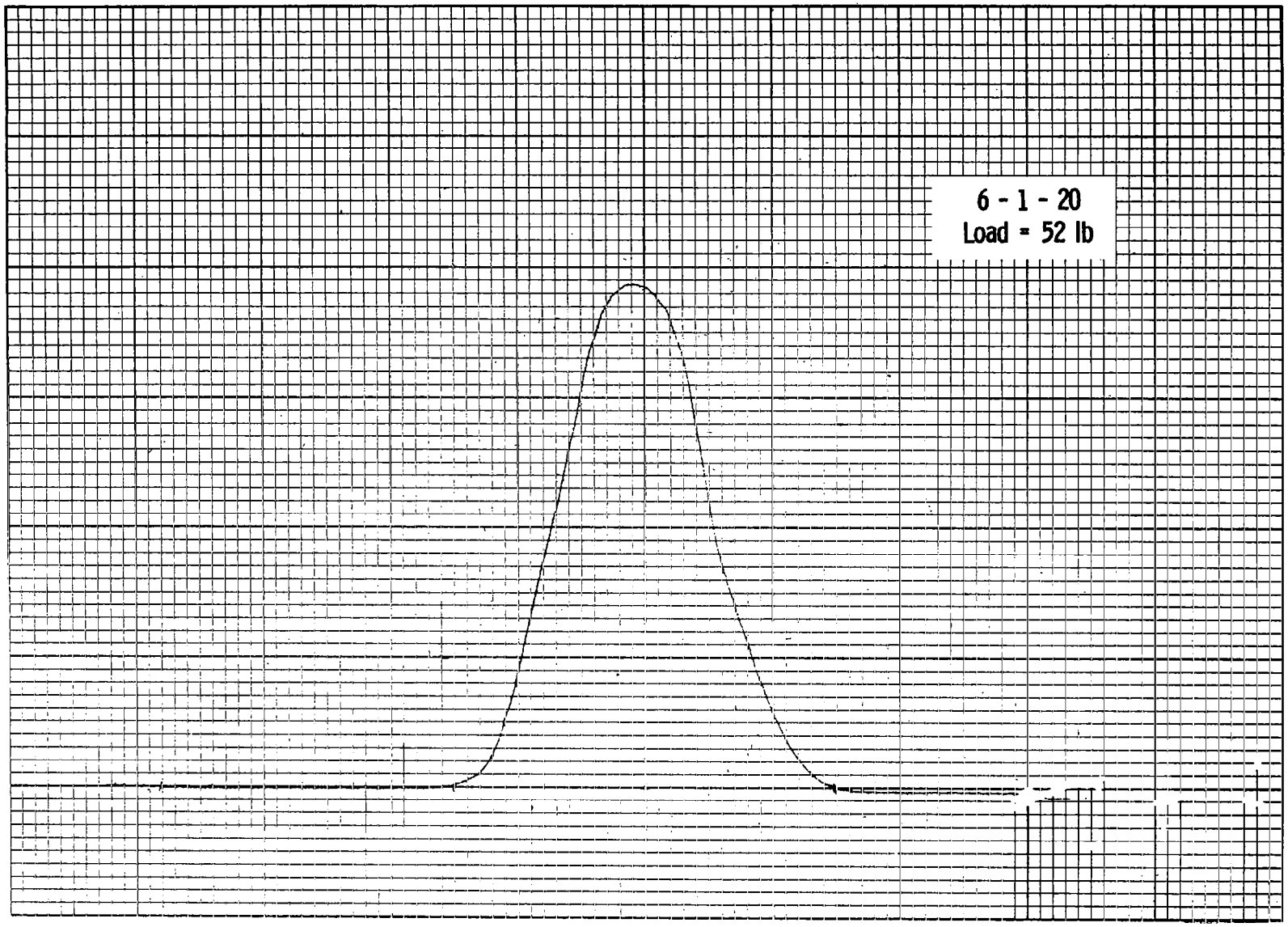

Figure 15. Pressure distribution curve.

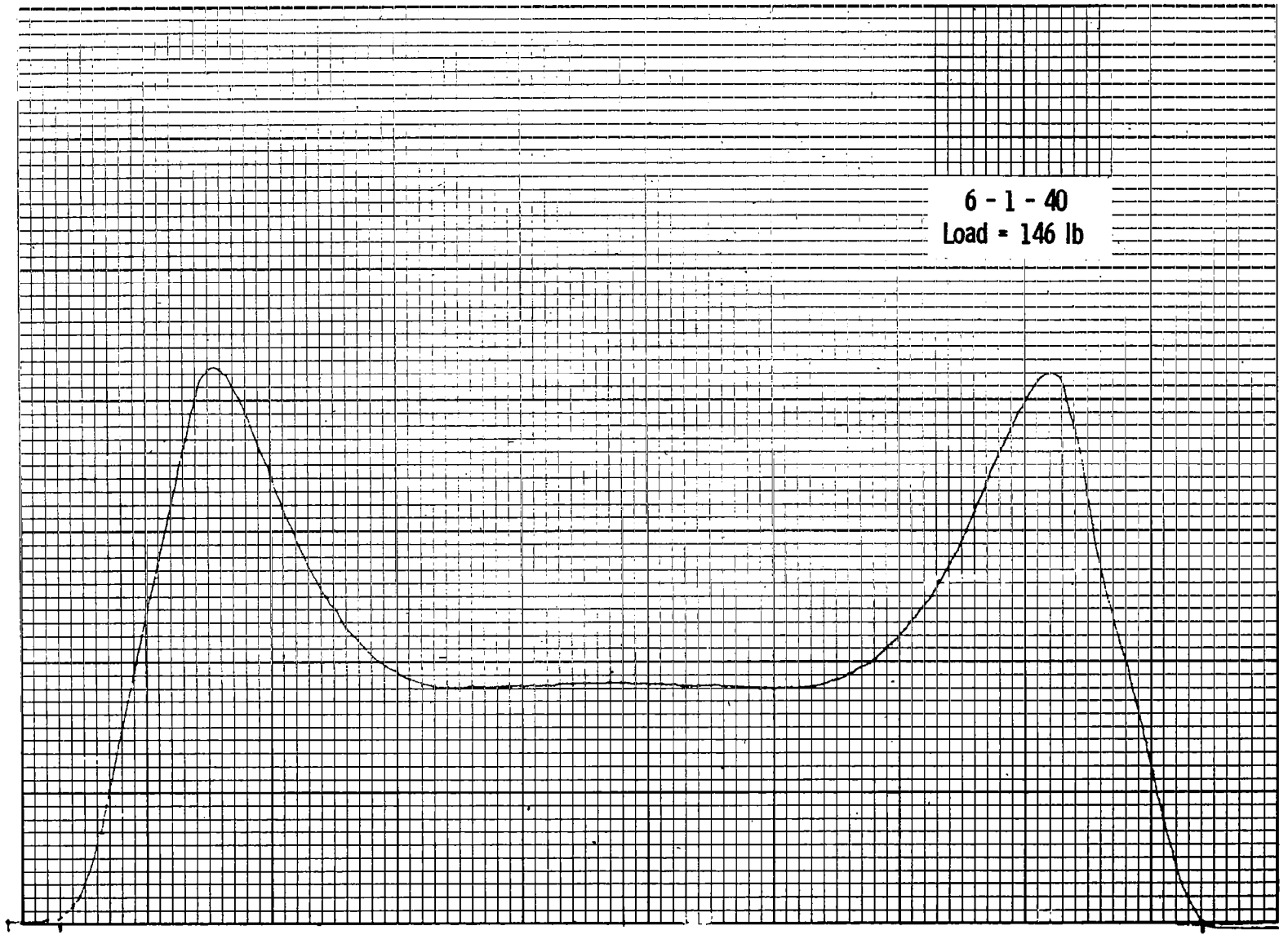

Figure 16. Pressure distribution curve.

specifically to distributions in the fore and aft directions, and not to distributions across the width, although there similar considerations undoubtedly apply.

VI. DATA ANALYSIS AND CORRELATION

Discussion of such an extensive mass of data is considerably simplified if a shorthand notation is defined allowing easy reference to particular pieces of data. The system adopted here uses three different numbers, each separated from another by a dash in order to identify a particular set of conditions. The first number, always lying between 1 and 10, defines the model number as given in Table I. The second digit, lying between 1 and 5, denotes the type of coating applied to the outer surface of the model. The number 1 represents no additional coating. Number 2 represents the 1/16 in. thick hard rubber sheet as described in Table II, while the number 3 describes the 1/4 in. thick soft rubber sheet described in the same table. The number 4 refers to a foam rubber coating used only once in this series of tests and not extensively reported. The last of the three digits represents the dimensionless reflection δ/a expressed in thousandths. By such a scheme, the data for model number 4 with a 1/16 in. hard rubber coating at a dimensionless deflection $\delta/a = 0.020$, would be denoted 4-2-20.

Reduction of the data obtained in the test program previously described basically involves condensing the results into some form conveying an overall picture of the phenomena. There are several possible techniques for doing this. One is to measure the ratio of maximum pressure near the edge of the contact patch to the pressure at the center of the contact patch. This gives a dimensionless picture or value of the nature of the shear discontinuity contribution to pressure distribution. Some of the data obtained in these tests

was analyzed in this fashion and the results are given in Figures 17(a) and 17(b). In one type of behavior, illustrated in Figure 17(a), the ratio of peak pressure over central pressure tends to increase continuously as the dimensionless deflection increases. This is shown in that figure for models 1-1 and 6-2. On the other hand, a somewhat different type of behavior is observable in which the ratio of peak pressure to midpoint pressure starts at some low value, rises to a peak, and then decreases as the dimensionless deflection grows. This is illustrated in Figure 17(b) by the data from models 4-1 and 7-1. It is not completely clear exactly why the differences between the data of Figures 17(a) and 17(b) should be so large, except that it is strongly suspected that if the dimensionless deflections of Figure 17(a) were increased yet farther, the curves of that figure would show maximum values similar to those in Figure 17(b). This would mean that the somewhat softer surfaces of the data used in Figure 17(a) causes a delay or retardation in the occurrence of the peak values of this dimensionless pressure ratio.

All of the data analyzed in this fashion is presented in Table III.

Another method for analyzing this data is to note that the parabolic curves shown in Figures 10 and 11 may be split into two essentially symmetric parts, each half measured about a center line. Each of these two parts will represent half a parabola to a first approximation, whose centroid is located approximately 3/8 of the half length of the contact patch away from the center position. On the other hand, pressure distribution curves exhibiting large shear discontinuity effects, such as shown in Figures 12 and 13 may also be subdivided into two essentially symmetric halves. Each of these will exhibit

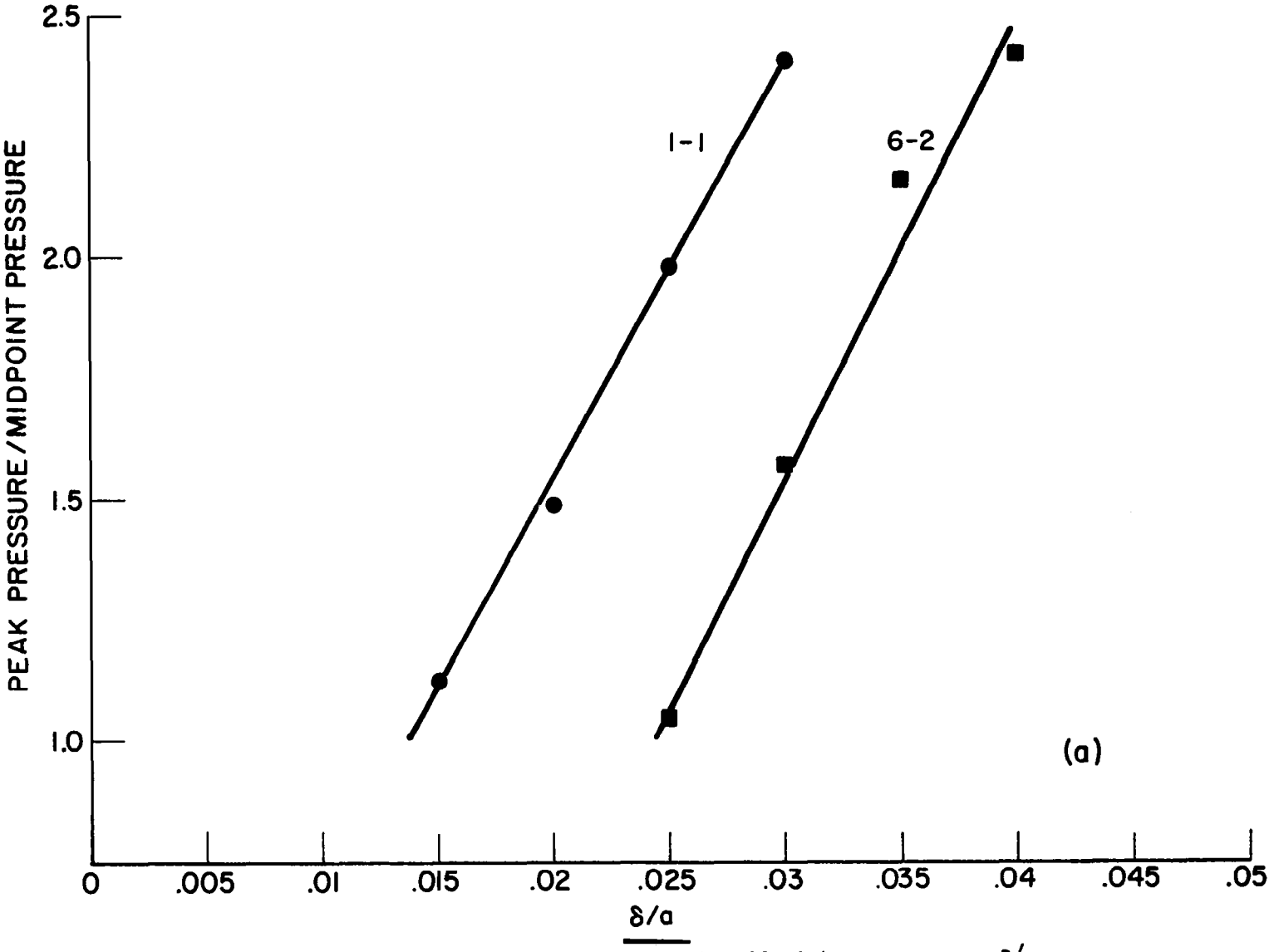

Figure 17. Ratio of peak pressure to midpoint pressure vs. δ/a.

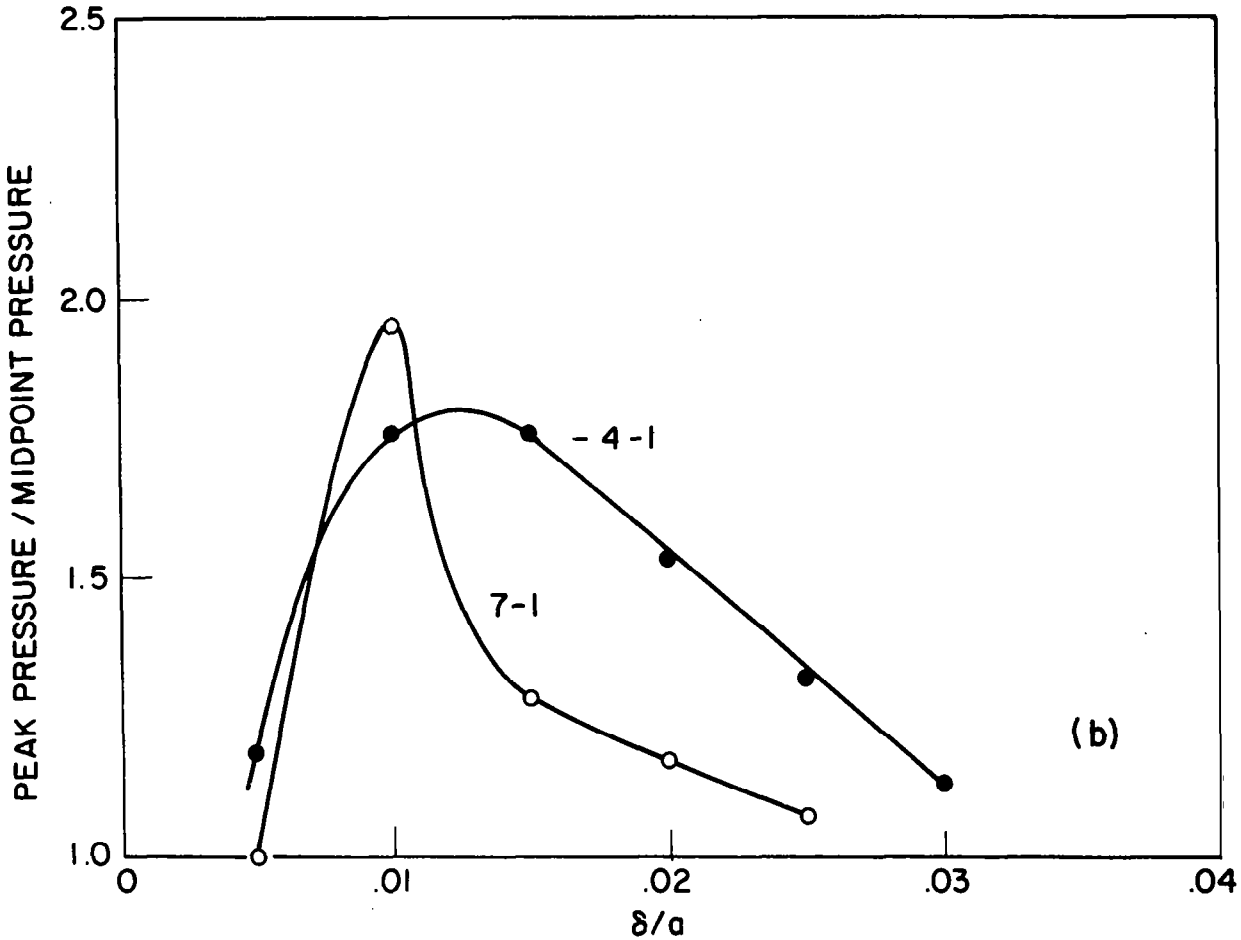

Figure 17. (Concluded)

TABLE III

TABULATED PRESSURE RATIO DATA

Model No.	δ/a	-1 Plain	-2 Black Rubber	-3 Brown Rubber	-4 Foam Rubber
1	5	1.0	1.0	1.0	1.0
	10	1.0	1.0	1.0	1.0
	15	1.12	1.0	1.0	1.0
	20	1.49	1.0	1.0	1.0
	25	1.98	1.07	1.0	1.0
	30	2.40	1.128	1.0	1.0
	35				
	40				
4	5	1.187	1.0	1.0	
	10	1.76	1.45	1.0	
	15	1.765	1.15	1.0	
	20	1.535	0.945	1.0	
	25	1.32	0.79	1.0	
	30	1.135	0.671	1.0	
	35				
	40				
5	5	1.112	1.056	1.0	
	10	1.01	1.0	1.0	
	15	0.921	1.0	1.0	
	20	0.872	1.0	1.0	
	25	0.779	1.0	1.0	
	30	0.672	1.0	1.0	
	35				
	40				
6	5	1.0	1.0	1.0	
	10	1.0	1.0	1.0	
	15	1.325	1.0	1.0	
	20	2.50	1.0	1.0	
	25	2.72	1.05	1.0	
	30	2.30	1.57	1.0	
	35		2.15	1.0	
	40		2.42	1.0	
7	5	1.0	1.0	1.0	
	10	1.95	1.39	1.0	
	15	1.28	1.35	1.0	
	20	1.17	1.08	1.0	
	25	1.075	0.925	1.0	
	30				
	35				
	40				
8	5	1.0			
	10	1.0			
	15	1.0			
	20	1.0			
	25	1.0			
	30	1.0			
	35				
	40				

centroids located considerably farther from the center line than the 3/8 value previously given for parabolic shapes. This leads to the concept that location of the centroid of half of such a curve measures the importance of shear discontinuity influences. For that reason, the fractional location of the centroid of the pressure distribution curve for each of the cases measured is presented in Table IV. This data was obtained by splitting each pressure distribution curve into the two essentially symmetric parts are previously mentioned, then determining the pressure distribution centroid for each of the two parts, and finally averaging them into a single value. One may again see that the general role of decreasing Π_1 and increasing Π_2 is to increase the centroidal distance of the pressure distribution area. In addition, increasing deflection also accentuates this effect. Some of this data is illustrated in Figures 18(a) through 18(e).

Each of the pressure distribution curves on given wheel were taken at a consistent vertical scale, although such vertical scales were adjusted from wheel to wheel to provide reasonably scaled records for recording purposes. Thus, the mean pressure may be obtained by dividing the total area of the contact patch curve by the length of the contact patch area. This will give useful information concerning the influence of deflection on the mean or average pressure distribution intensity. It is necessary to recognize that this information is not valid in direct comparisons between model to model for two reasons. The first is that the vertical scales involved are not necessarily the same. The second reason is that these pressure distribution records were taken at different positions along the width of the models in question, and

TABLE IV

TABULATED PRESSURE DISTRIBUTION CENTROIDS

Model No.	δ/a	-1 Plain	-2 Black Rubber	-3 Brown Rubber	-4 Foam Rubber
1	5	0.375	0.327	0.375	0.33
	10	0.370	0.378	0.435	0.395
	15	0.4875	0.379	0.432	0.408
	20	0.474	0.413	0.435	0.403
	25	0.574	0.447	0.436	0.446
	30	0.762		0.446	0.407
	35				
	40				
4	5	0.552	0.365	0.349	
	10	0.554	0.505	0.395	
	15	0.529	0.468	0.408	
	20	0.529	0.472	0.416	
	25	0.510	0.451	0.416	
	30	0.482	0.433	0.414	
	35				
	40				
5	5	0.492	0.380	0.376	
	10	0.483	0.425	0.395	
	15	0.423	0.430	0.400	
	20	0.472	0.426	0.400	
	25	0.458	0.419	0.398	
	30	0.447			
	35				
	40				
6	5	0.266	0.337	0.326	
	10	0.297	0.349	0.373	
	15	0.387	0.343	0.381	
	20	0.485	0.349	0.370	
	25	0.522	0.396	0.379	
	30	0.530	0.453	0.384	
	35		0.479	0.396	
	40		0.497	0.398	
7	5	0.316	0.288	0.374	
	10	0.480	0.437	0.409	
	15	0.495	0.449	0.398	
	20	0.485	0.460	0.411	
	25	0.482	0.445	0.414	
	30				
	35				
	40				
8	5	0.33			
	10	0.405			
	15	0.388			
	20	0.392			
	25	0.389			
	30	0.397			
	35				
	40				

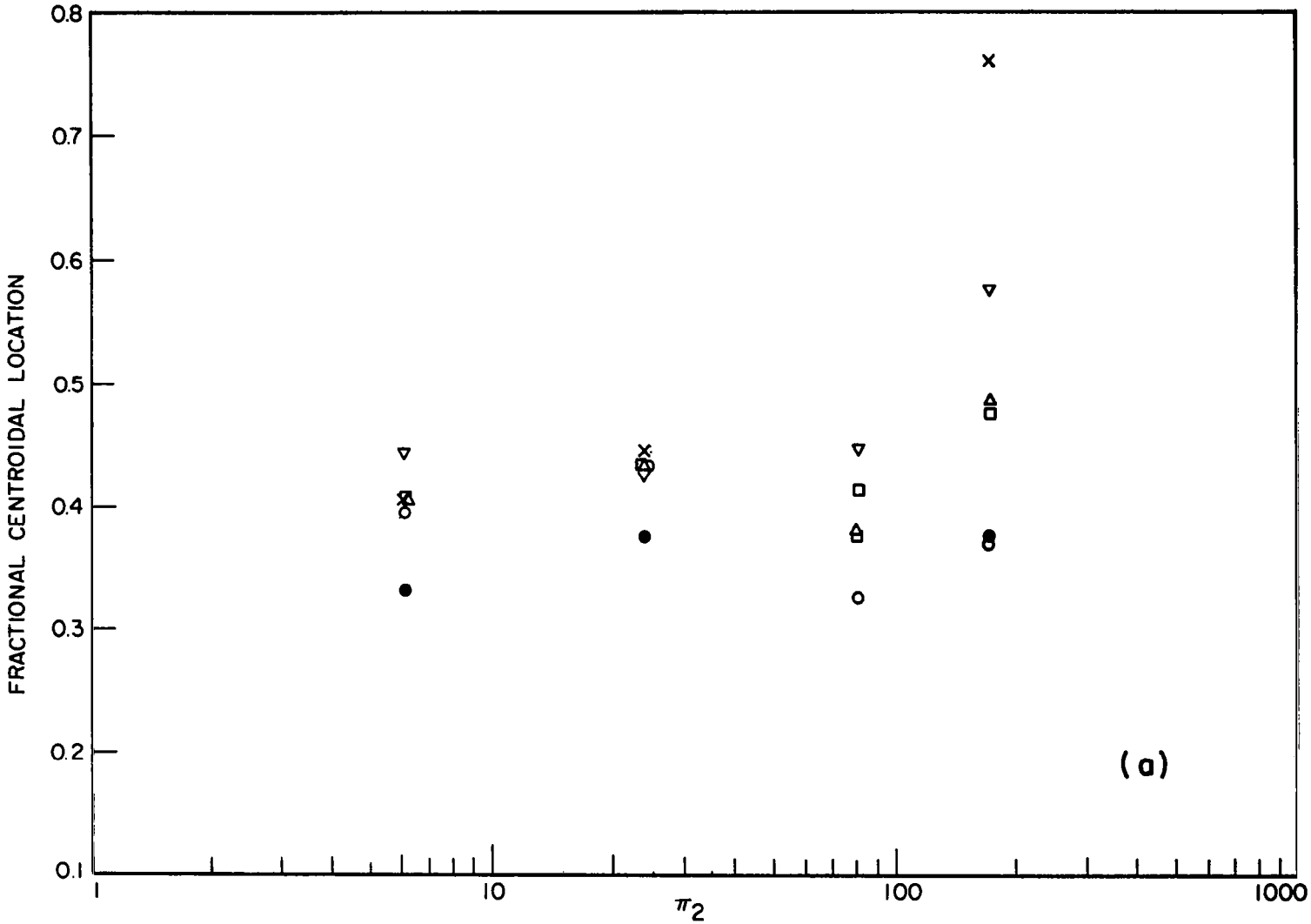

(a) Model 1

Figure 18. Pressure distribution centroid vs. Π_2.

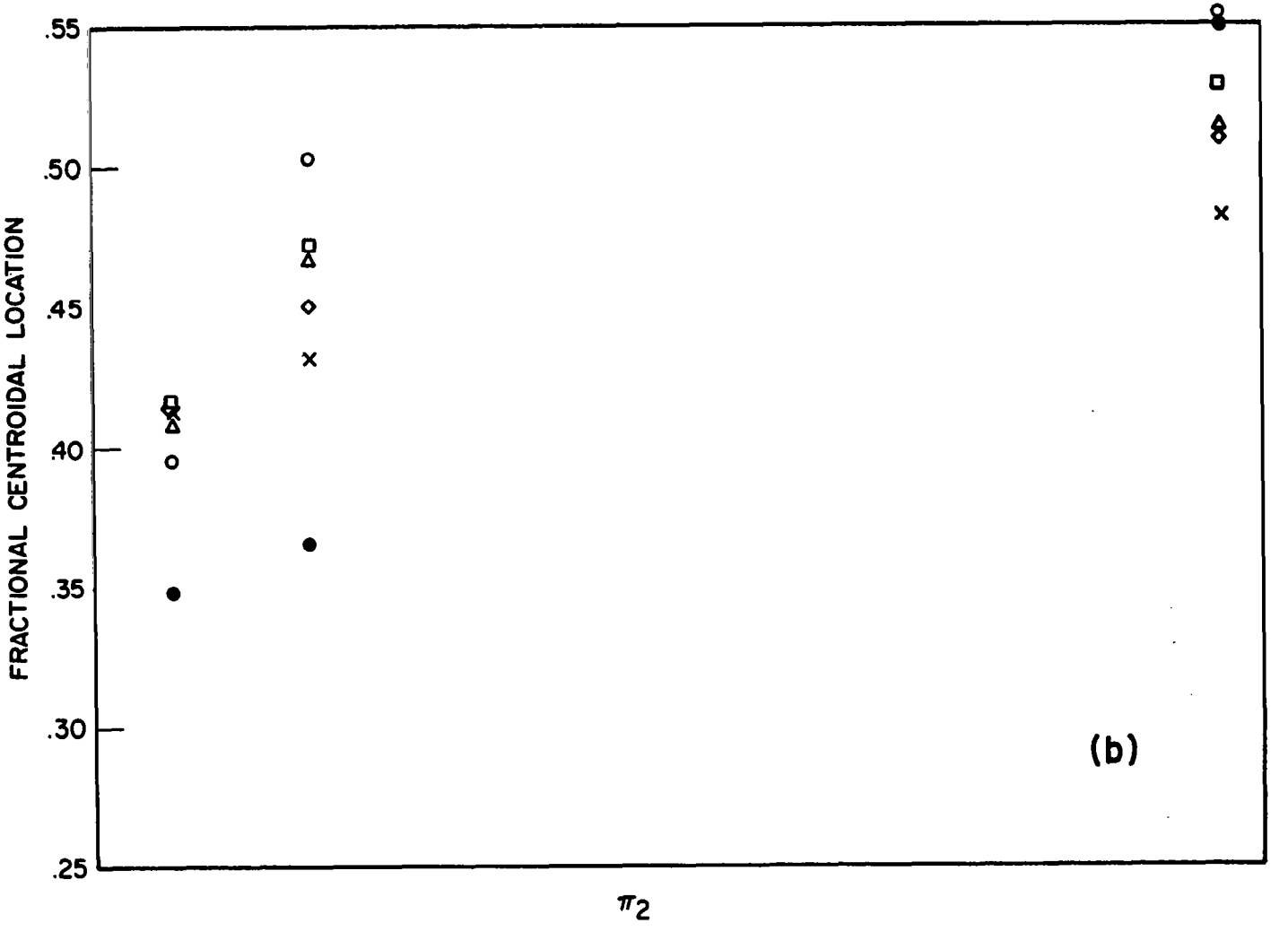

(b) Model 4

Figure 18. (Continued)

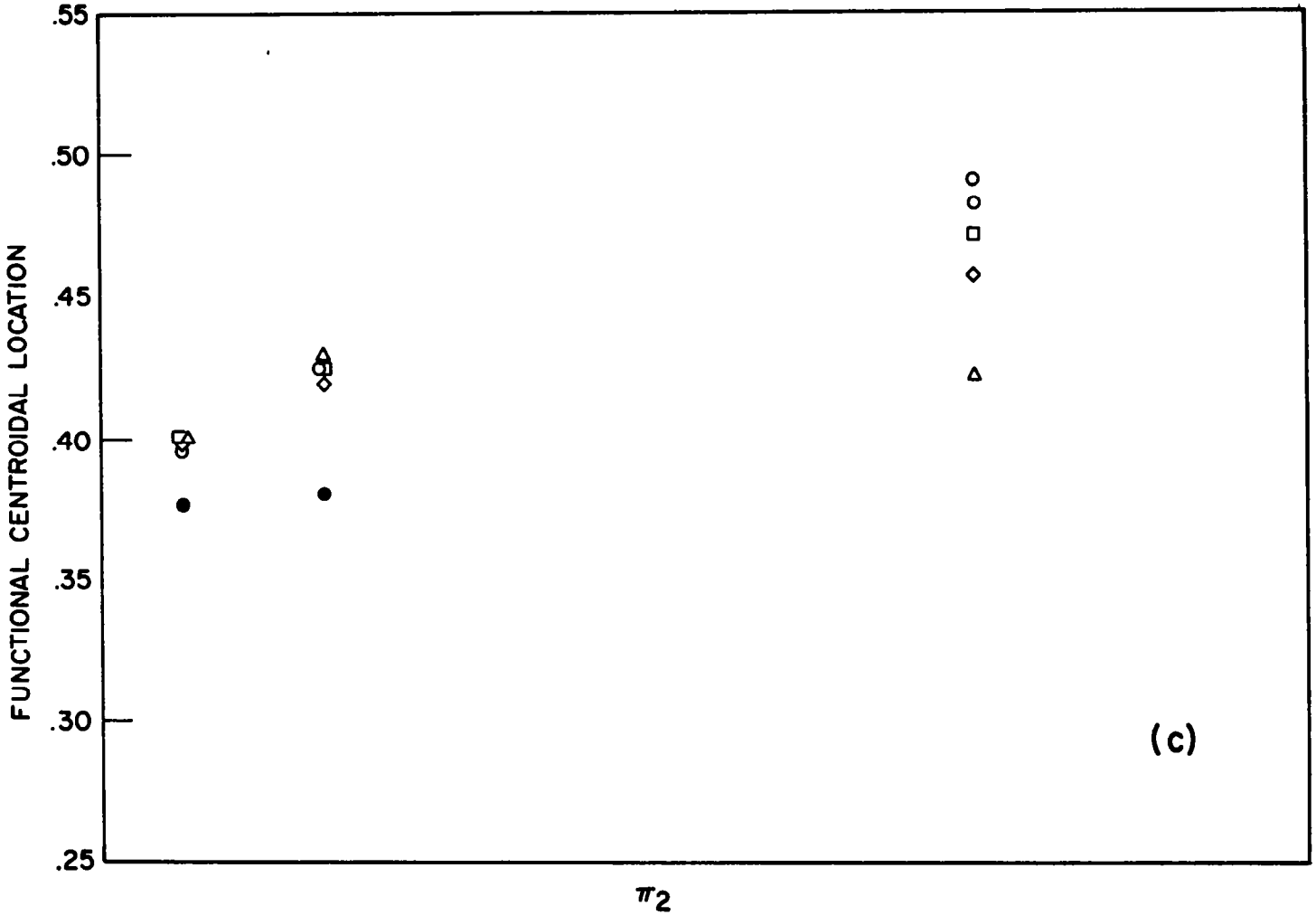

(c) Model 5

Figure 18. (Continued)

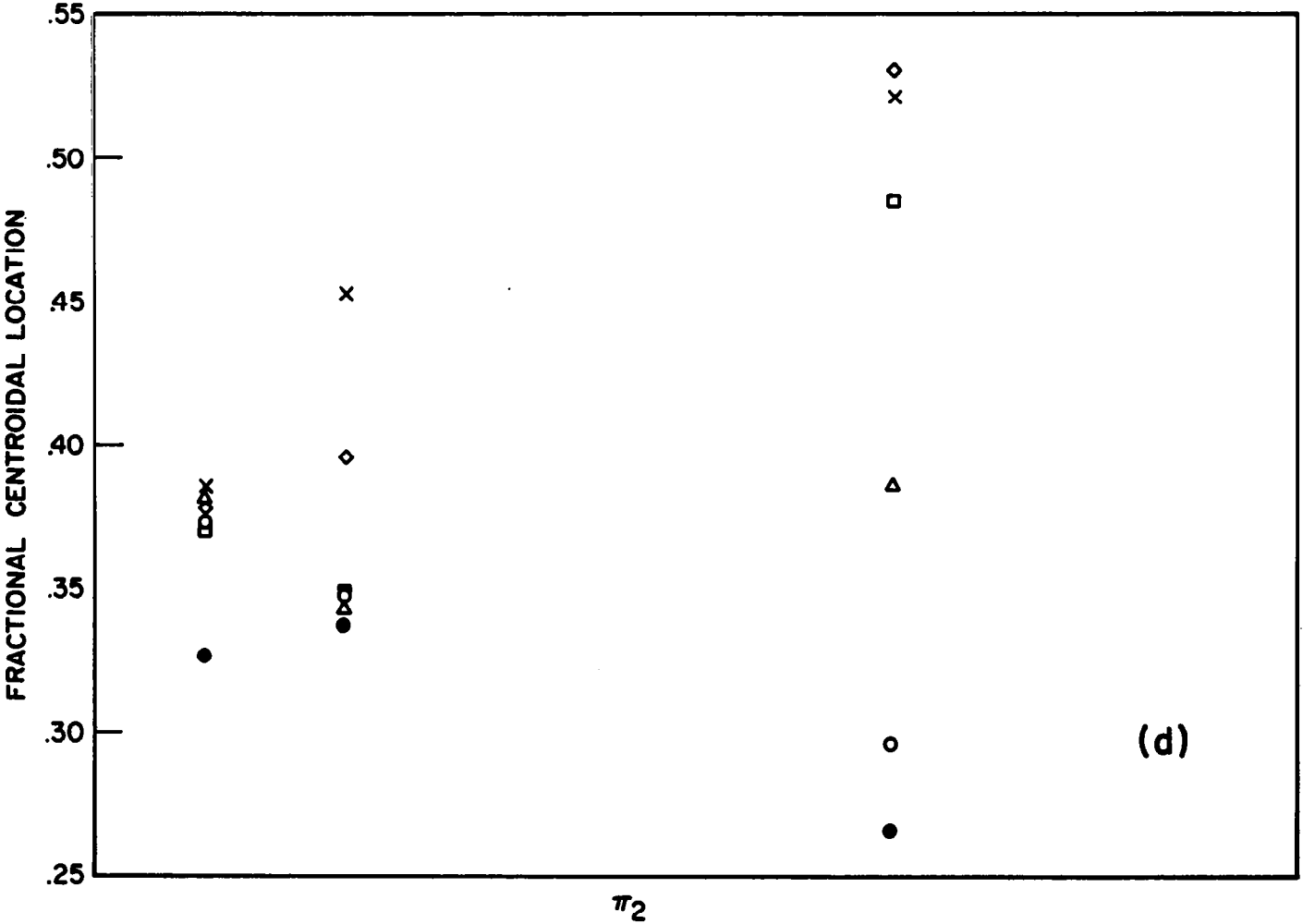

(d) Model 6

Figure 18. (Continued)

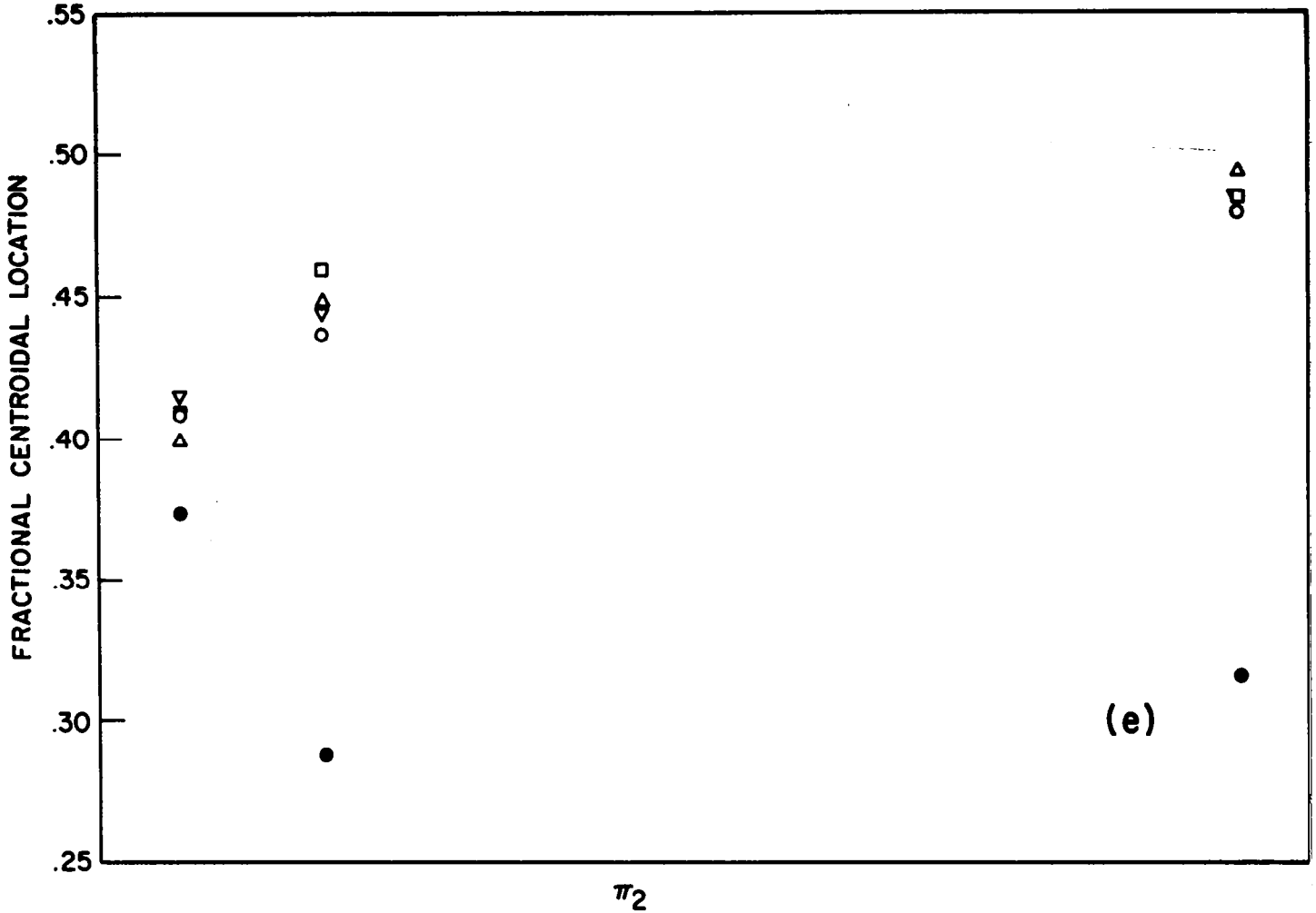

(e) Model 7

Figure 18. (Concluded)

there are variations in the amplitude of such records associated with the position of the pressure transducer along the width of the specimen, although the shapes are not influenced much, if at all, by such positioning. For these reasons, the mean pressure intensity is only valuable when viewed with each individual model as influenced by dimensionless deflection. In view of the fact that in real pneumatic tires the major contribution to the mean contact pressure is made by the inflation pressure, which is absent in these studies, no attempt will be made here to analyze the mean pressure distribution.

As mentioned at the beginning of this section, the various interactions taking place in these contact pressure curves are complex, and it is probably best to attempt to convey much of the information about them by direct presentation of such contact pressure records. For that reason, they are reproduced in the Appendix in their entirety.

VII. REFERENCES

1. Clark, S. K., "The Rolling Tire Under Load," SAE Paper No. 650493, 1965.

2. Dodge, R. N., "The Dynamic Stiffness of a Pneumatic Tire Model," SAE Paper No. 650491, 1965.

3. Tielking, J. T., "Plane Vibration Characteristics of a Pneumatic Tire Model," SAE Paper No. 650492, 1965.

4. Spengos, A. C., "Experimental Investigation of Rolling Contact," J. Appl. Mech., 32, No. 4, December, 1965.

VIII. ACKNOWLEDGMENTS

The equipment used to measure the pressure distribution curves given in this report was designed by Robert Cohen, and operated by Robert Cohen and Jacob David. Much of the credit for this report must go to them.

IX. APPENDIX. LONGITUDINAL PRESSURE DISTRIBUTION

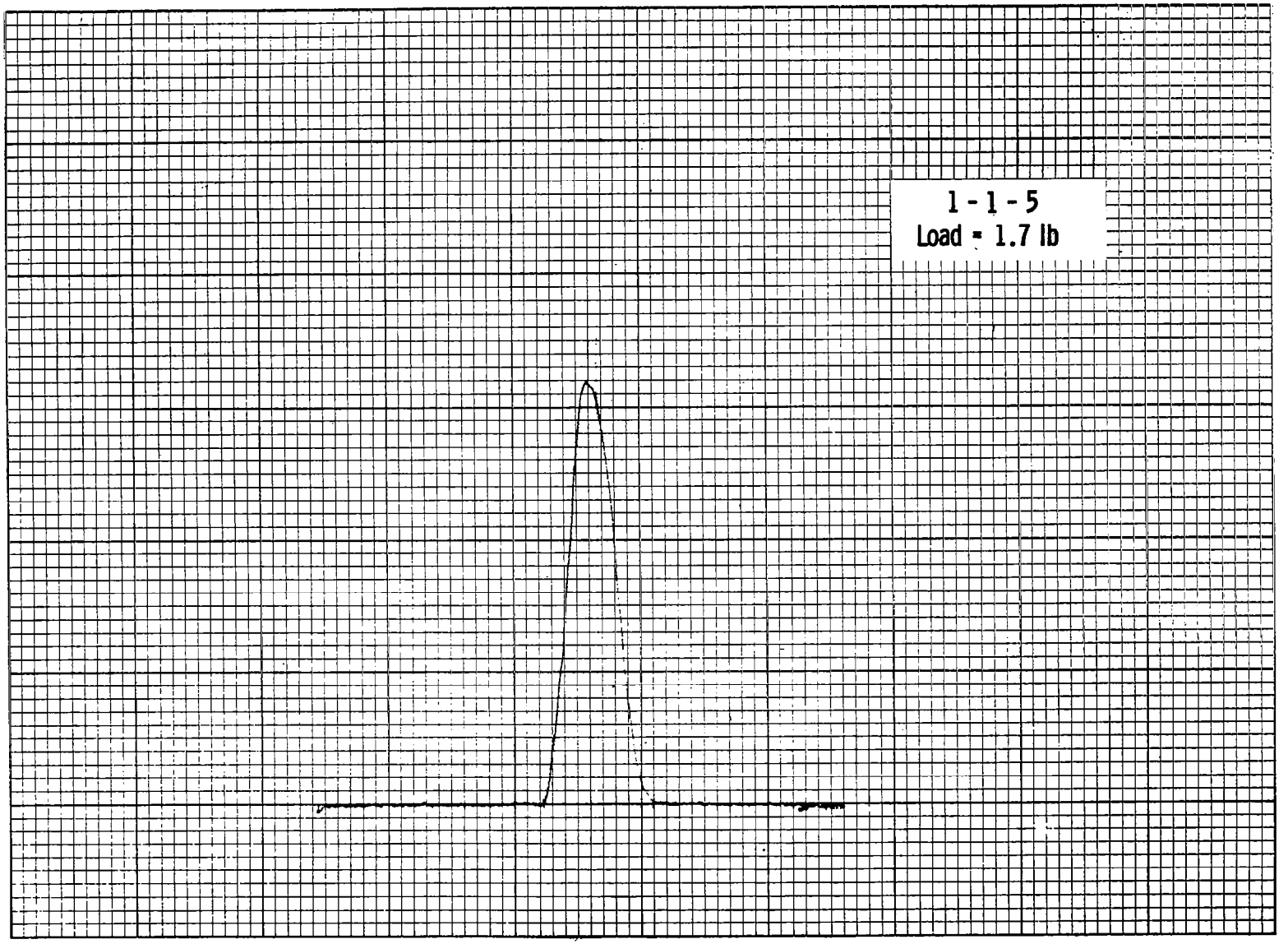
1 - 1 - 5
Load = 1.7 lb

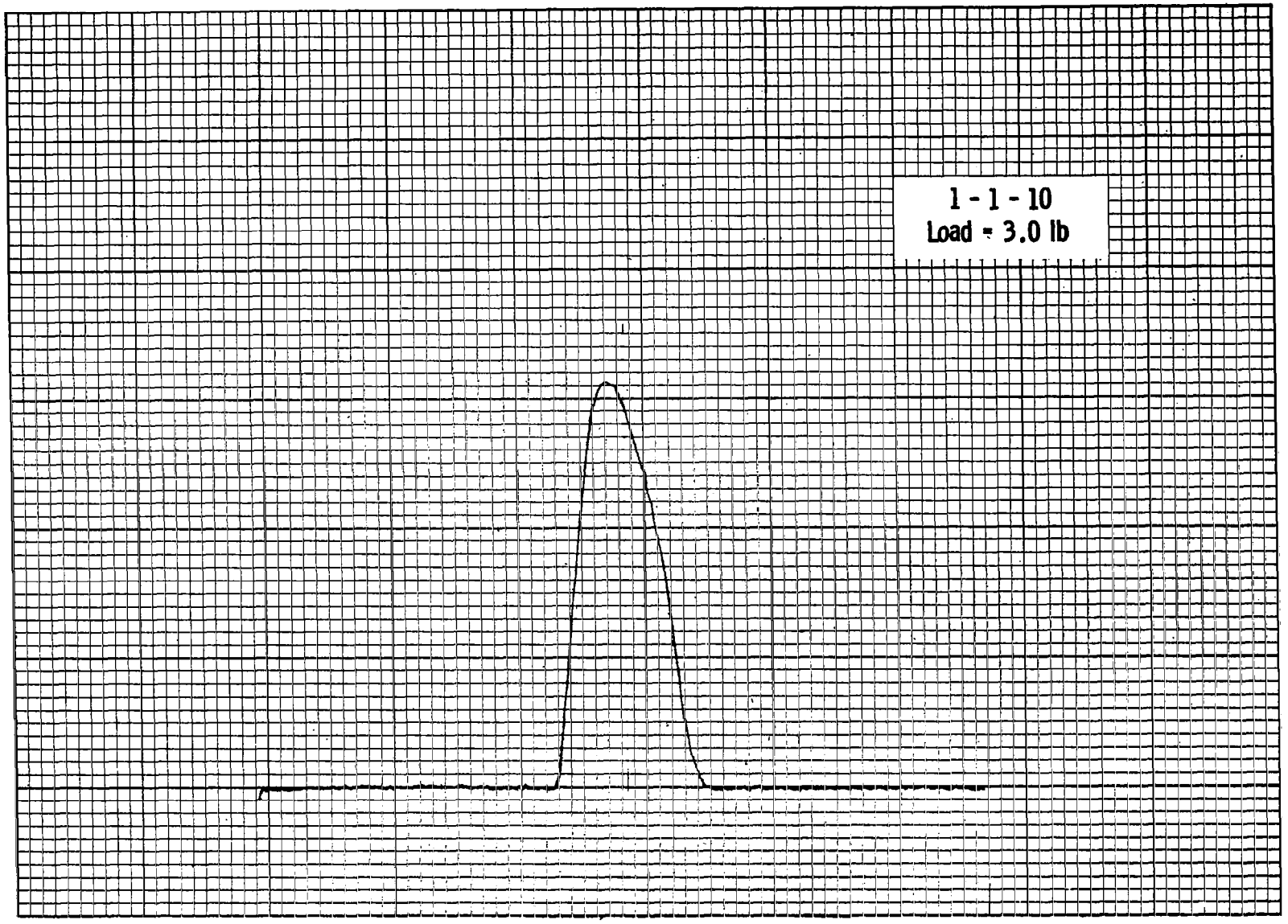
1 - 1 - 10
Load = 3.0 lb

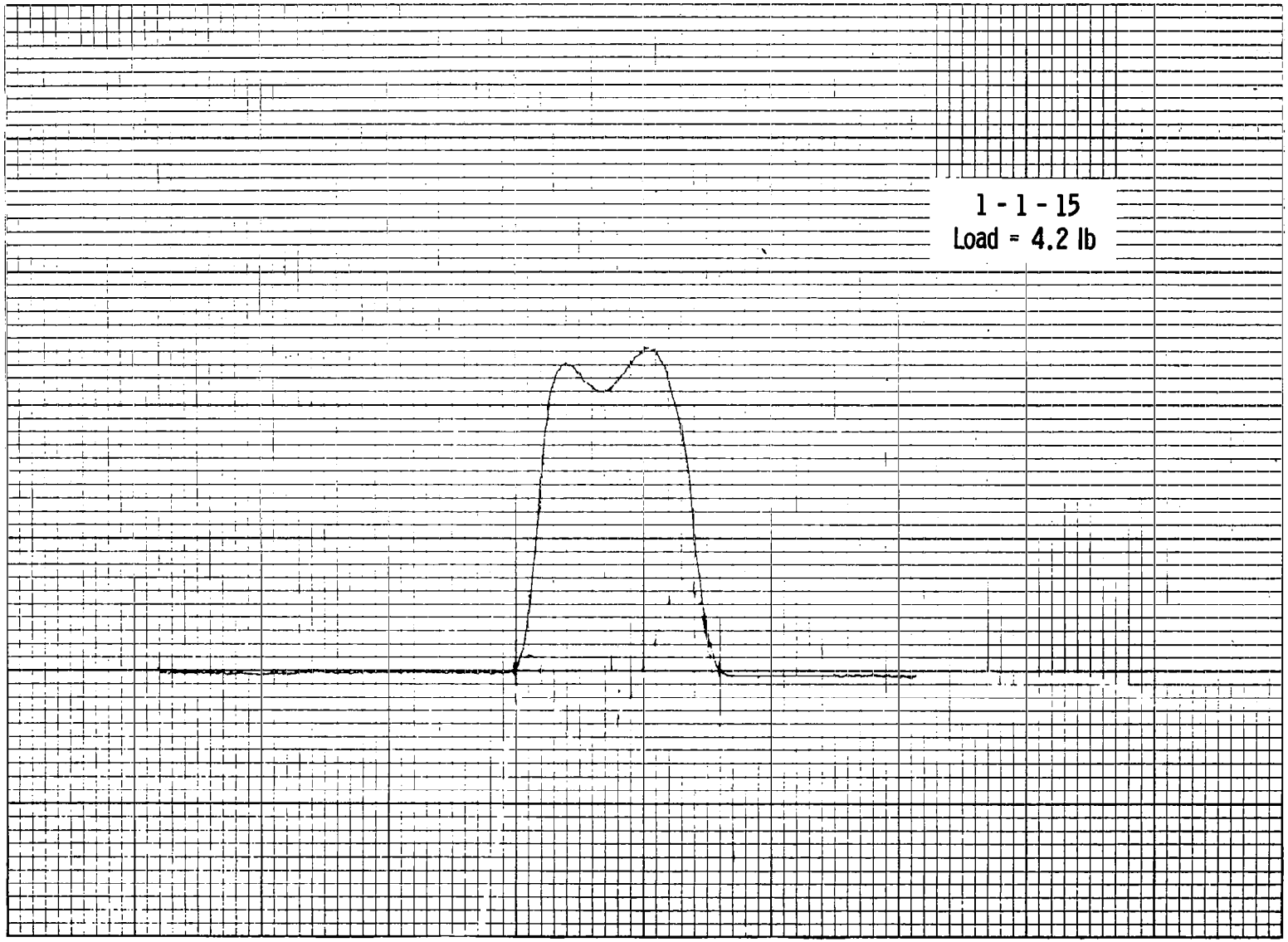
1 - 1 - 15
Load = 4.2 lb

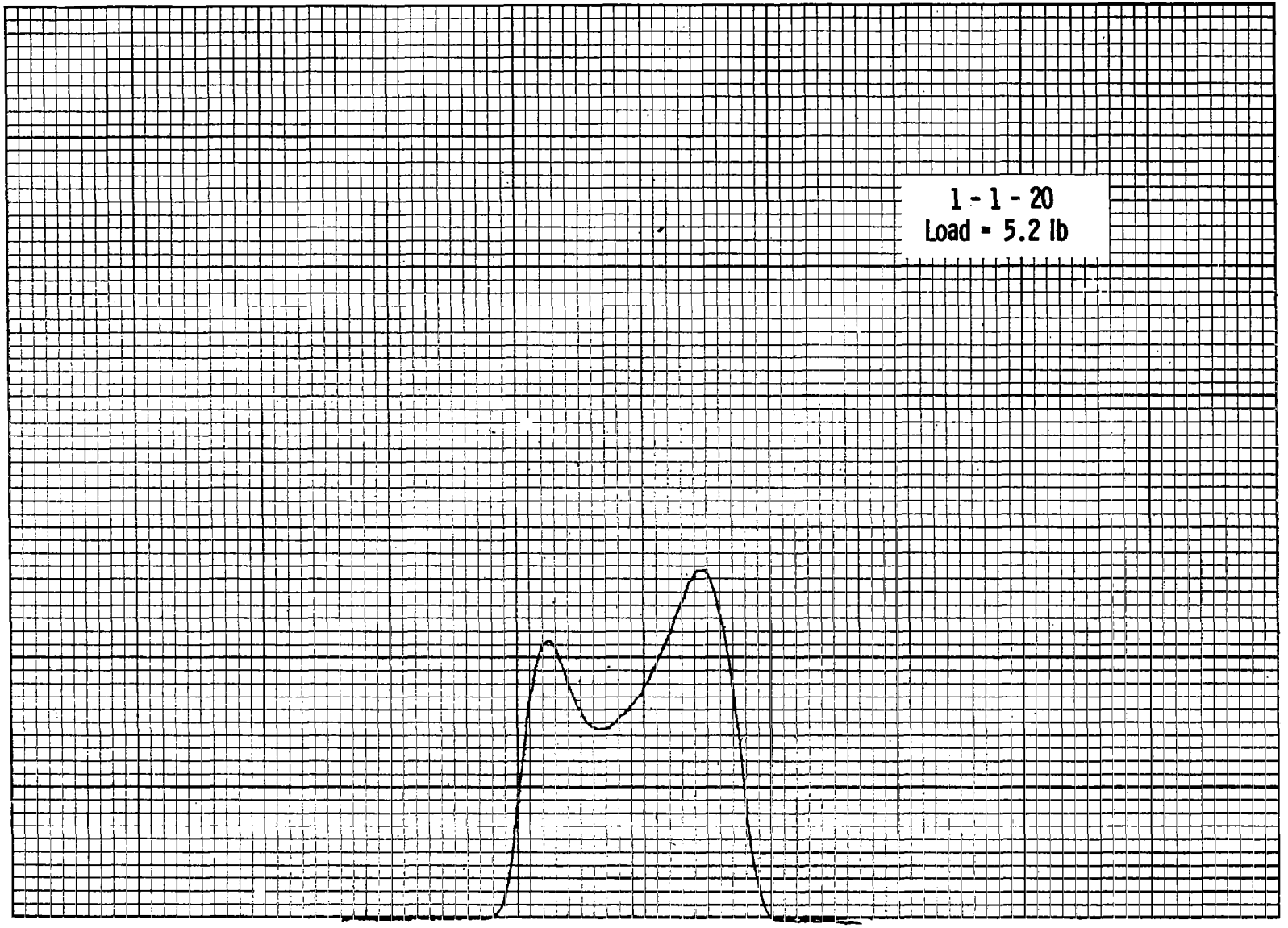
1 - 1 - 20
Load = 5.2 lb

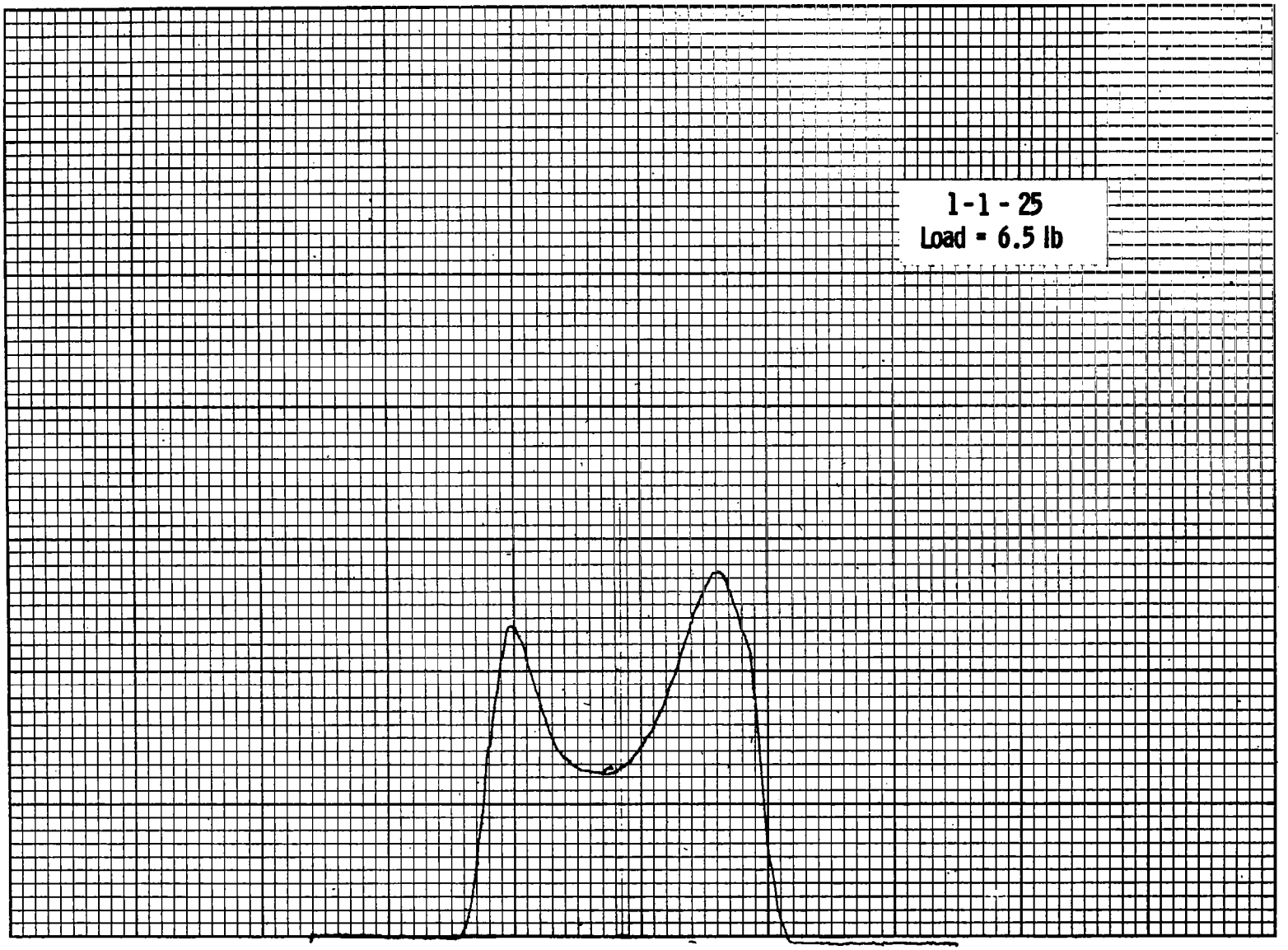
1-1-25
Load = 6.5 lb

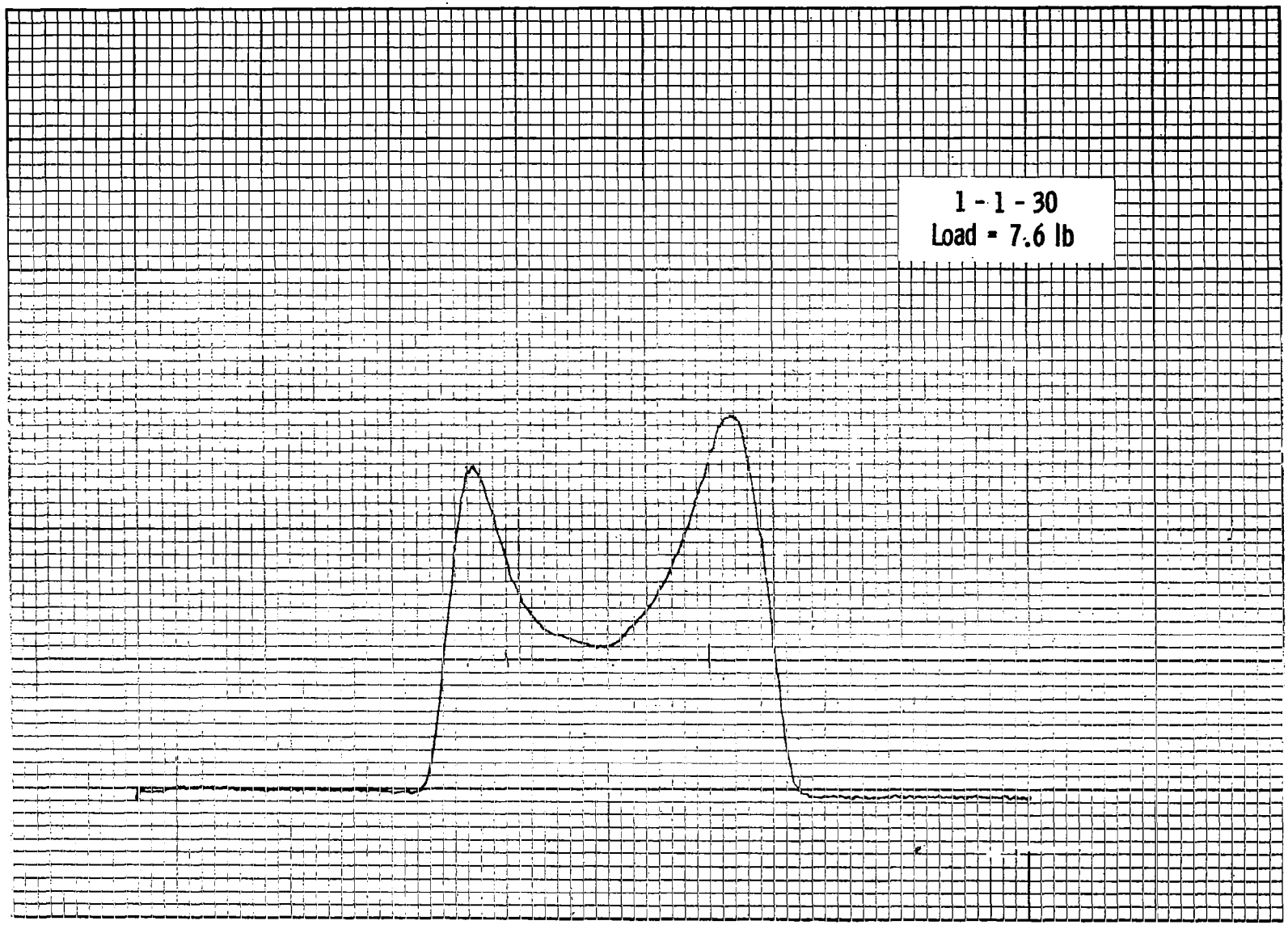
1 - 1 - 30
Load = 7.6 lb

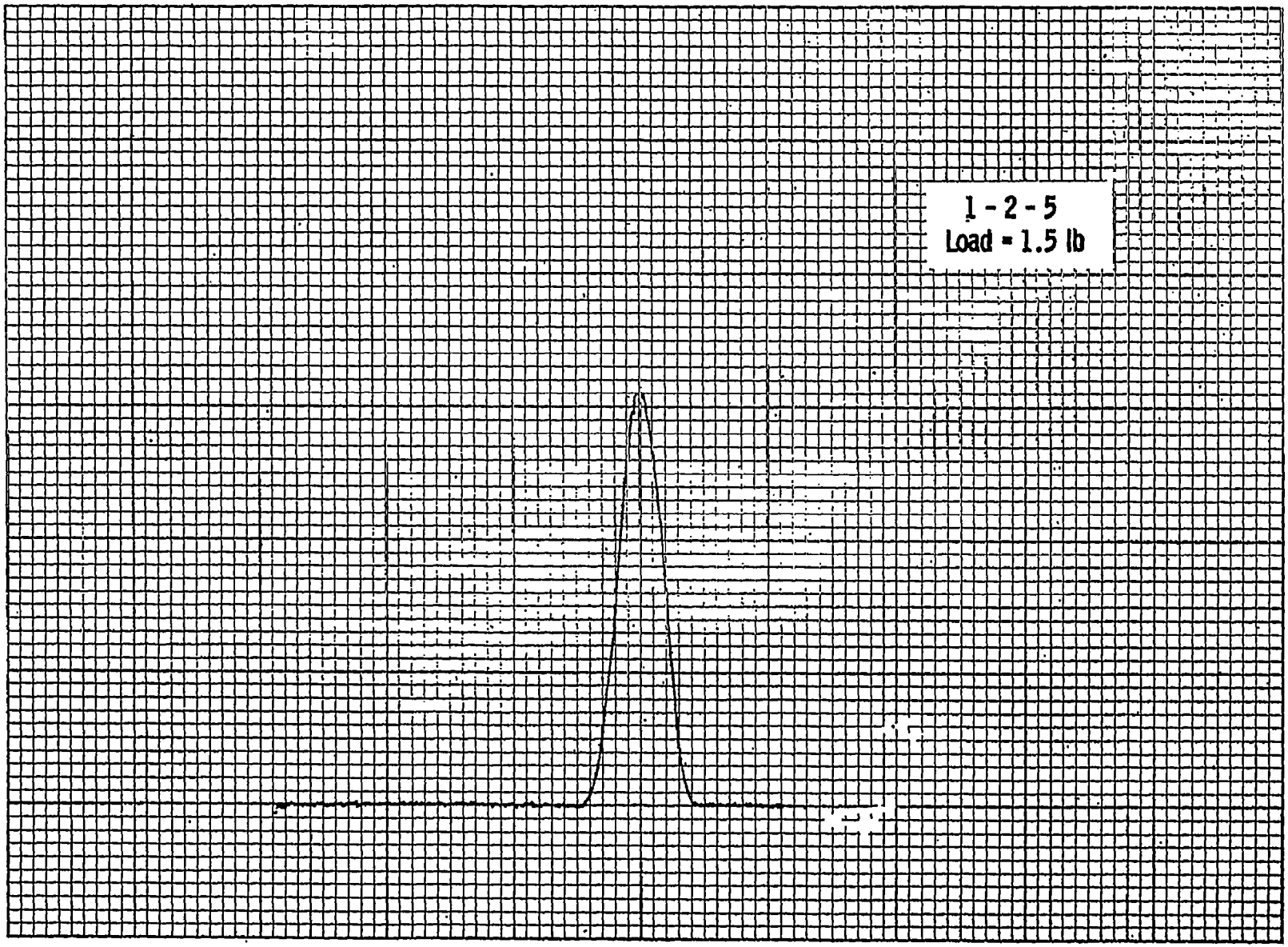
1 - 2 - 5
Load = 1.5 lb

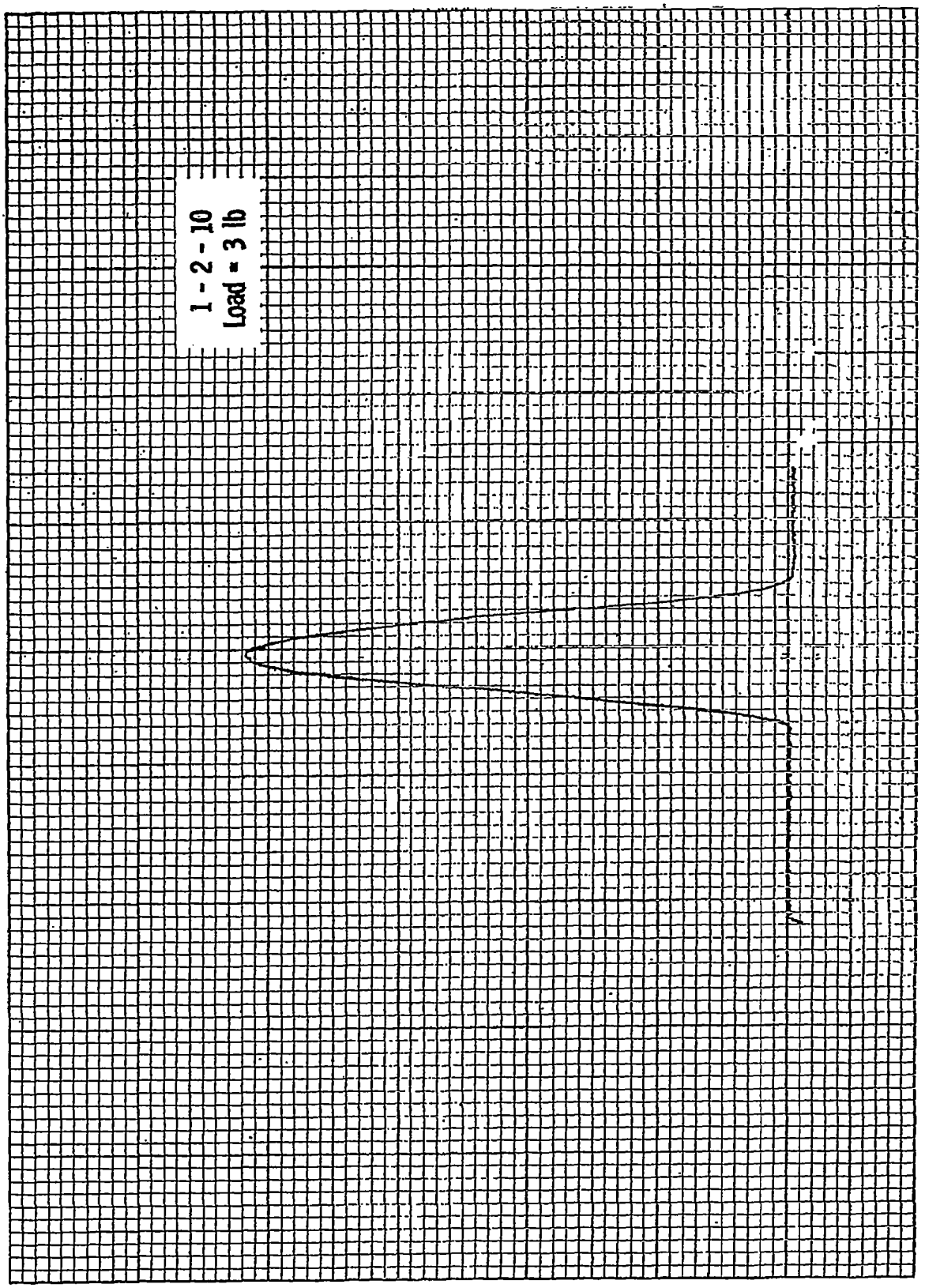
1 - 2 - 10
Load = 3 lb

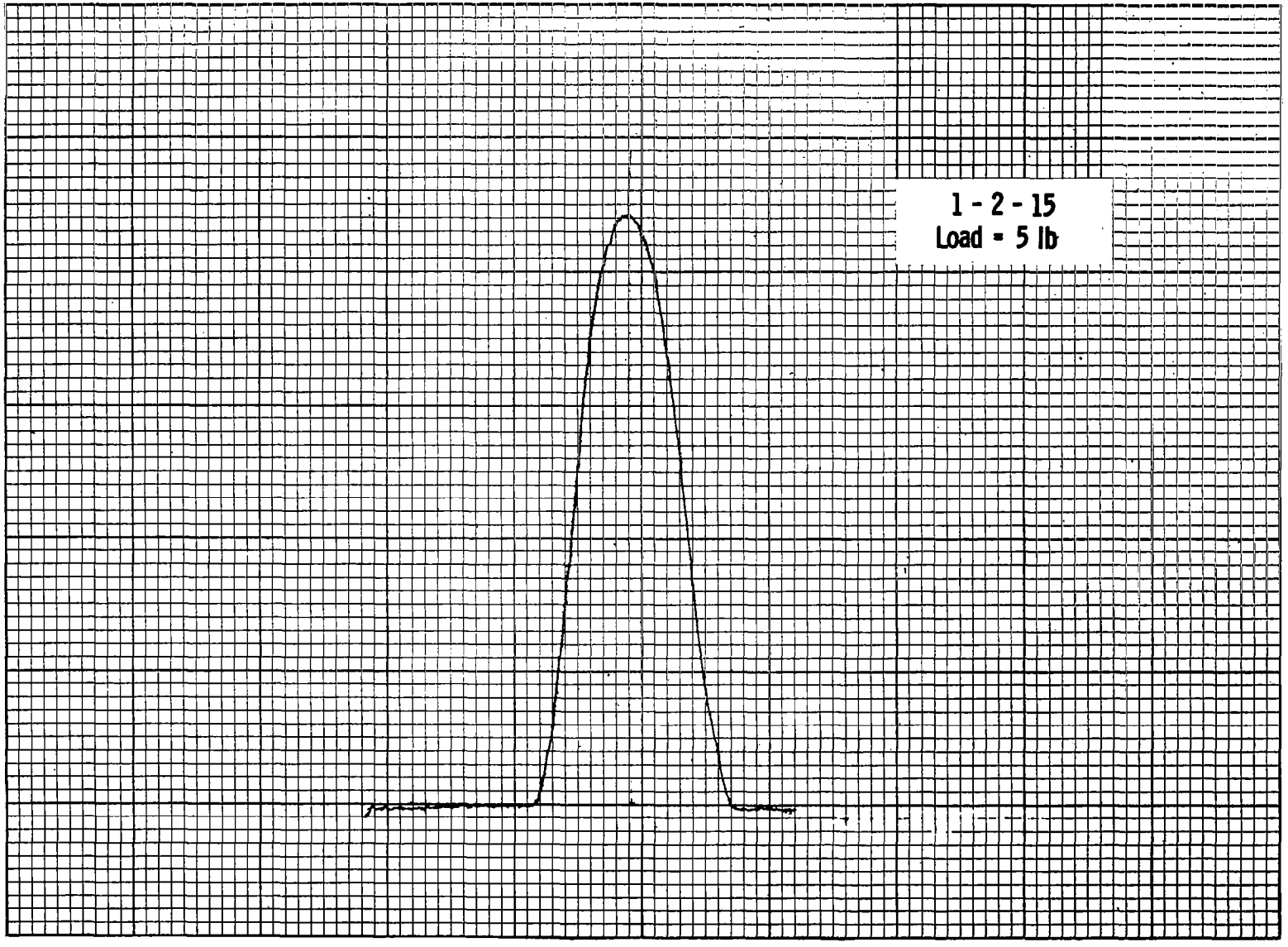
1 - 2 - 15
Load = 5 lb

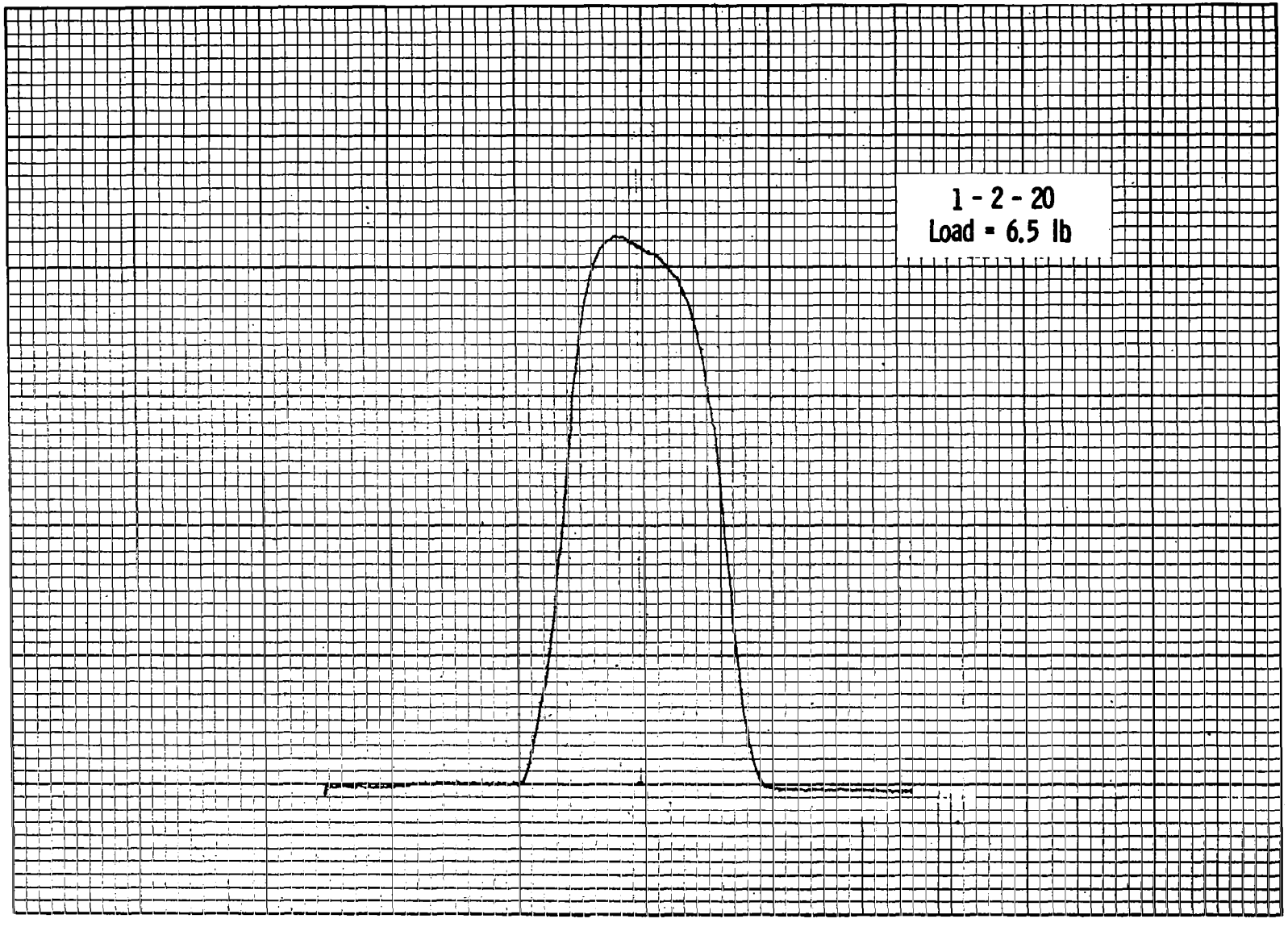
1 - 2 - 20
Load = 6.5 lb

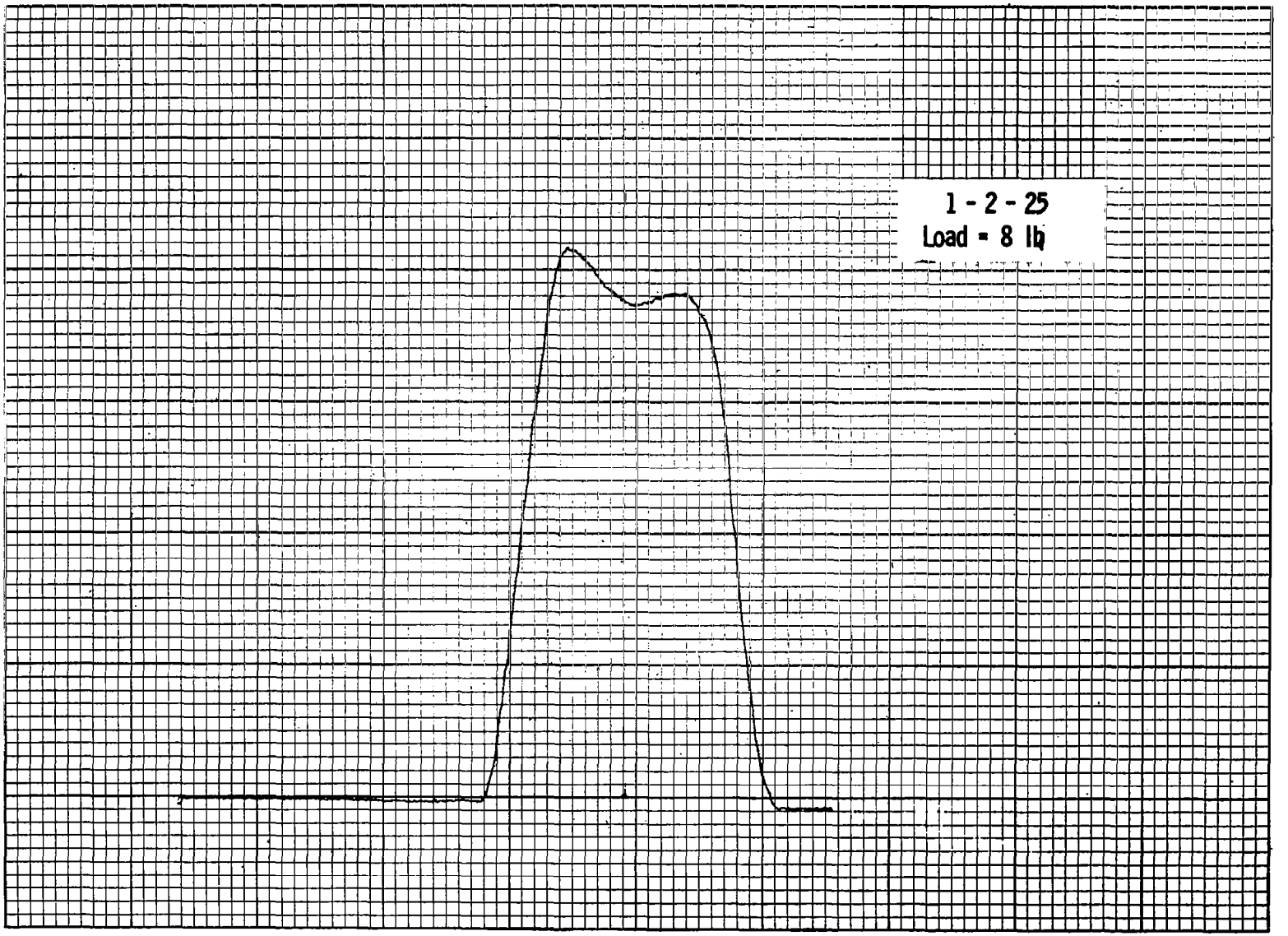
1 - 2 - 25
Load = 8 lb

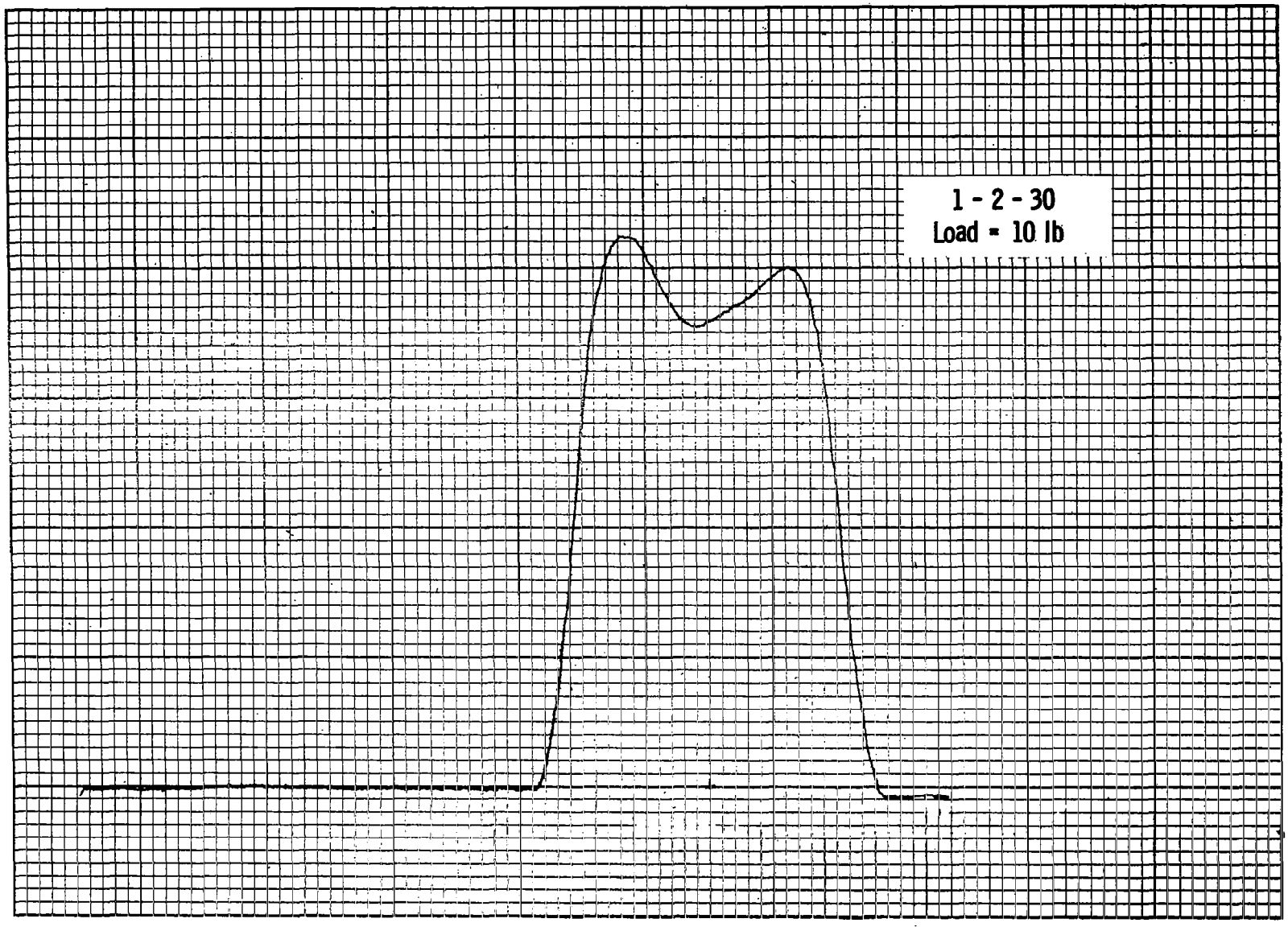
1 - 2 - 30
Load = 10 lb

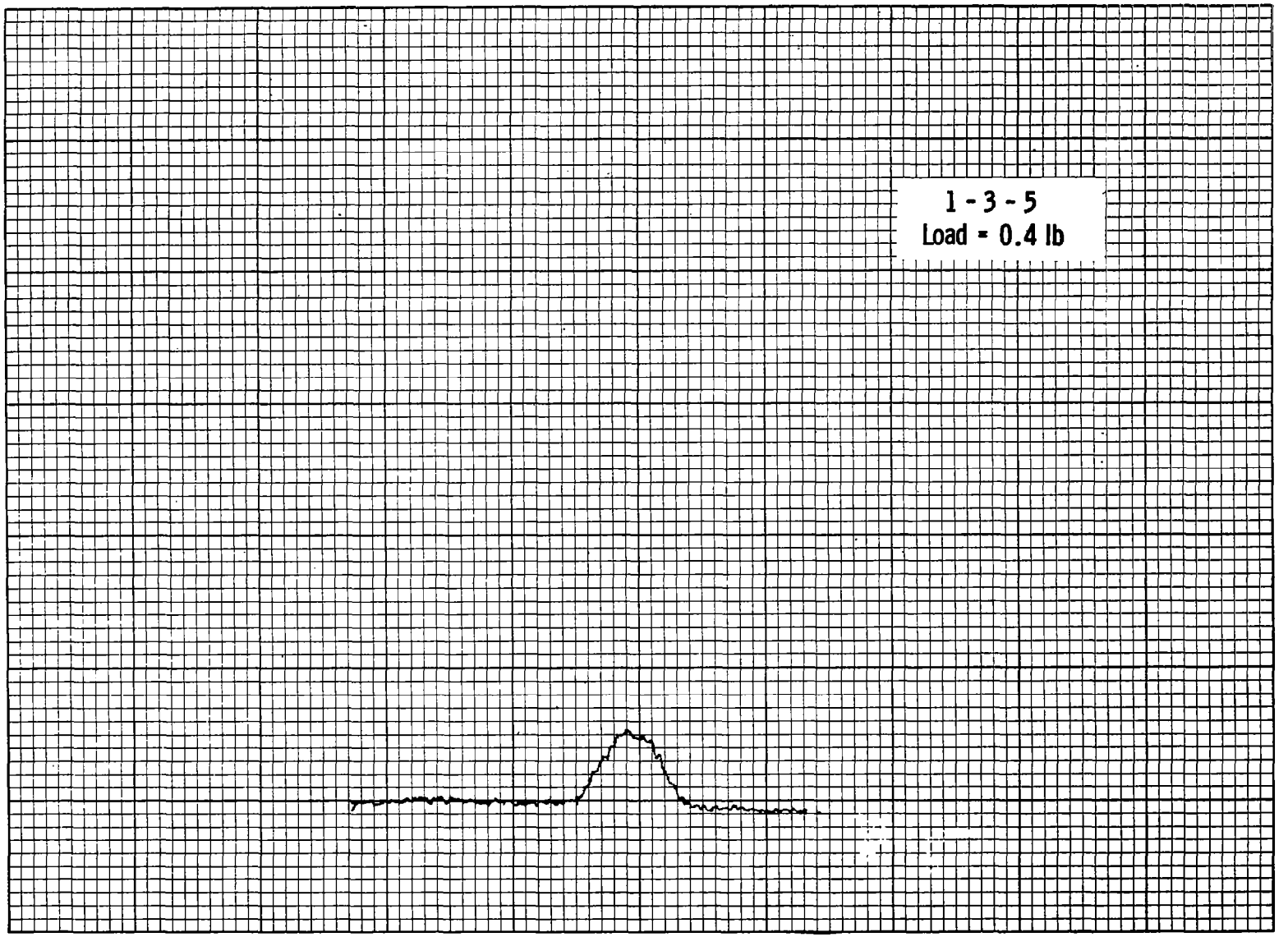
1 - 3 - 5
Load = 0.4 lb

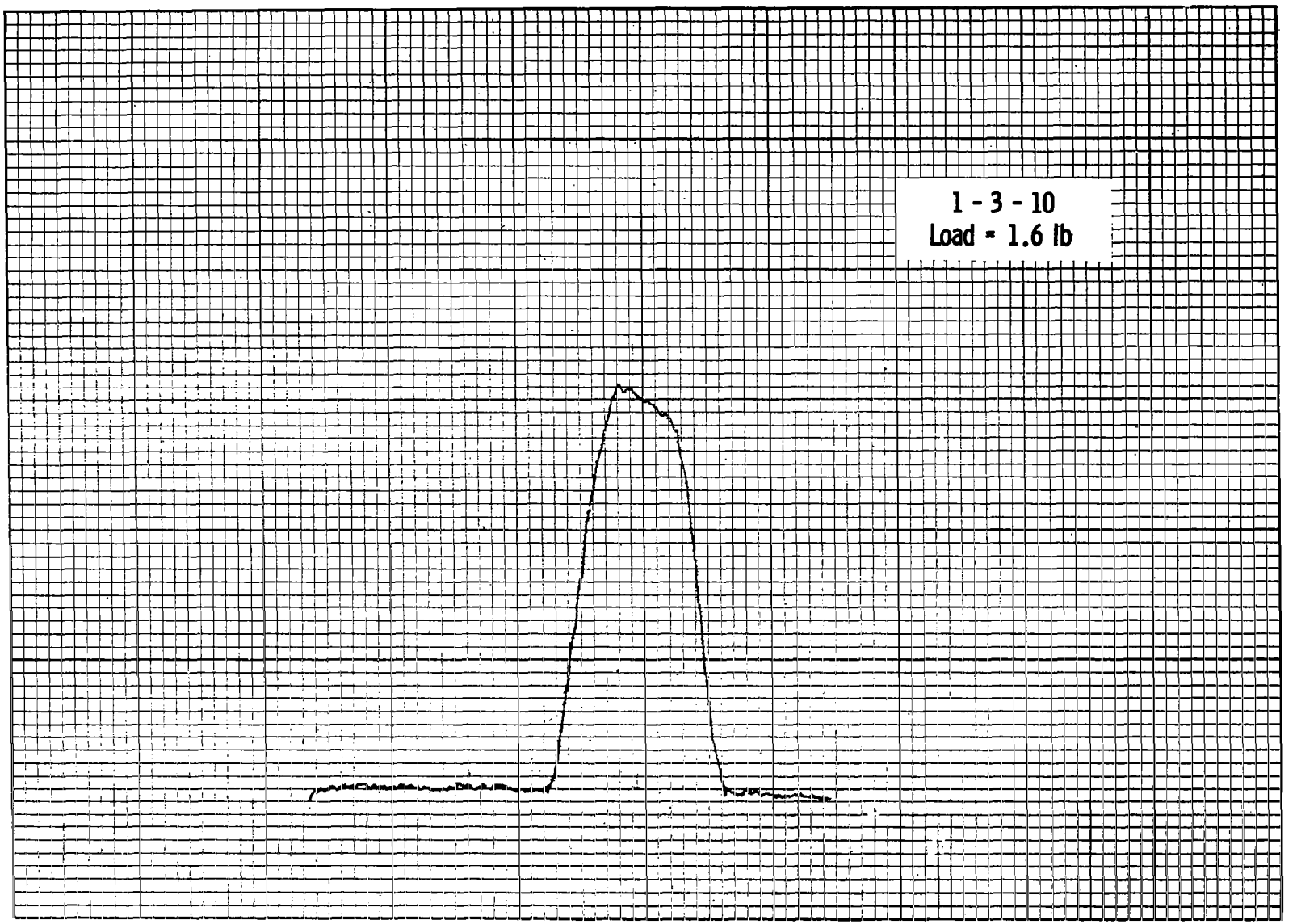
1 - 3 - 10
Load = 1.6 lb

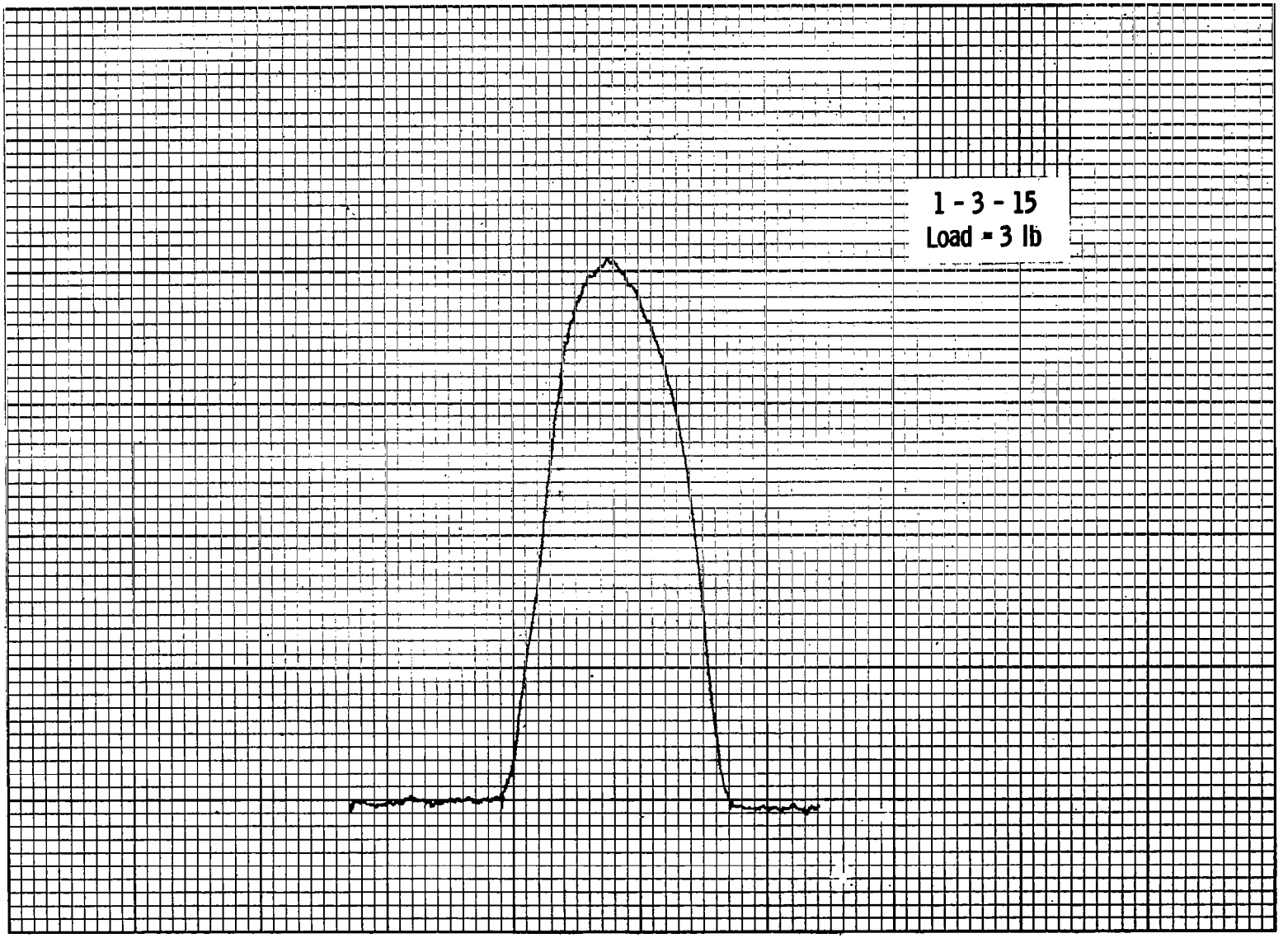
1 - 3 - 15
Load = 3 lb

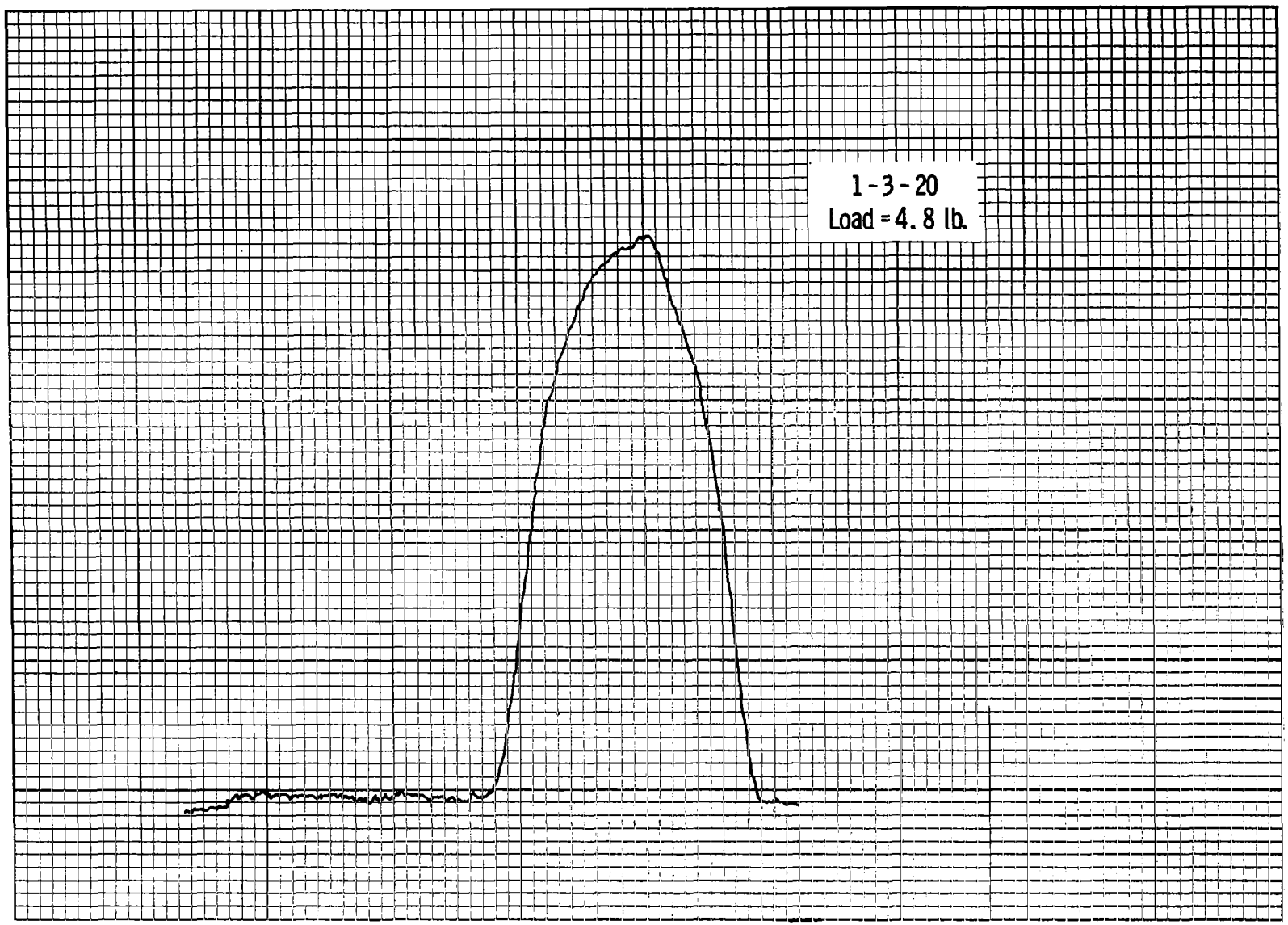
1-3-20
Load = 4.8 lb.

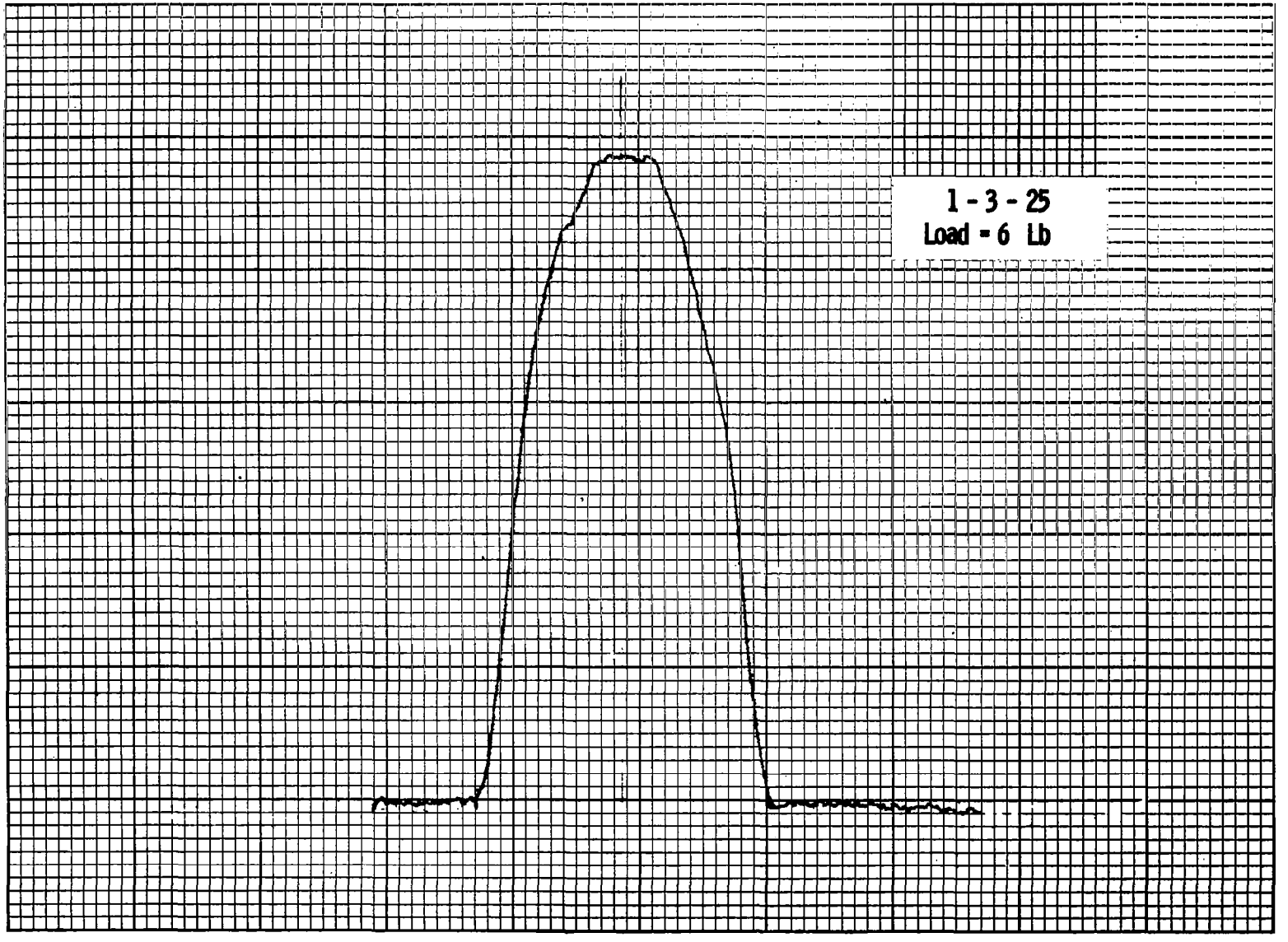
1 - 3 - 25
Load = 6 Lb

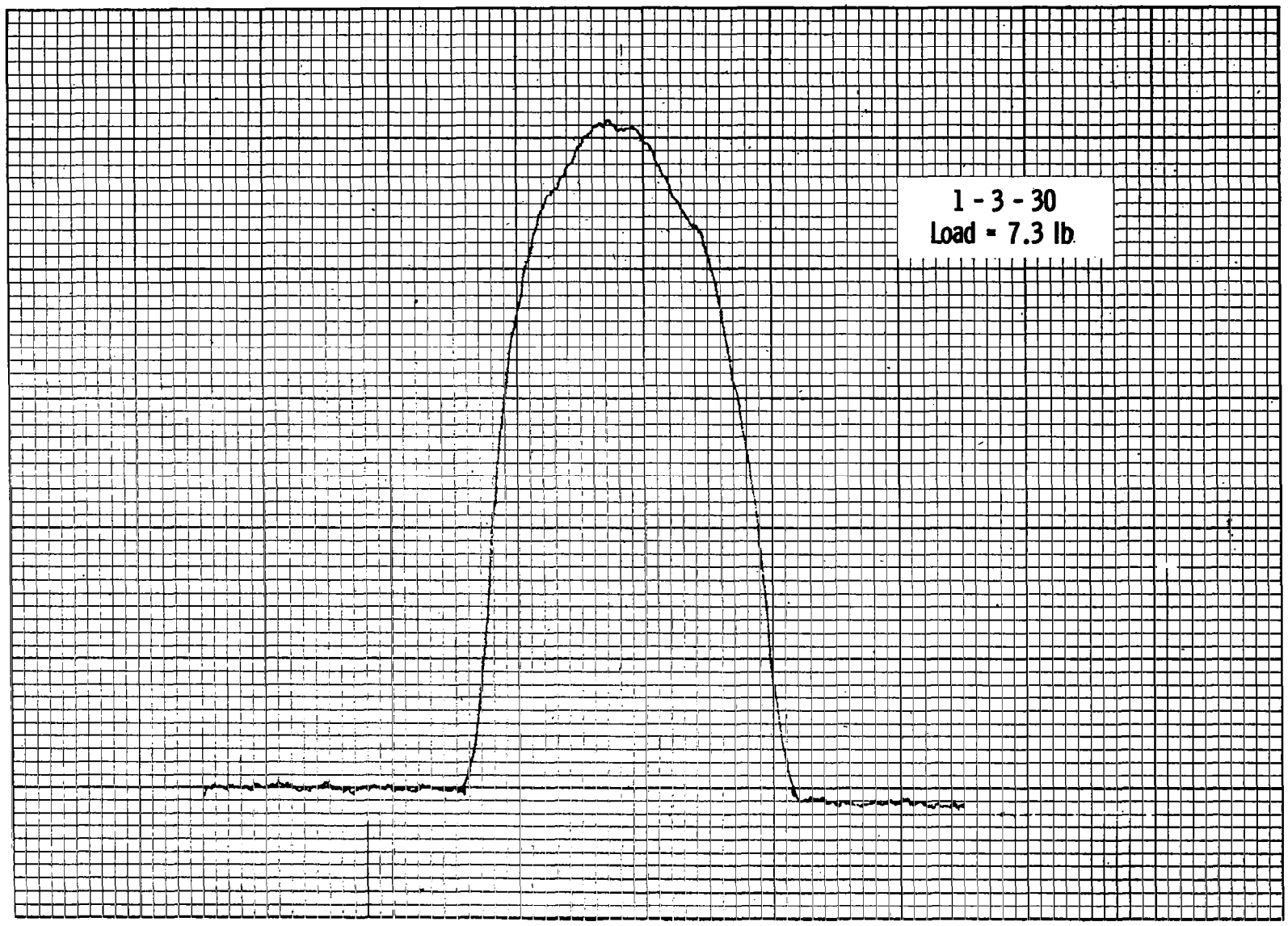
1 - 3 - 30
Load = 7.3 lb

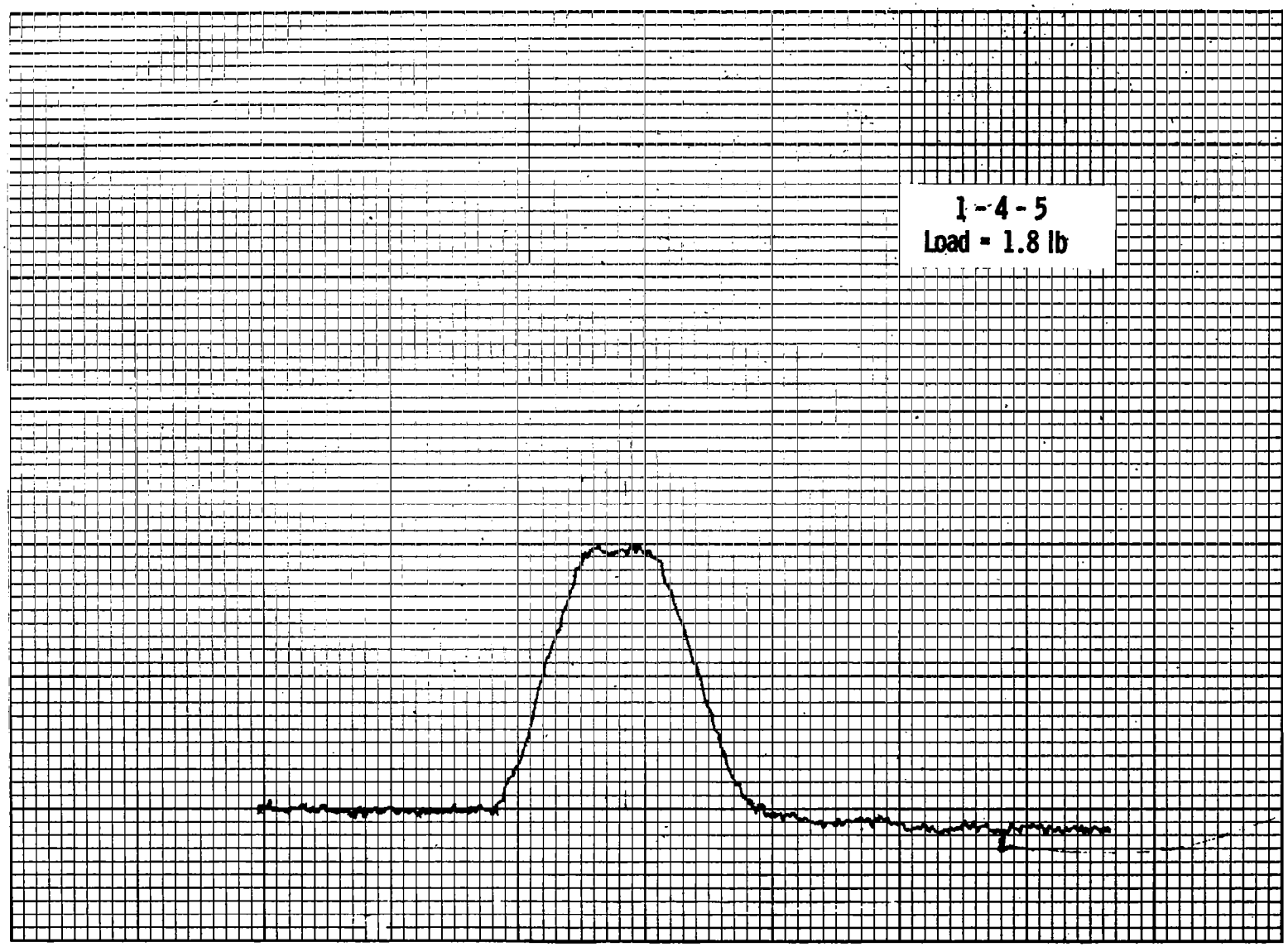
1-4-5
Load = 1.8 lb

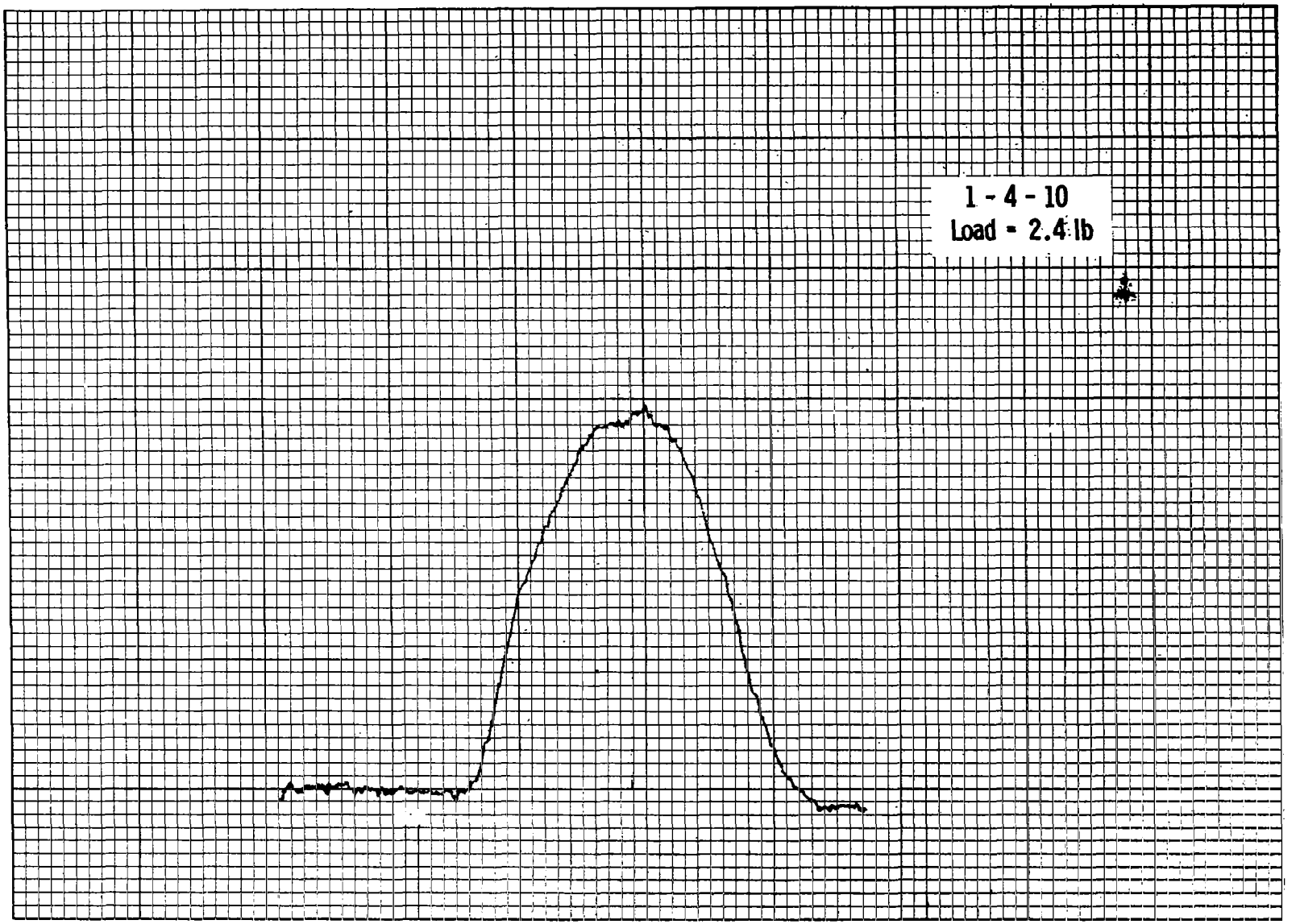
1 - 4 - 10
Load = 2.4 lb

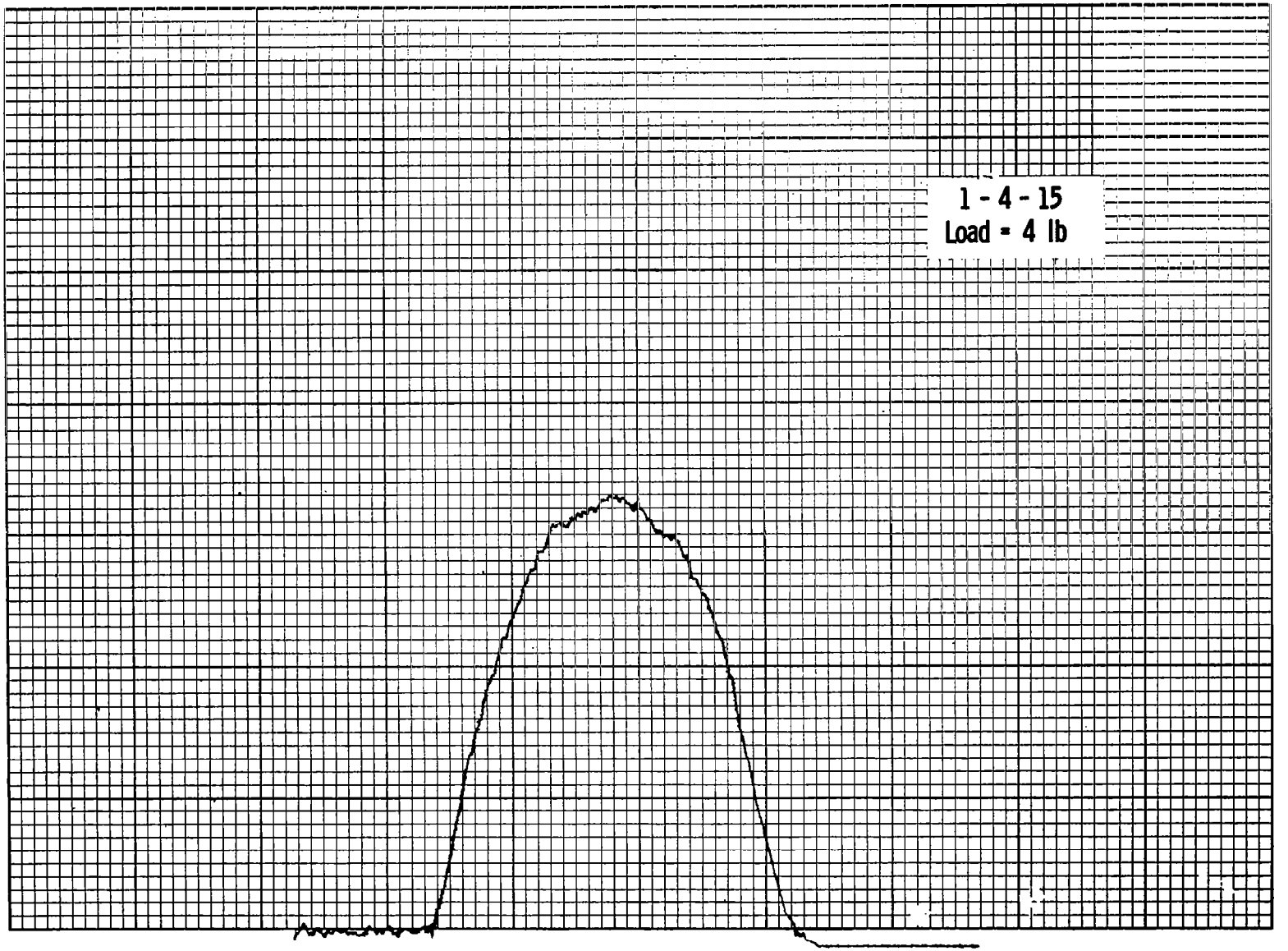
1 - 4 - 15
Load = 4 lb

1 - 4 - 20
Load = 5 lb

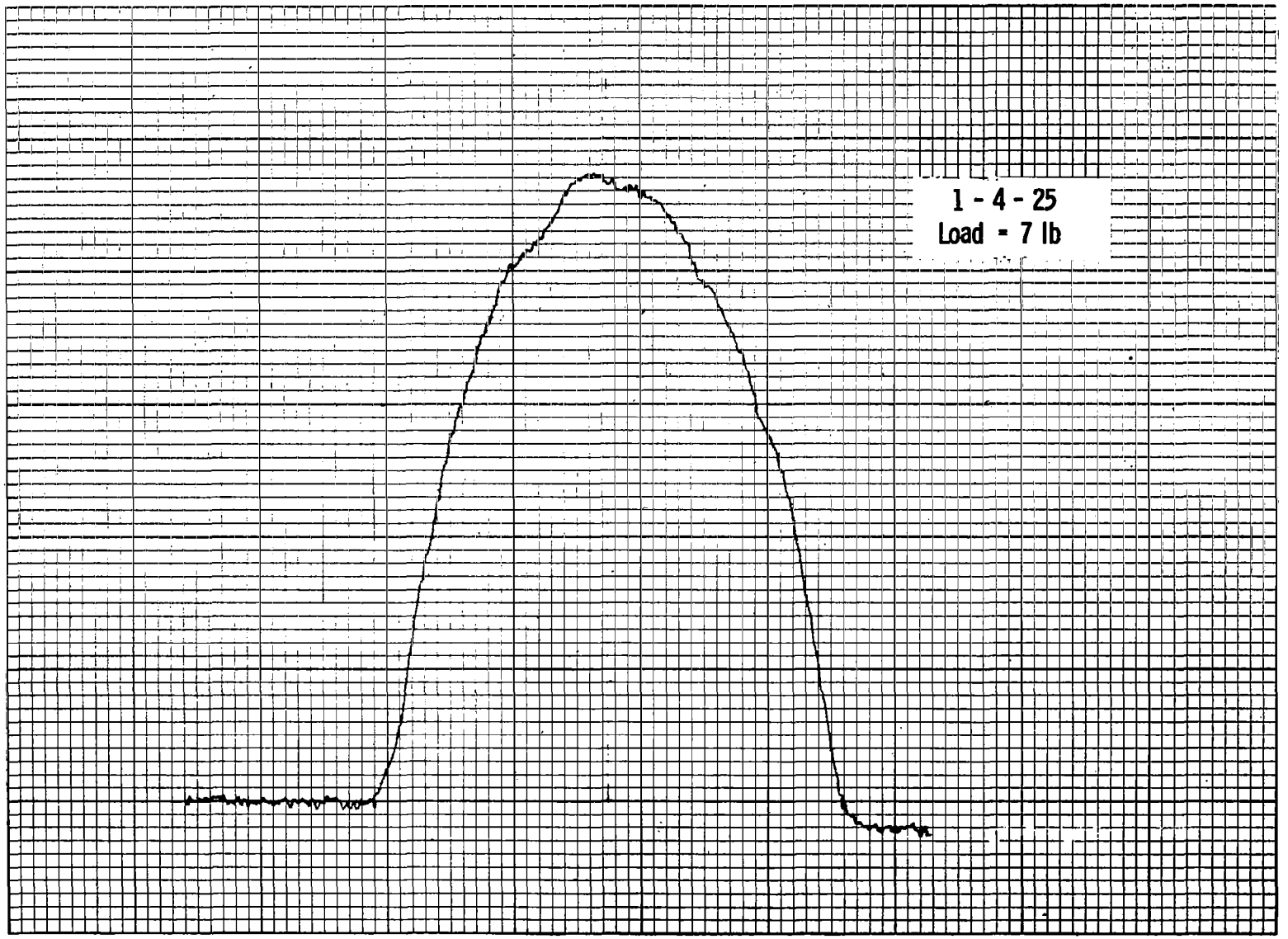
1 - 4 - 25
Load = 7 lb

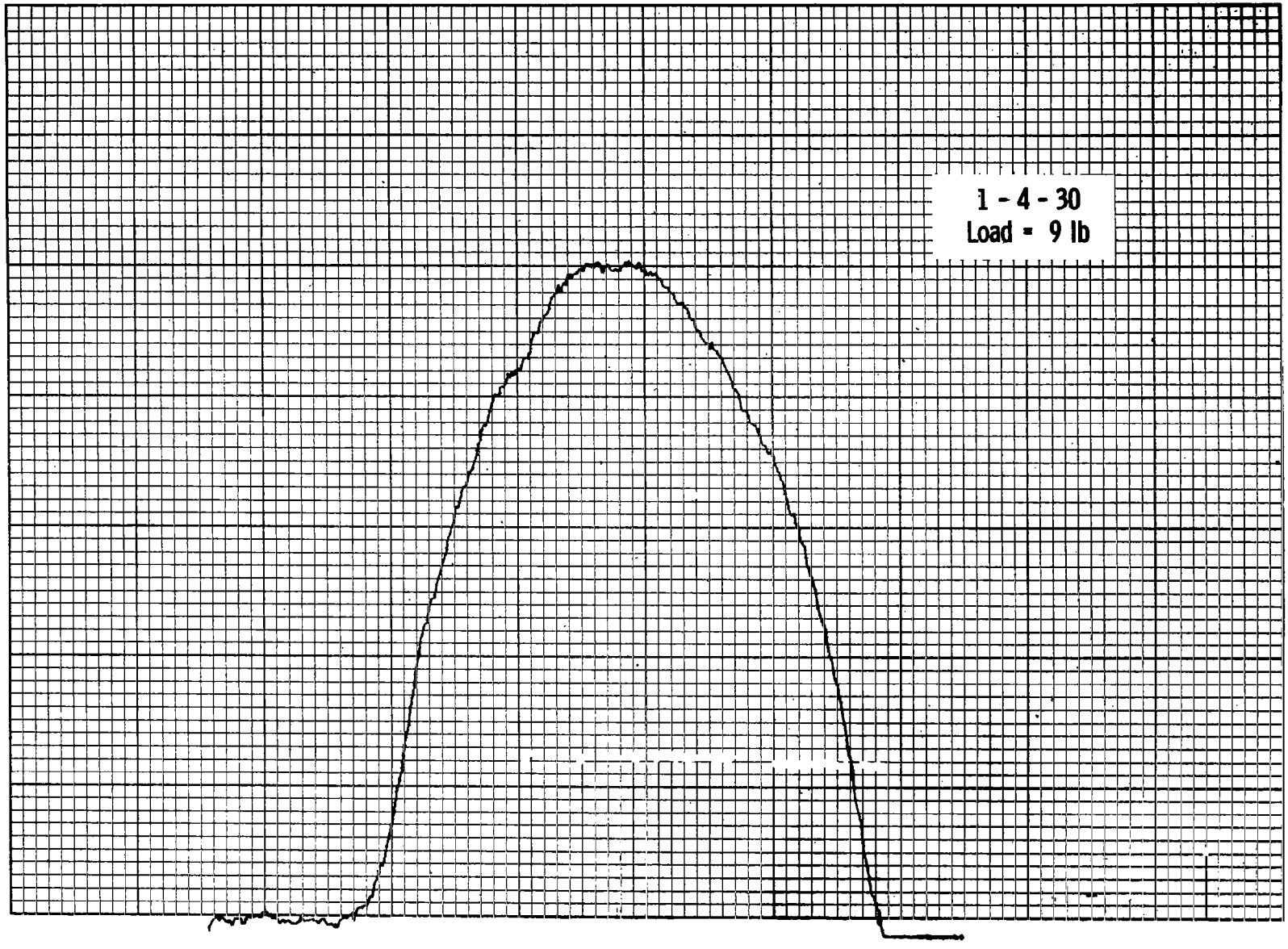
1 - 4 - 30
Load = 9 lb


4 - 1 - 5
Load = 8 lb

4 - 1 - 10
Load = 19 lb


4 - 1 - 15
Load = 36 lb

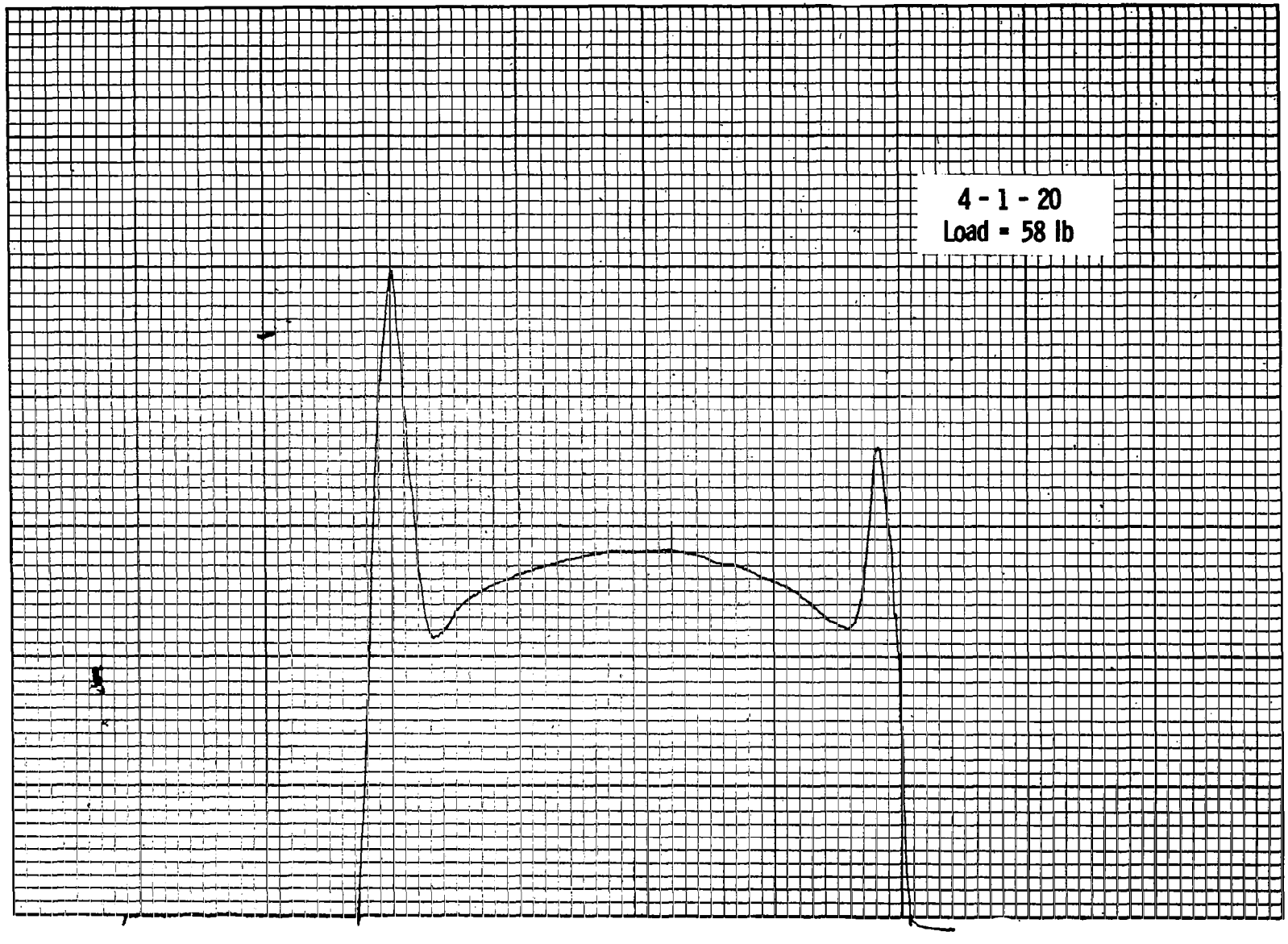
4 - 1 - 20
Load = 58 lb

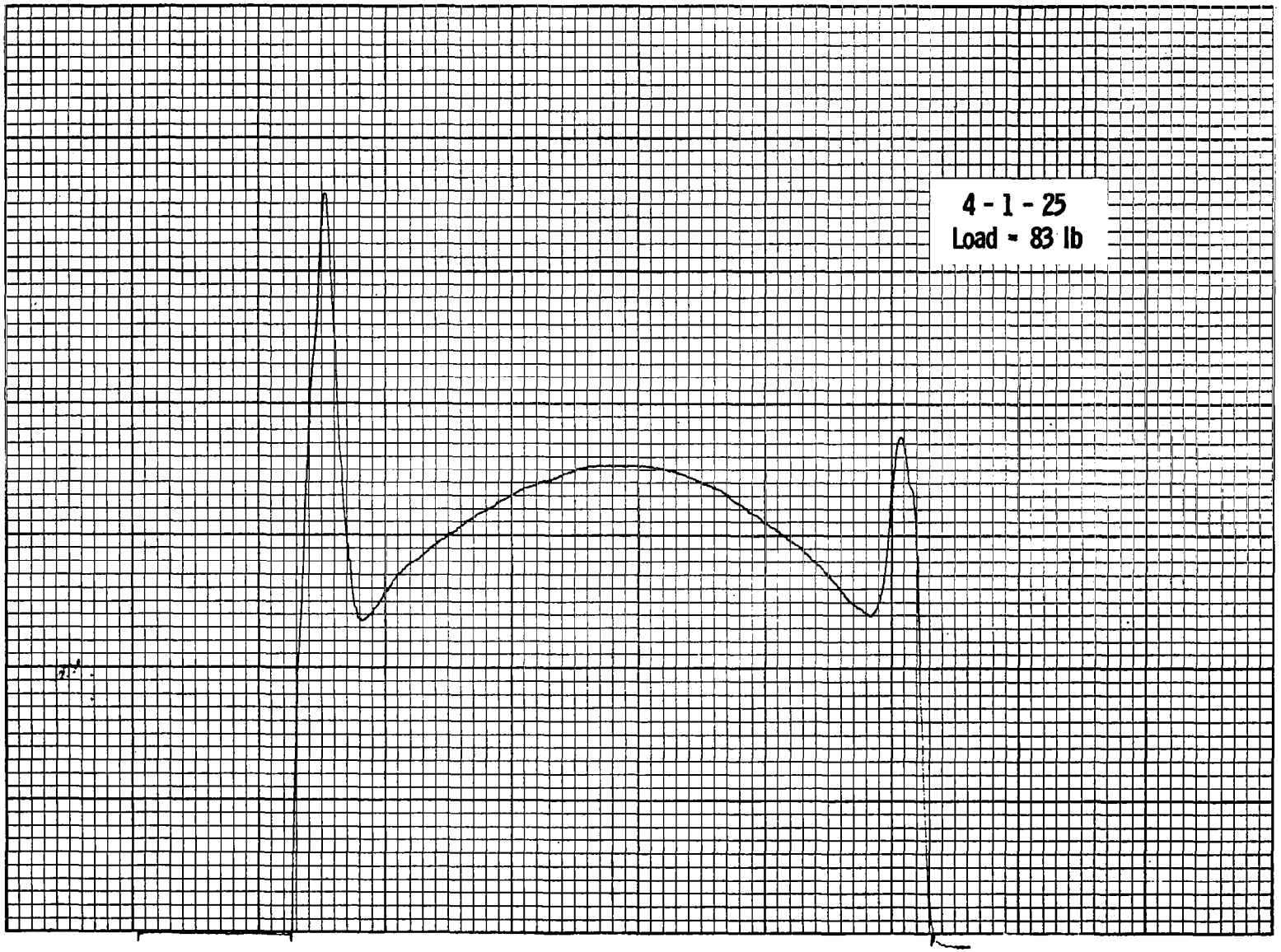
4 - 1 - 25
Load = 83 lb

4 - 1 - 30
Load = 122 lb

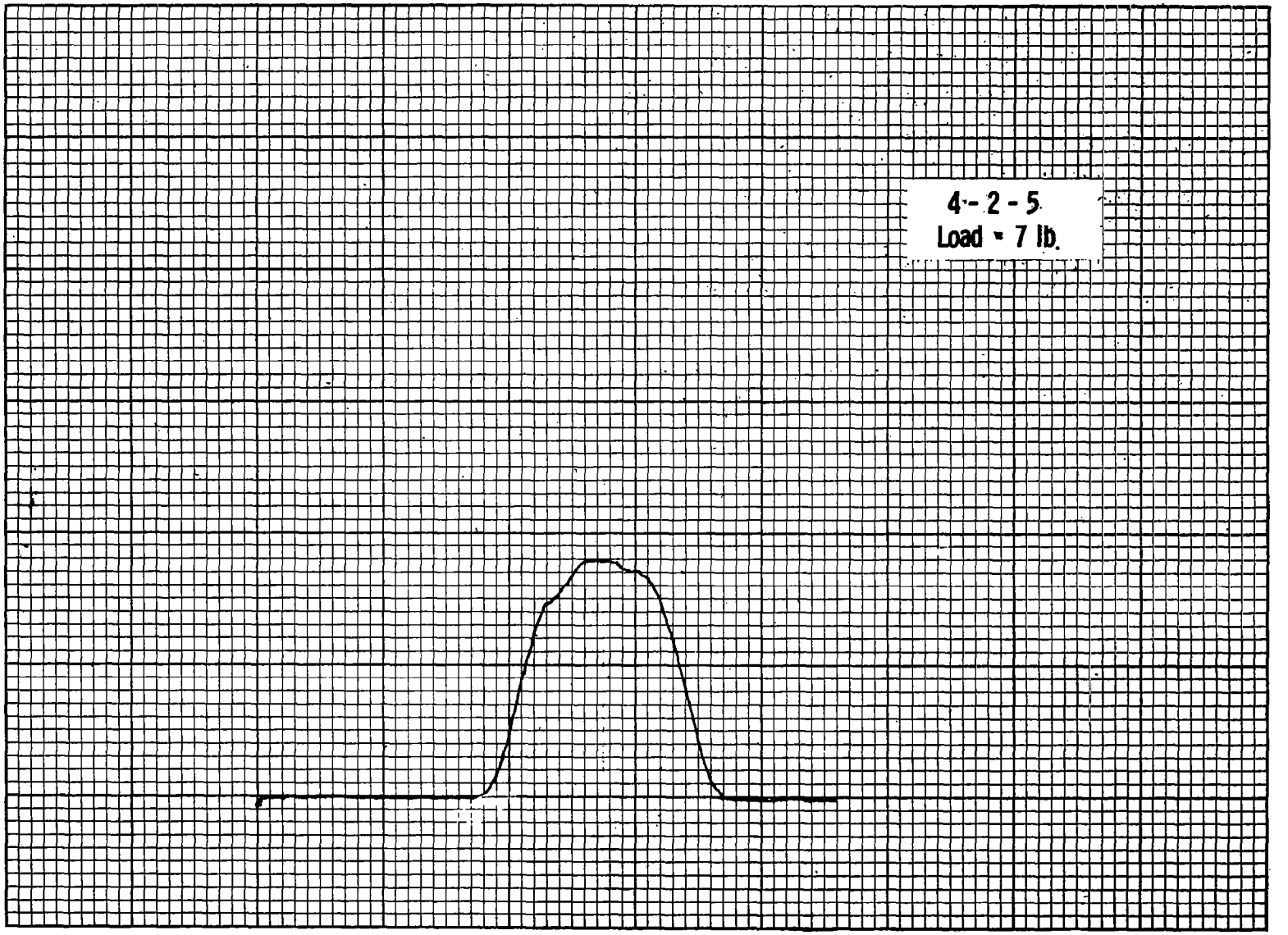
4 - 2 - 5
Load = 7 lb.

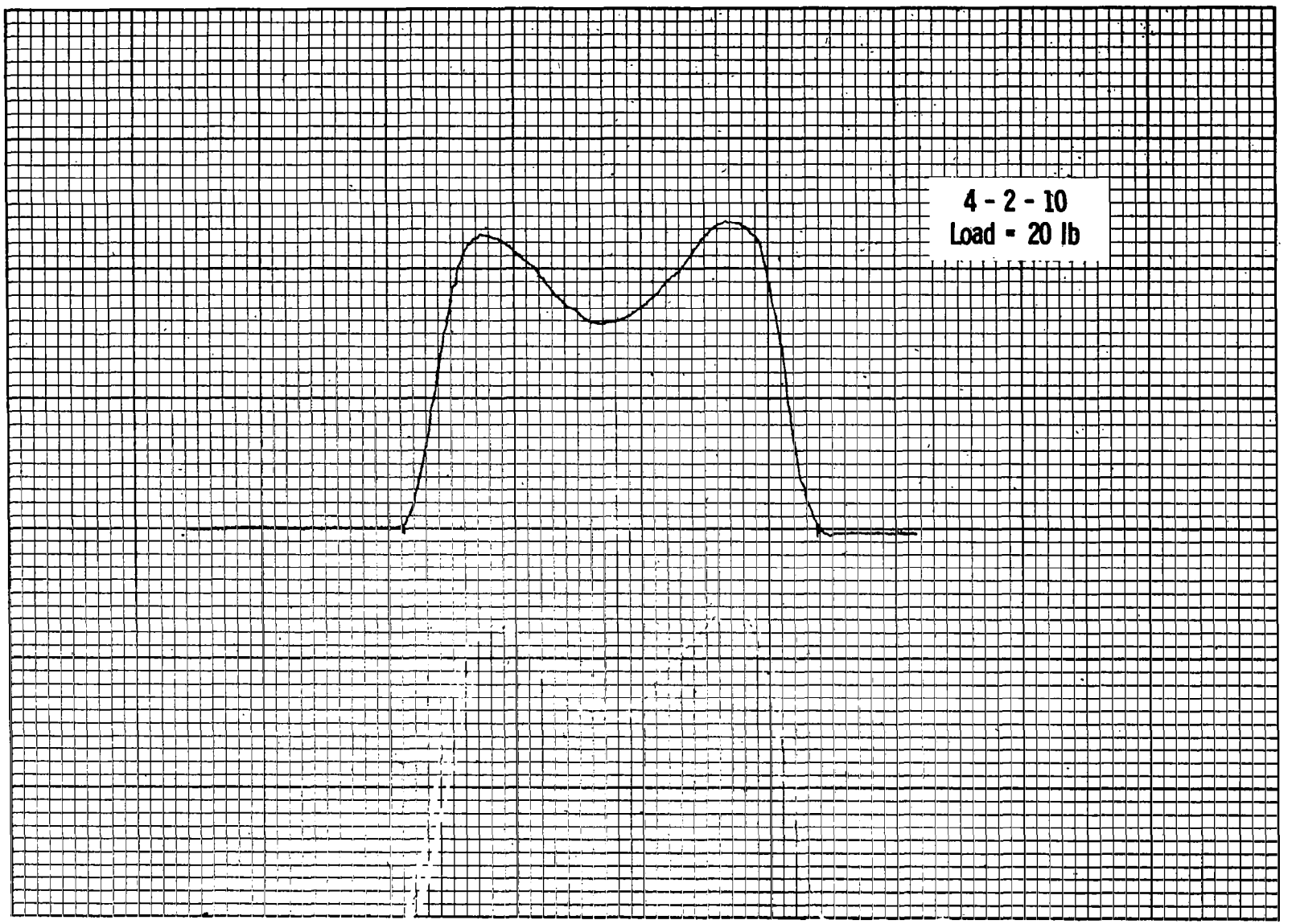
4 - 2 - 10
Load = 20 lb

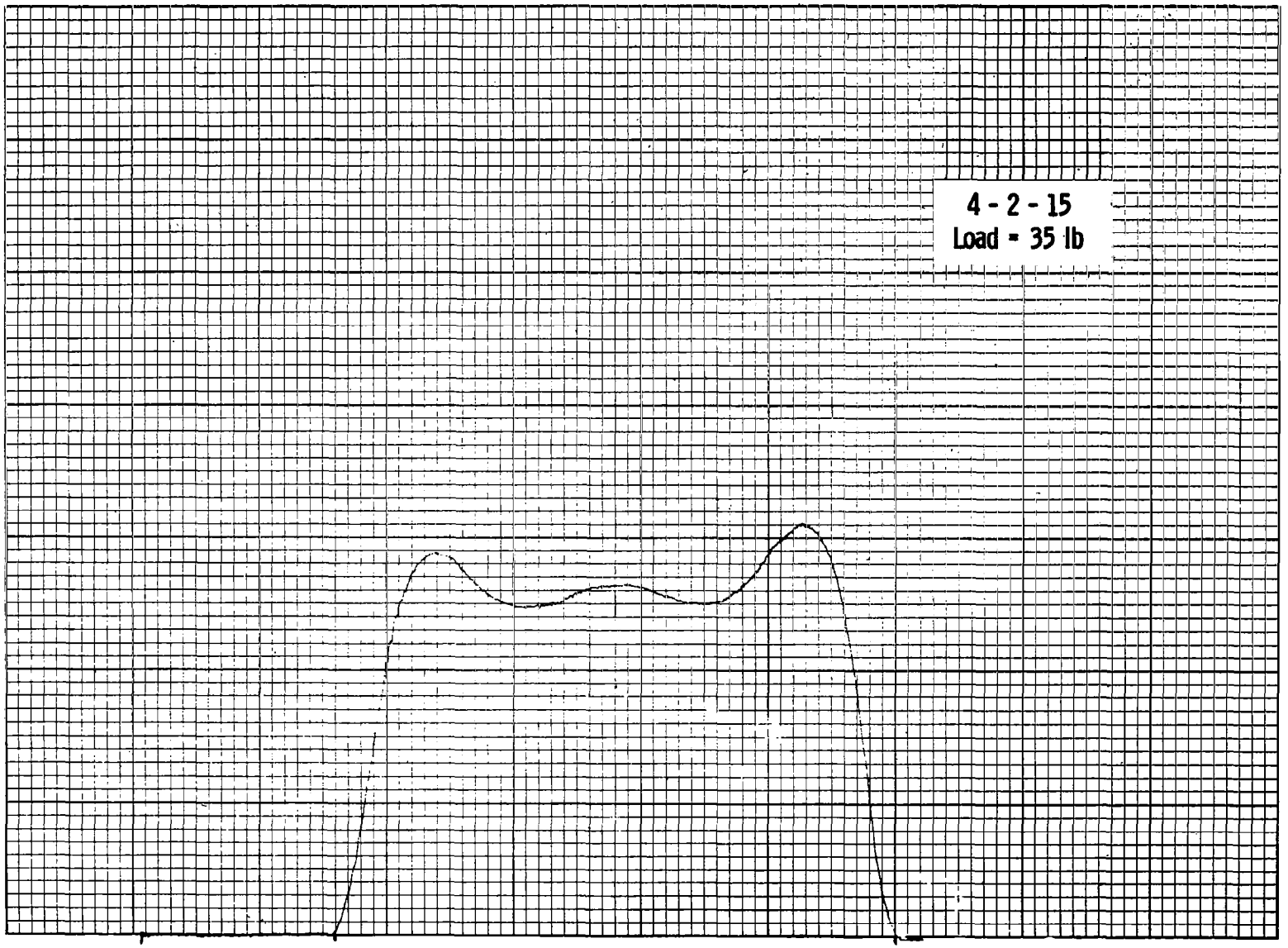
4 - 2 - 15
Load = 35 lb

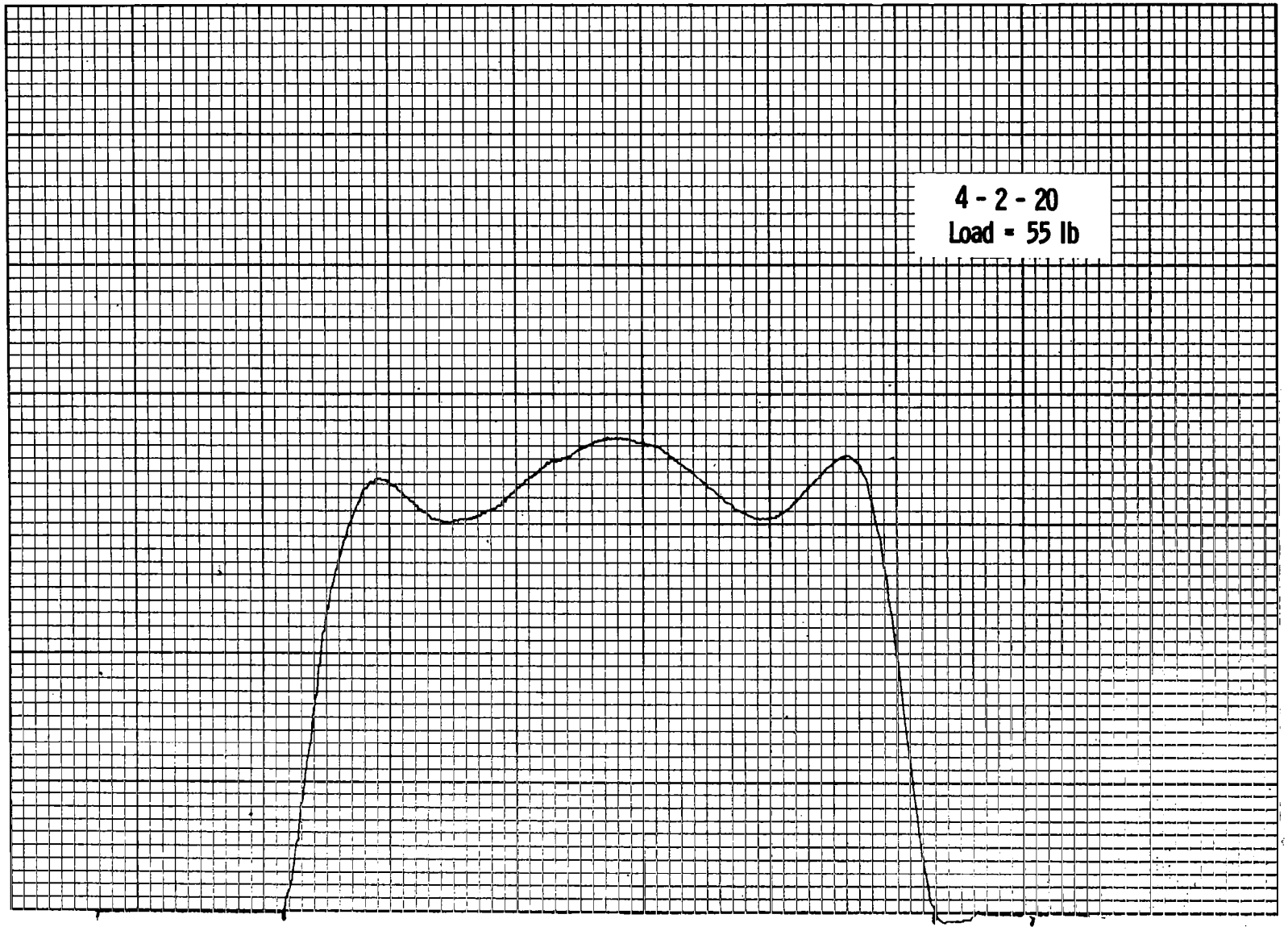
4 - 2 - 20
Load = 55 lb

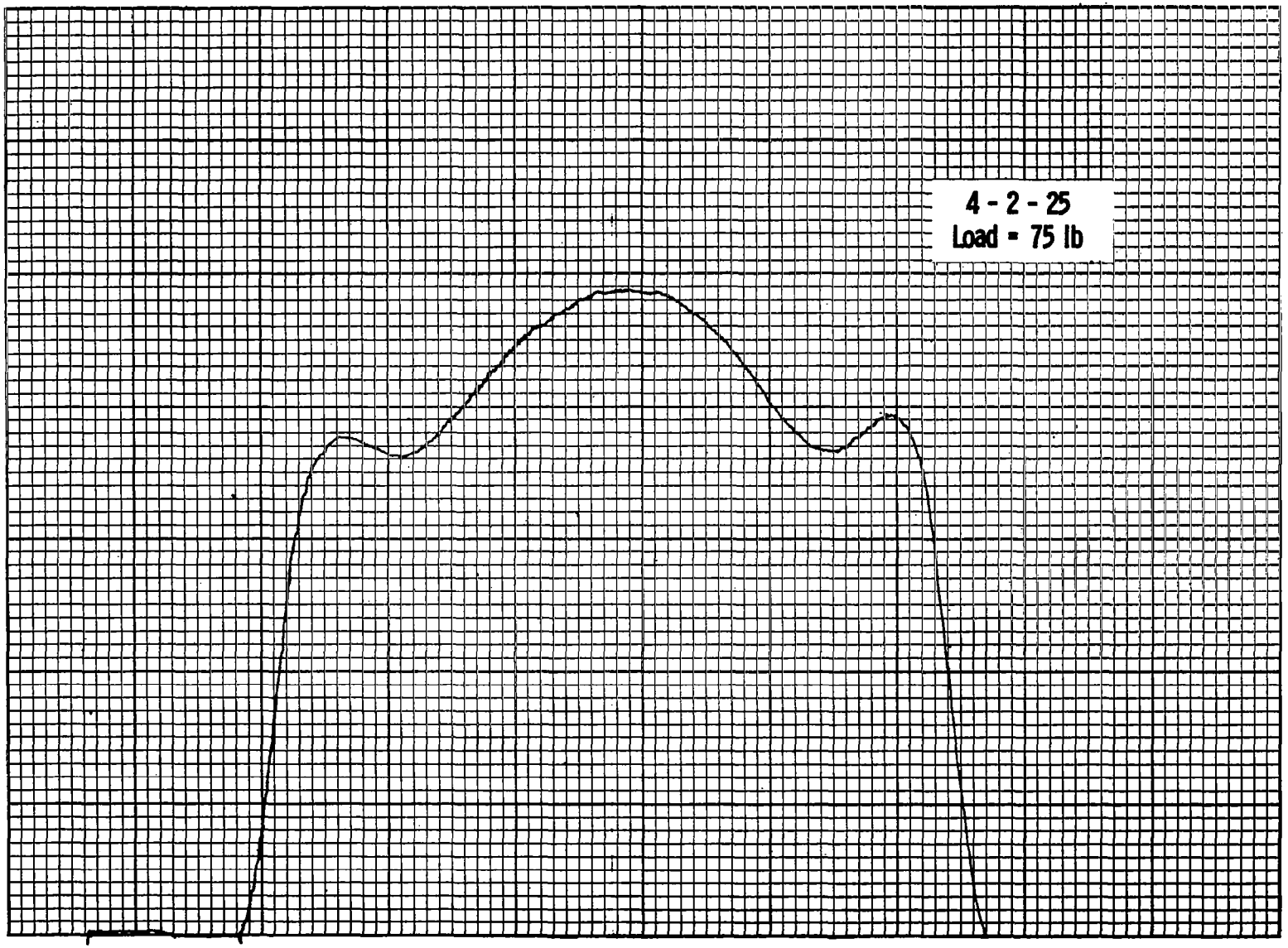
4 - 2 - 25
Load = 75 lb

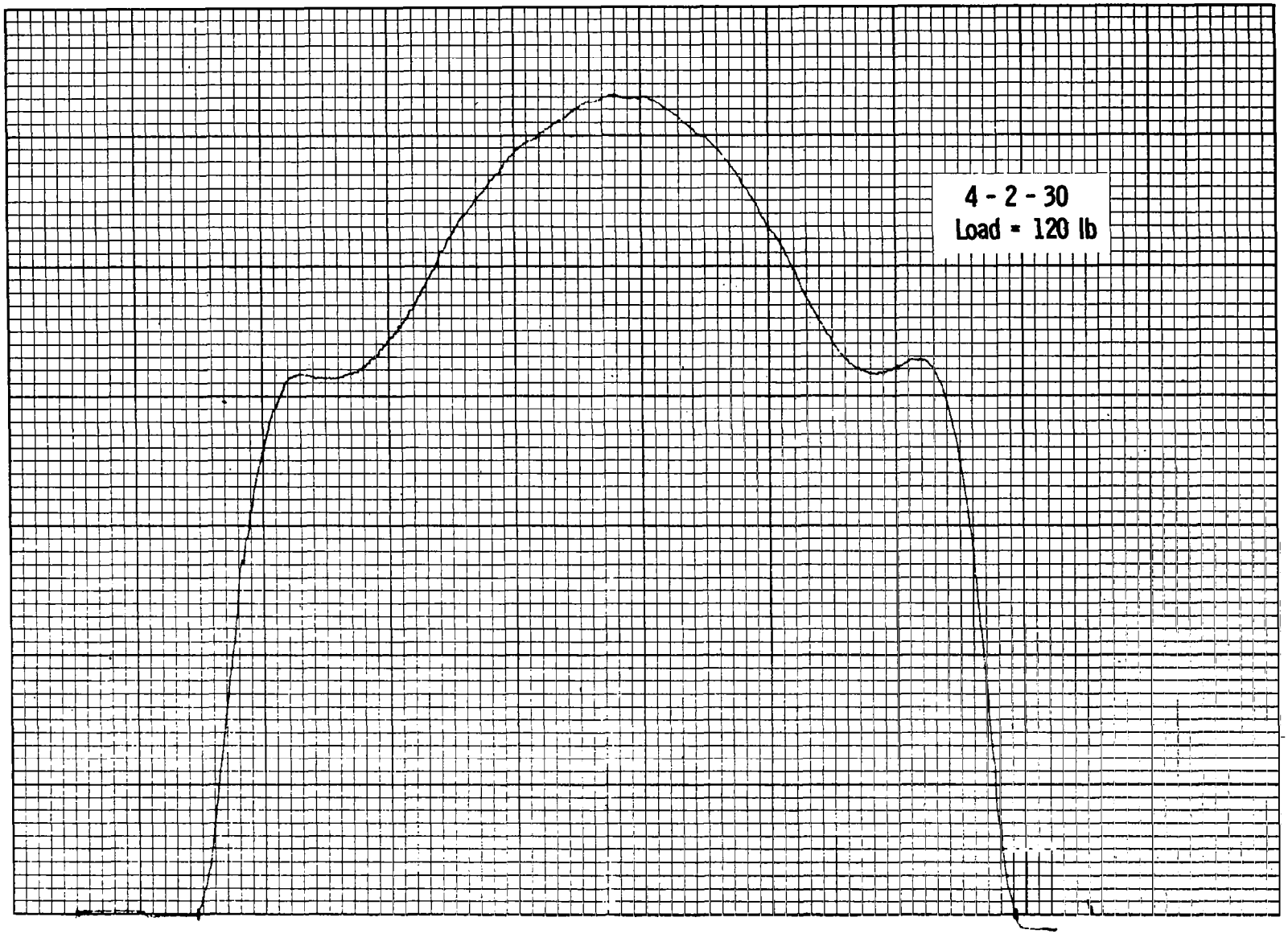
4 - 2 - 30
Load = 120 lb

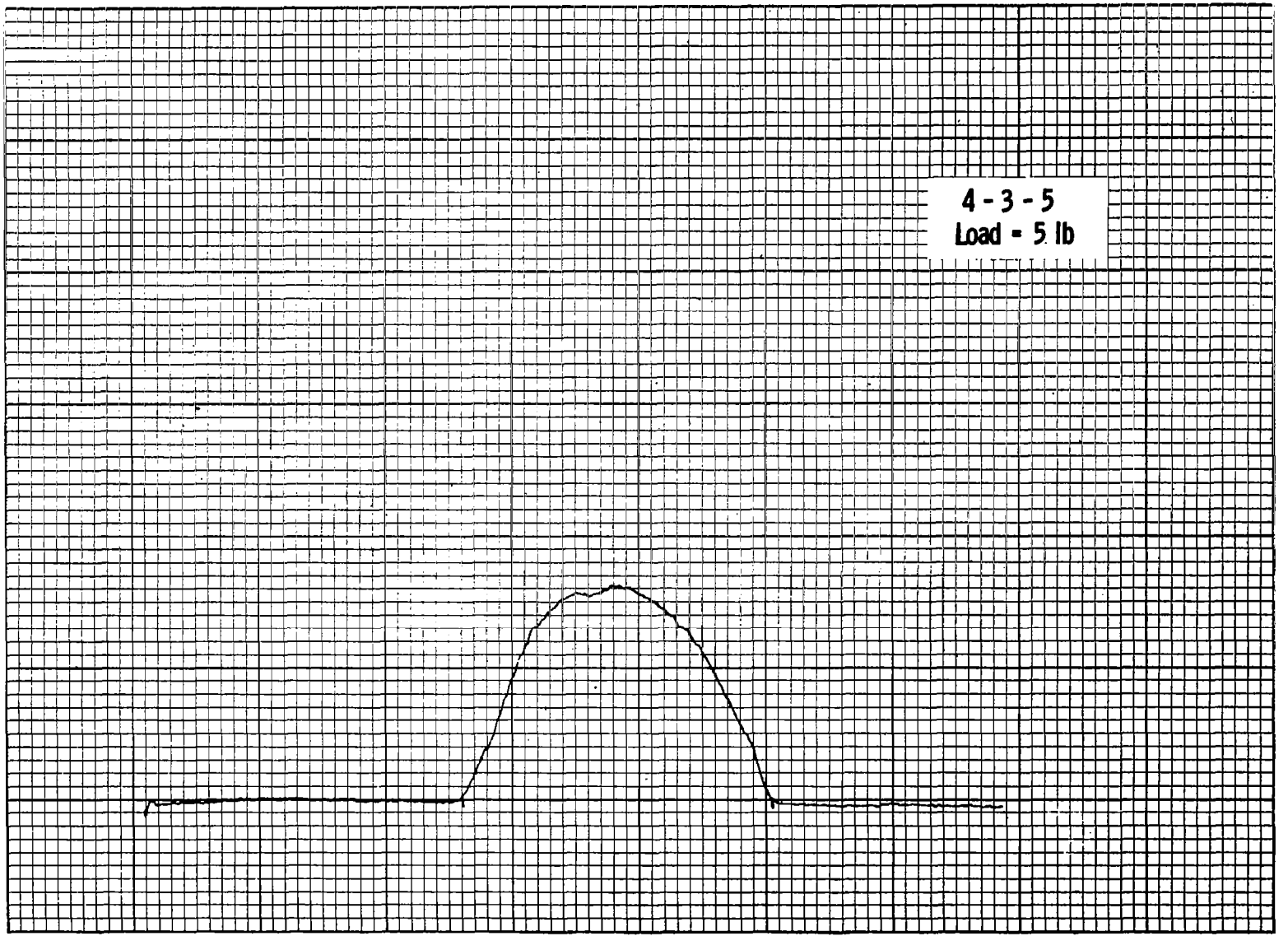
4 - 3 - 5
Load = 5 lb

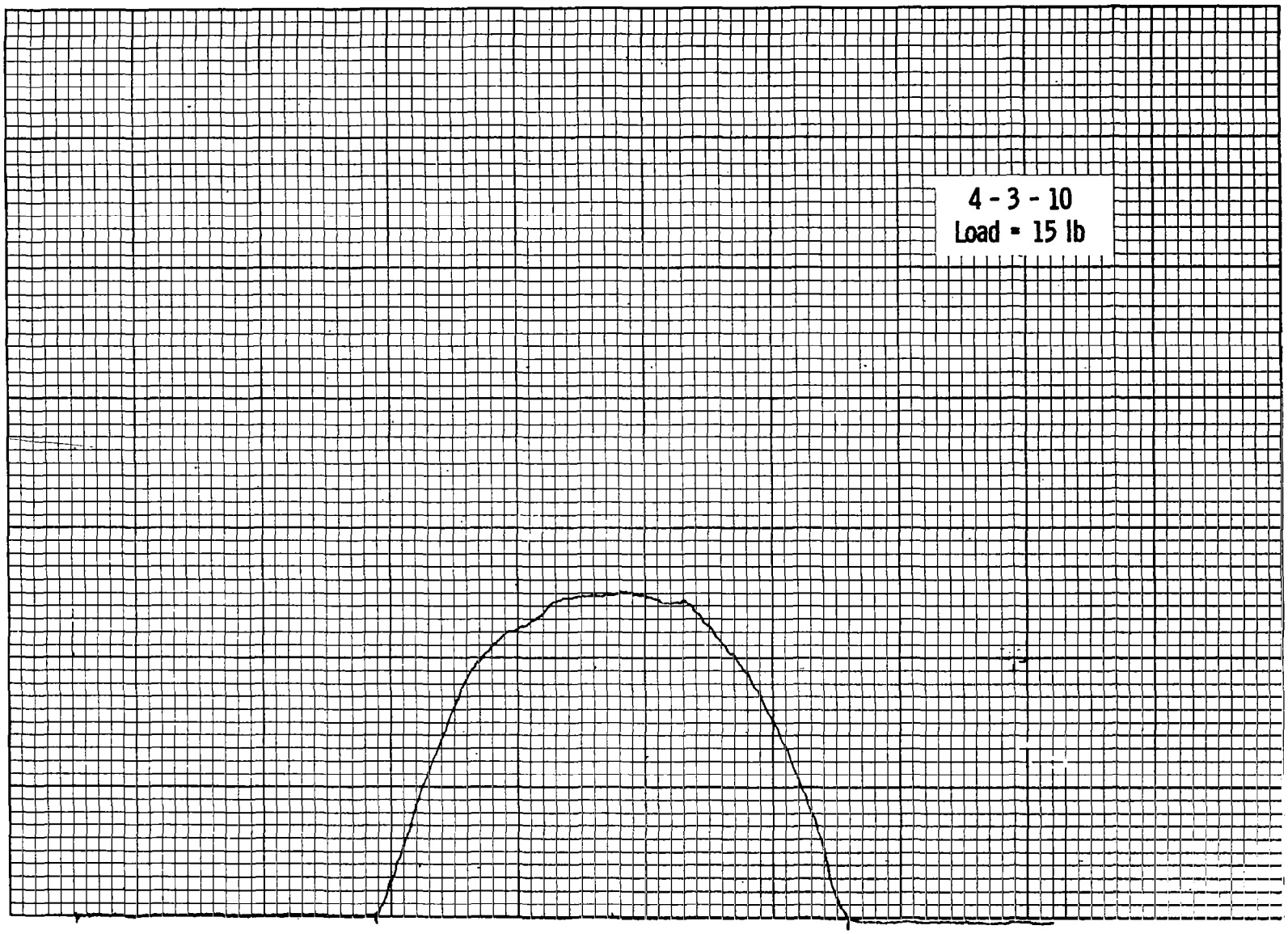
4 - 3 - 10
Load = 15 lb

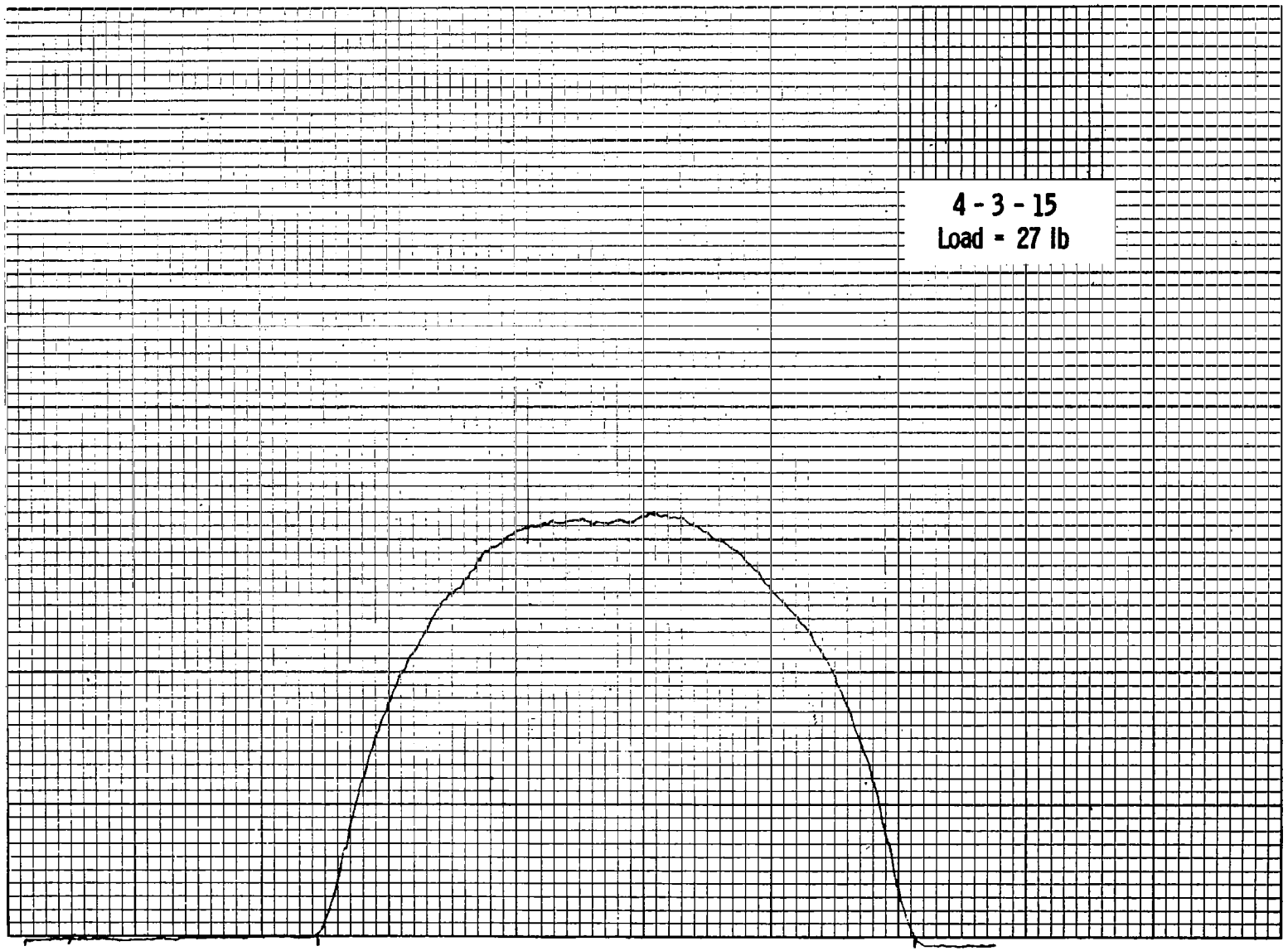
4 - 3 - 15
Load = 27 lb

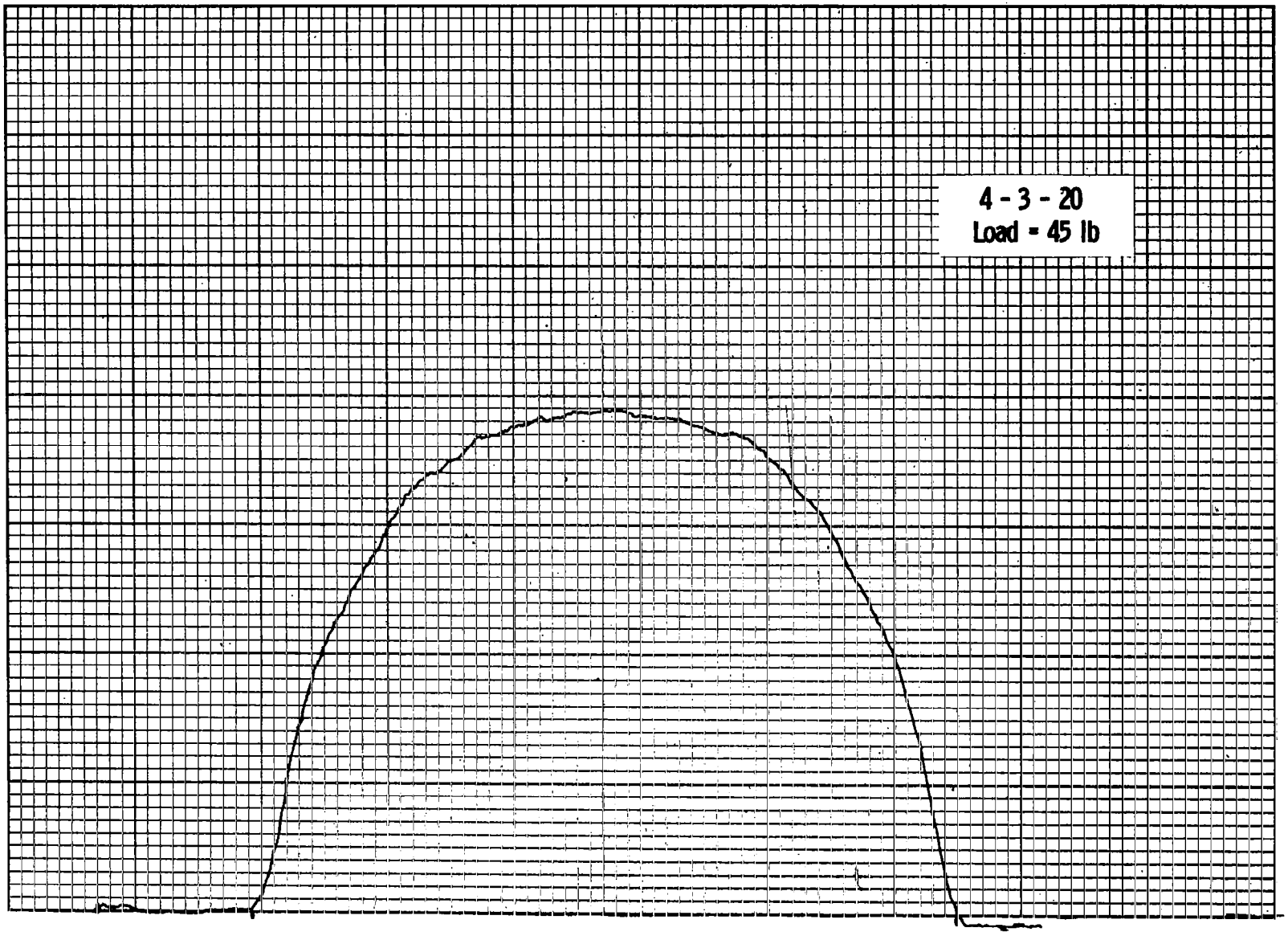
4 - 3 - 20
Load = 45 lb

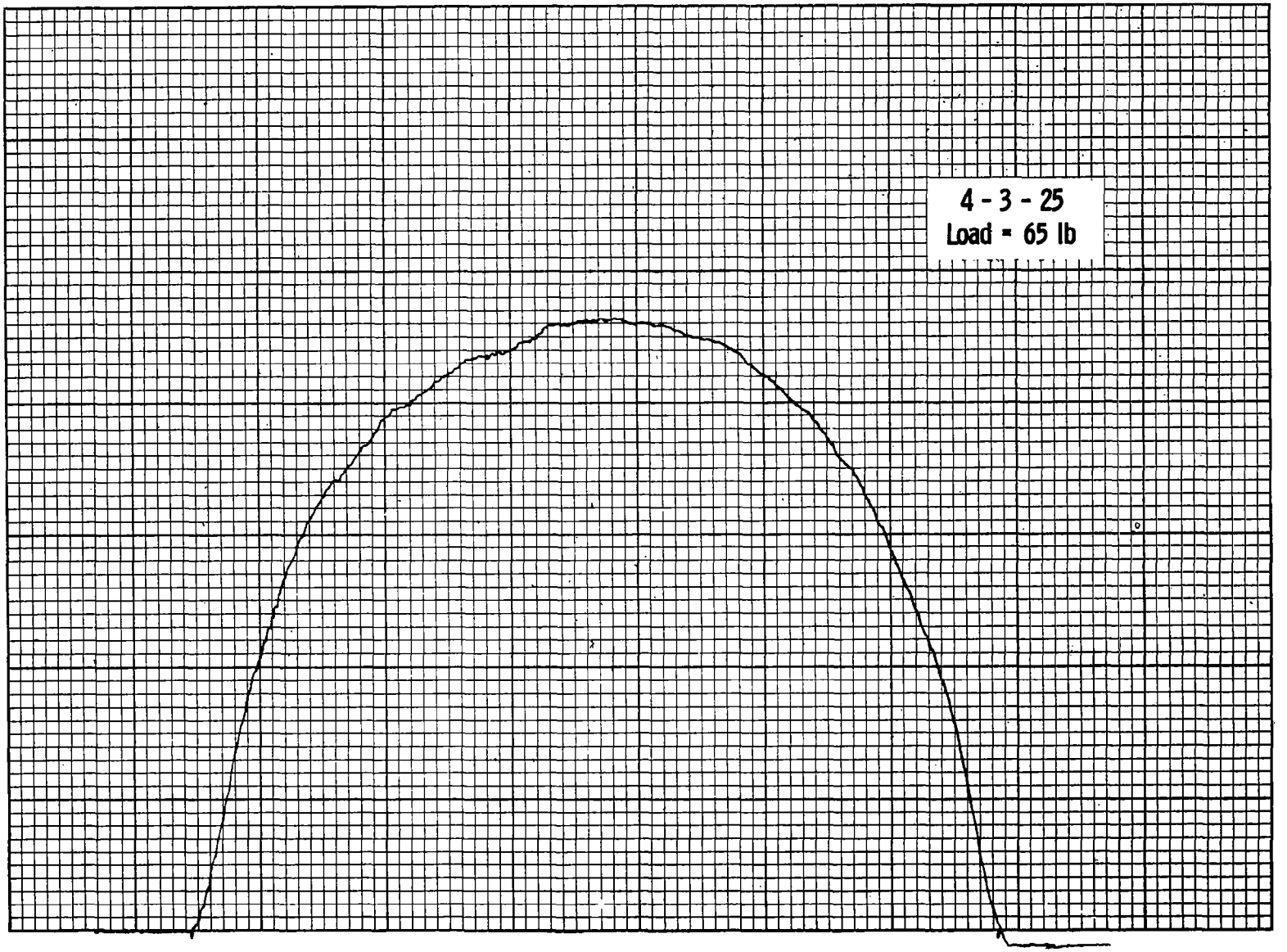
4 - 3 - 25
Load = 65 lb

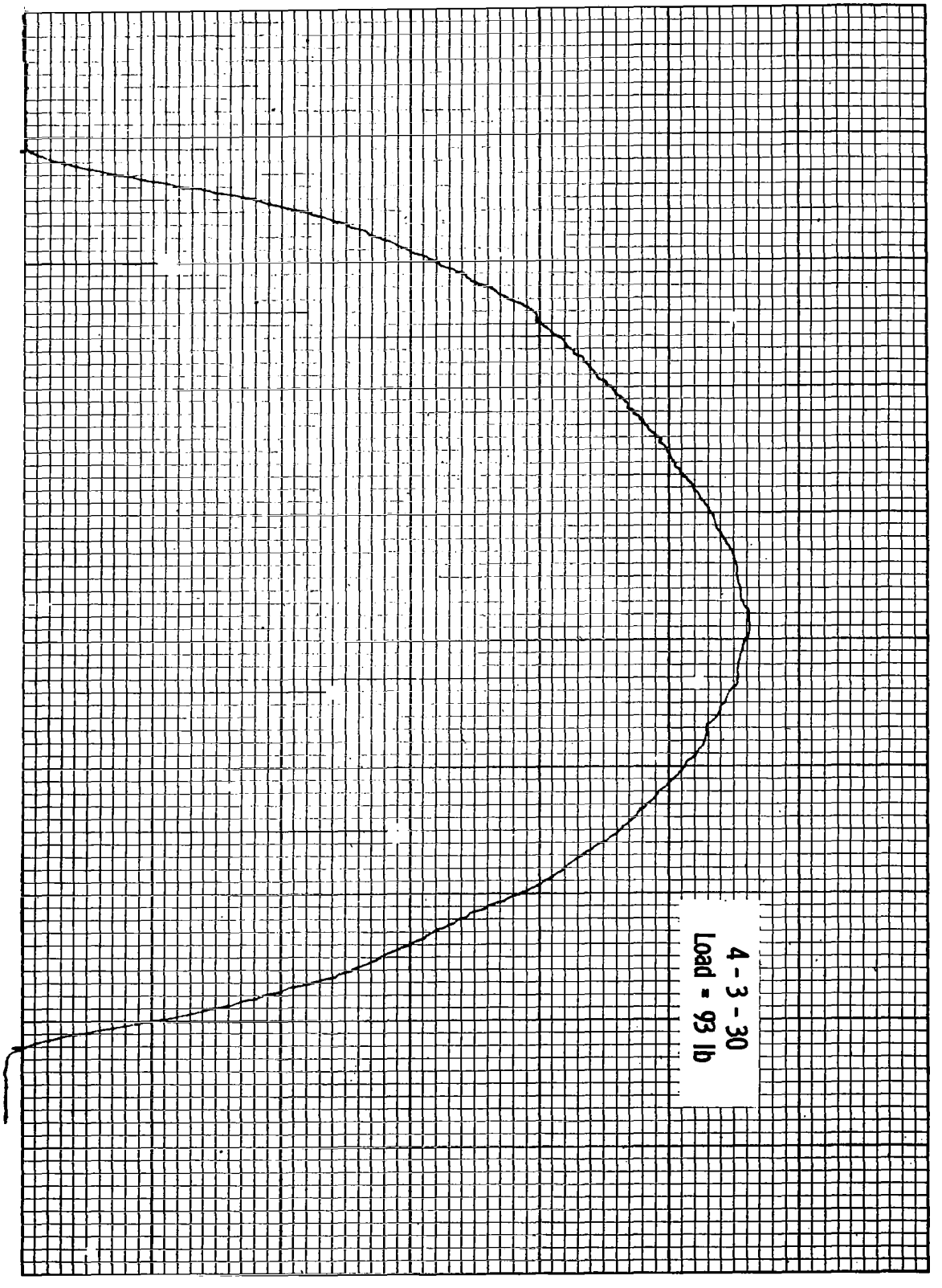
4 - 3 - 30
Load = 93 lb

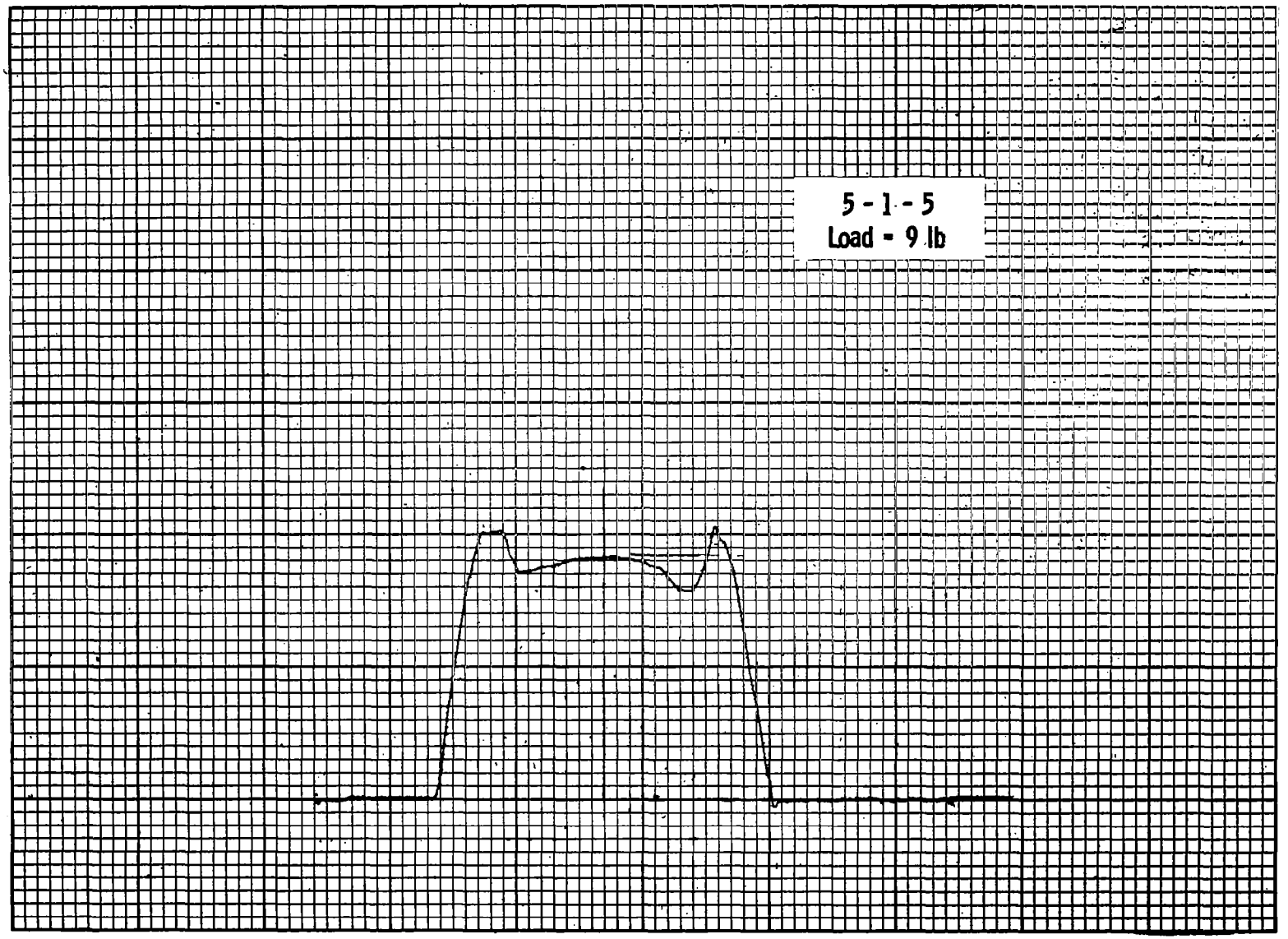
5 - 1 - 5
Load = 9 lb

5 - 1 - 10
Load = 25 lb

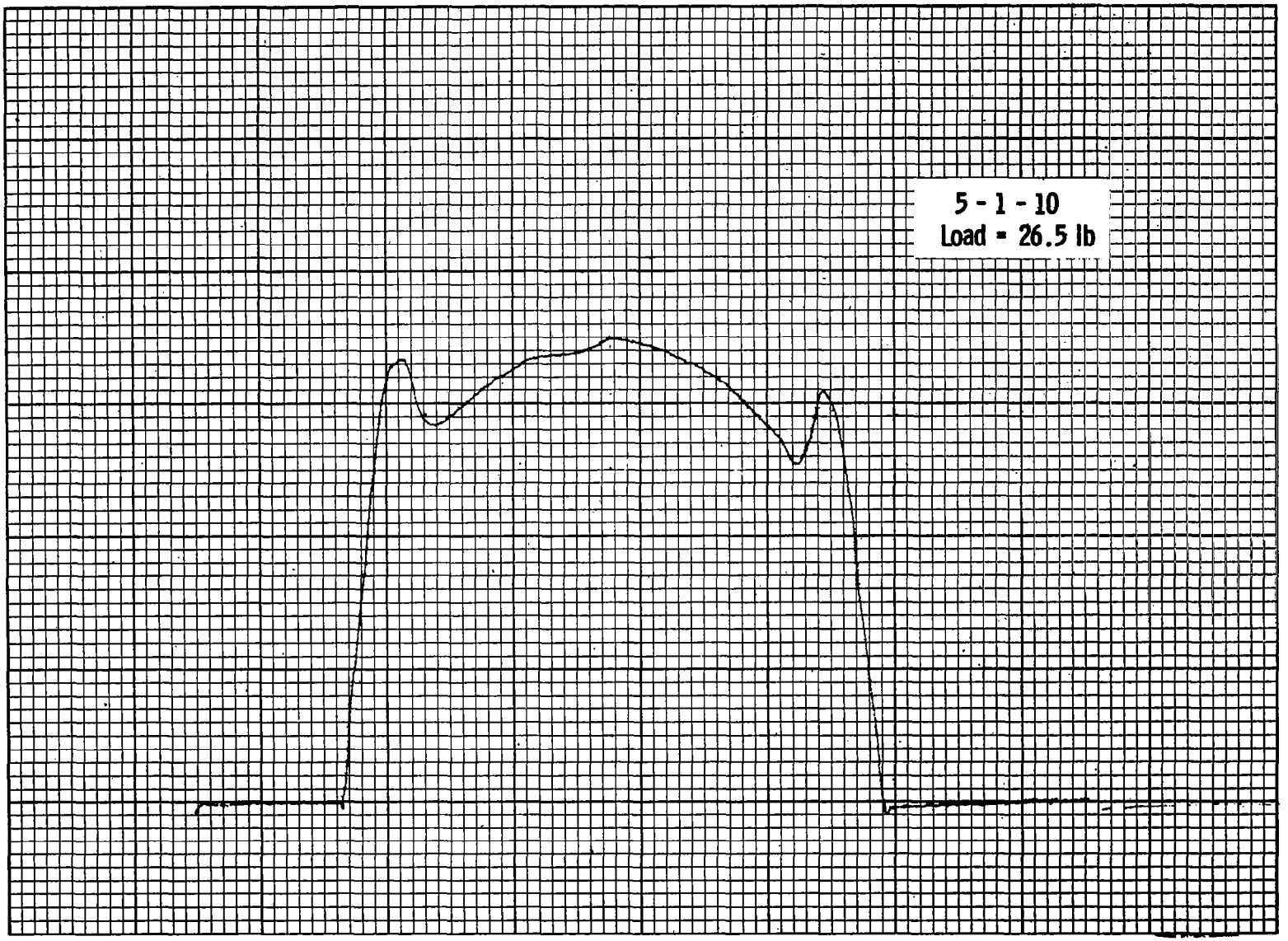
5 - 1 - 10
Load = 26.5 lb

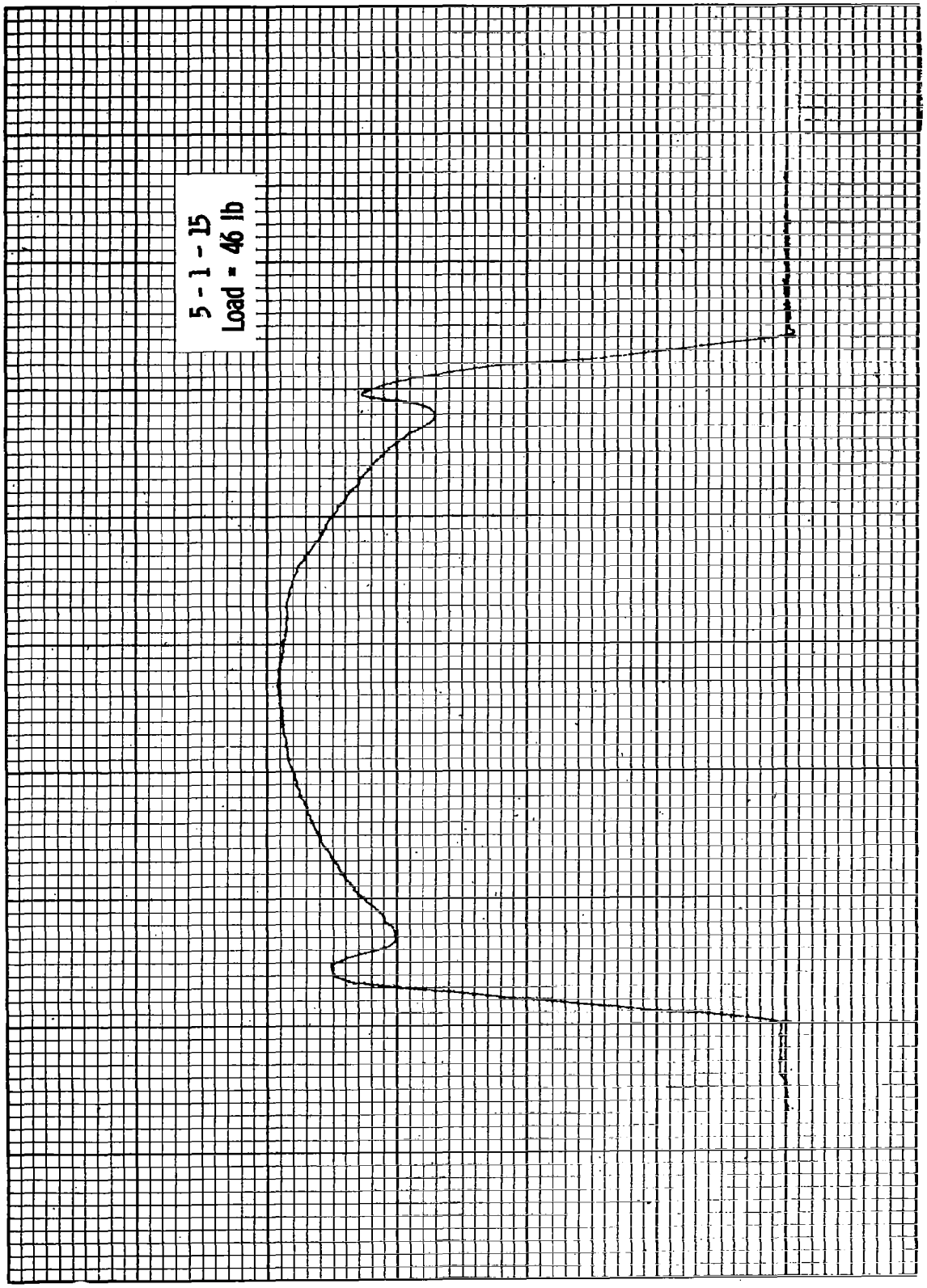
5 - 1 - 15
Load = 46 lb

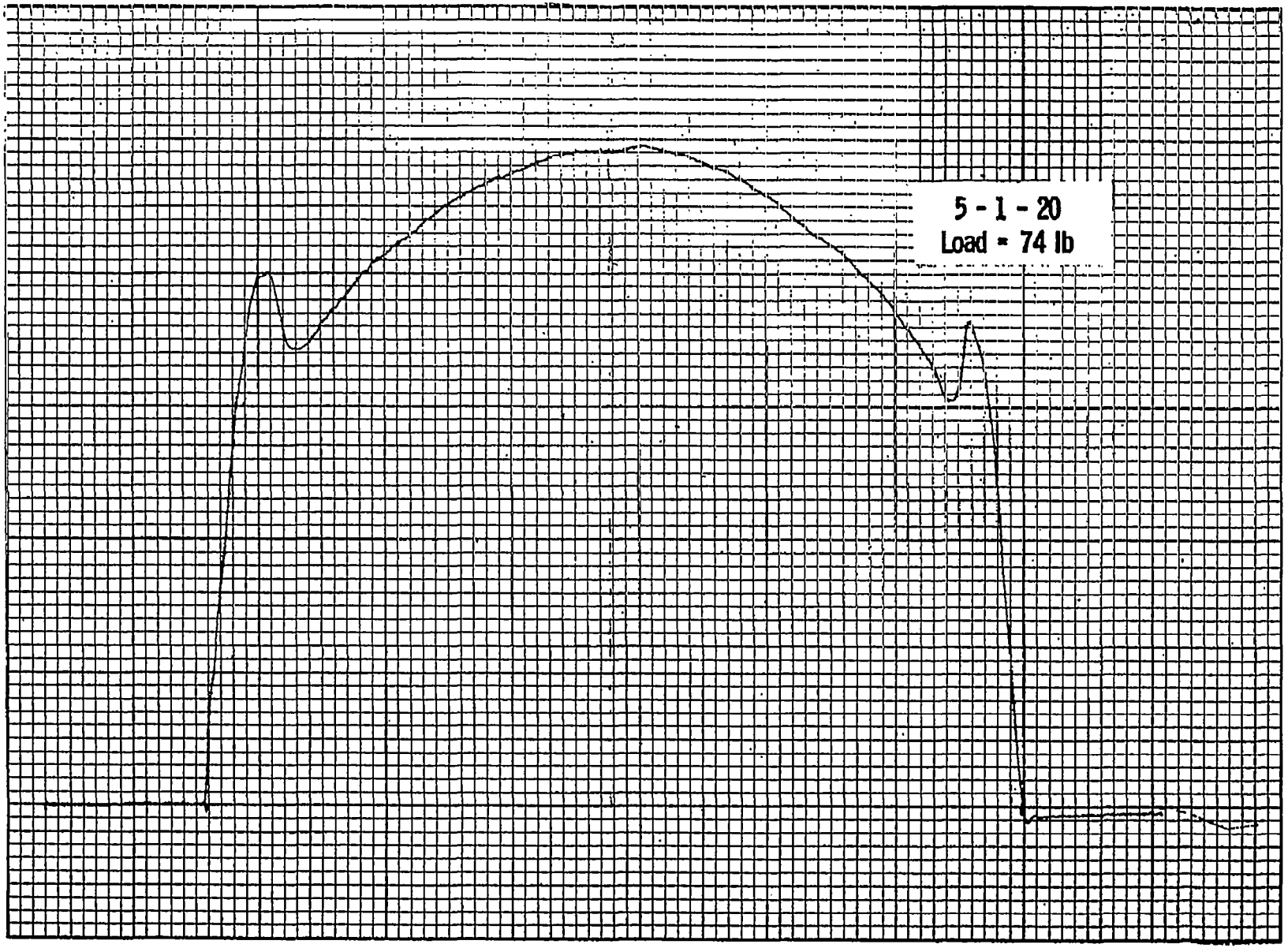
5 - 1 - 20
Load = 74 lb

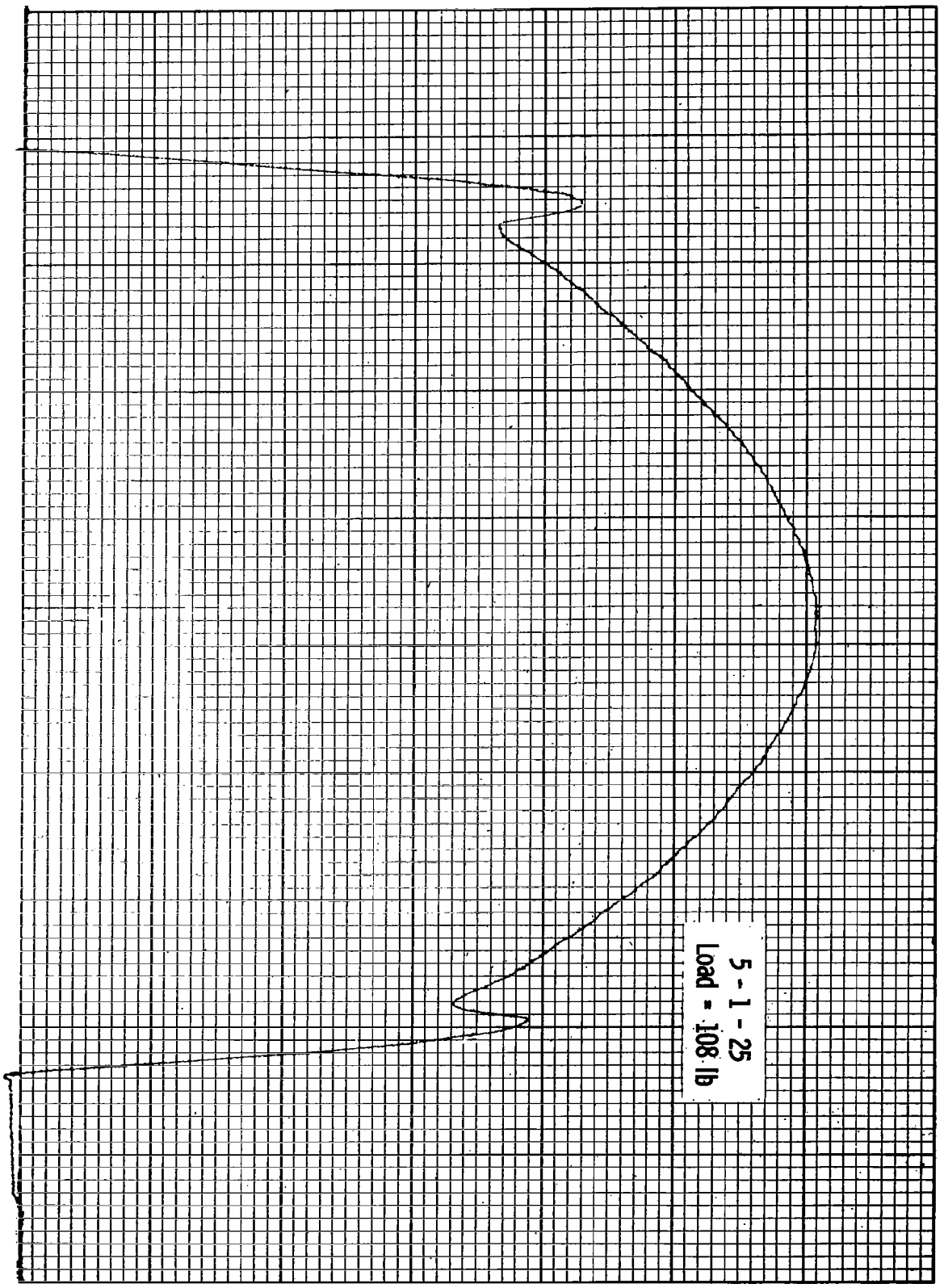
5 - 1 - 25
Load = 108 lb

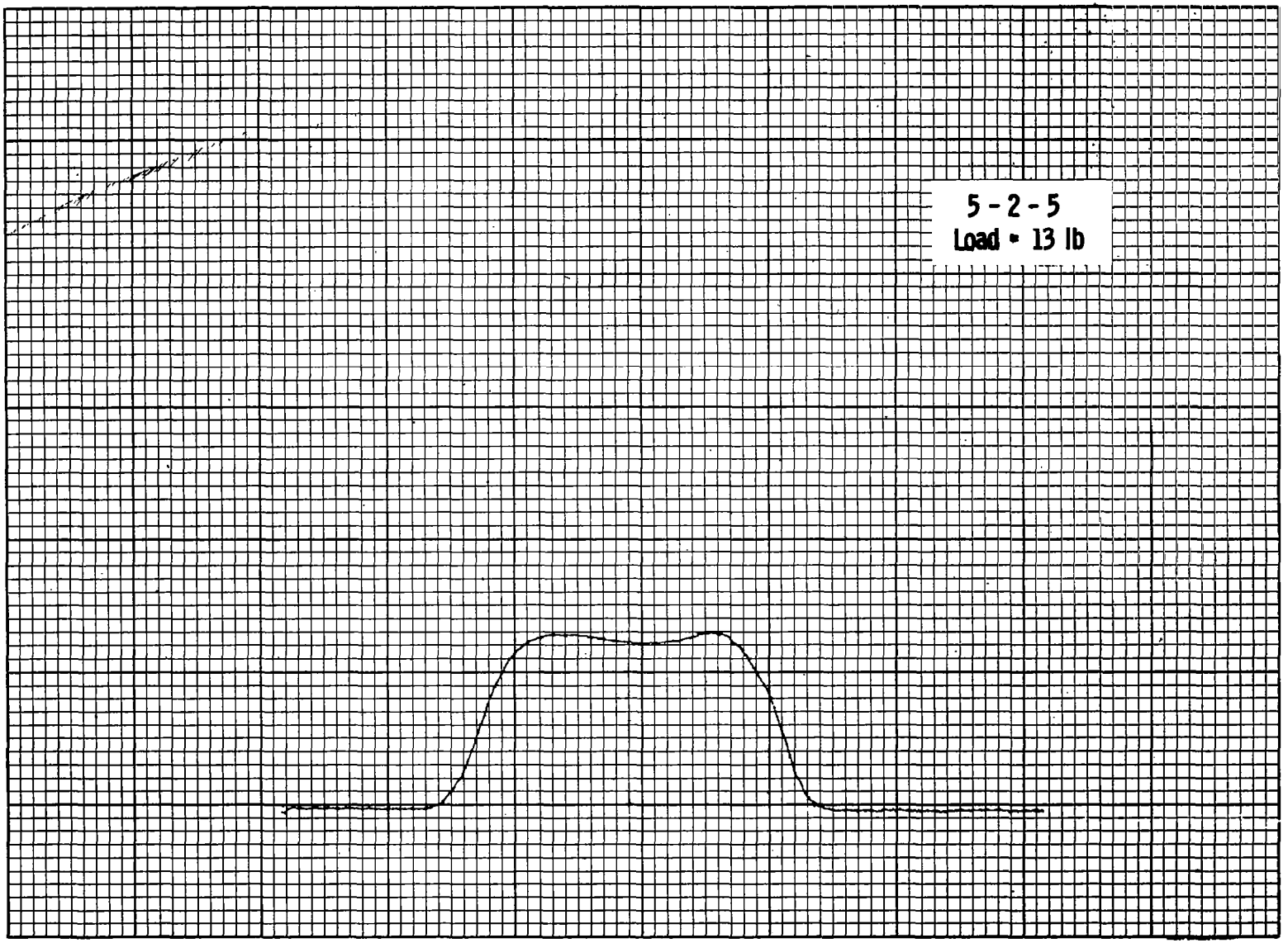
5 - 2 - 5
Load = 13 lb

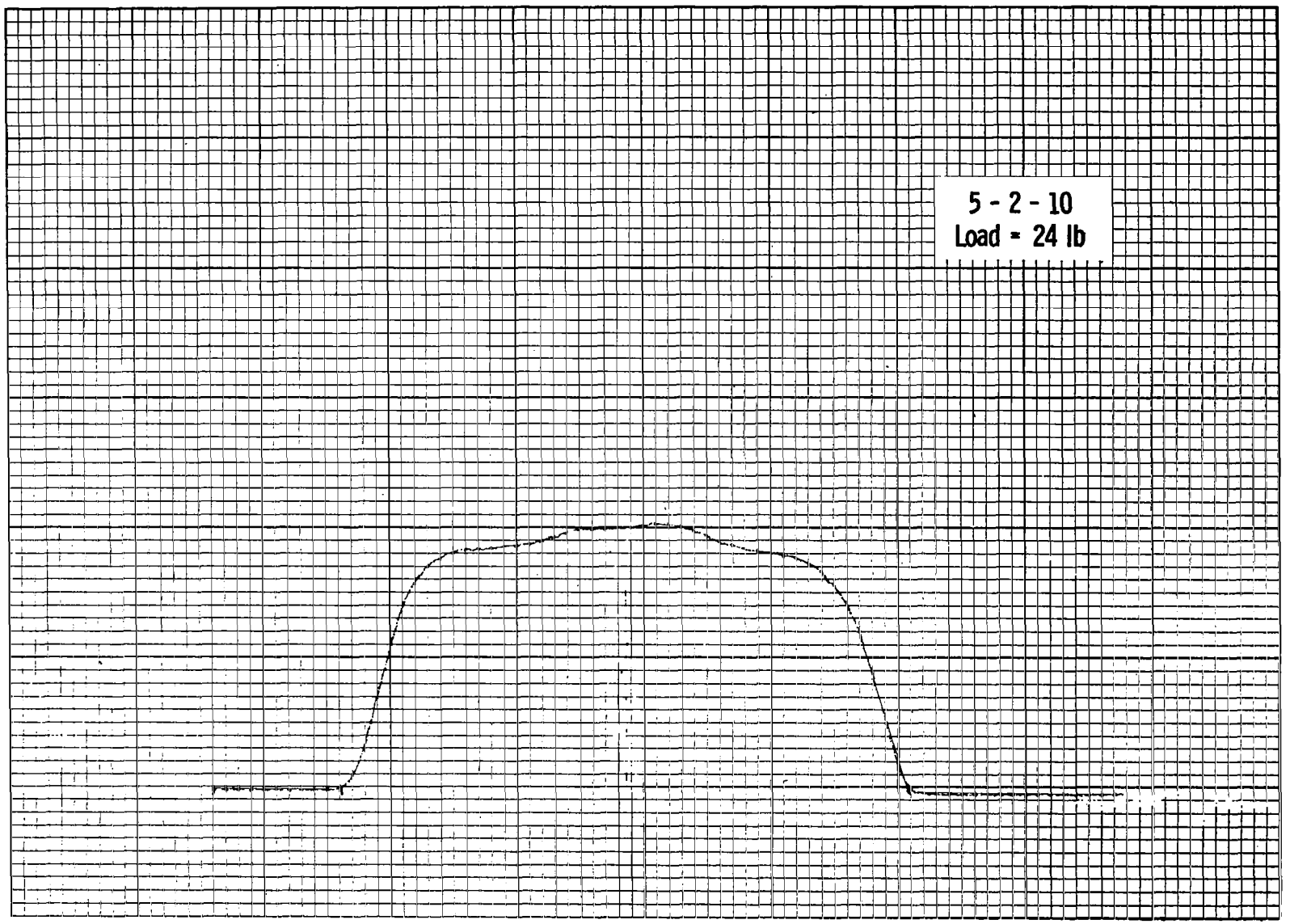
5 - 2 - 10
Load = 24 lb

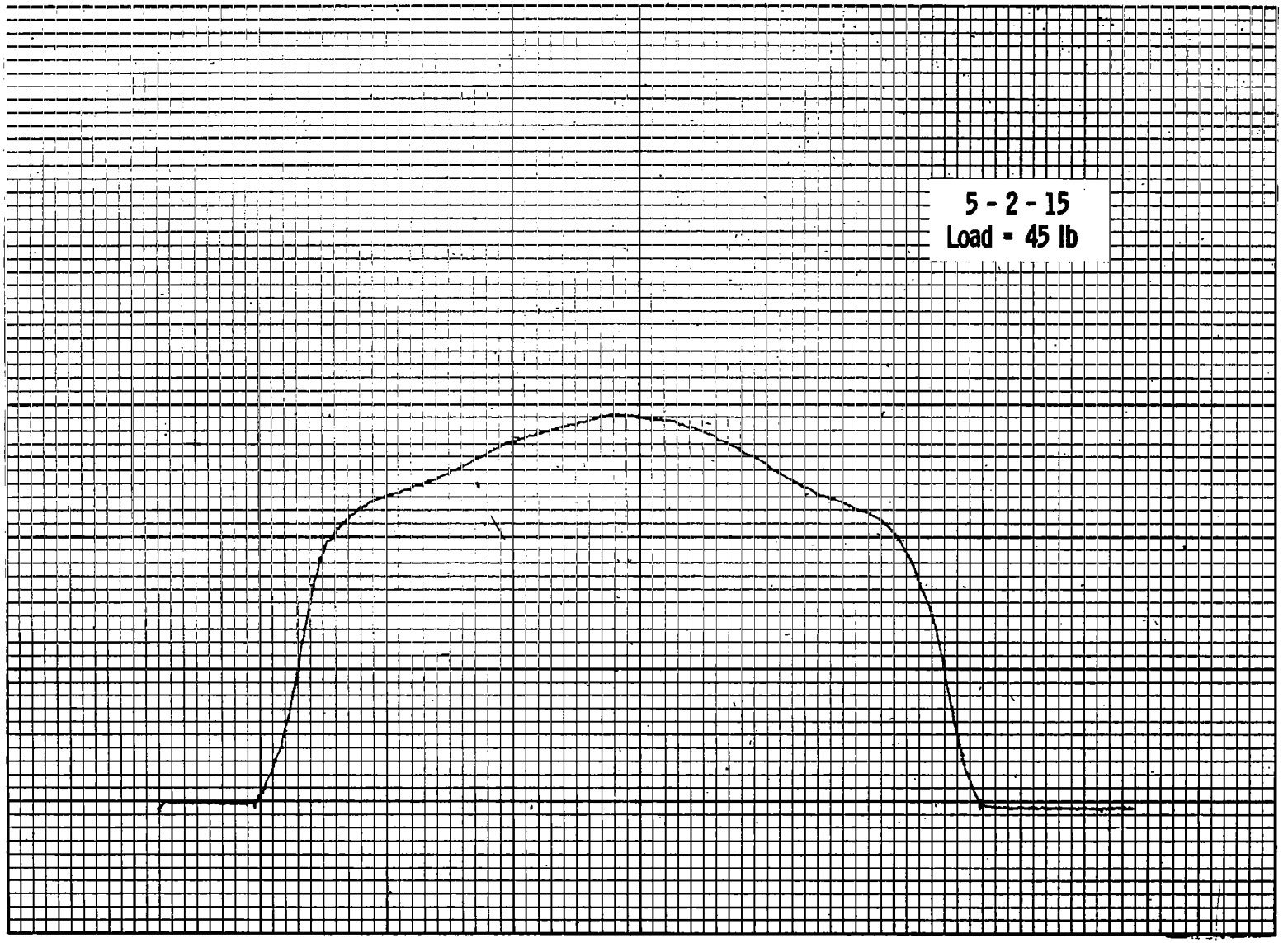
5 - 2 - 15
Load = 45 lb

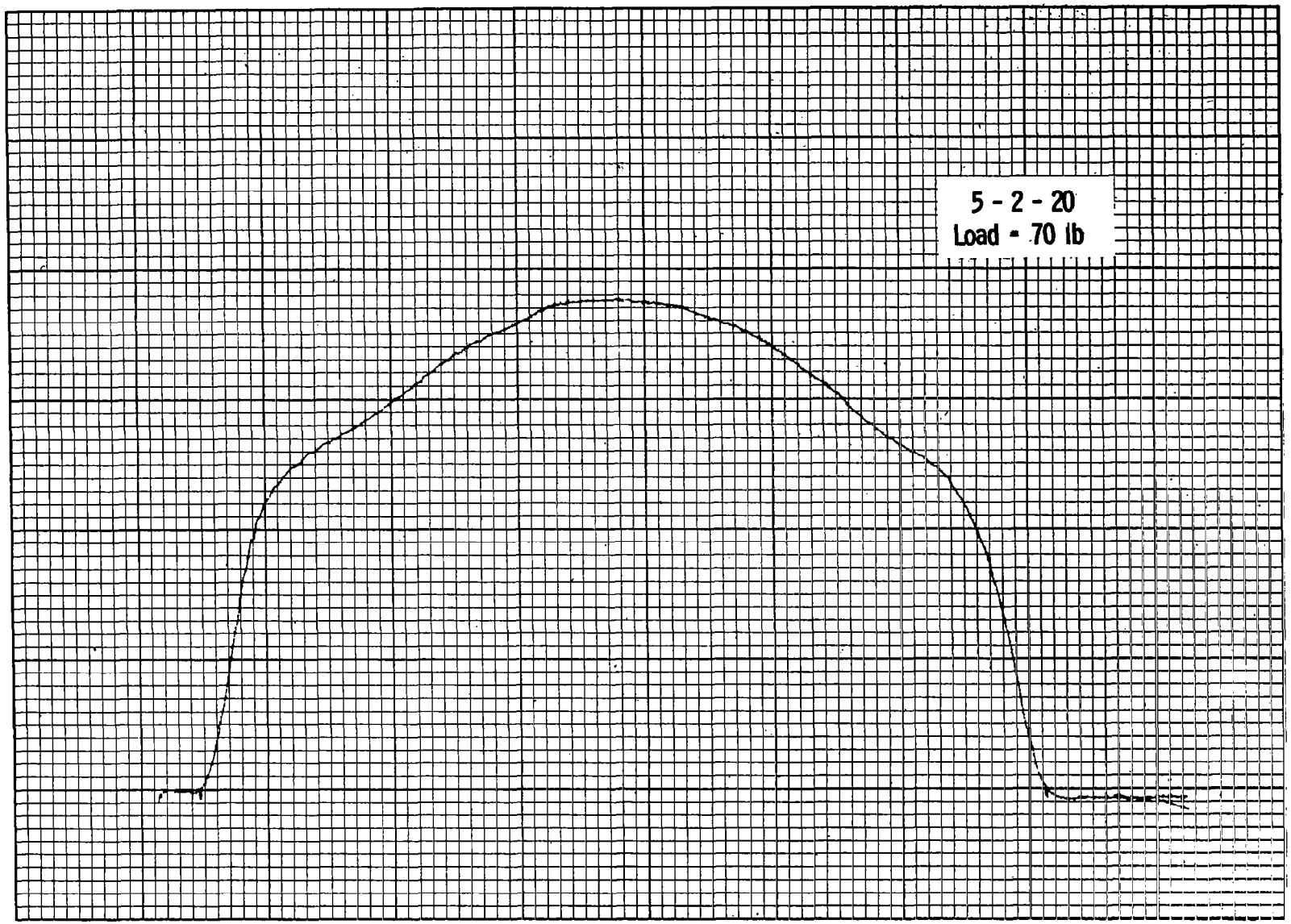
5 - 2 - 20
Load - 70 lb

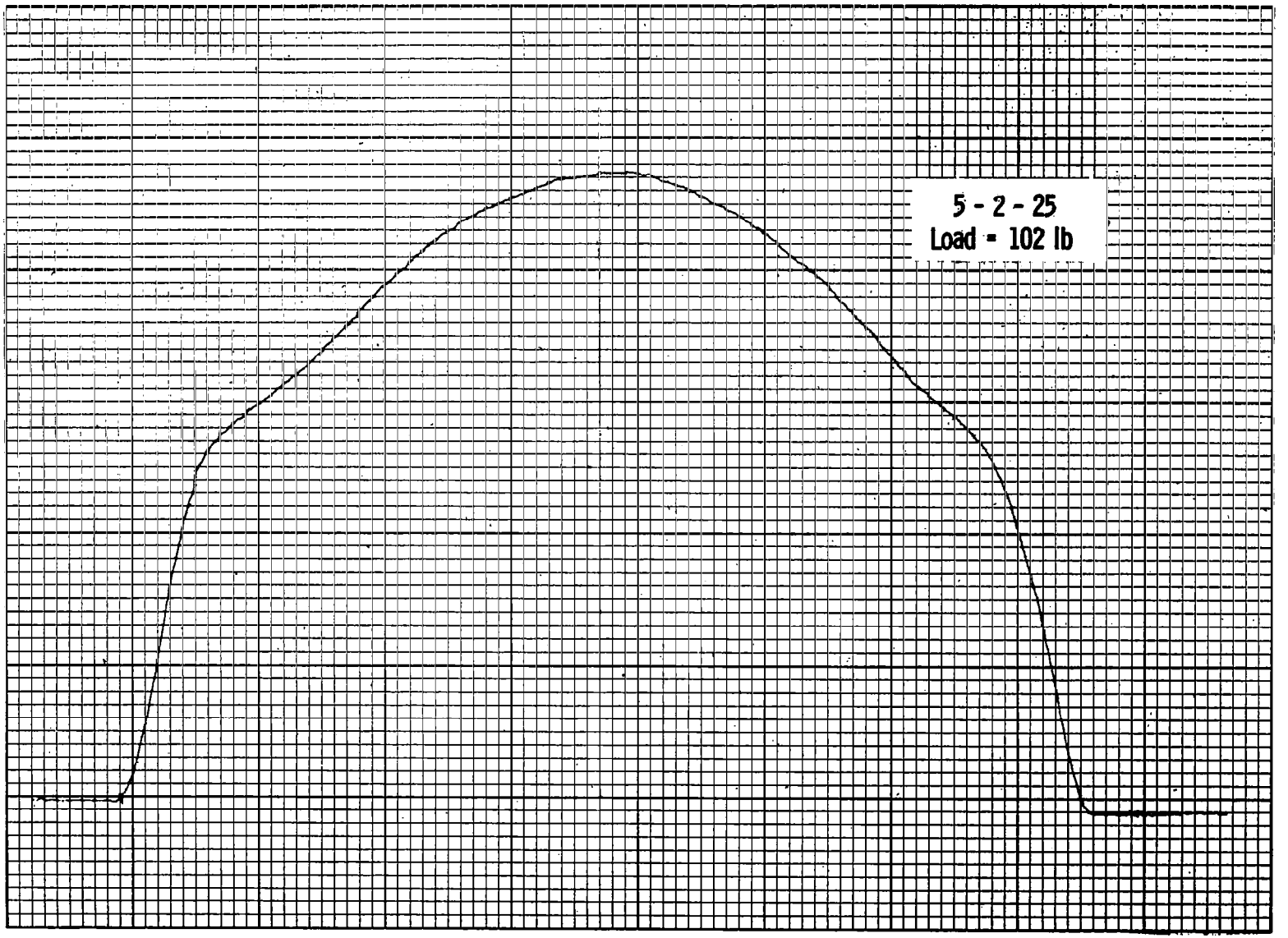
5 - 2 - 25
Load = 102 lb

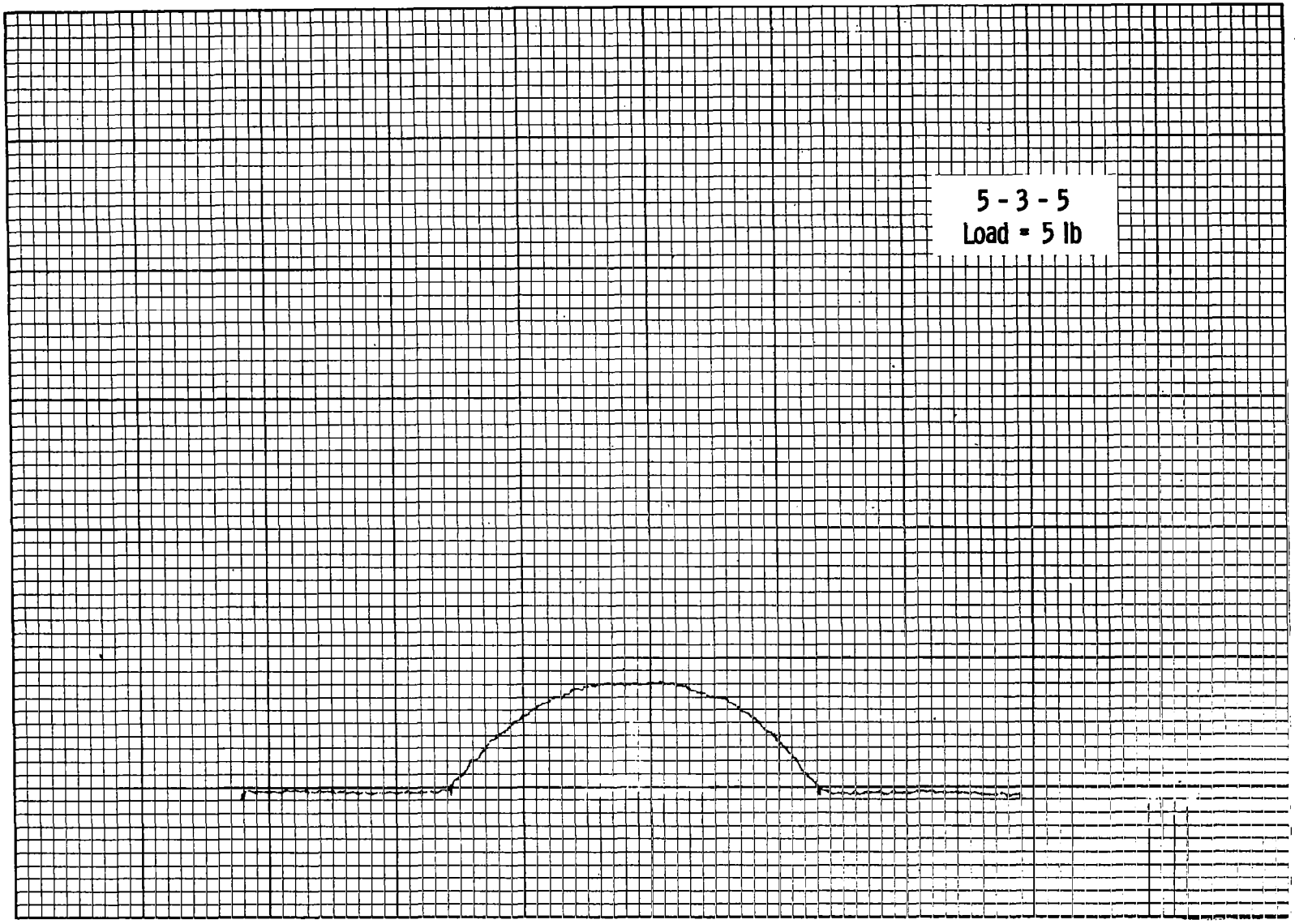
5 - 3 - 5
Load = 5 lb

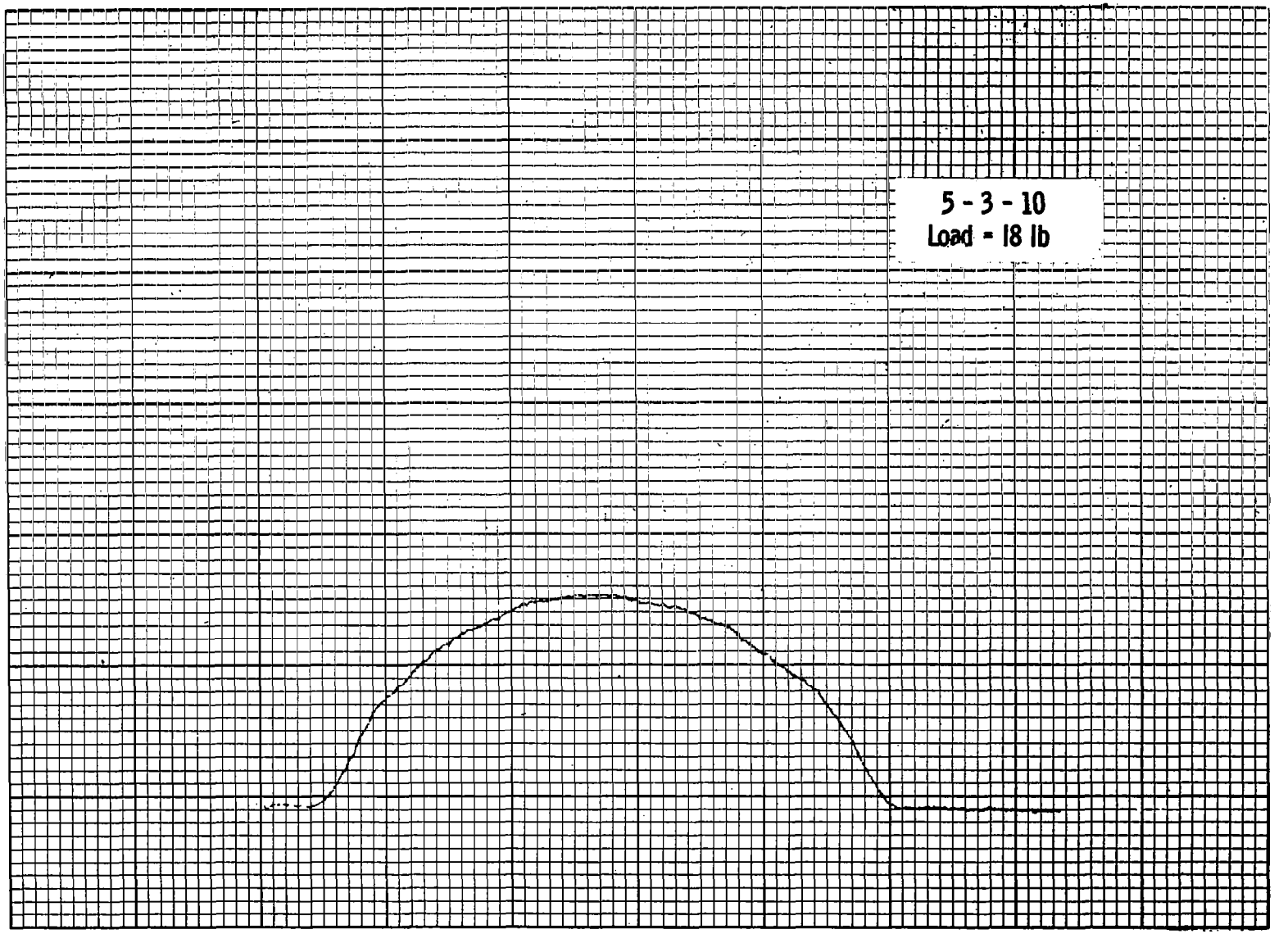
5 - 3 - 10
Load = 18 lb

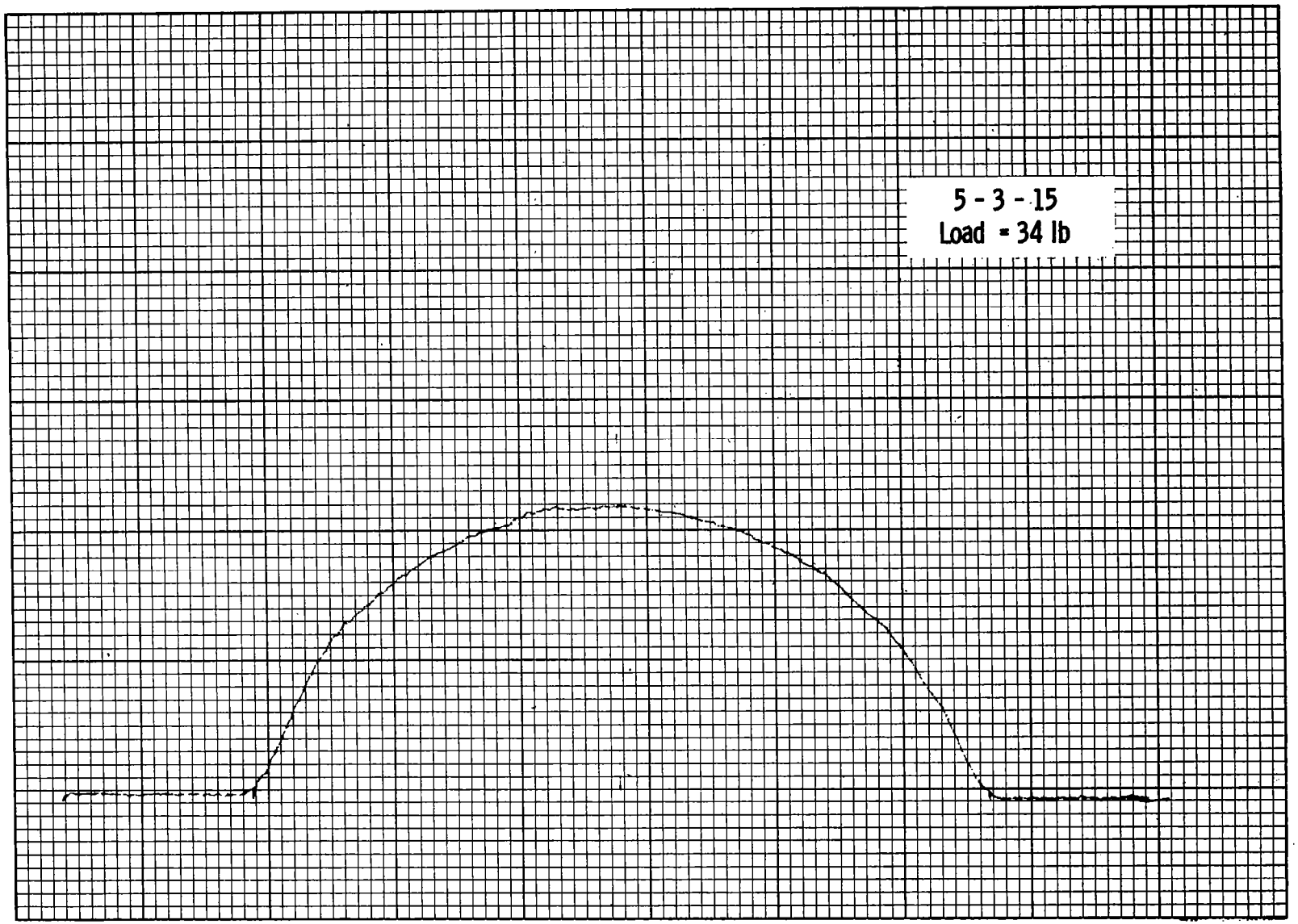
5 - 3 - 15
Load = 34 lb

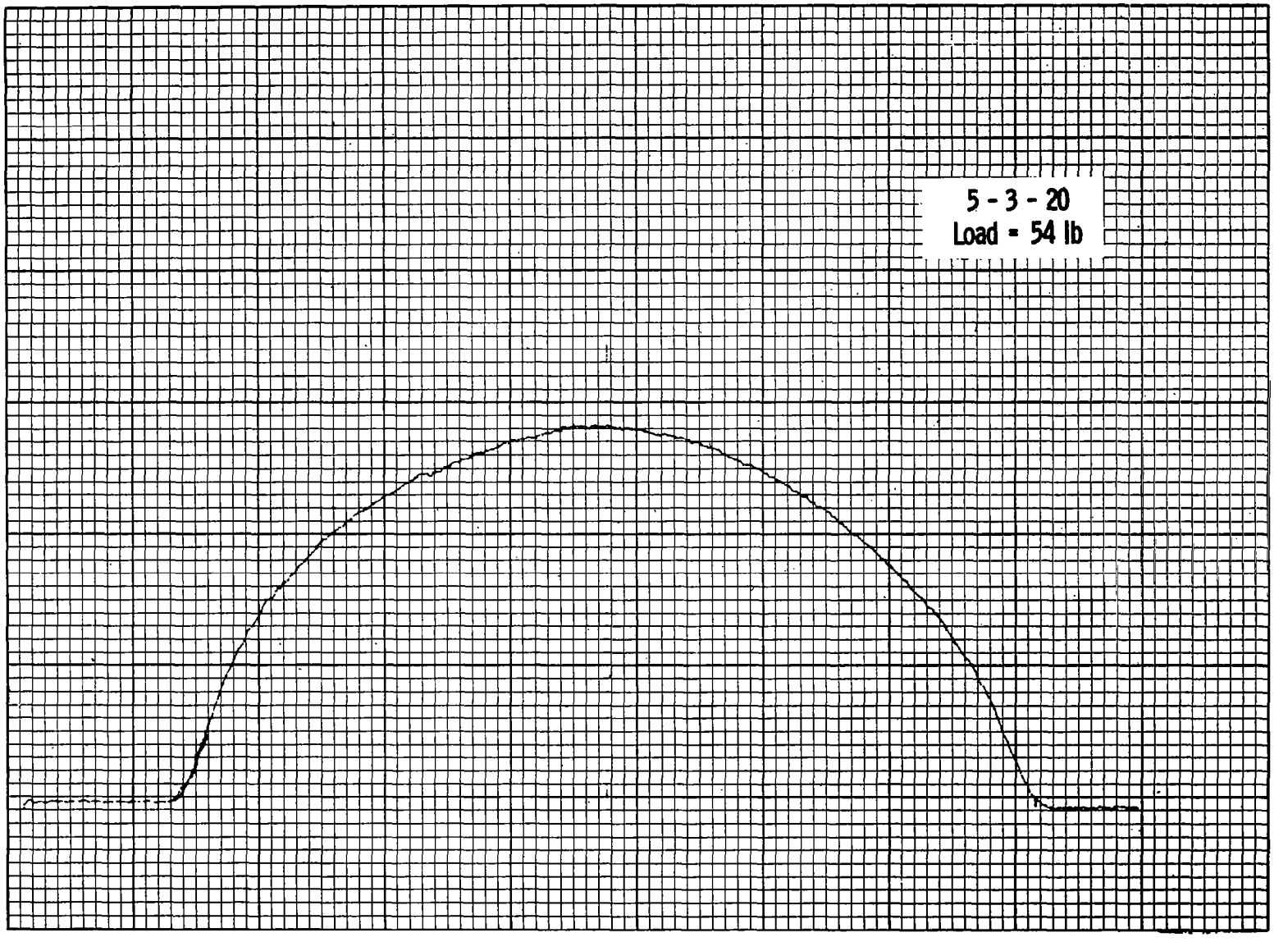
5 - 3 - 20
Load = 54 lb

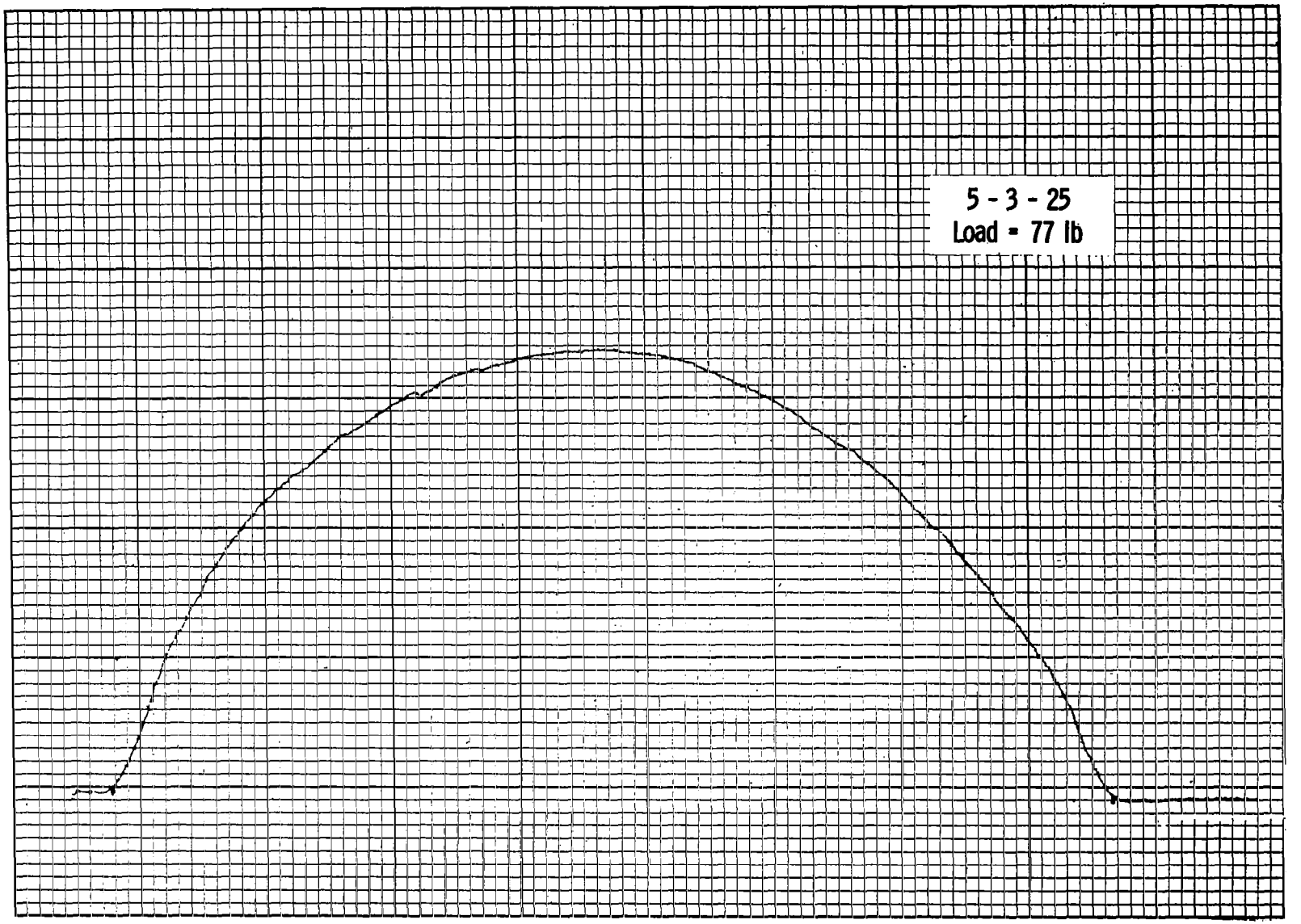
5 - 3 - 25
Load = 77 lb

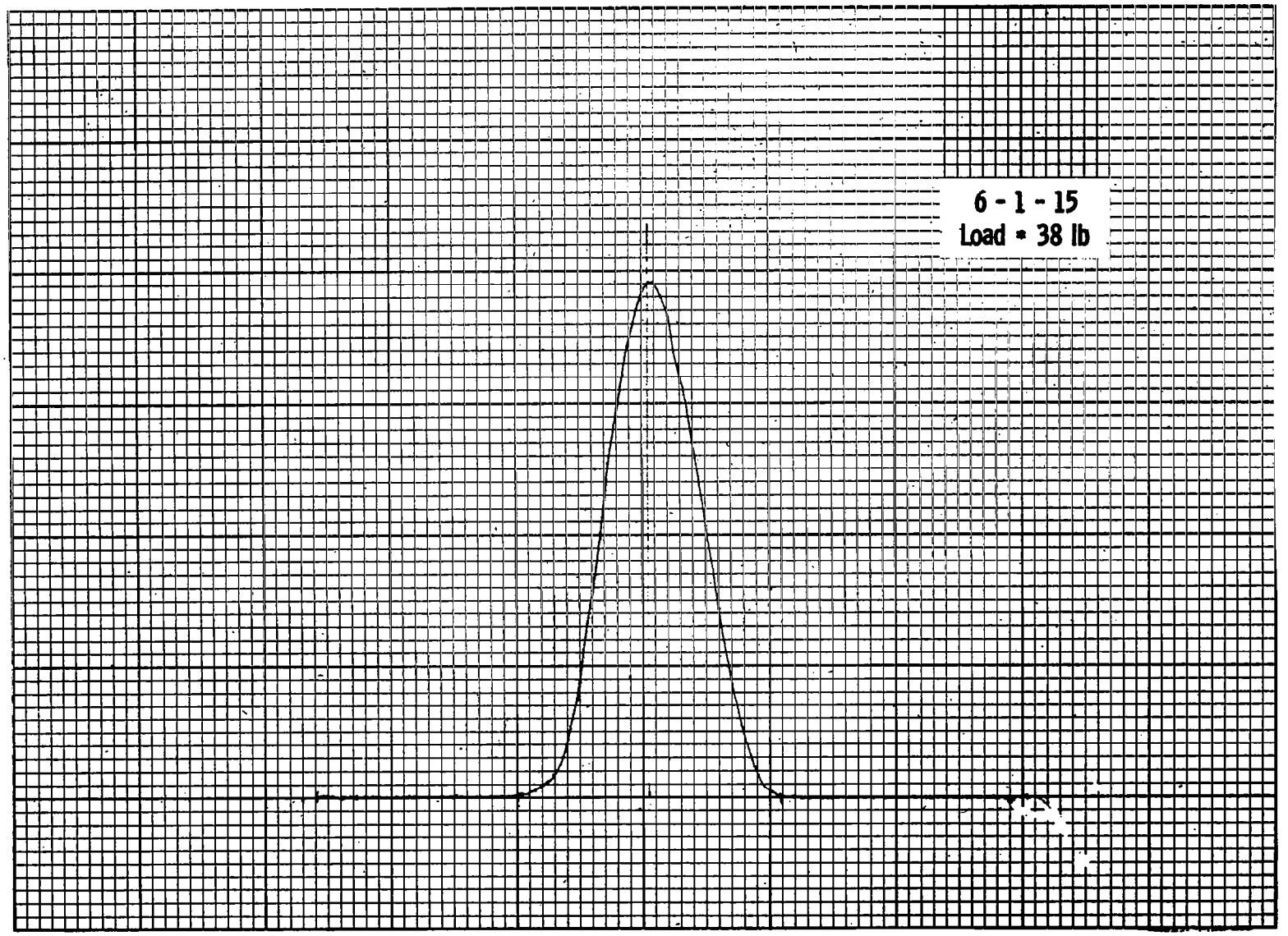
6 - 1 - 15
Load = 38 lb

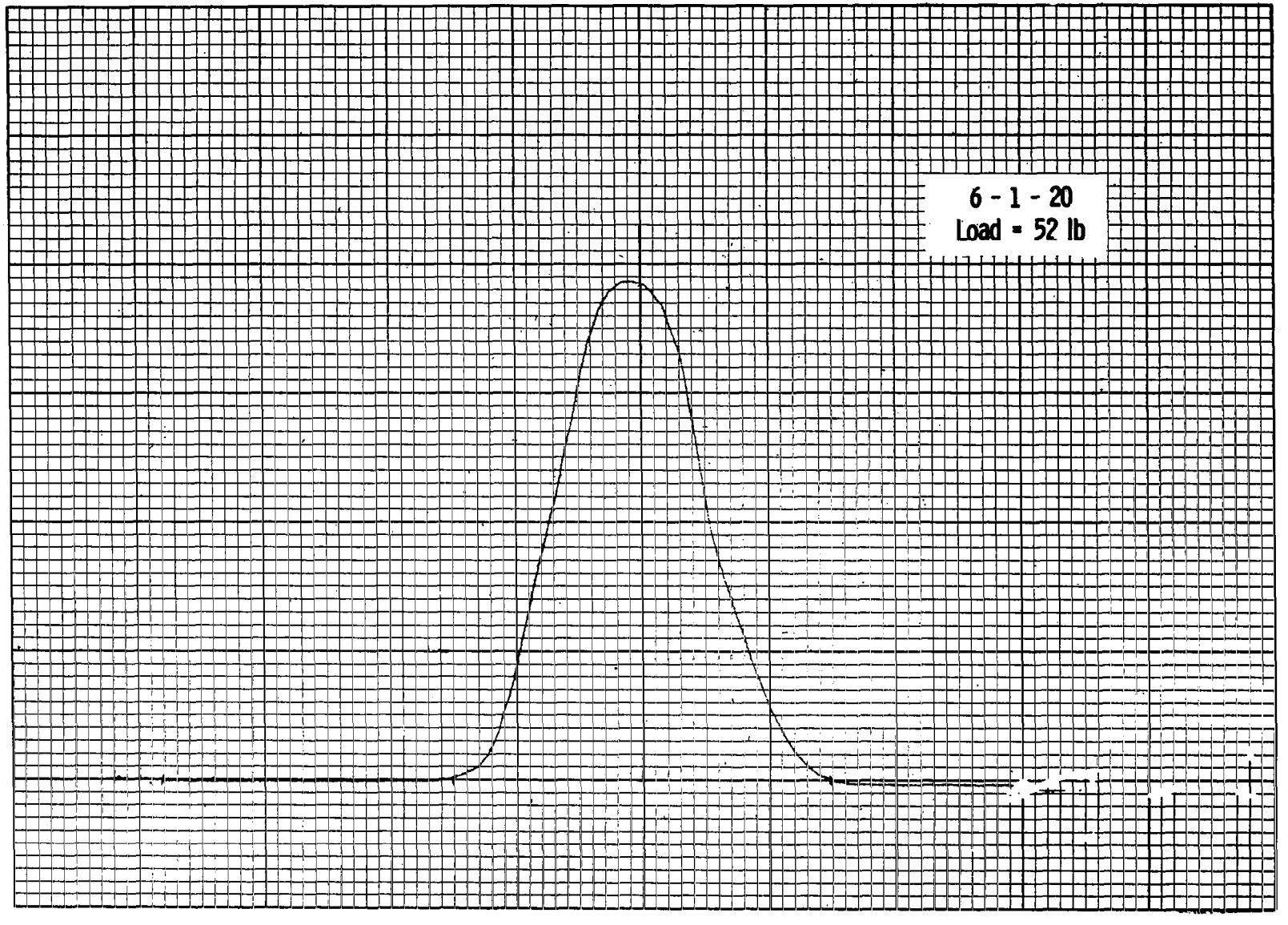
6 - 1 - 20
Load = 52 lb

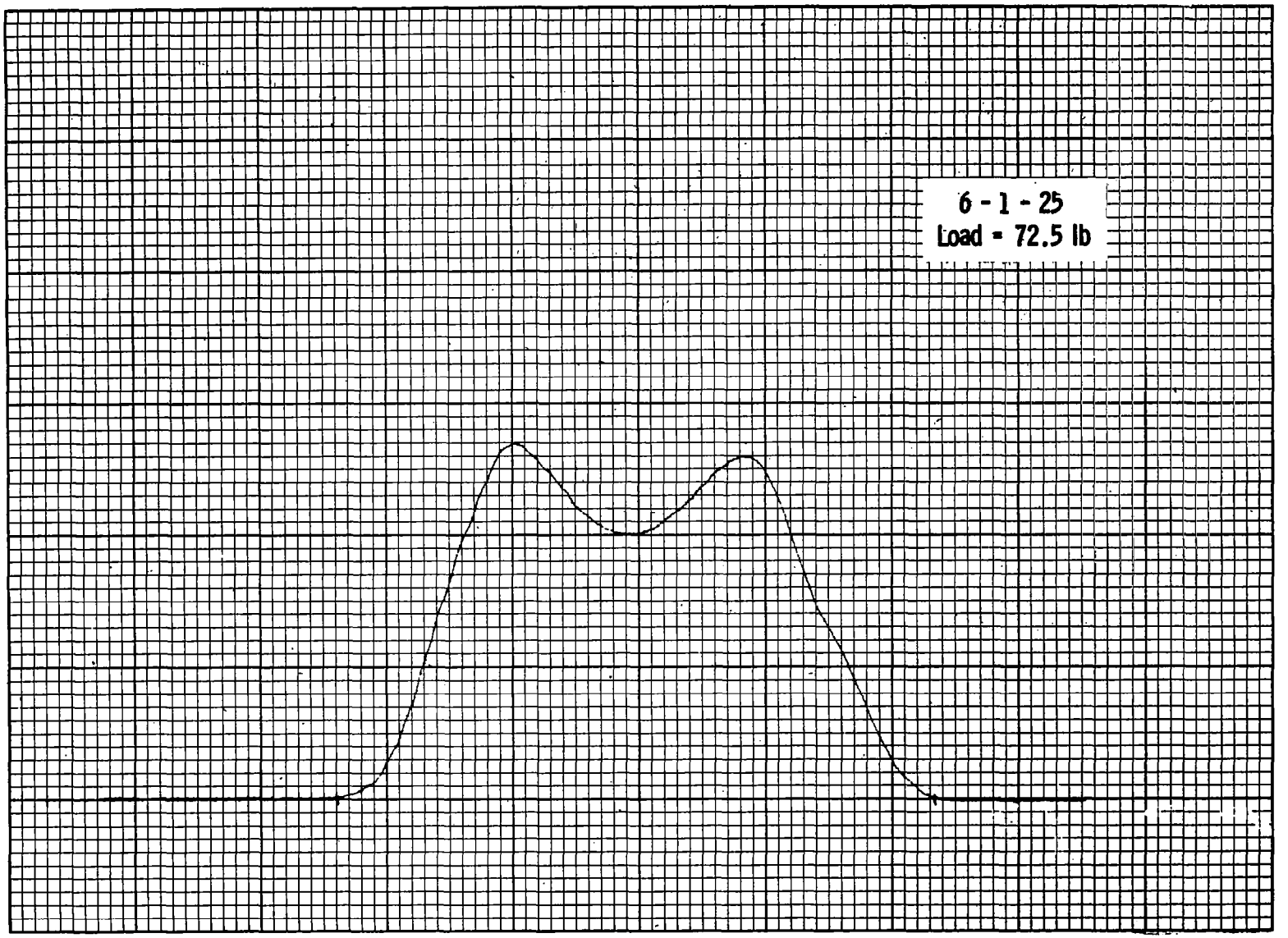
6 - 1 - 25
Load = 72.5 lb

6 - 1 - 30
Load = 94 lb

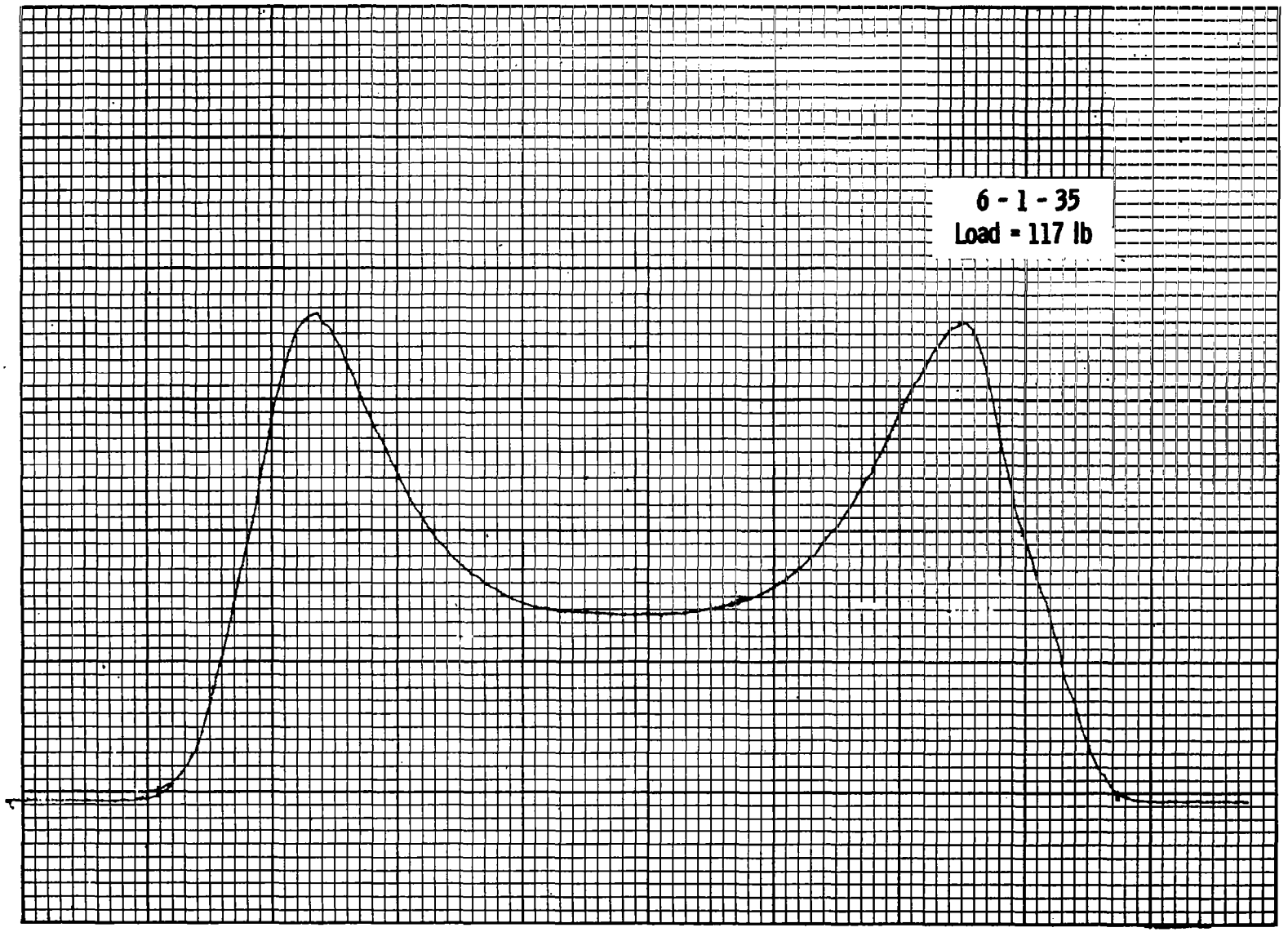
6 - 1 - 35
Load = 117 lb

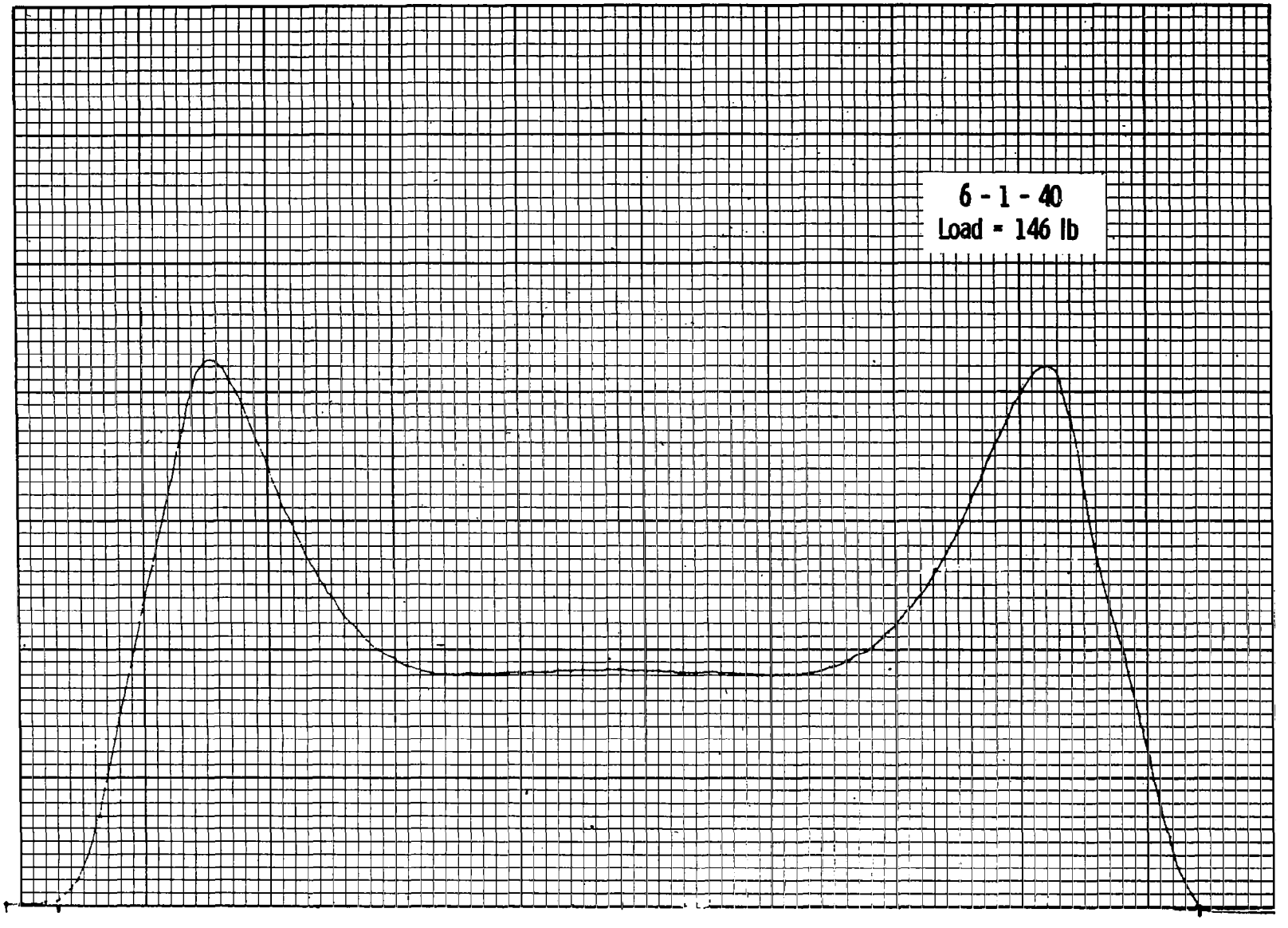
6 - 1 - 40
Load = 146 lb

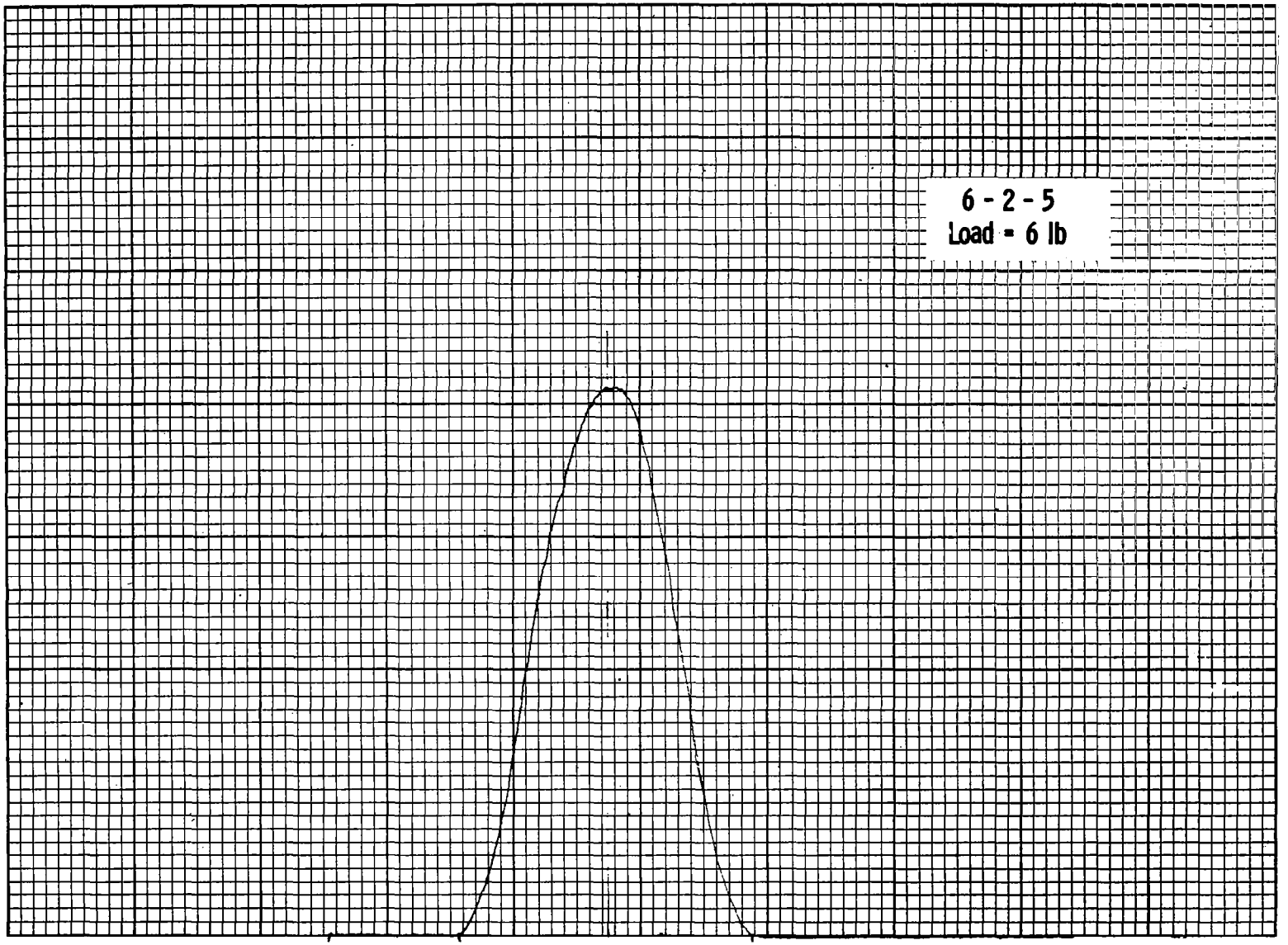
6 - 2 - 5
Load = 6 lb

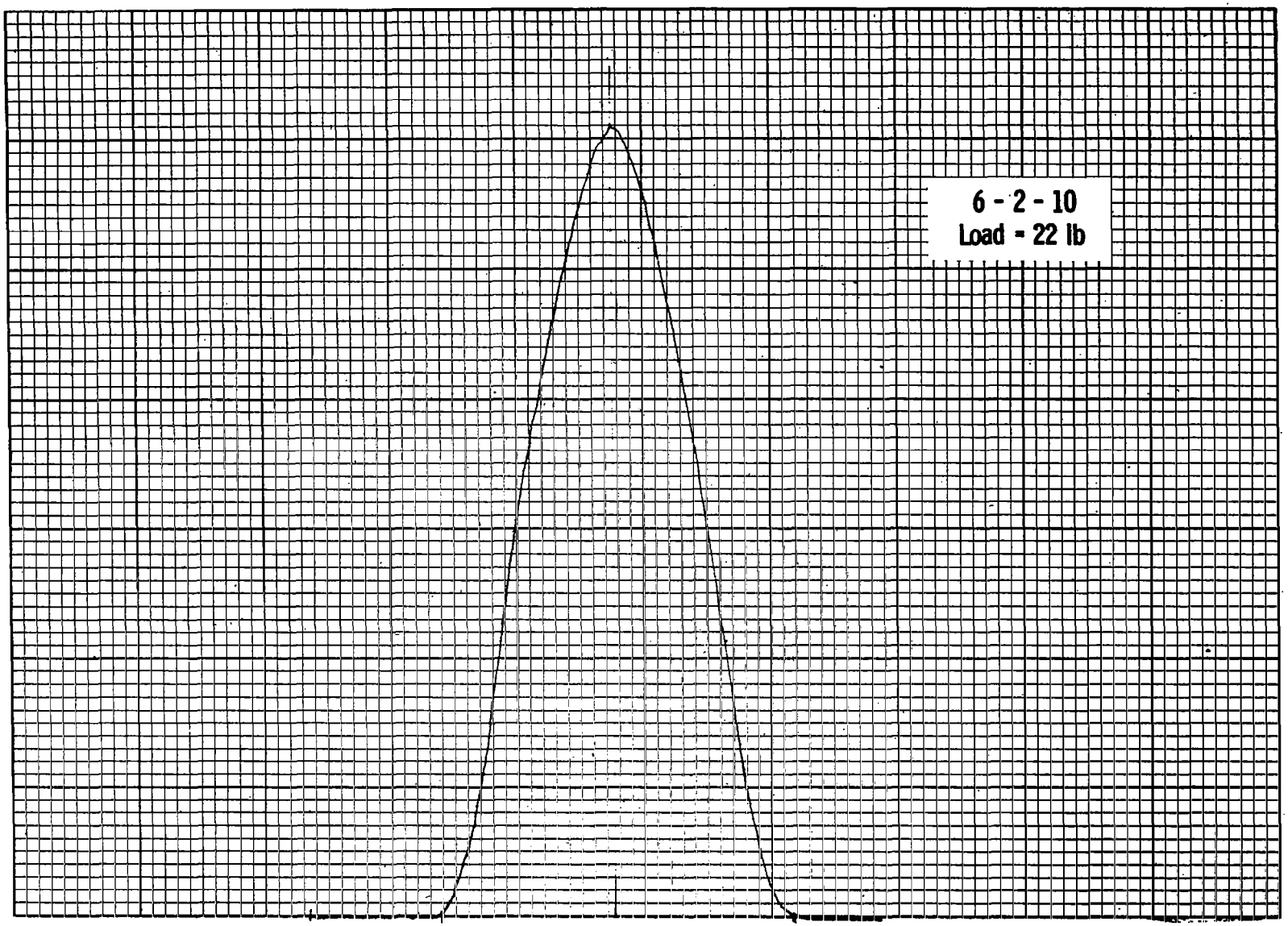
6 - 2 - 10
Load = 22 lb

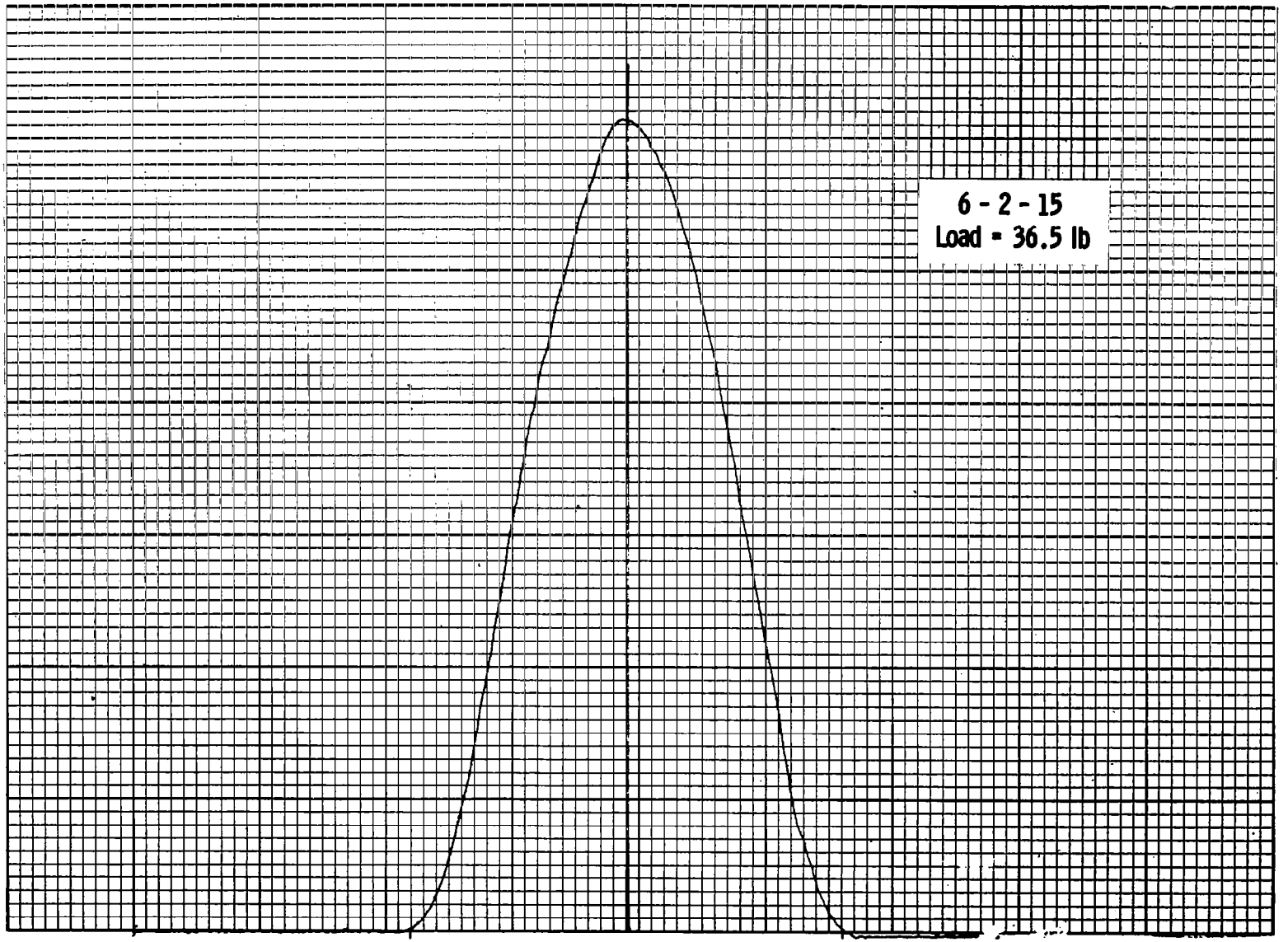
6 - 2 - 15
Load = 36.5 lb

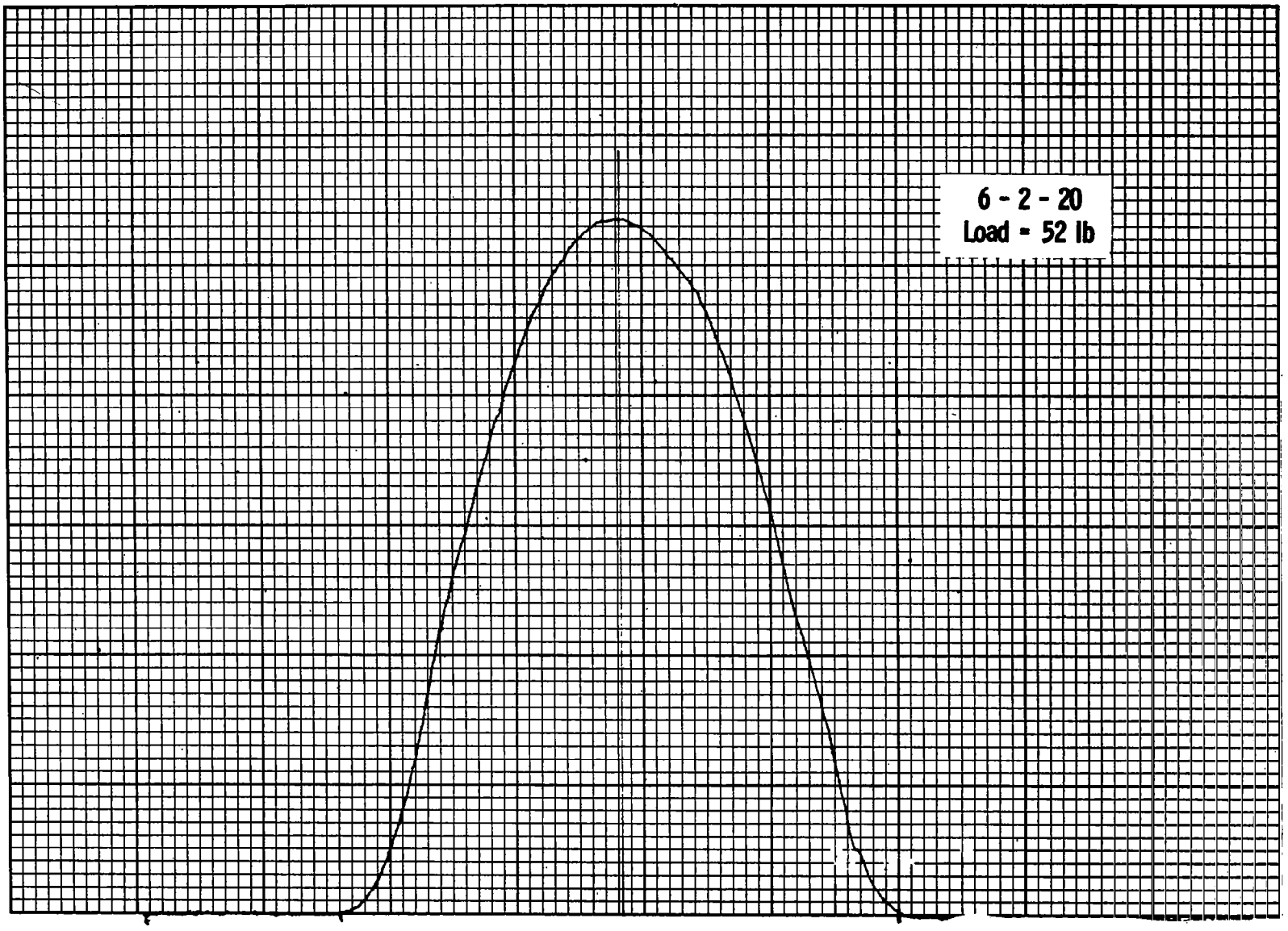
6 - 2 - 20
Load = 52 lb

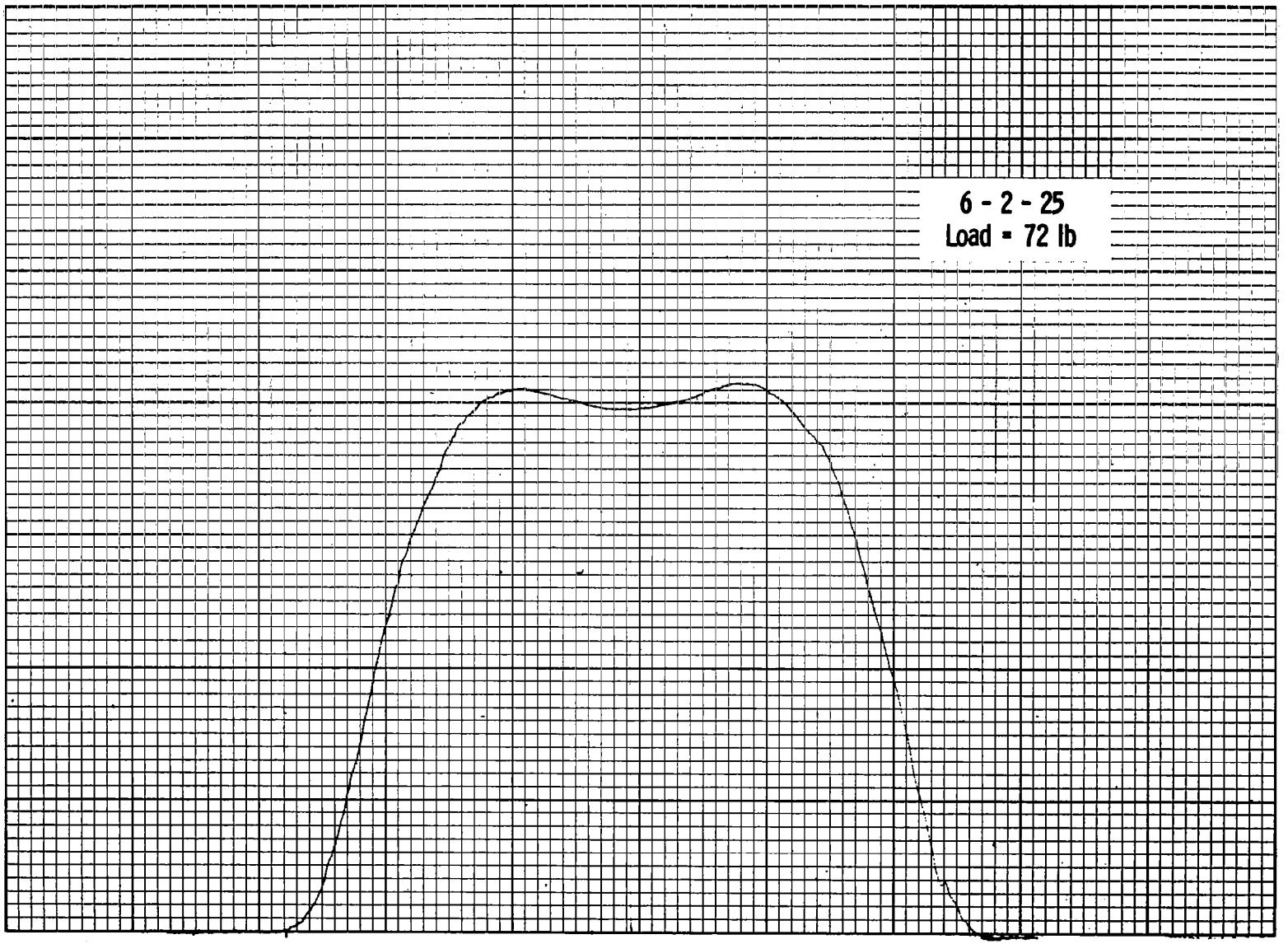
6 - 2 - 25
Load = 72 lb

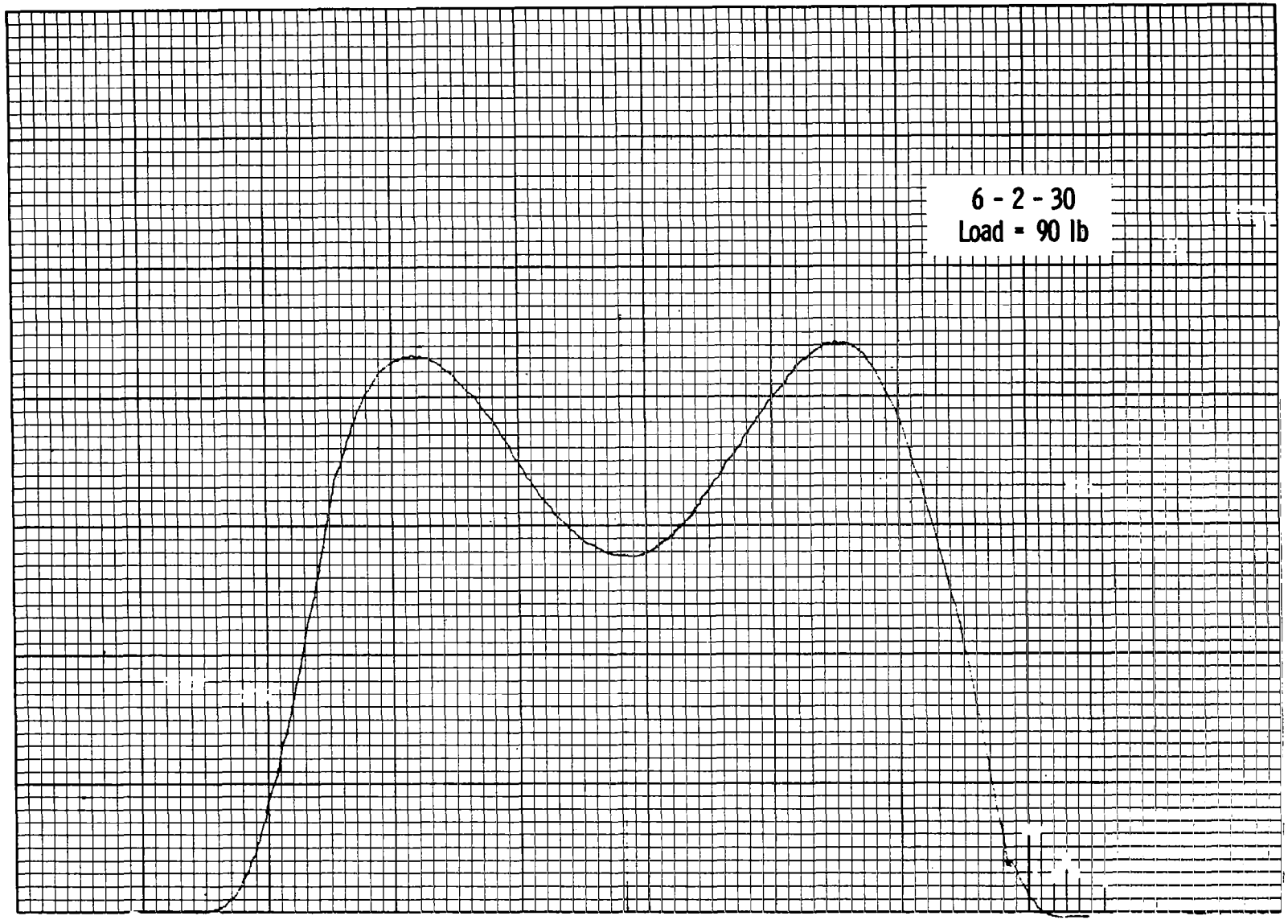
6 - 2 - 30
Load = 90 lb

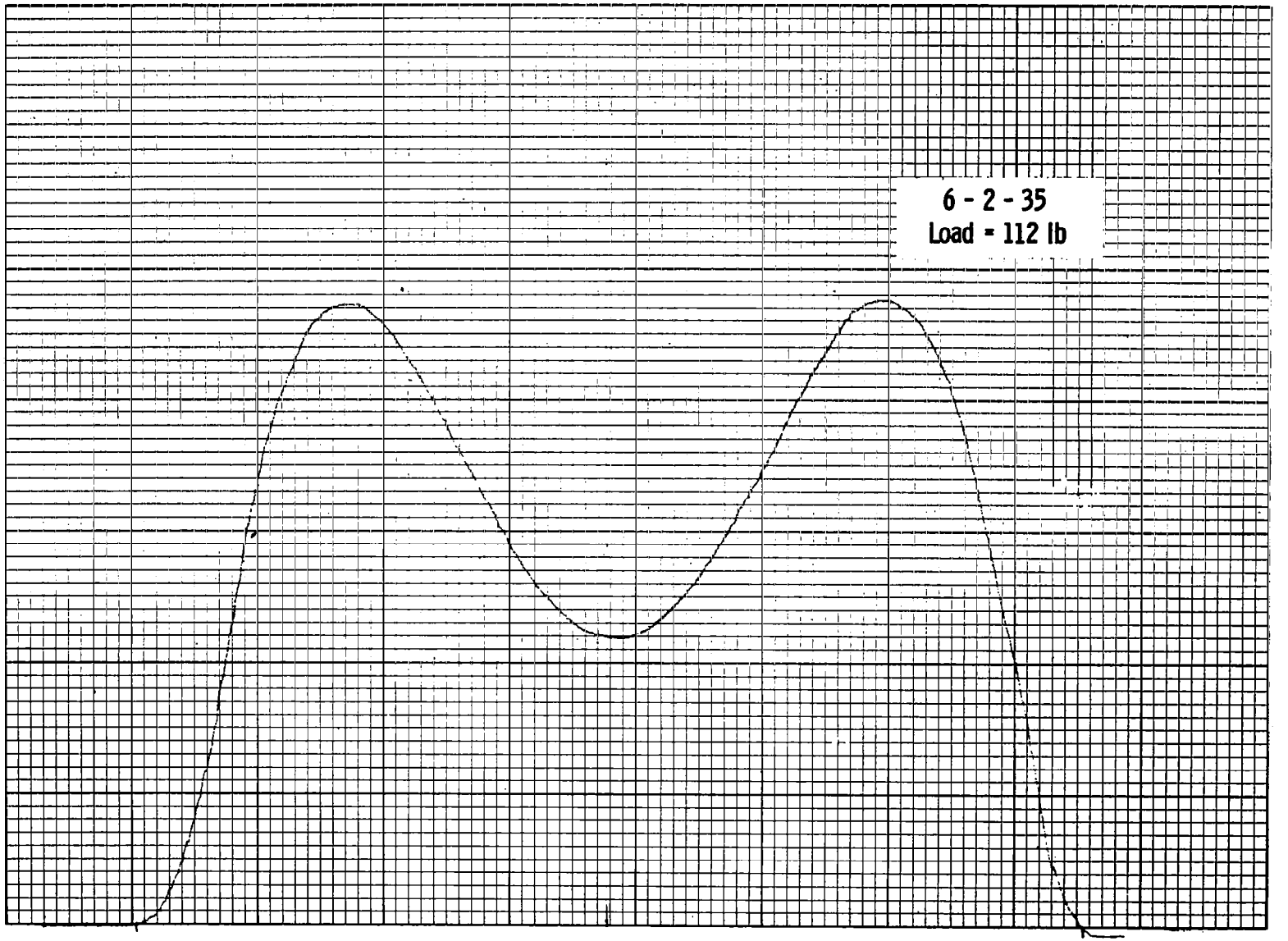
6 - 2 - 35
Load = 112 lb

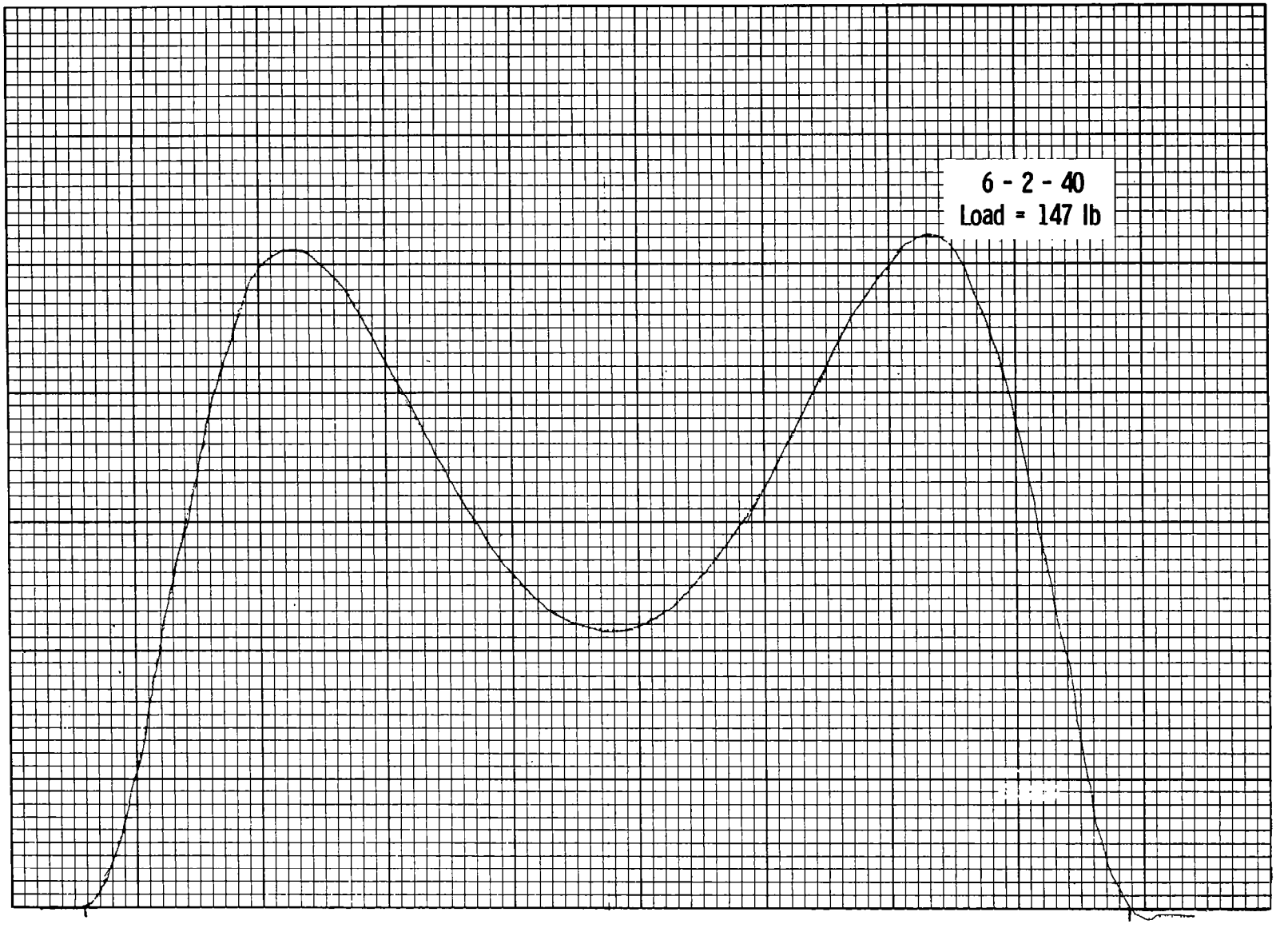
6 - 2 - 40
Load = 147 lb

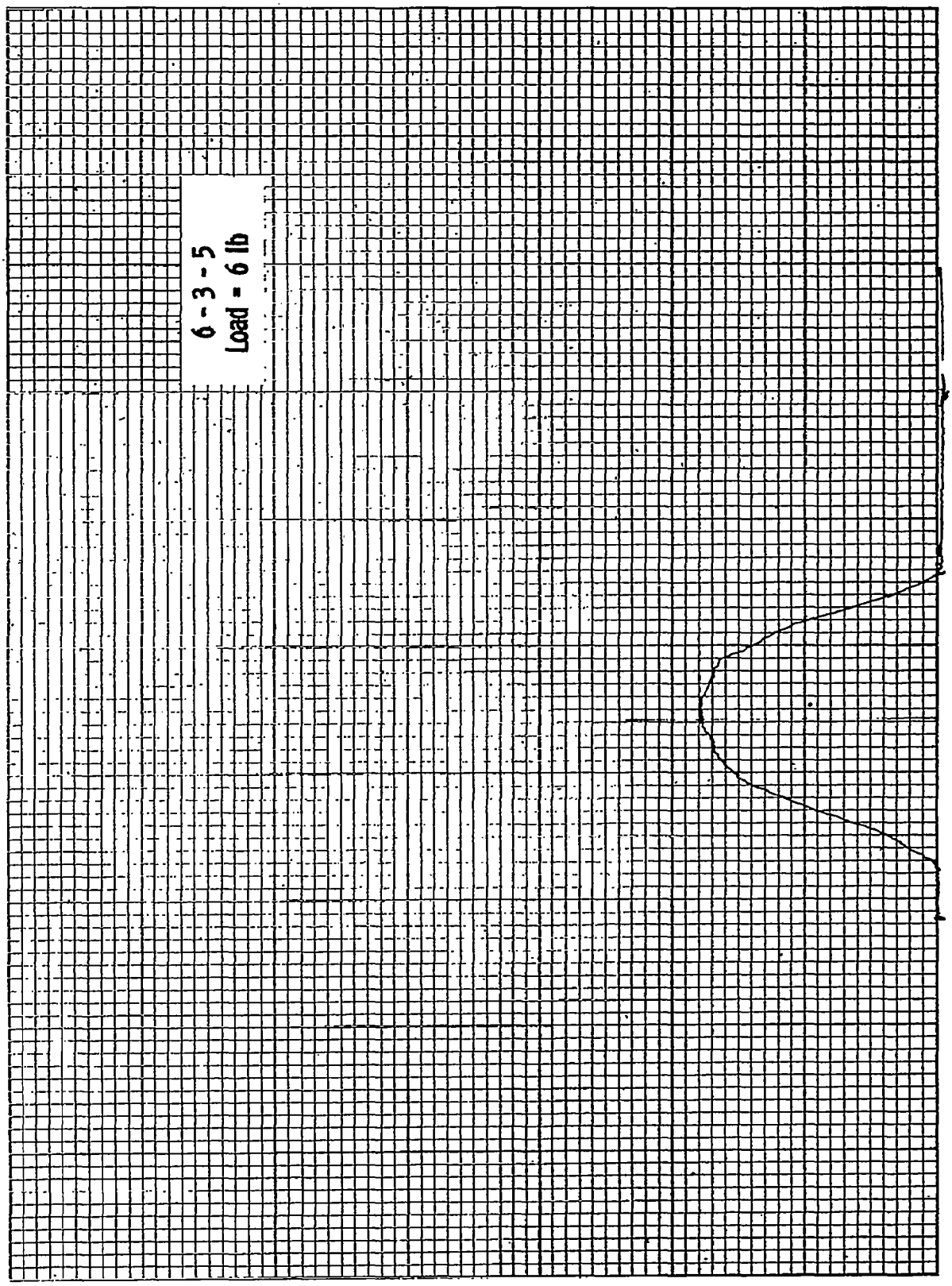
6 - 3 - 5
Load = 6 lb

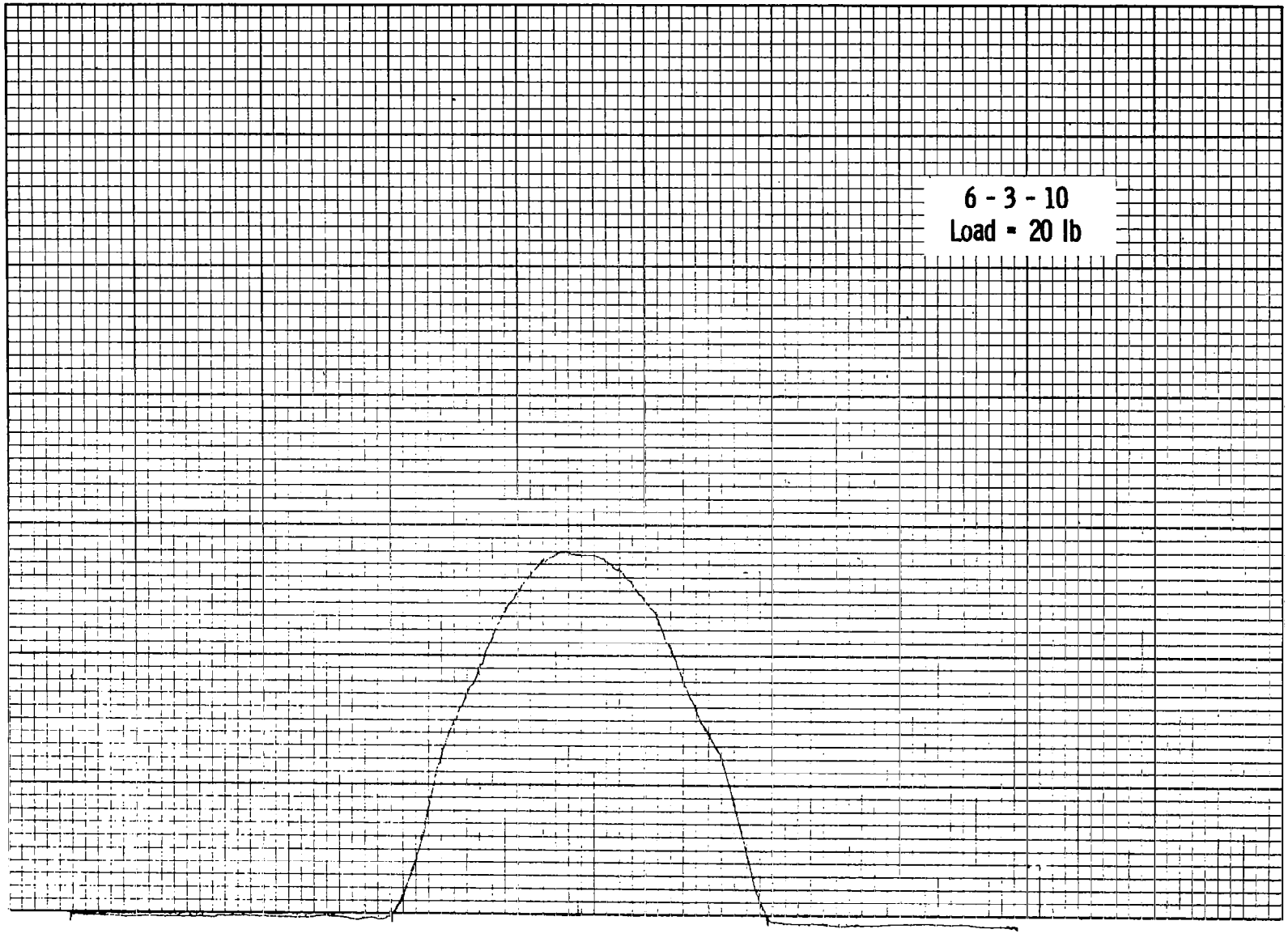
6 - 3 - 10
Load = 20 lb

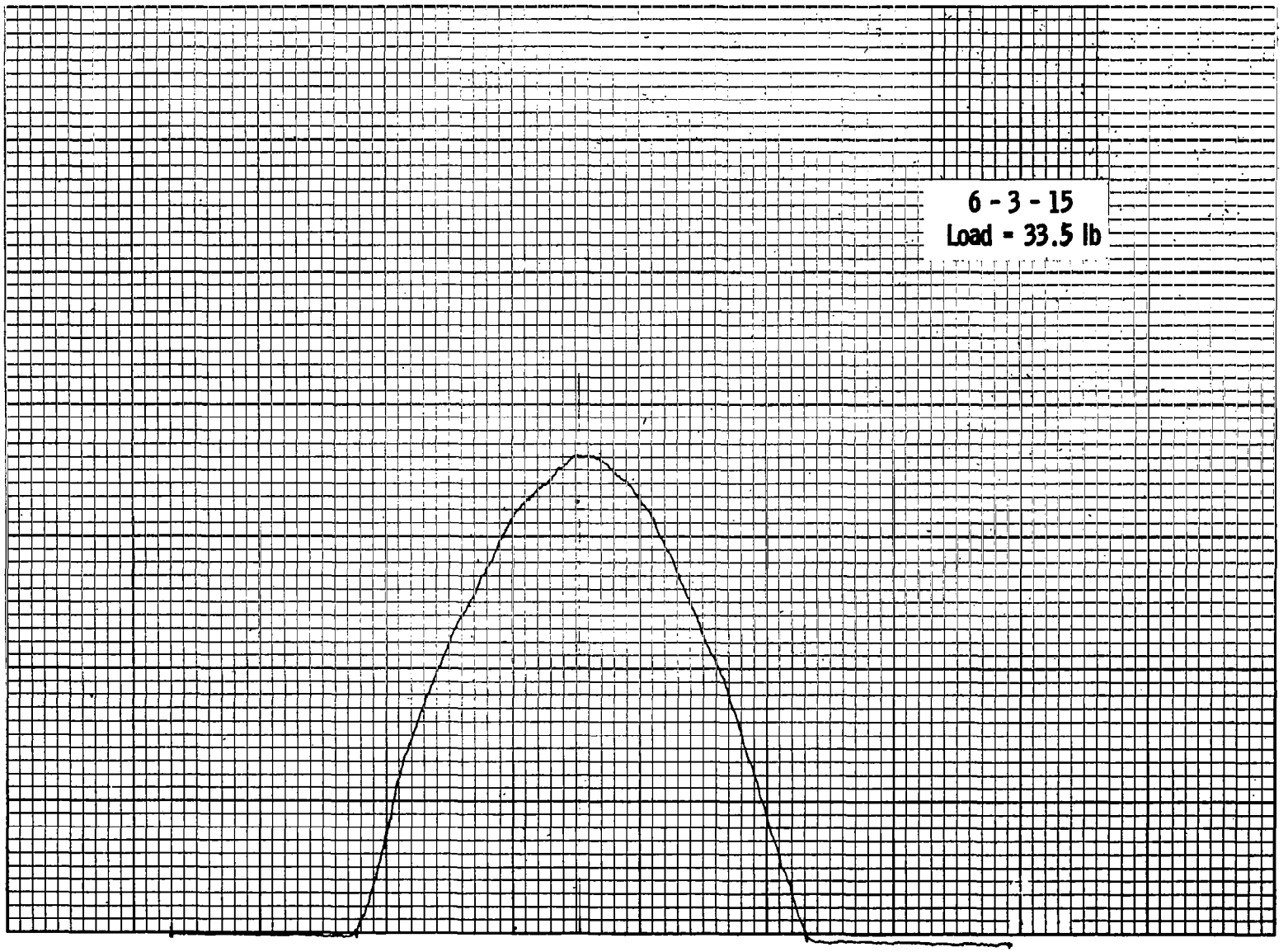
6 - 3 - 15
Load = 33.5 lb

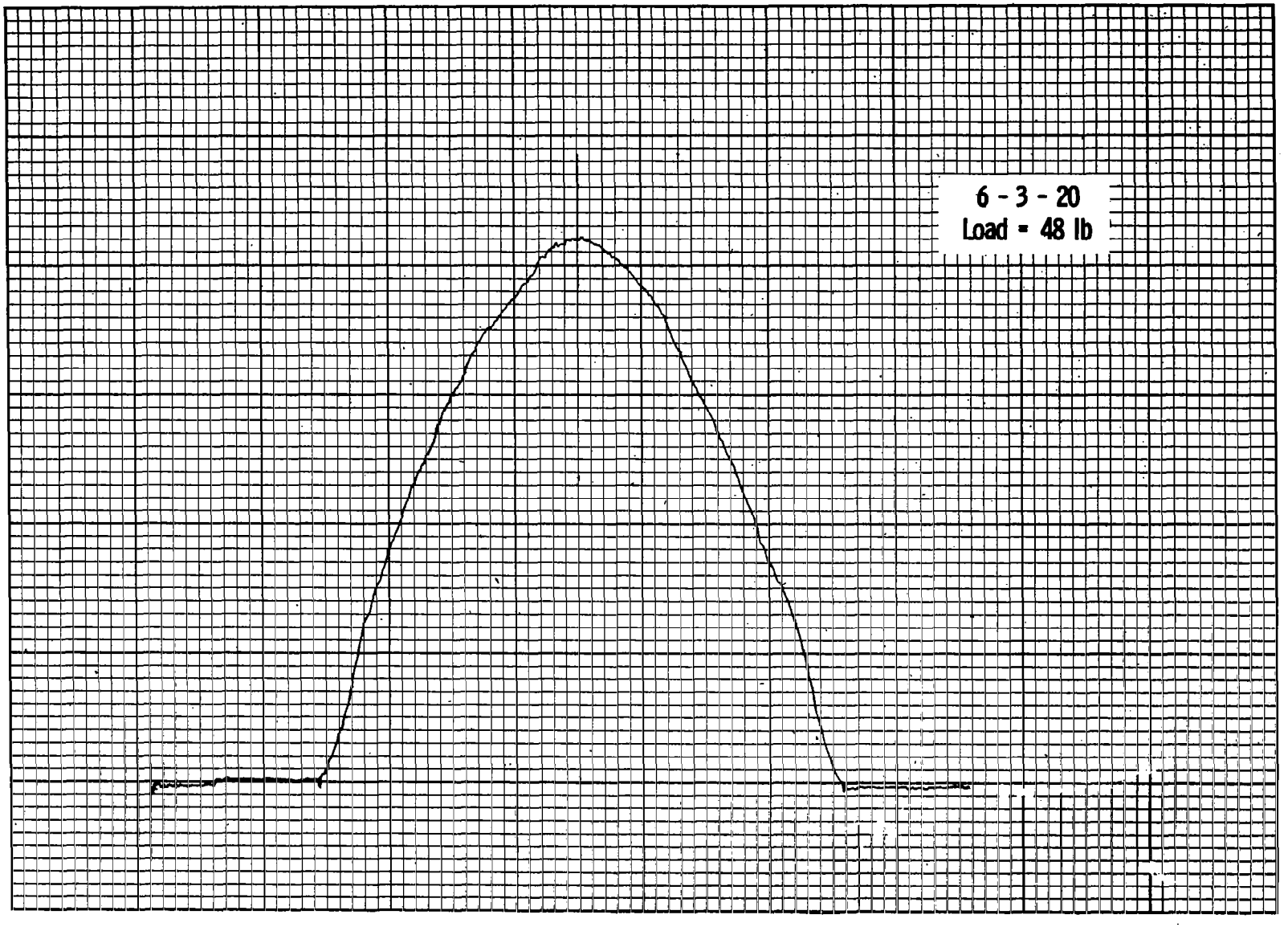
6 - 3 - 20
Load = 48 lb

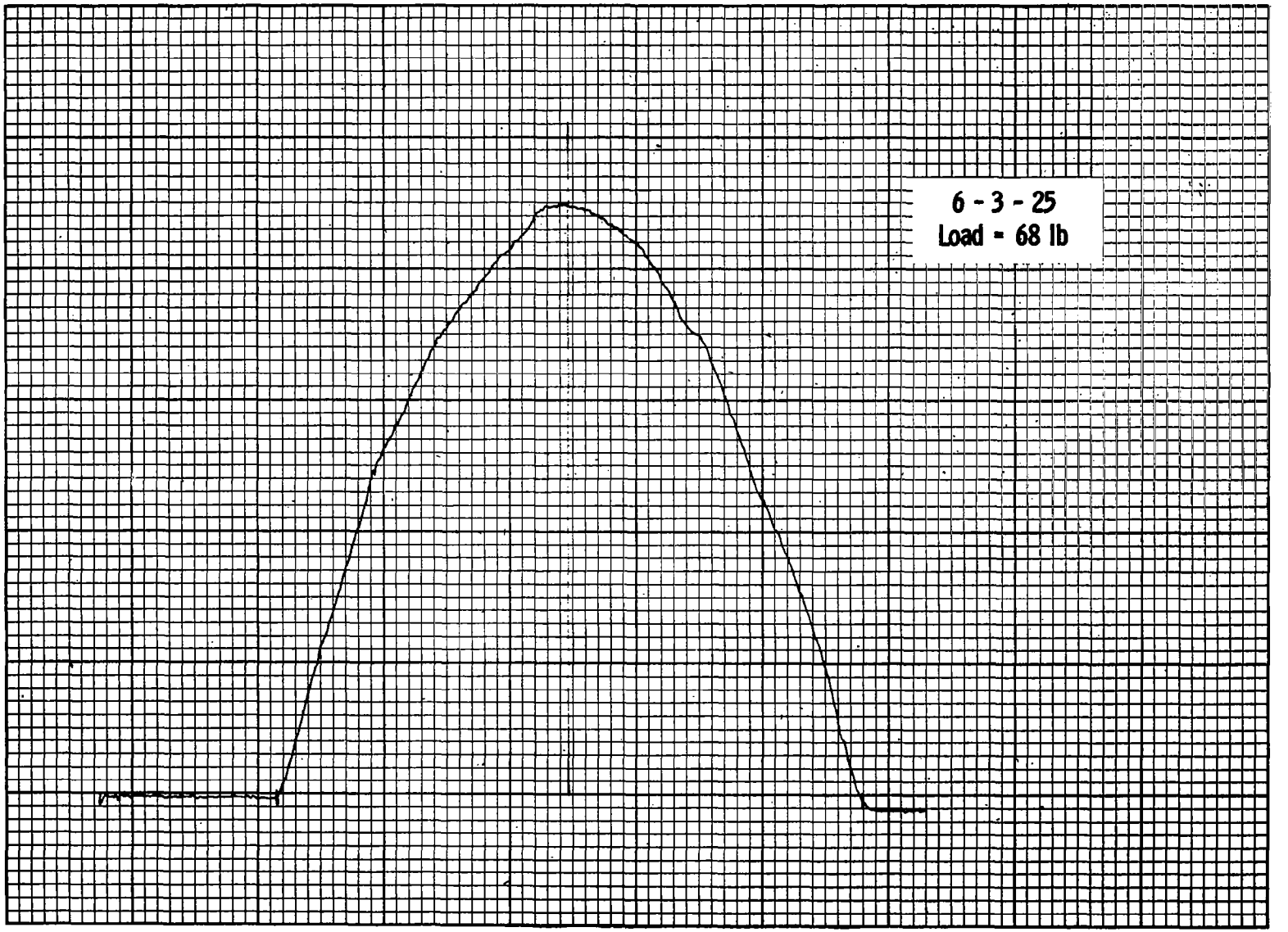
6 - 3 - 25
Load = 68 lb

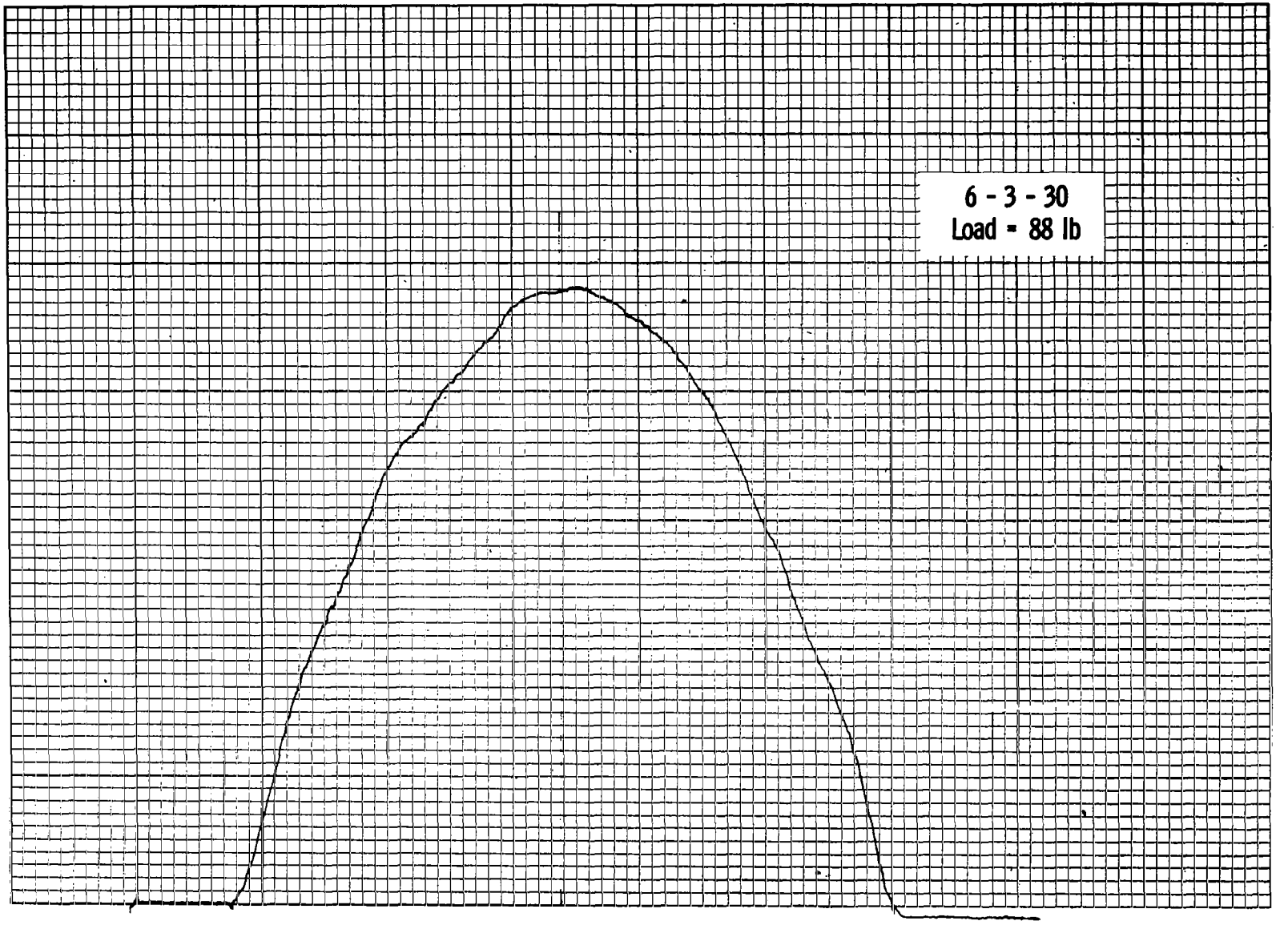
6 - 3 - 30
Load = 88 lb

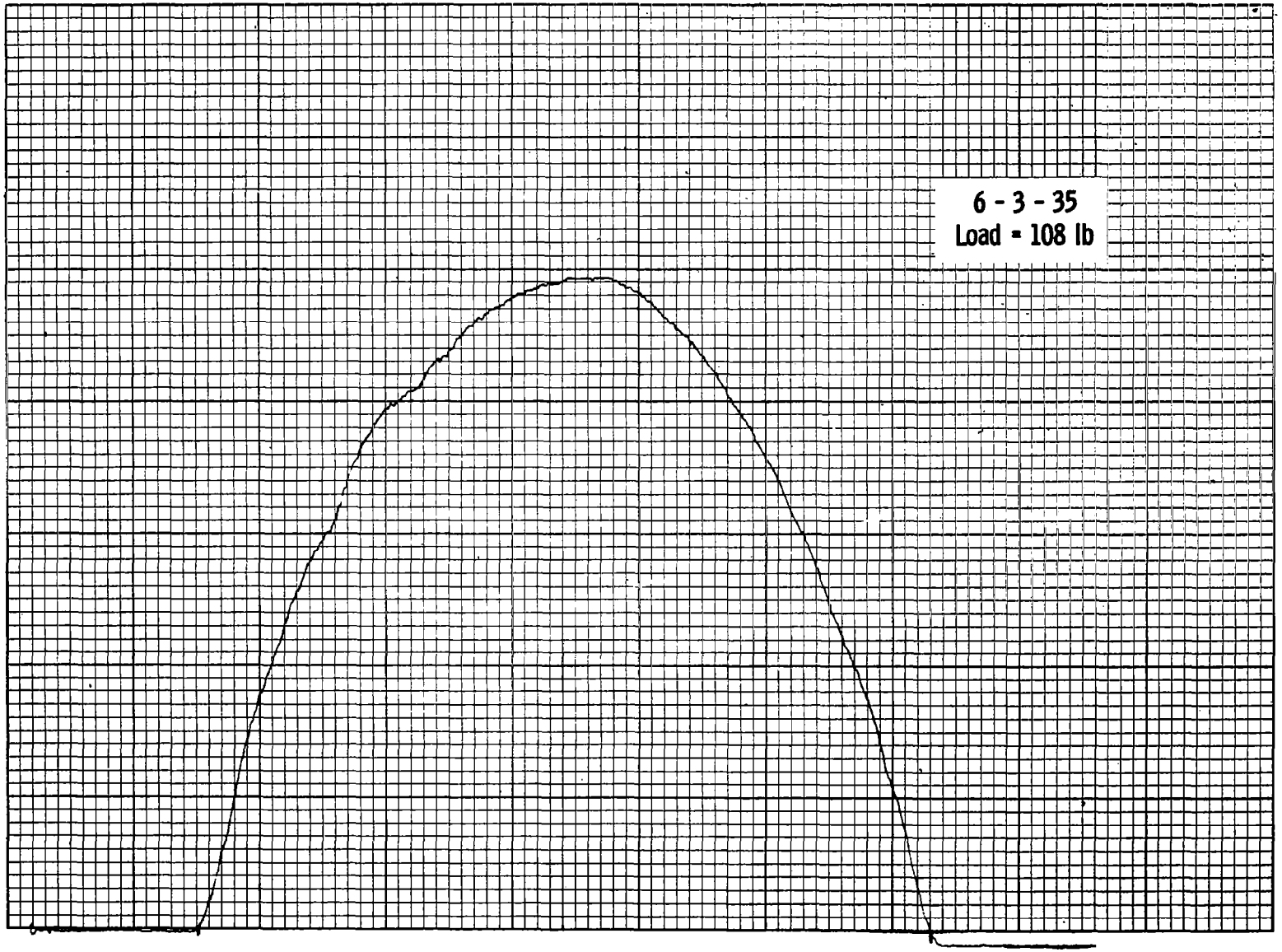
6 - 3 - 35
Load = 108 lb

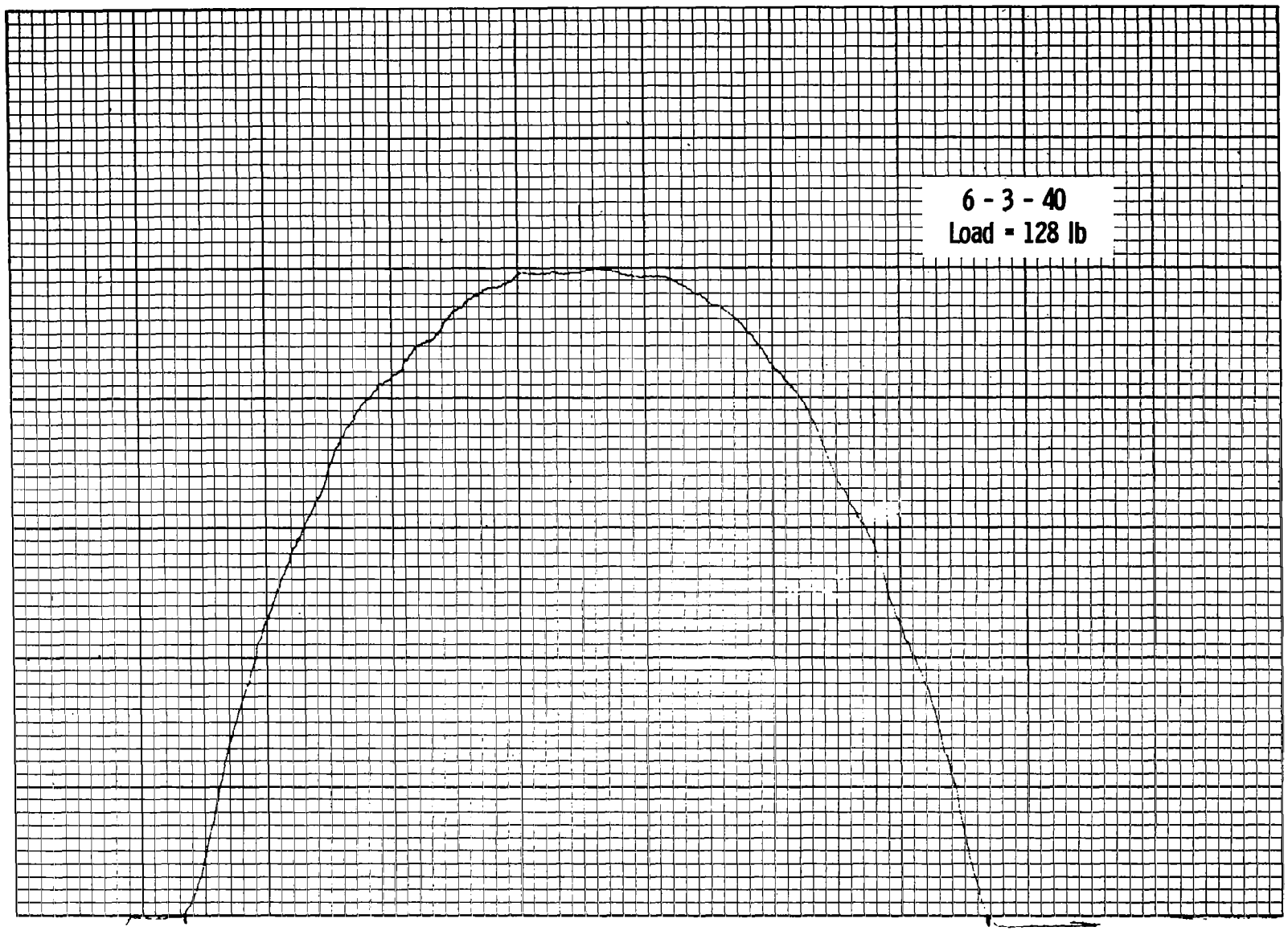
6 - 3 - 40
Load = 128 lb

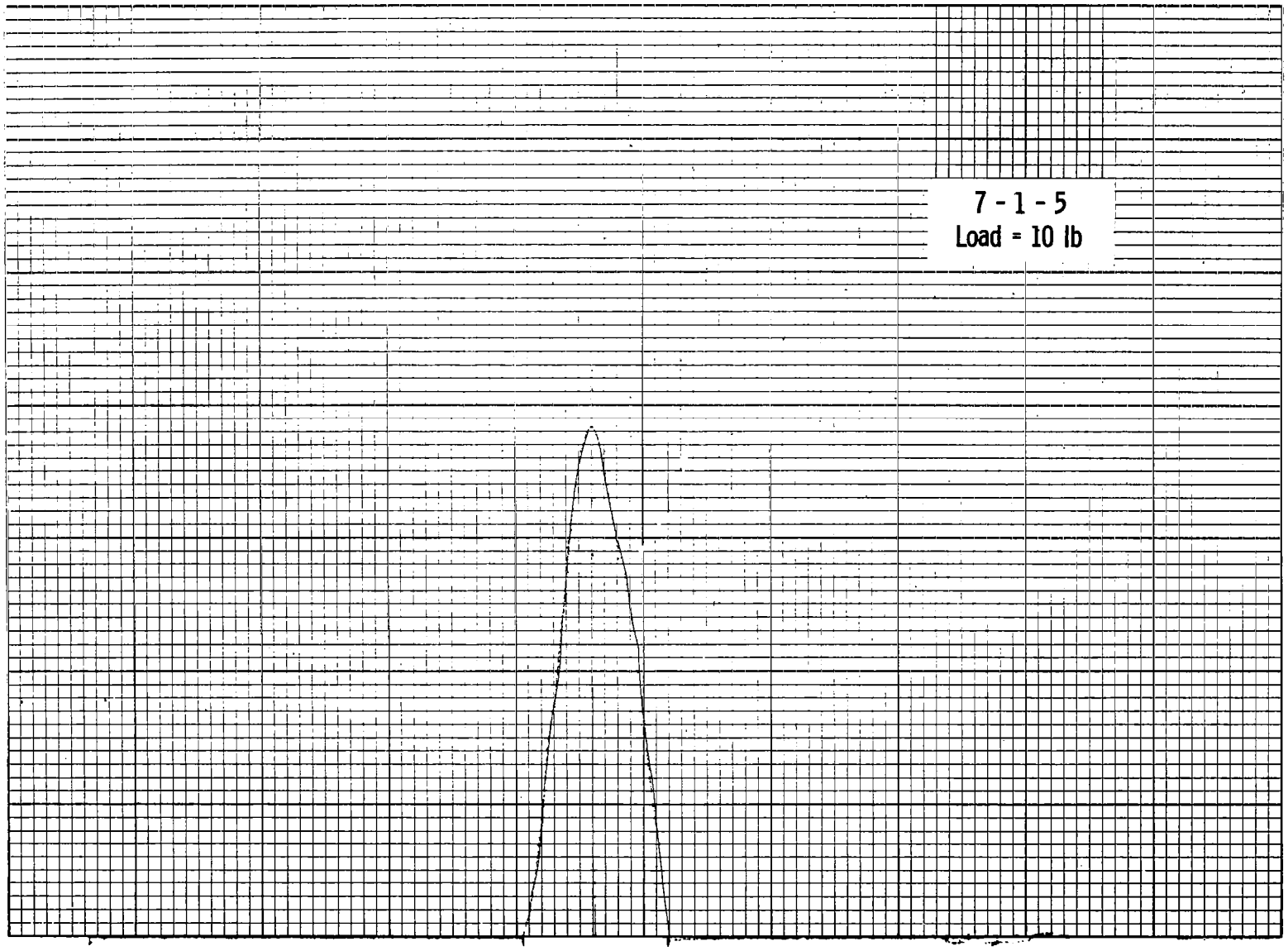
7 - 1 - 5
Load = 10 lb

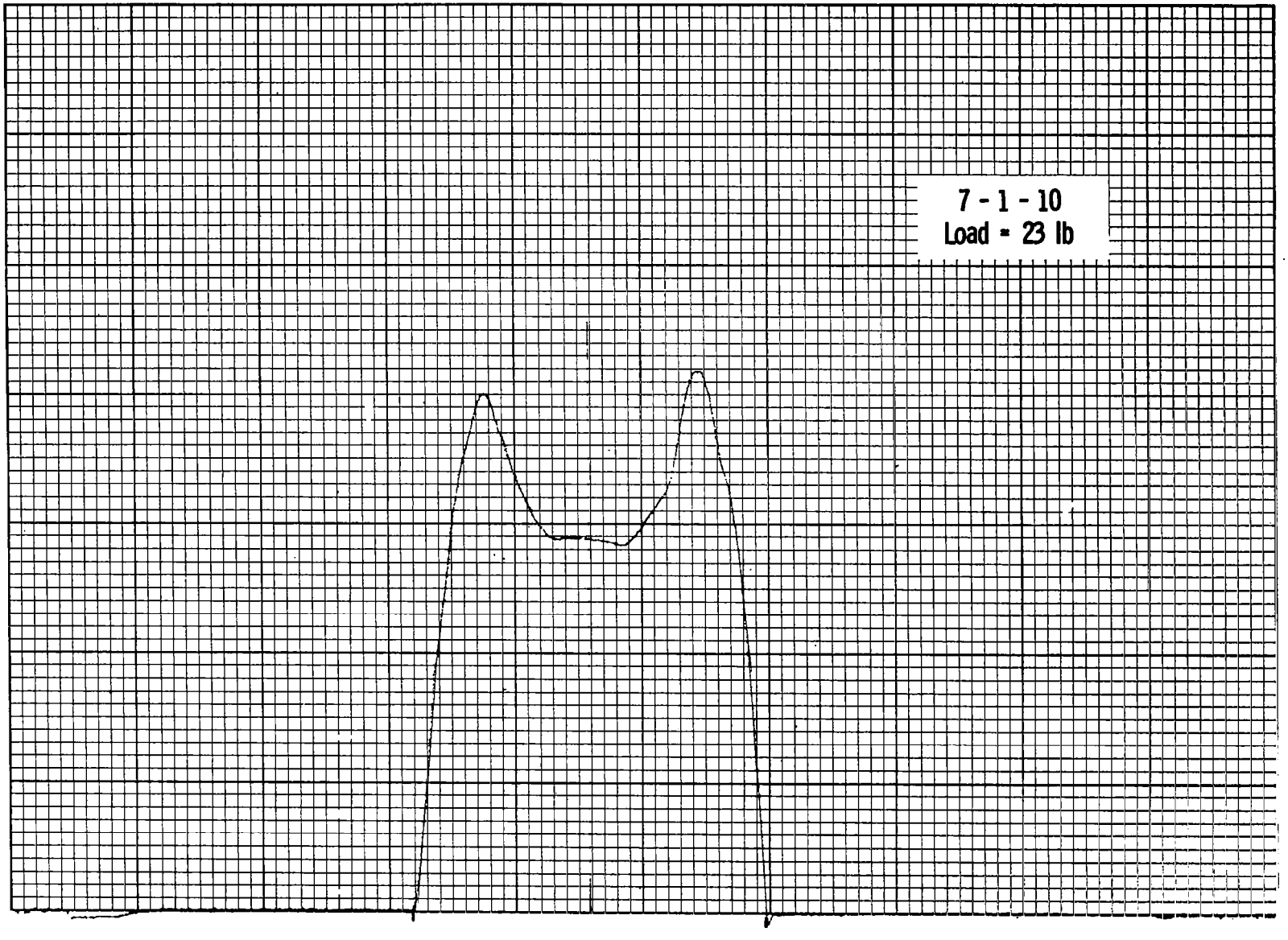
7 - 1 - 10
Load = 23 lb


7 - 1 - 15
Load = 45 lb


7 - 1 - 20
Load = 70 lb

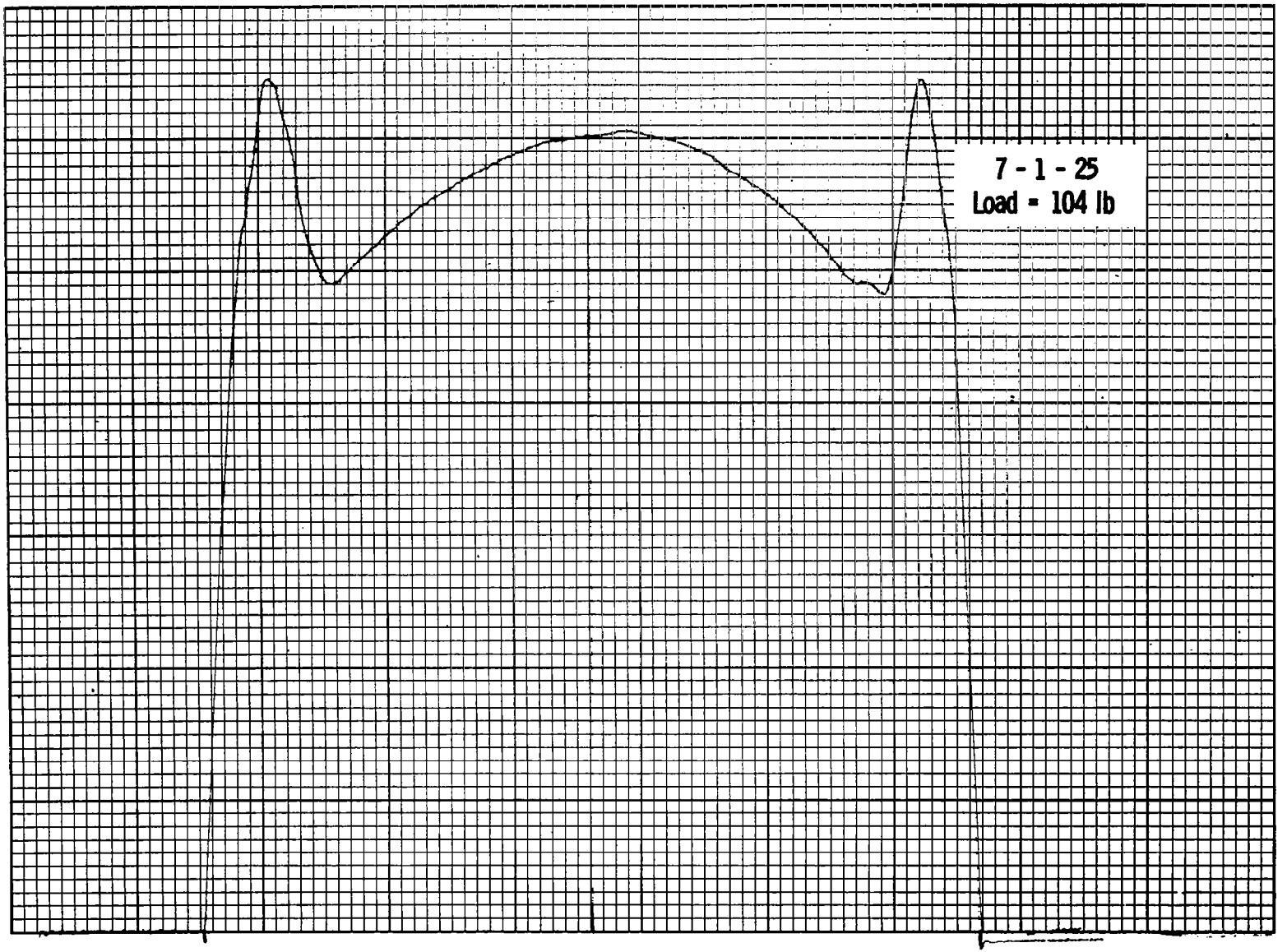
7 - 1 - 25
Load = 104 lb

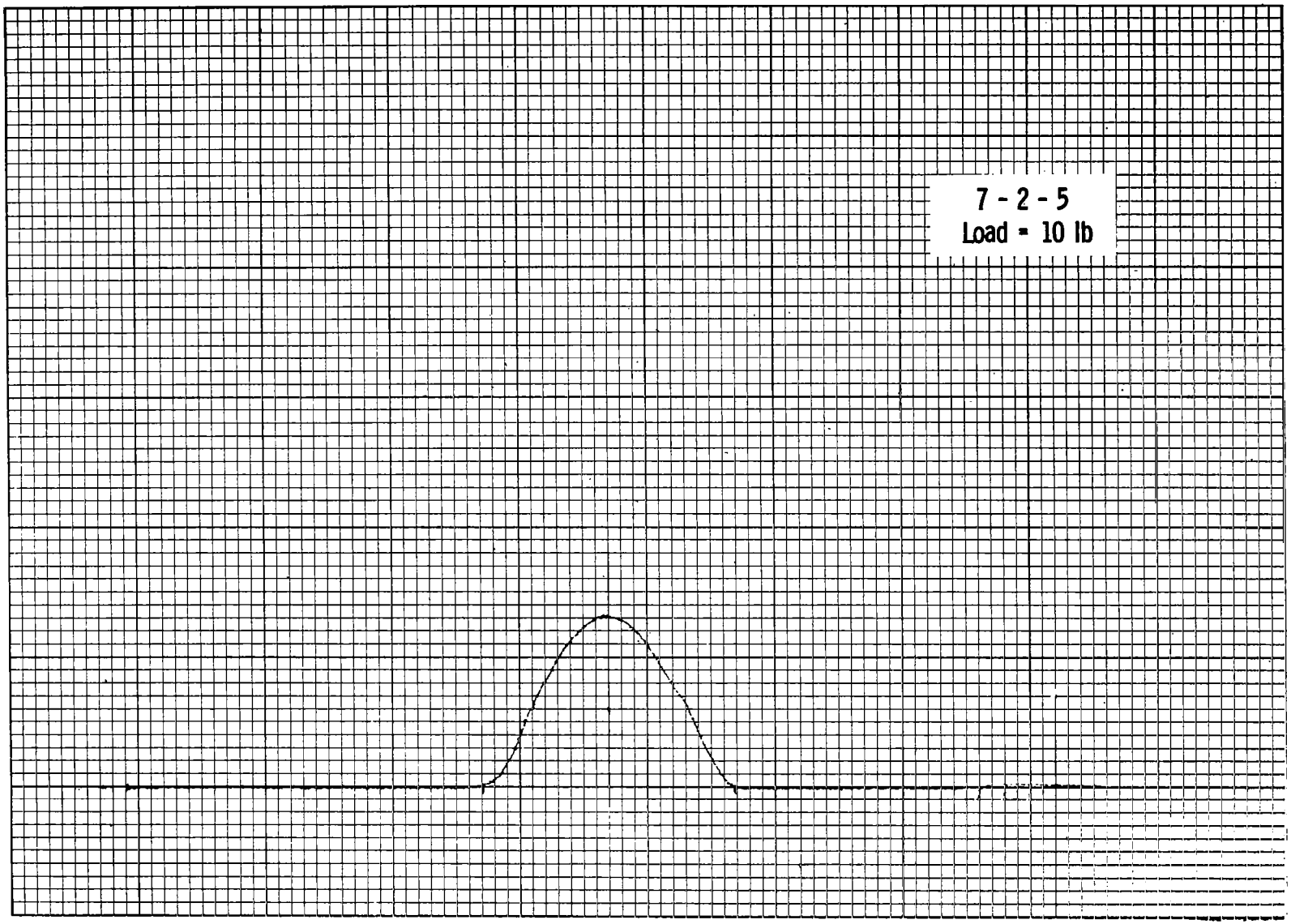
7 - 2 - 5
Load = 10 lb

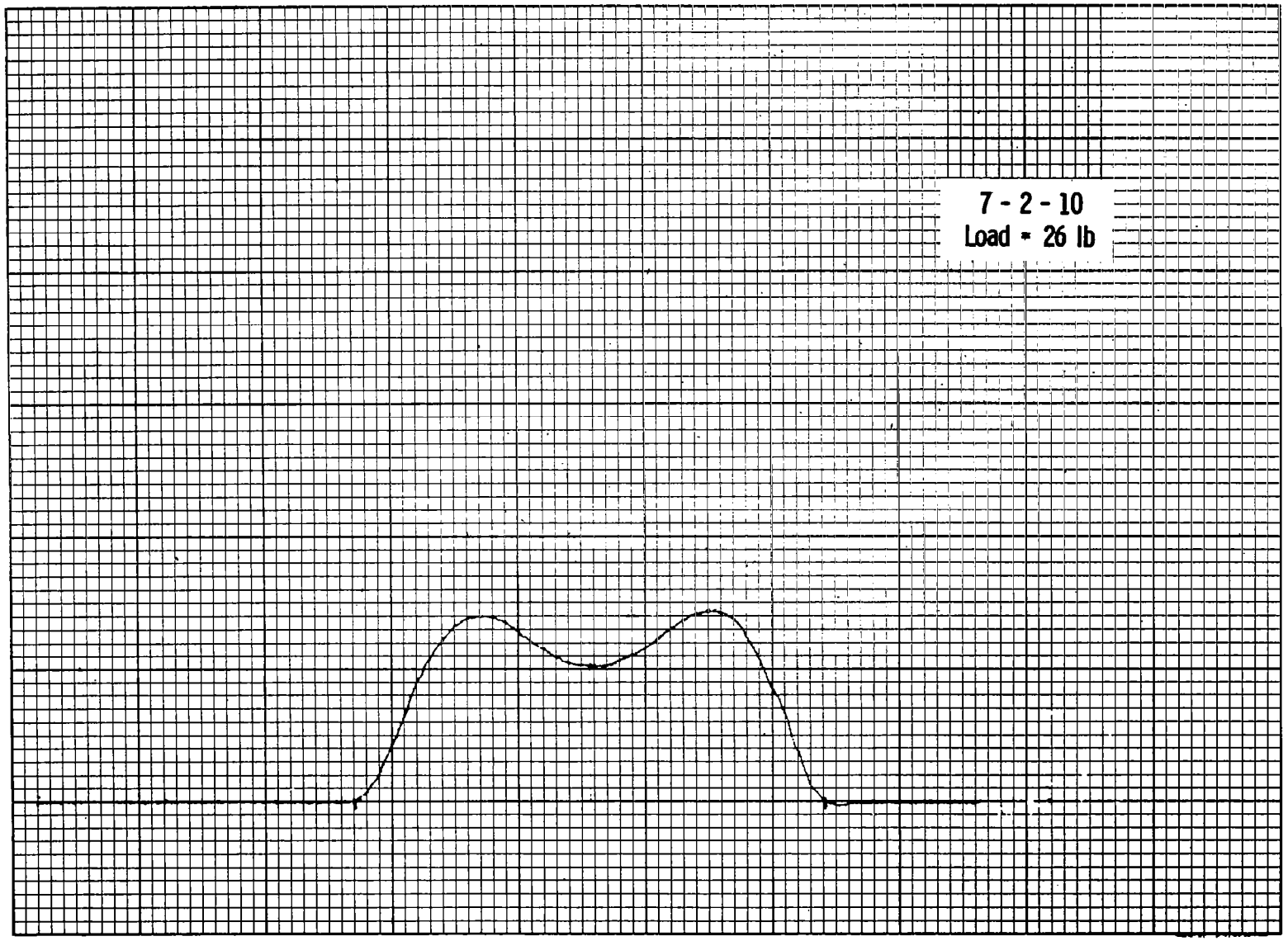
7 - 2 - 10
Load = 26 lb

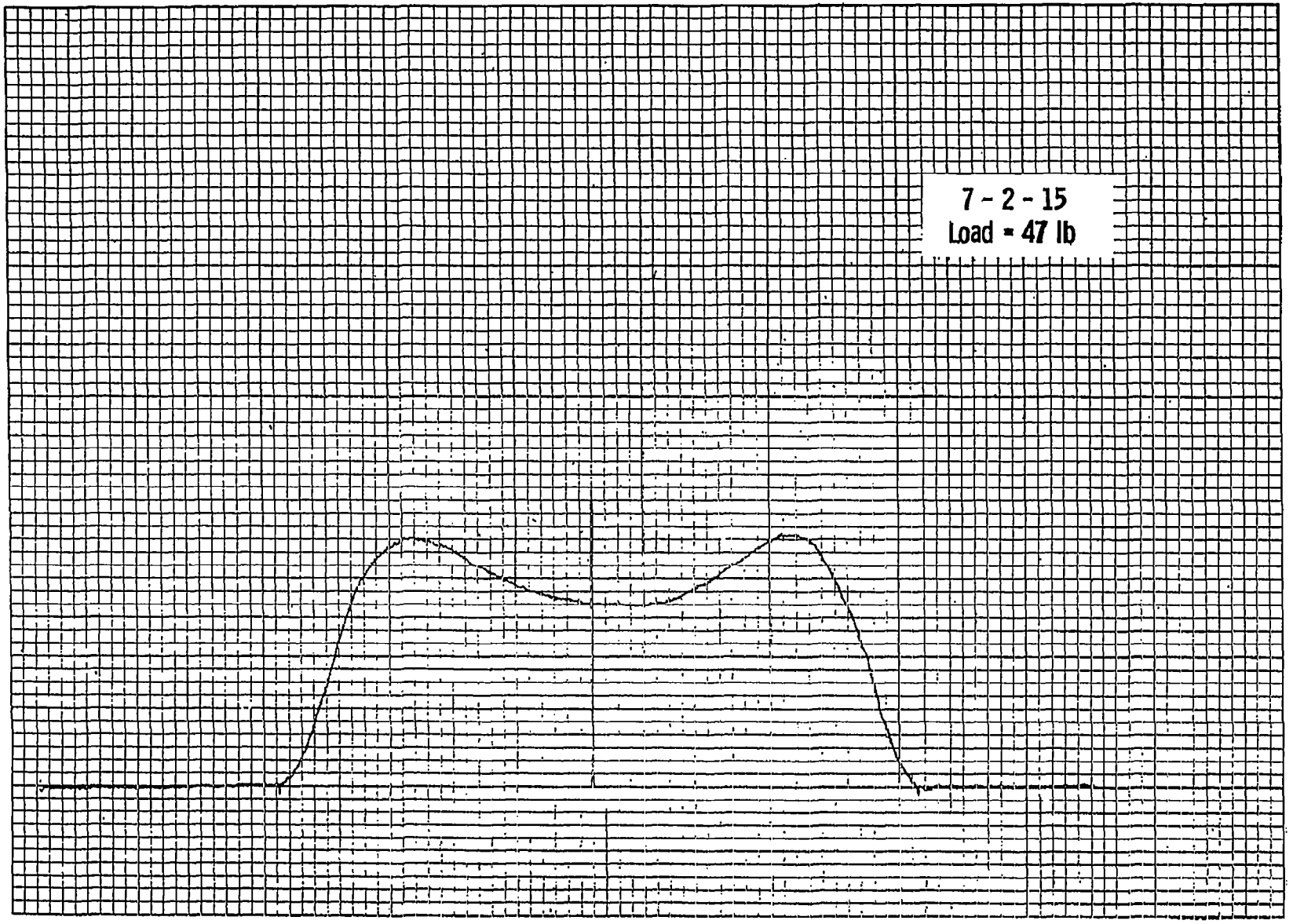
7 - 2 - 15
Load = 47 lb

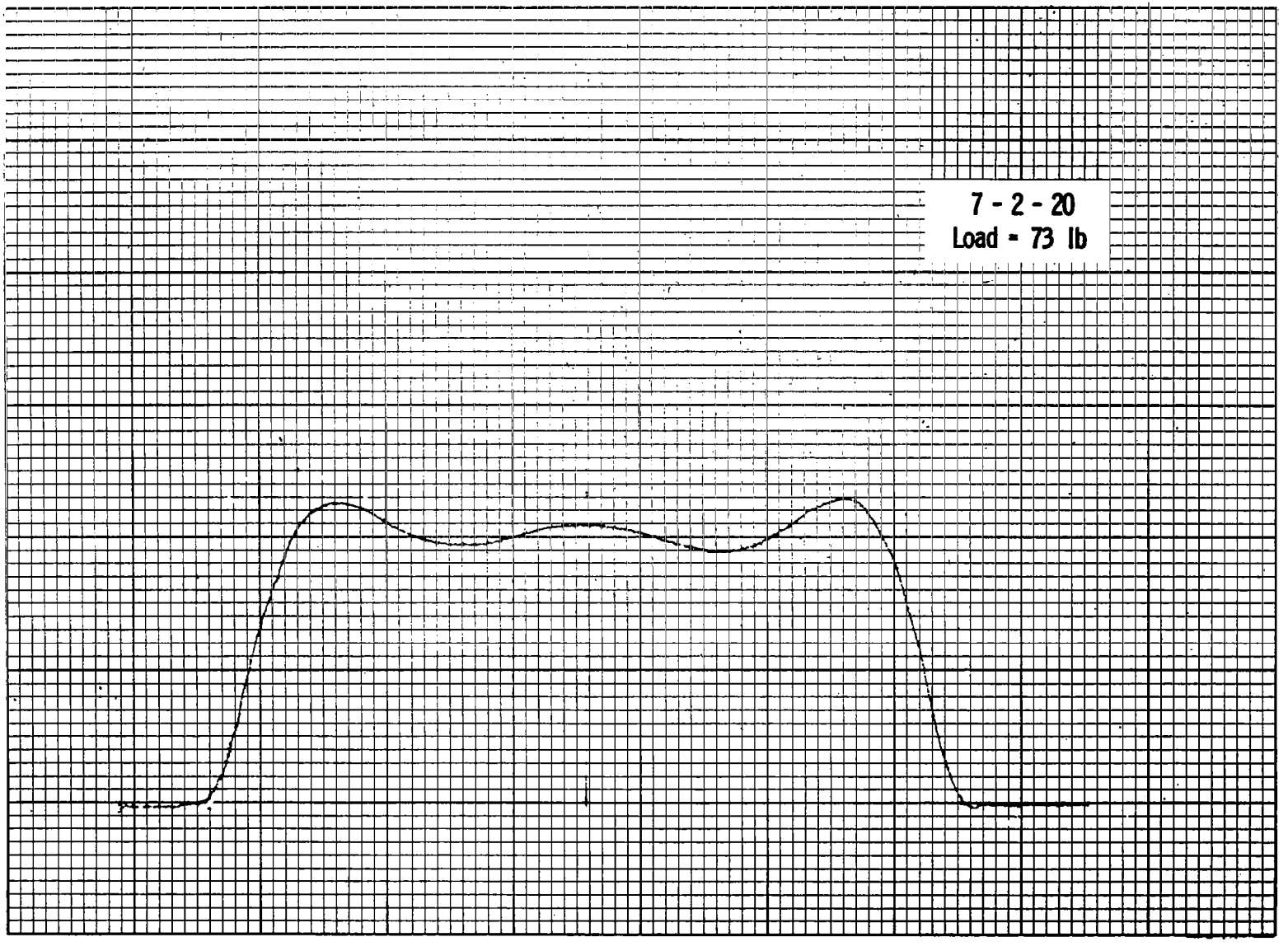
7 - 2 - 20
Load = 73 lb

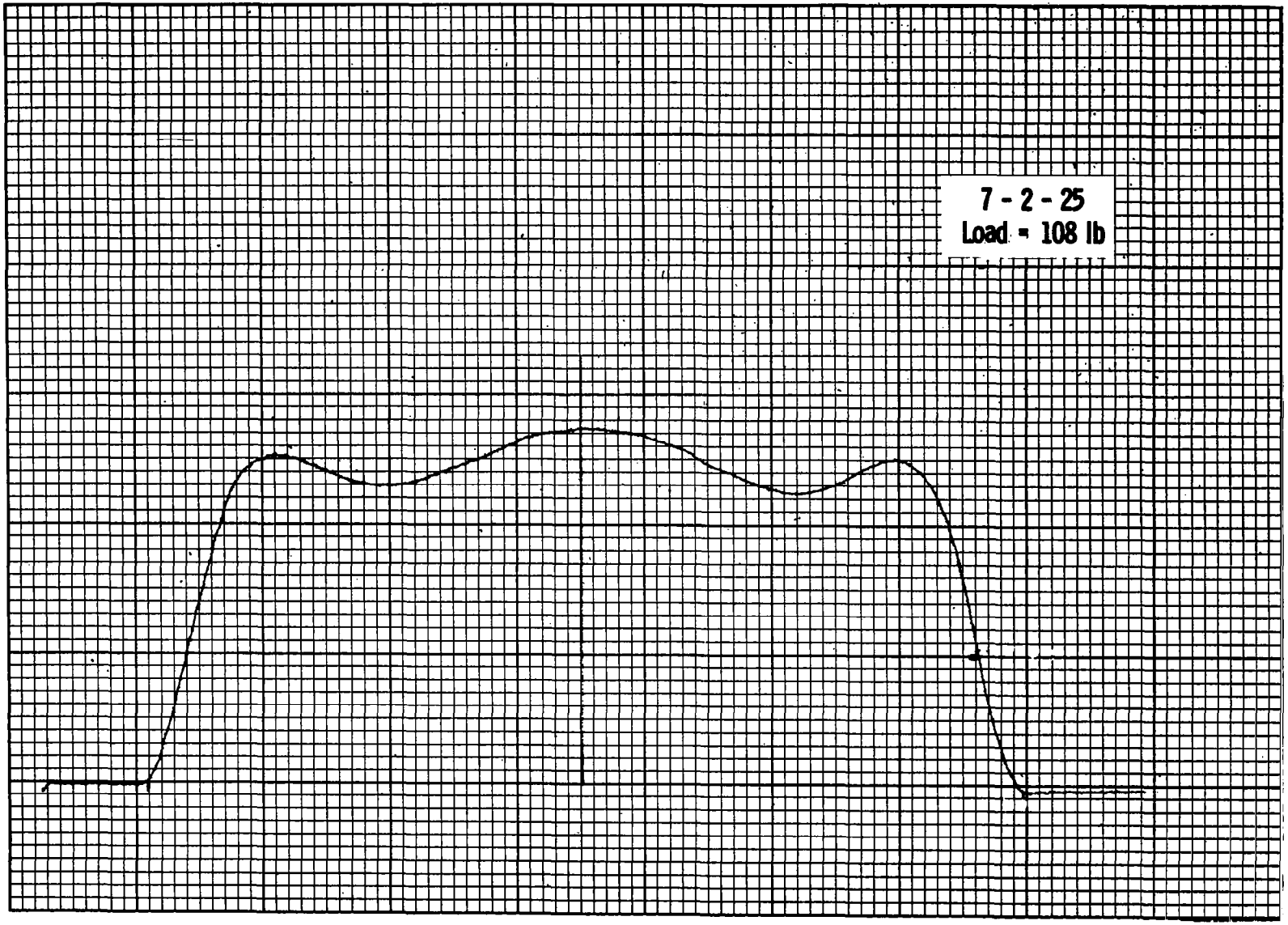
7 - 2 - 25
Load = 108 lb

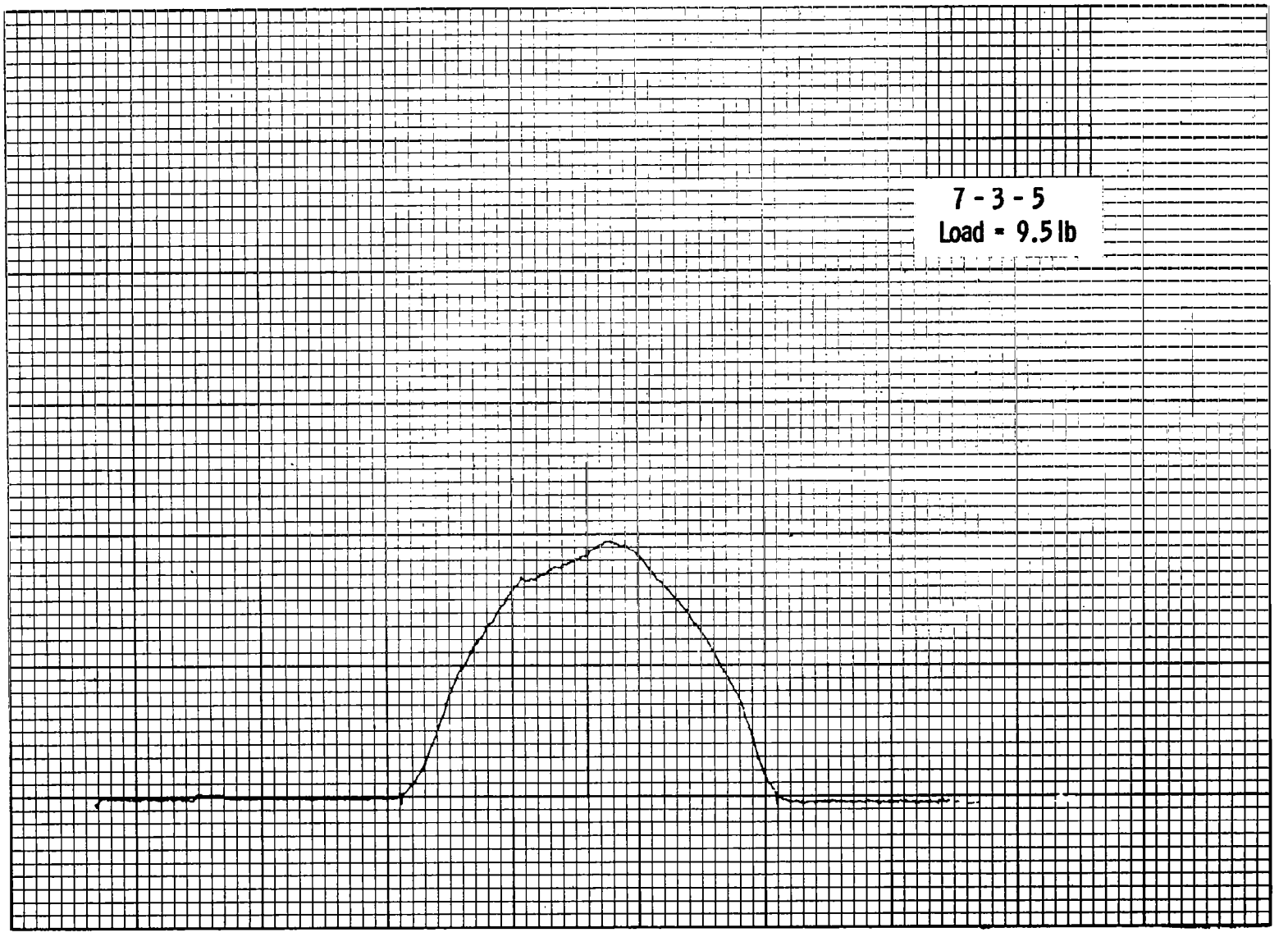
7 - 3 - 5
Load = 9.5 lb

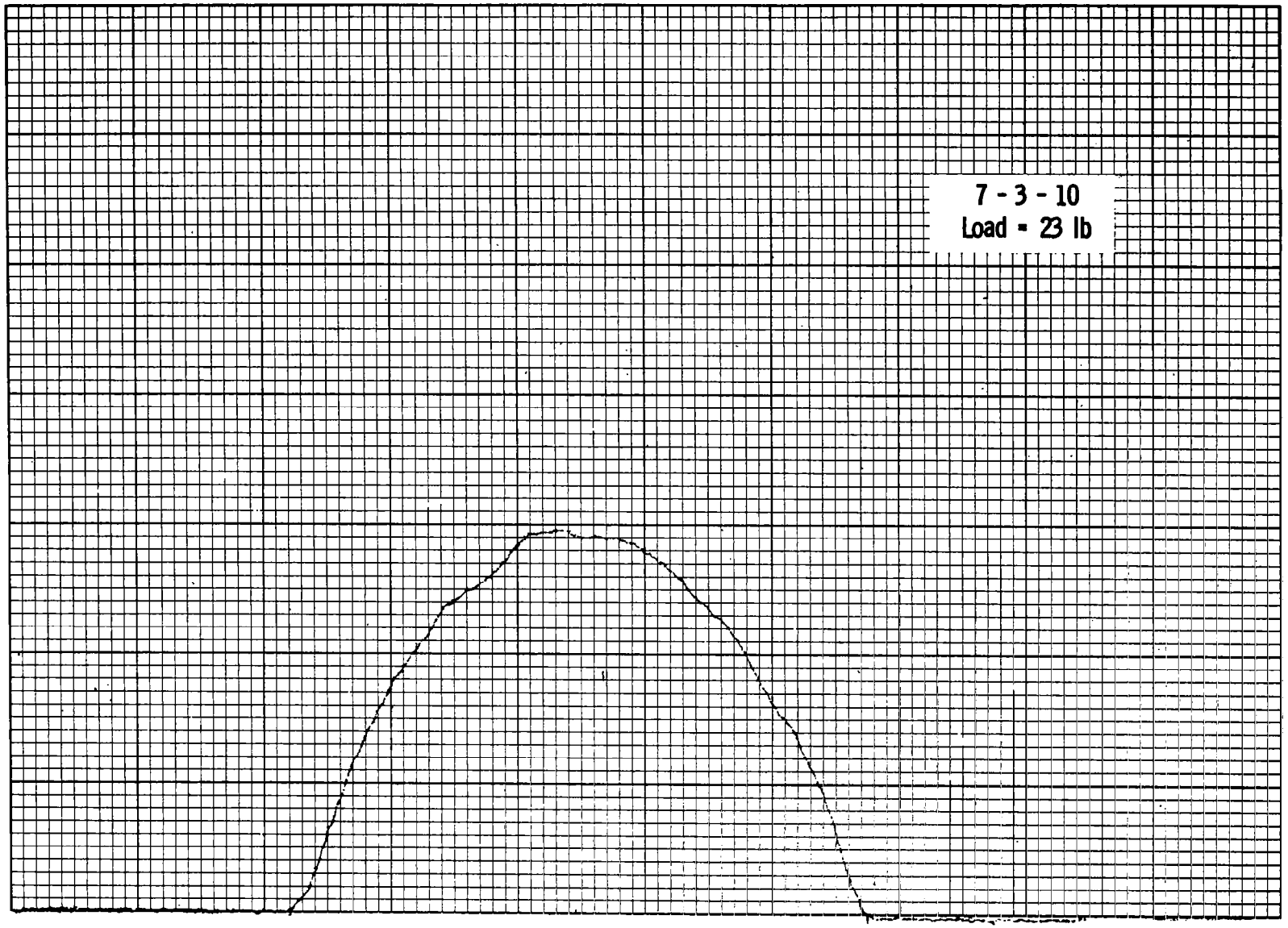
7 - 3 - 10
Load = 23 lb

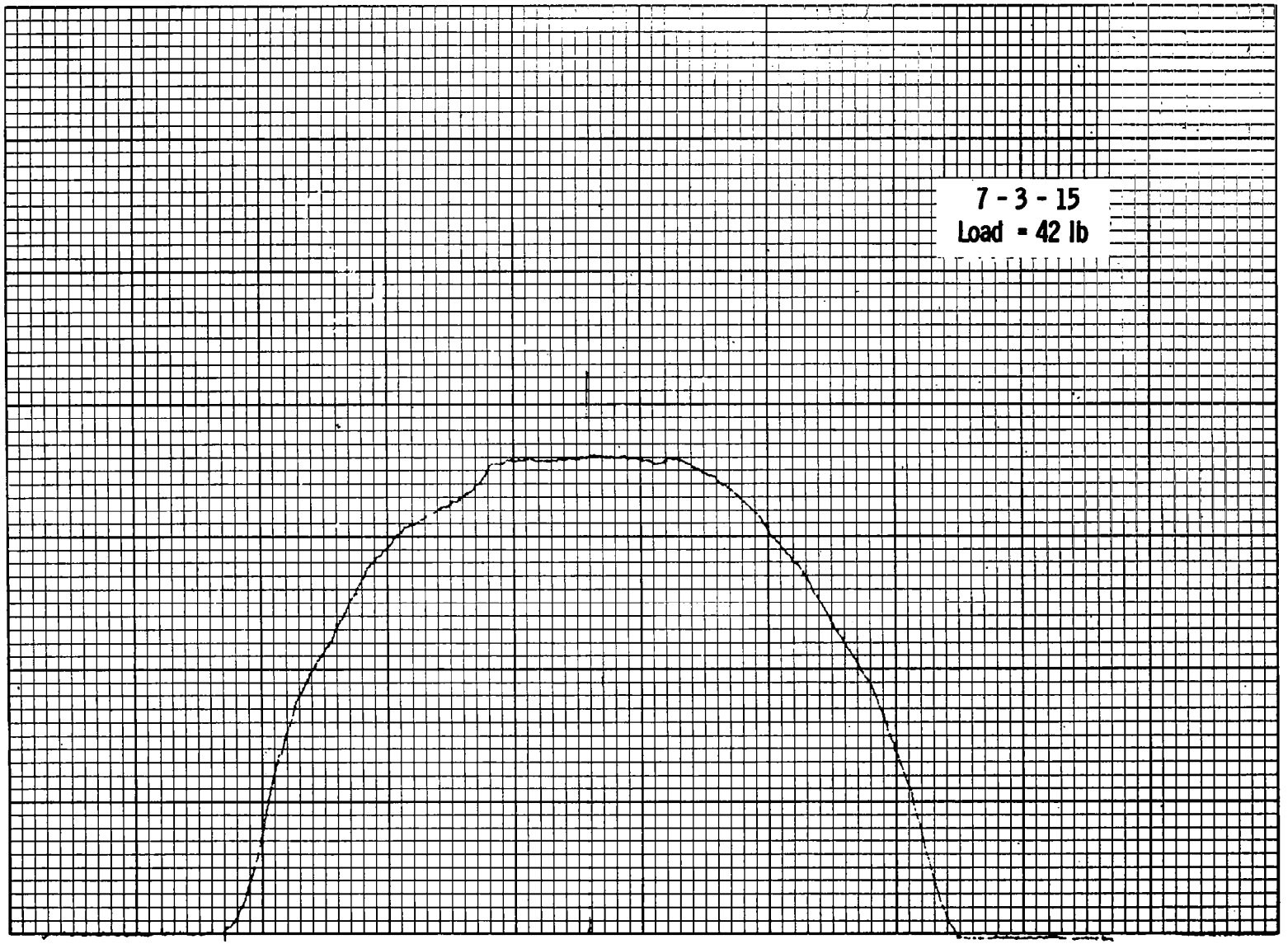
7 - 3 - 15
Load = 42 lb

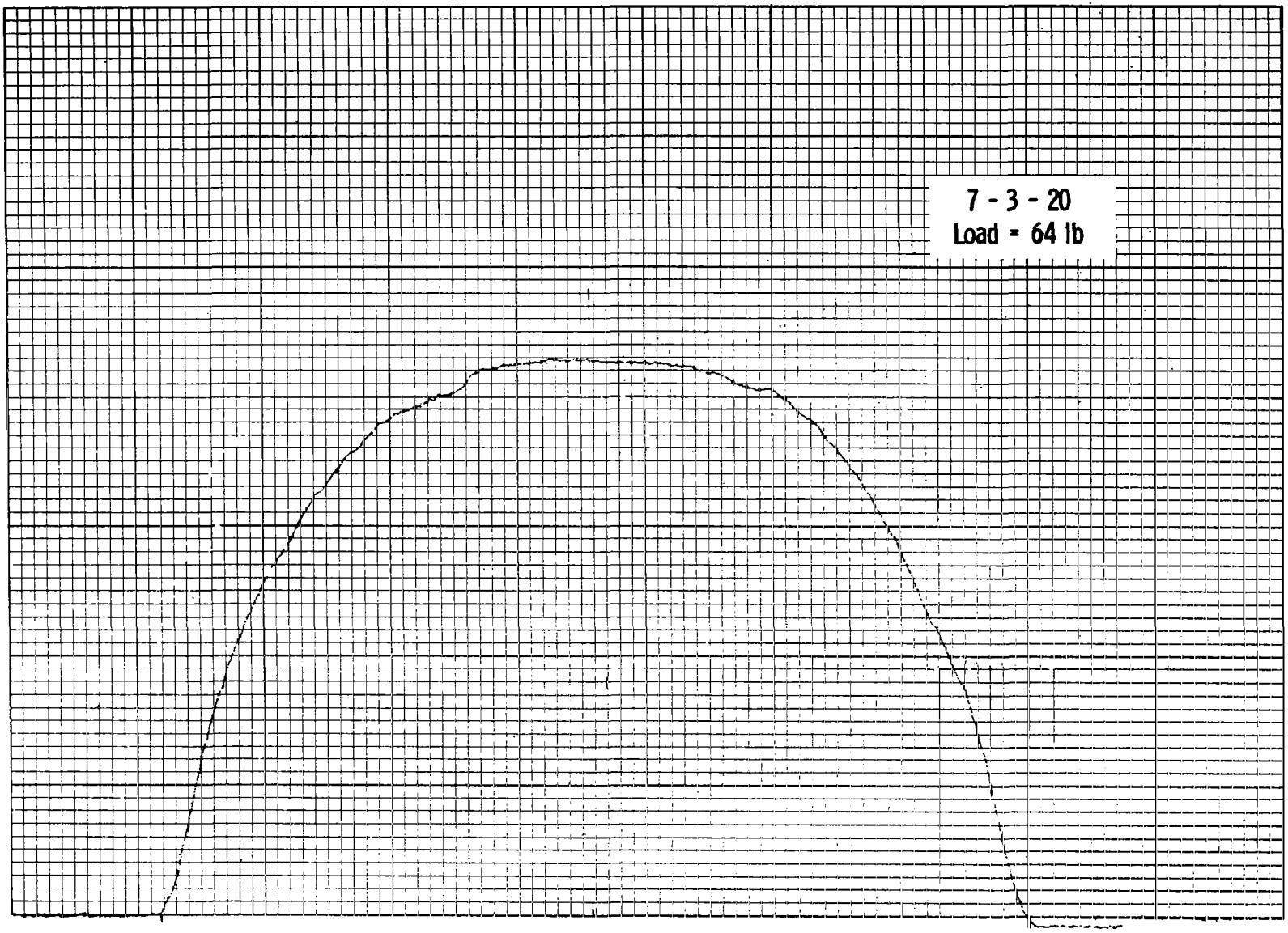
7 - 3 - 20
Load = 64 lb

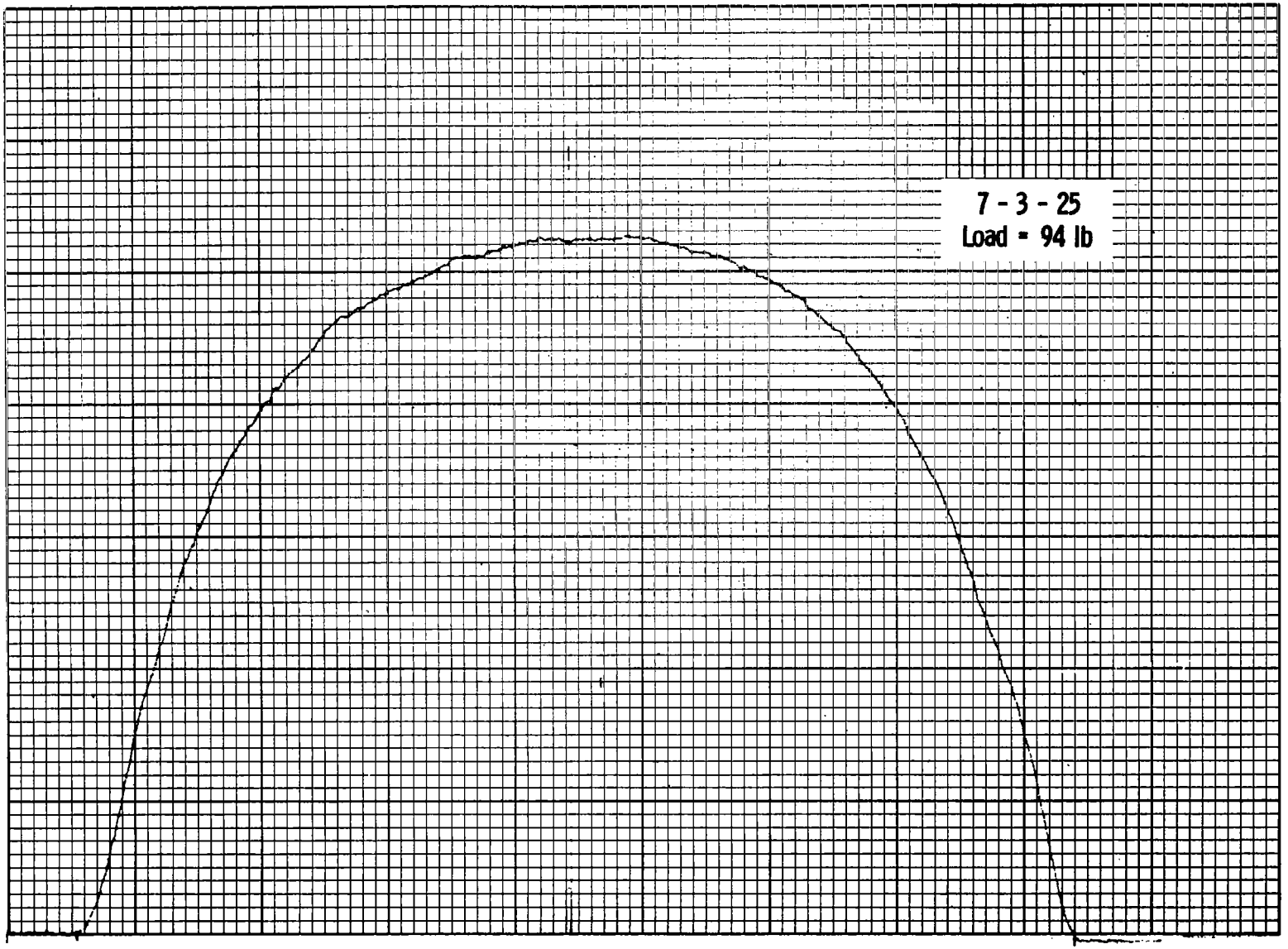
7 - 3 - 25
Load = 94 lb

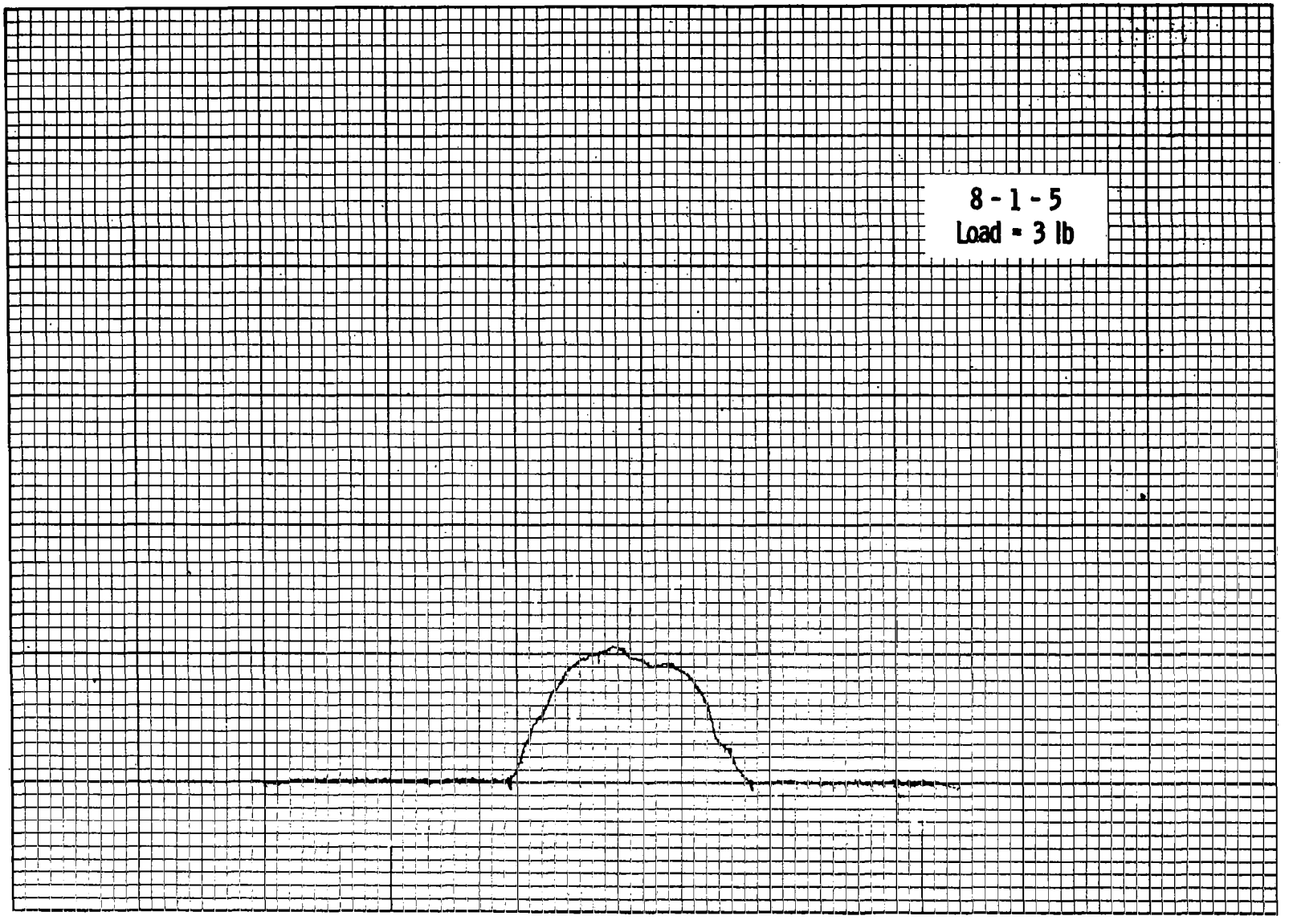
8 - 1 - 5
Load = 3 lb

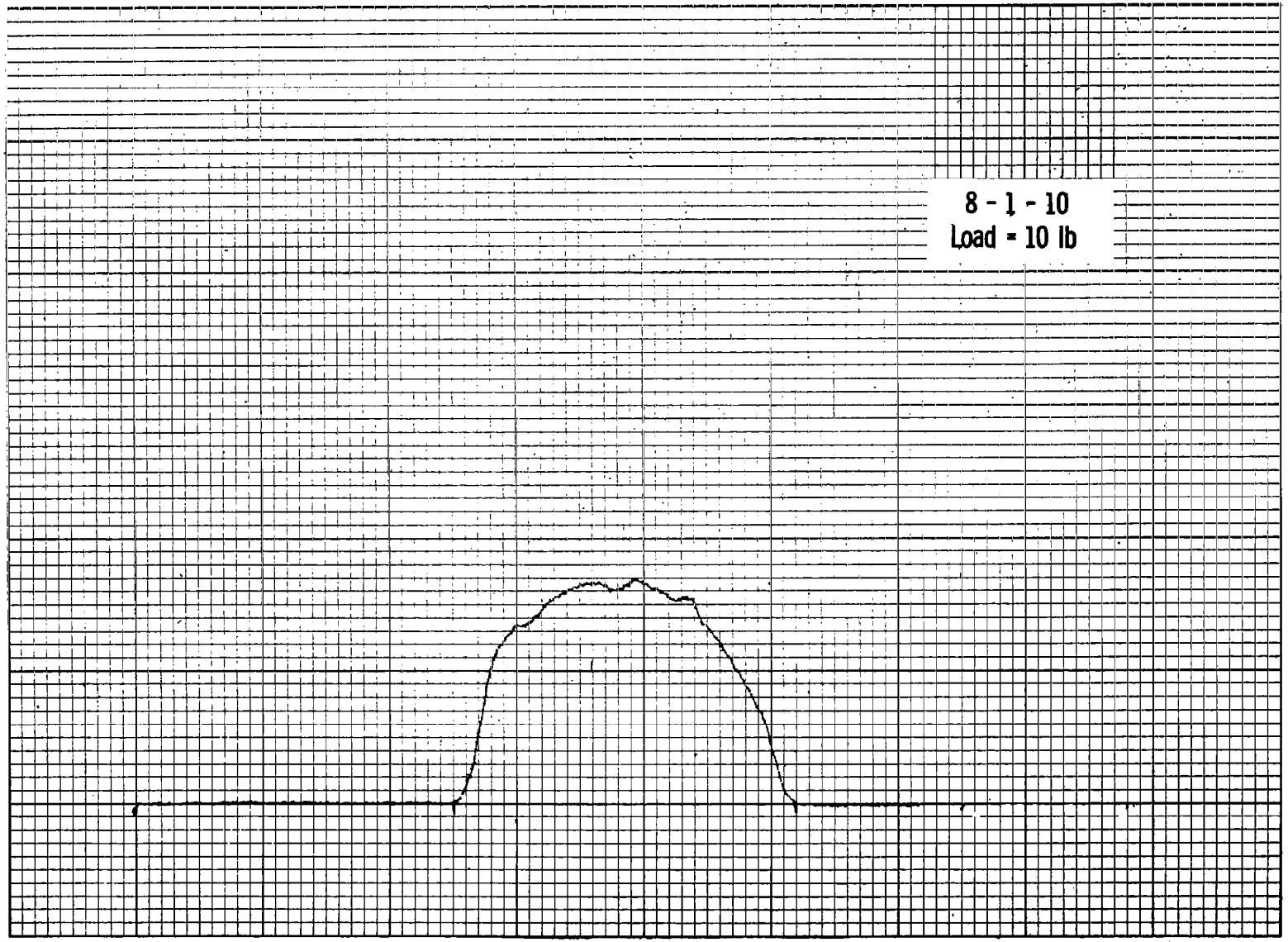
8 - 1 - 10
Load = 10 lb

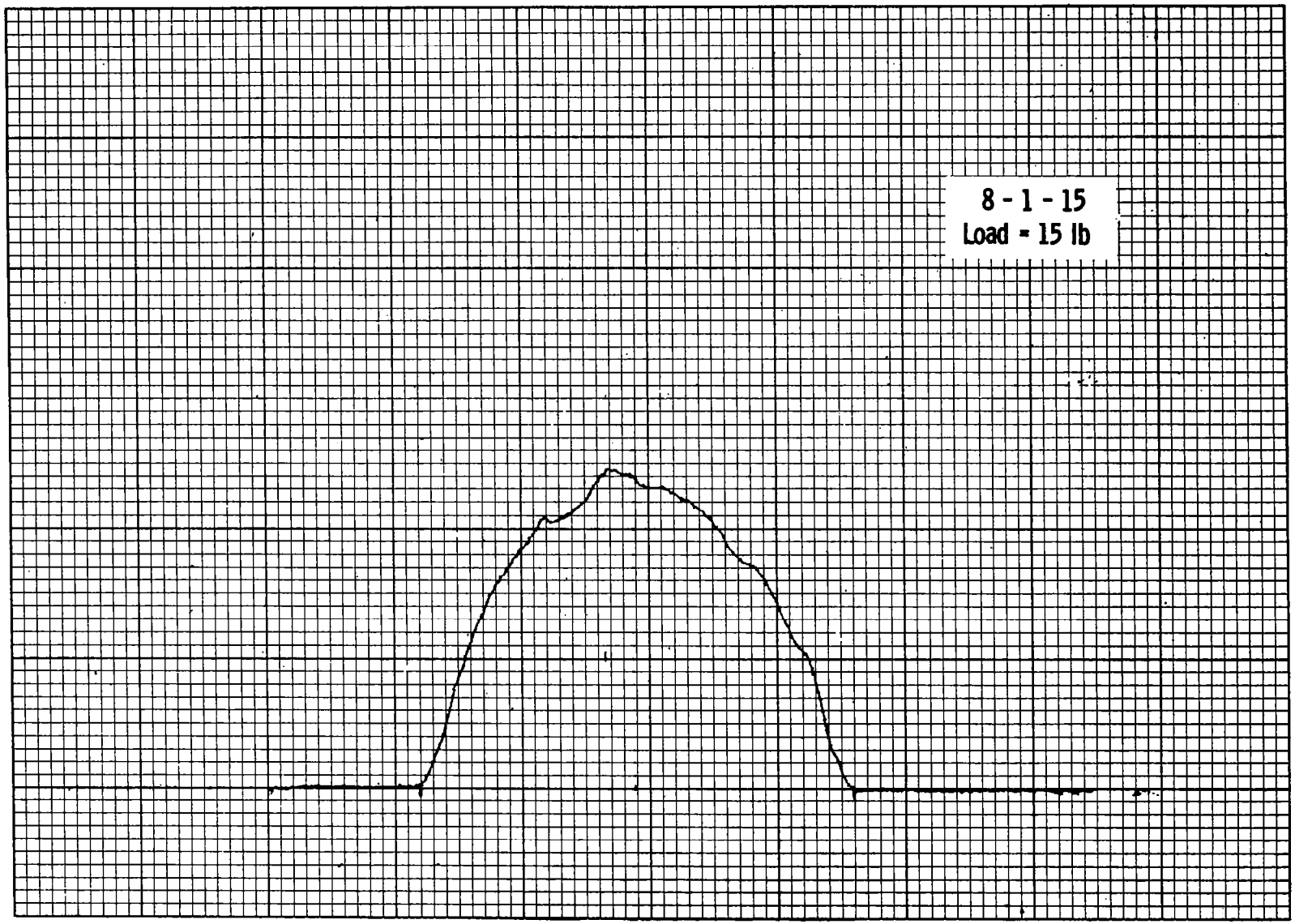
8 - 1 - 15
Load = 15 lb

8 - 1 - 20
Load = 26 lb

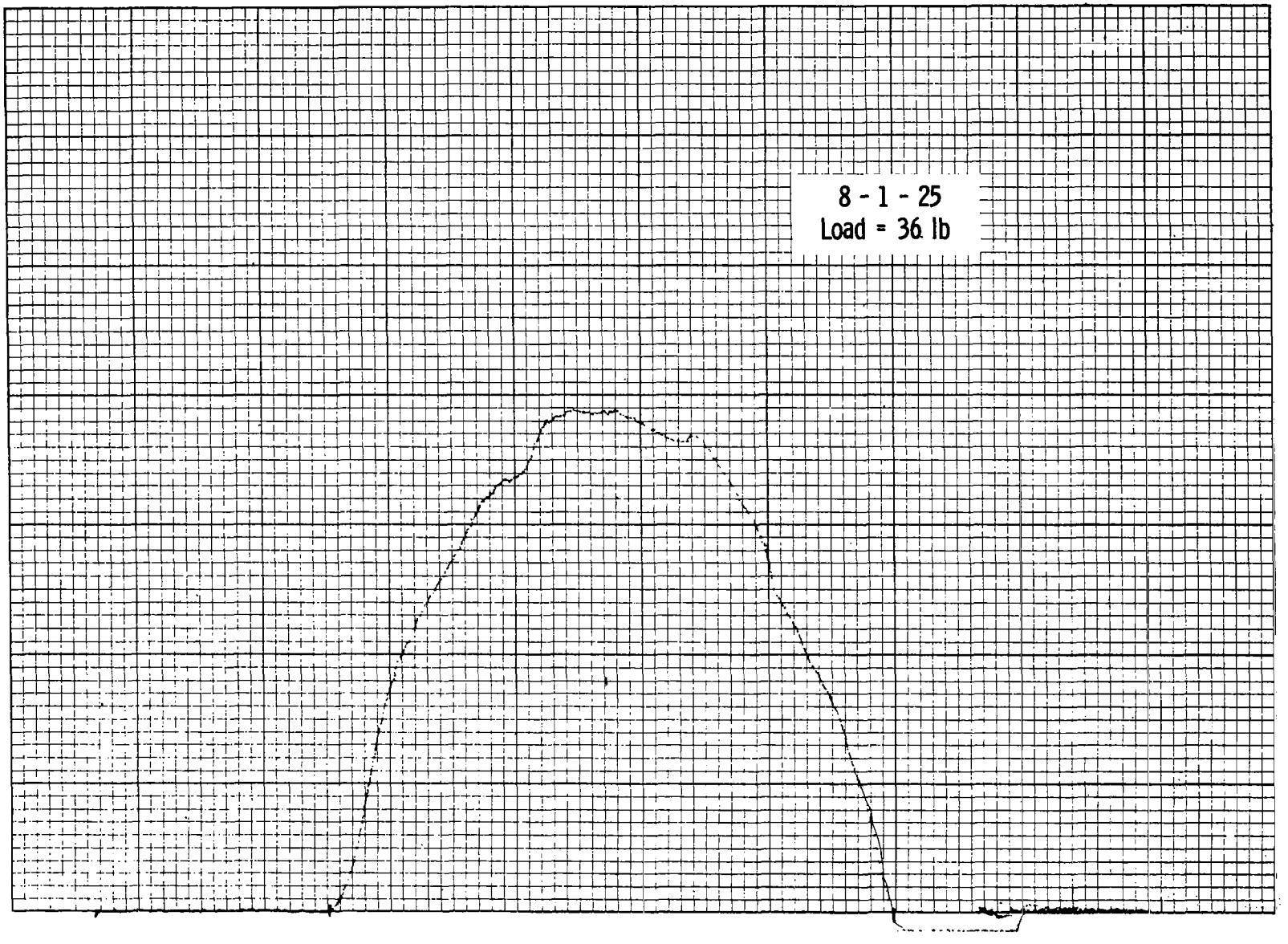
8 - 1 - 25
Load = 36 lb

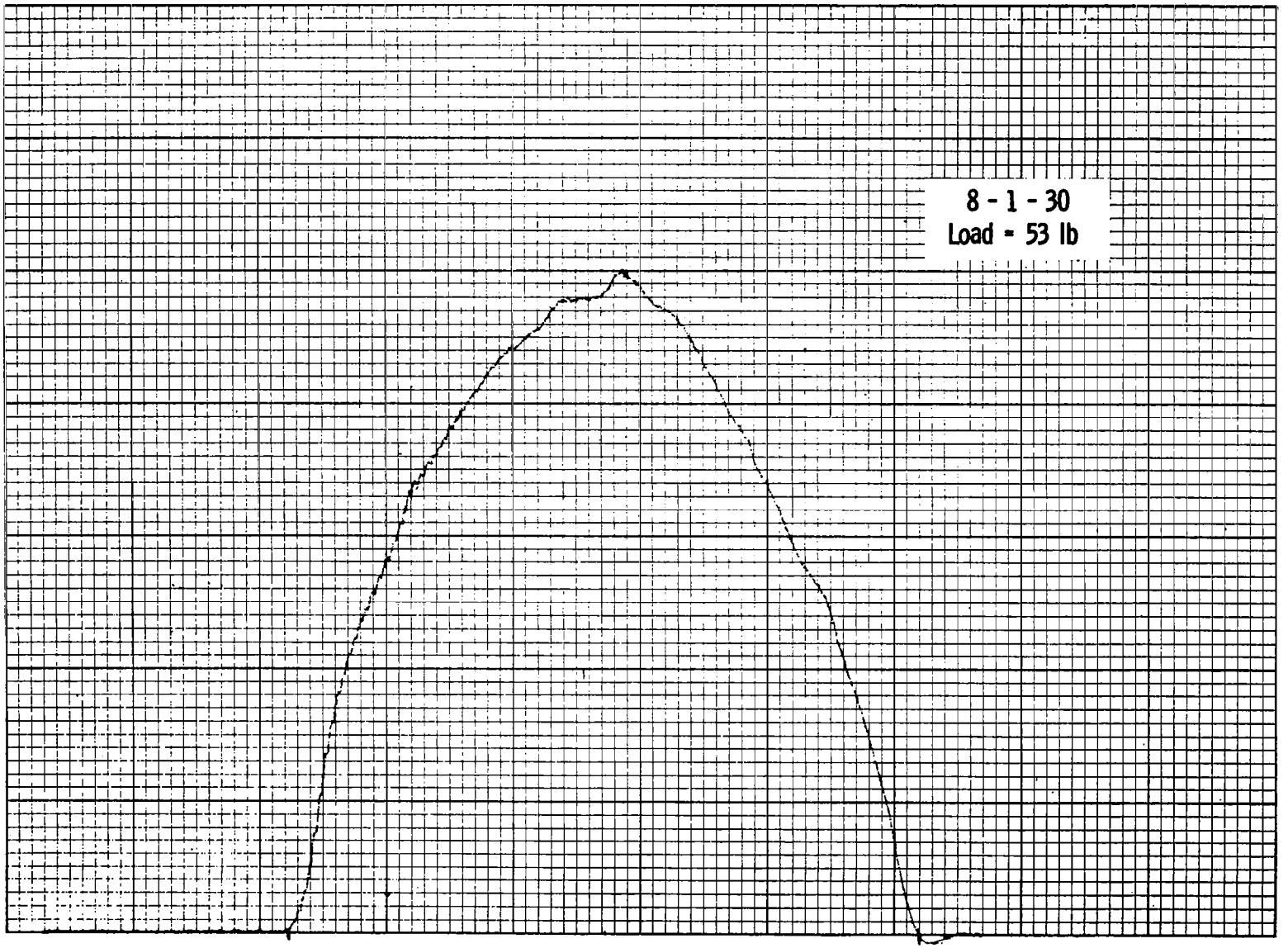
8 - 1 - 30
Load = 53 lb

9 - 1 - 10
Load = 90 lb

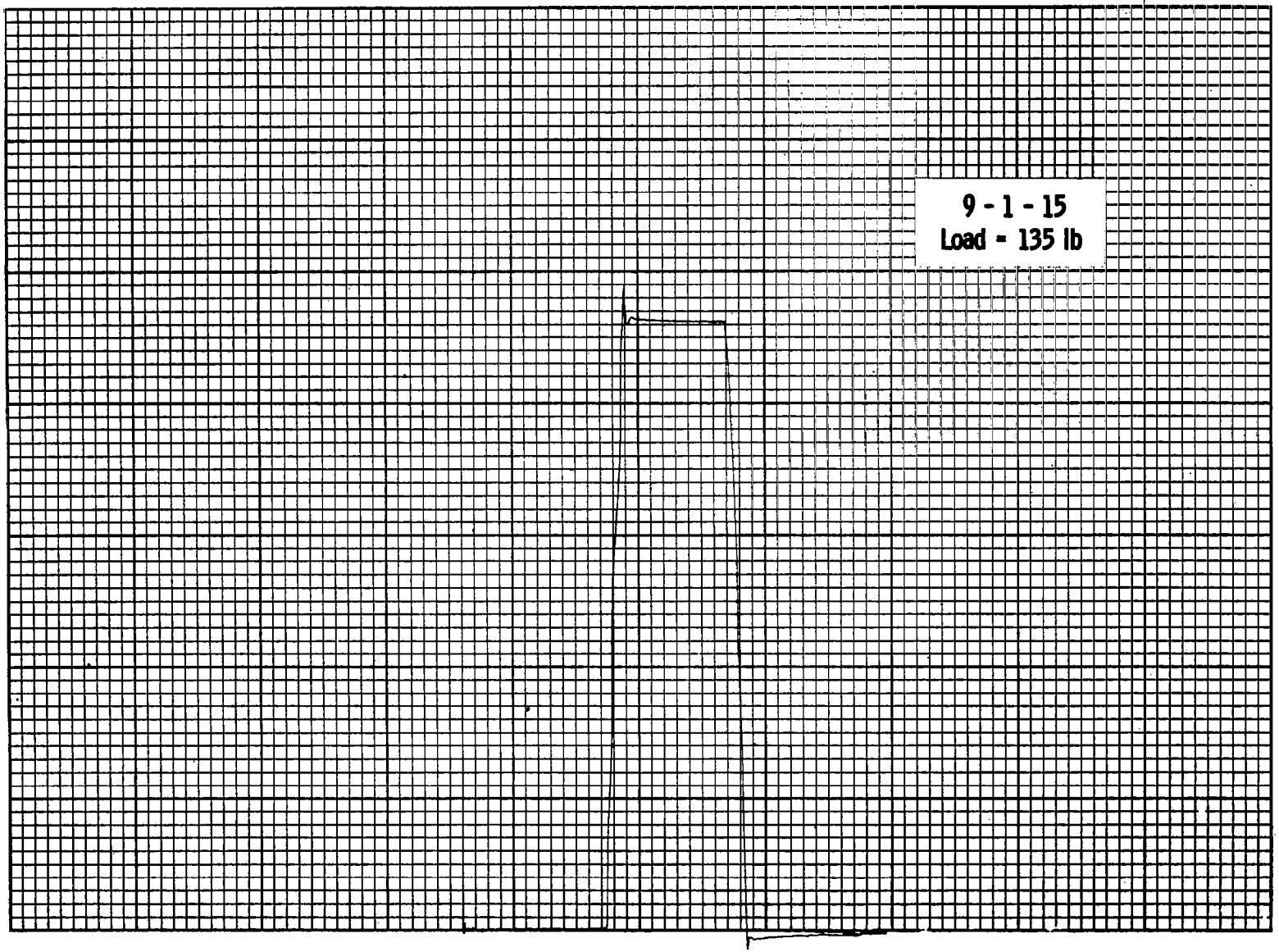
9 - 1 - 15
Load = 135 lb

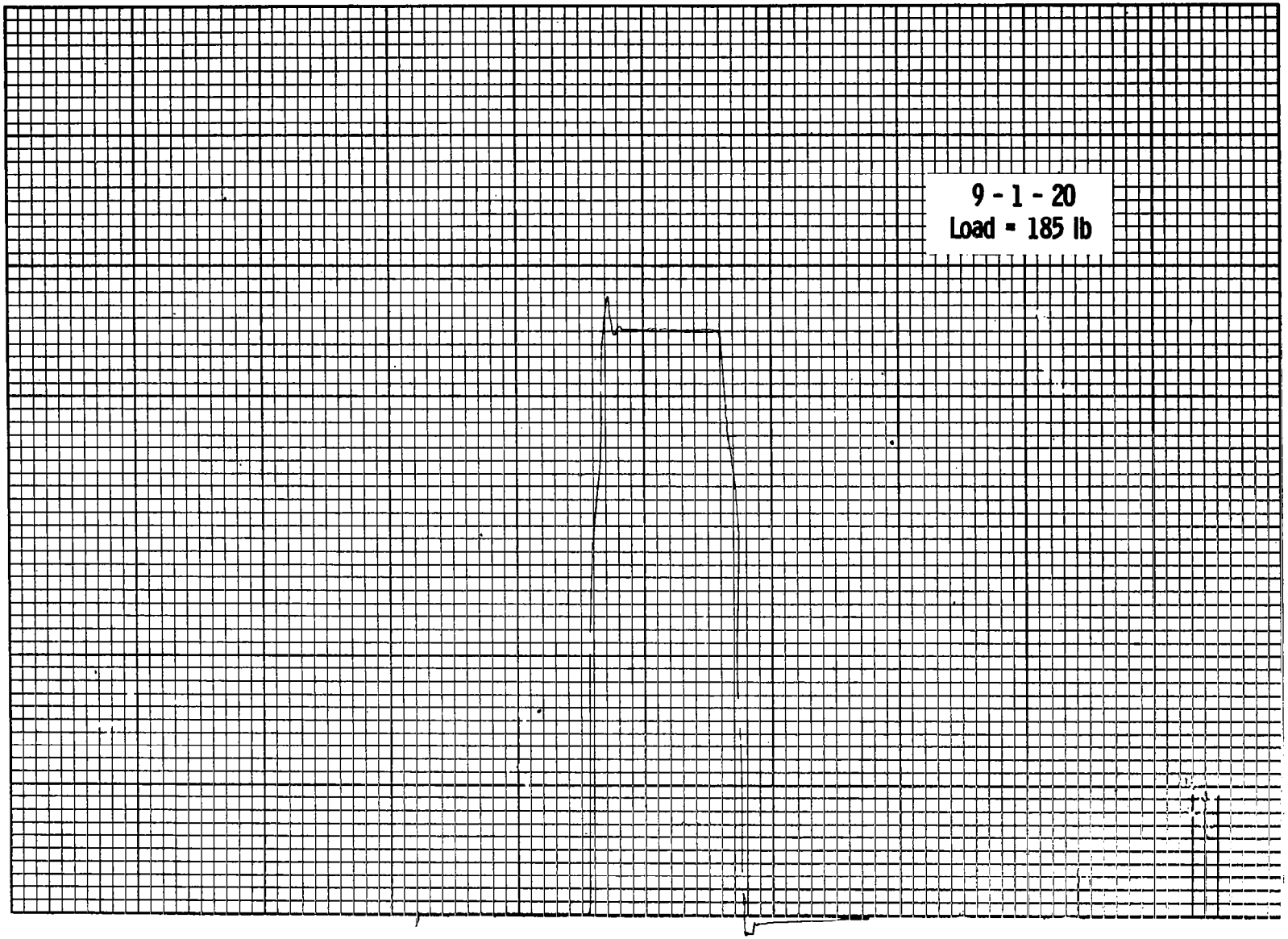
9 - 1 - 20
Load = 185 lb

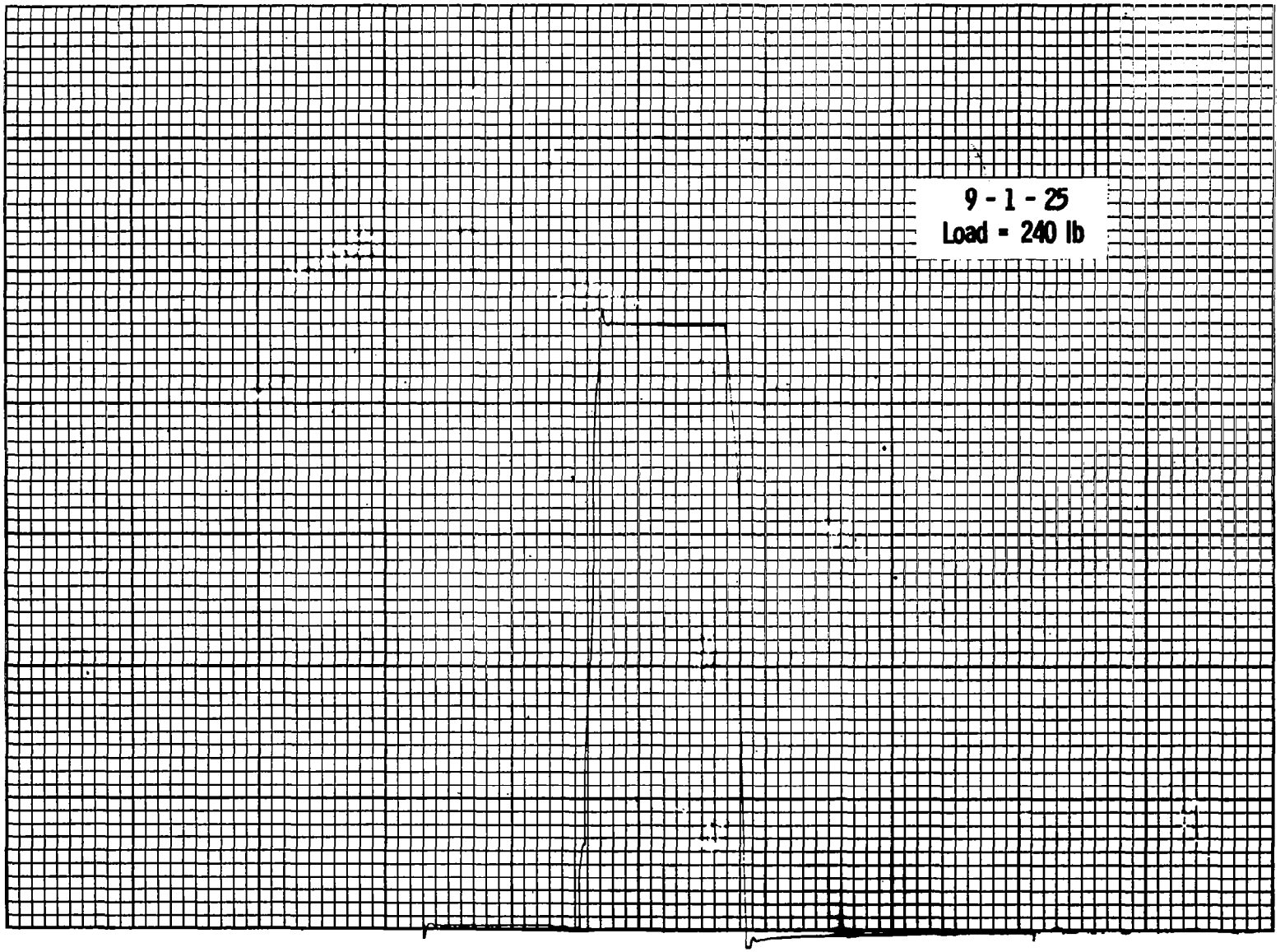
9 - 1 - 25
Load = 240 lb

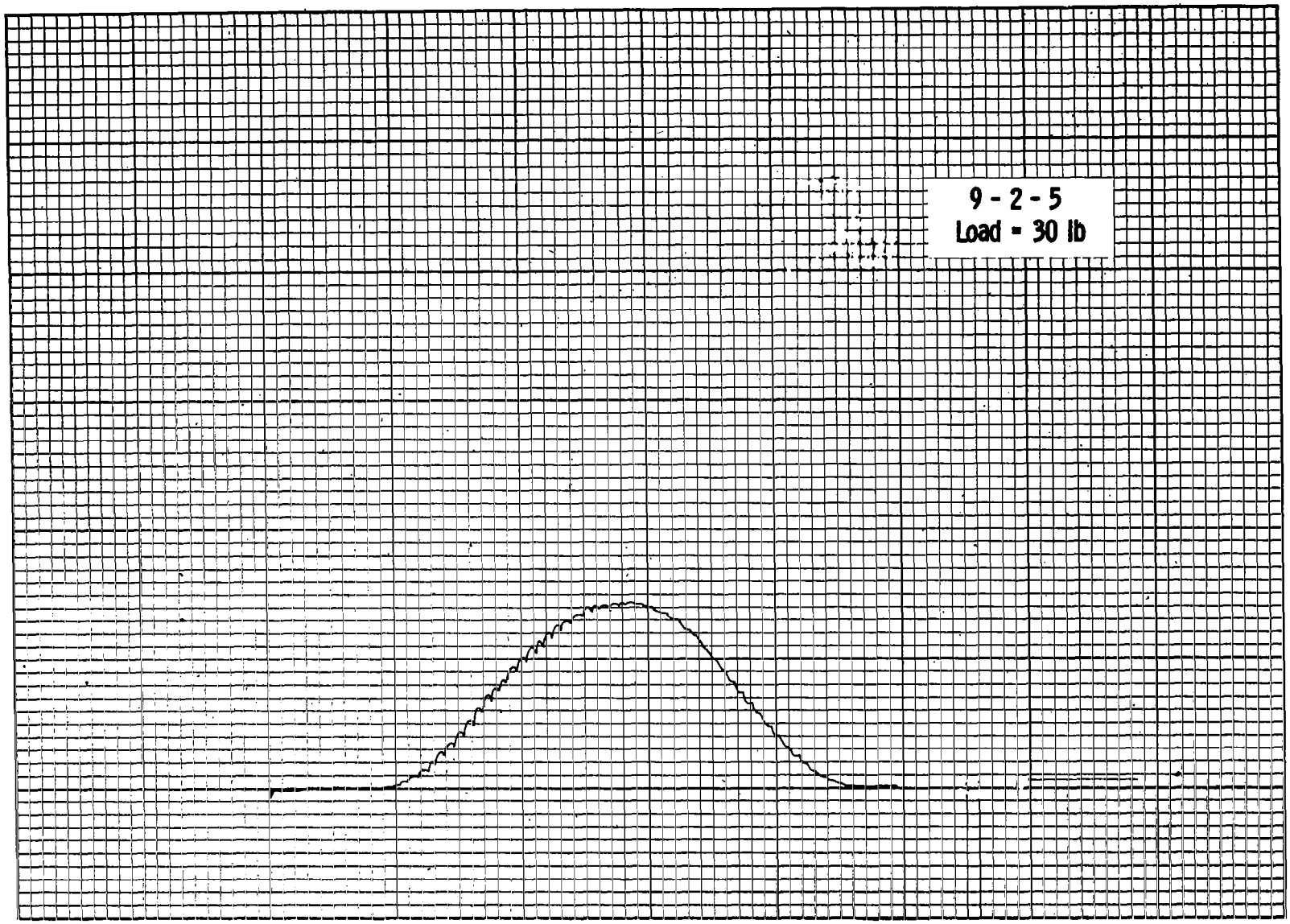
9 - 2 - 5
Load = 30 lb

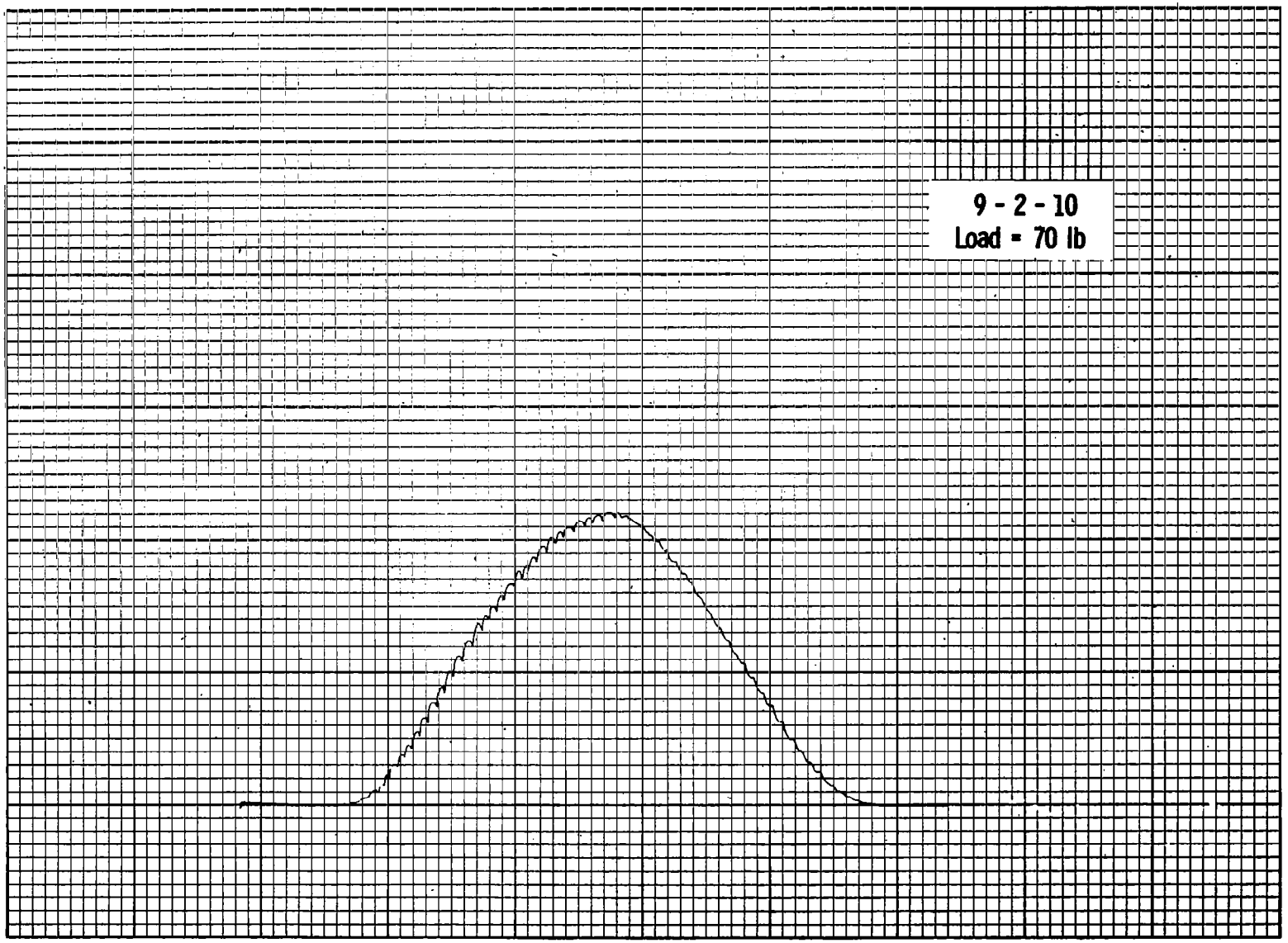
9 - 2 - 10
Load = 70 lb

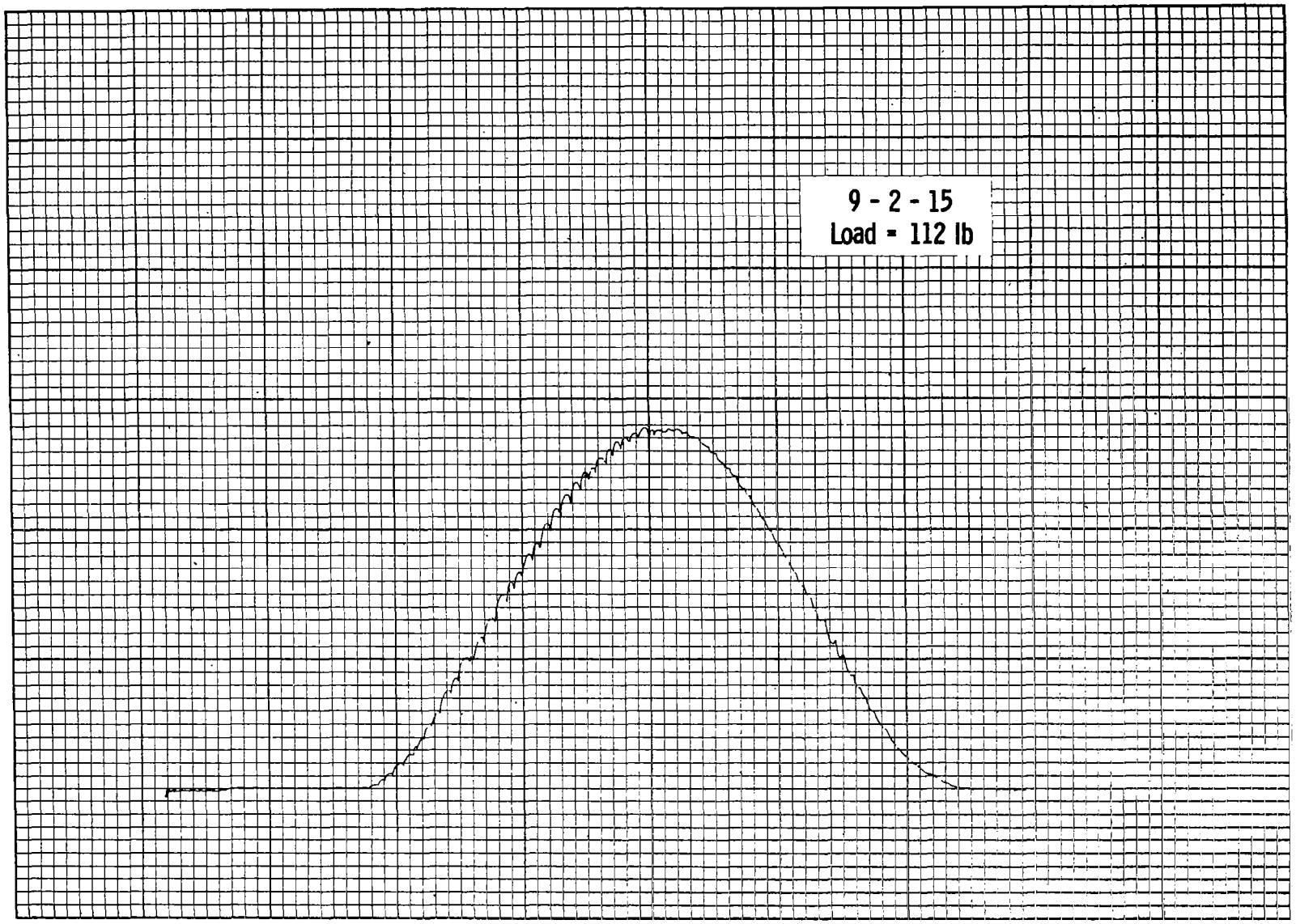
9 - 2 - 15
Load = 112 lb

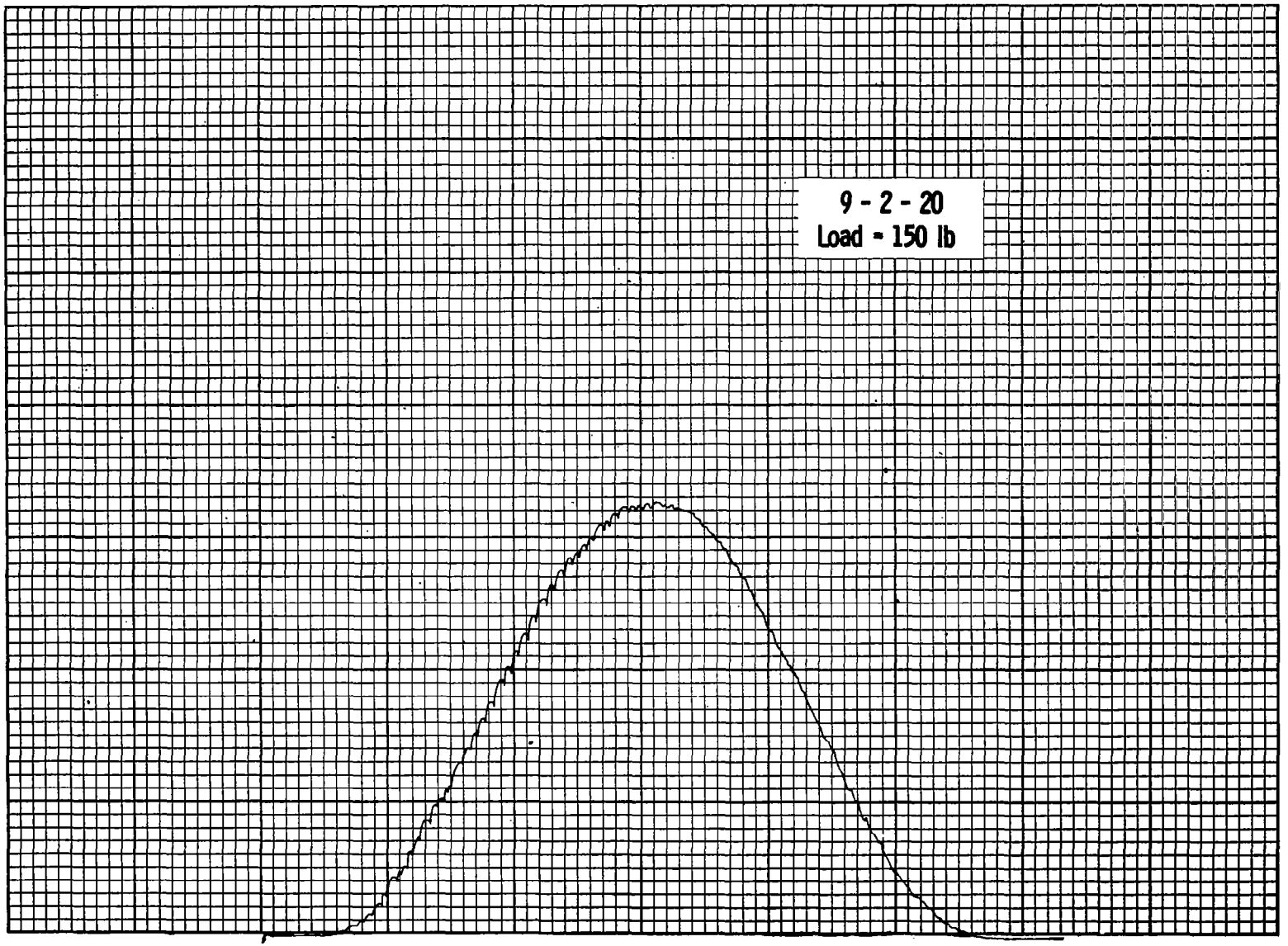
9 - 2 - 20
Load = 150 lb

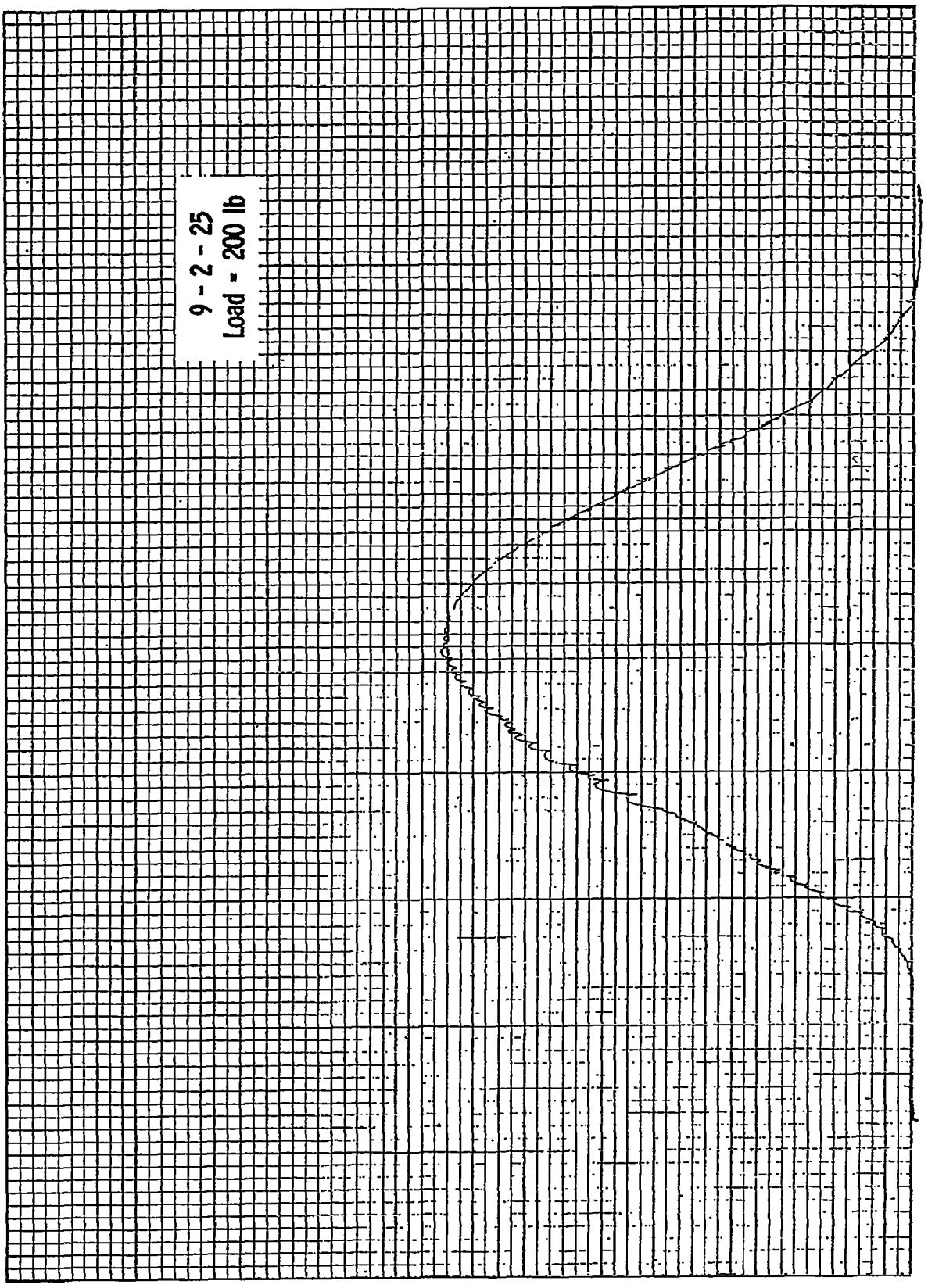
9 - 2 - 25
Load = 200 lb

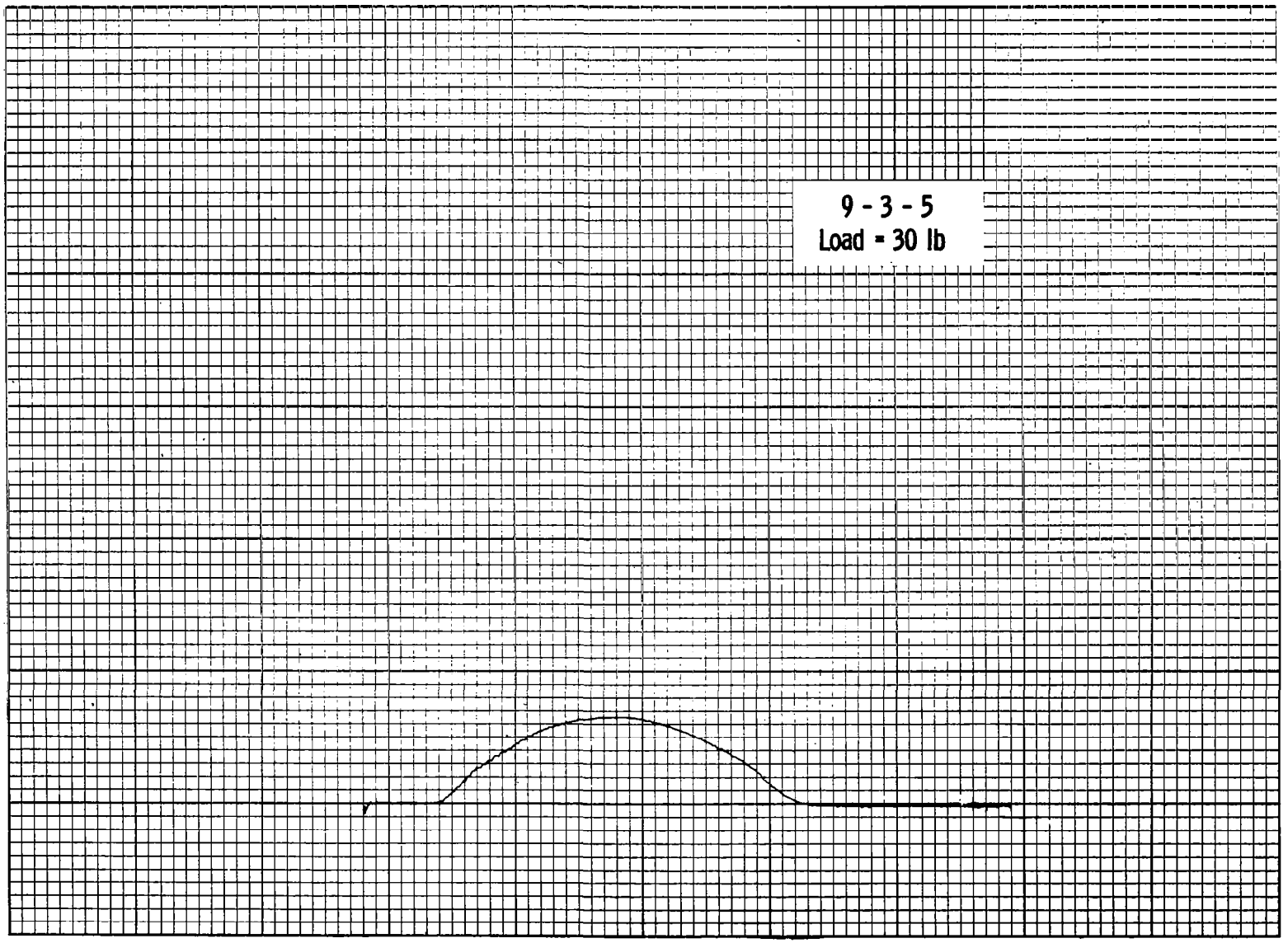
9 - 3 - 5
Load = 30 lb

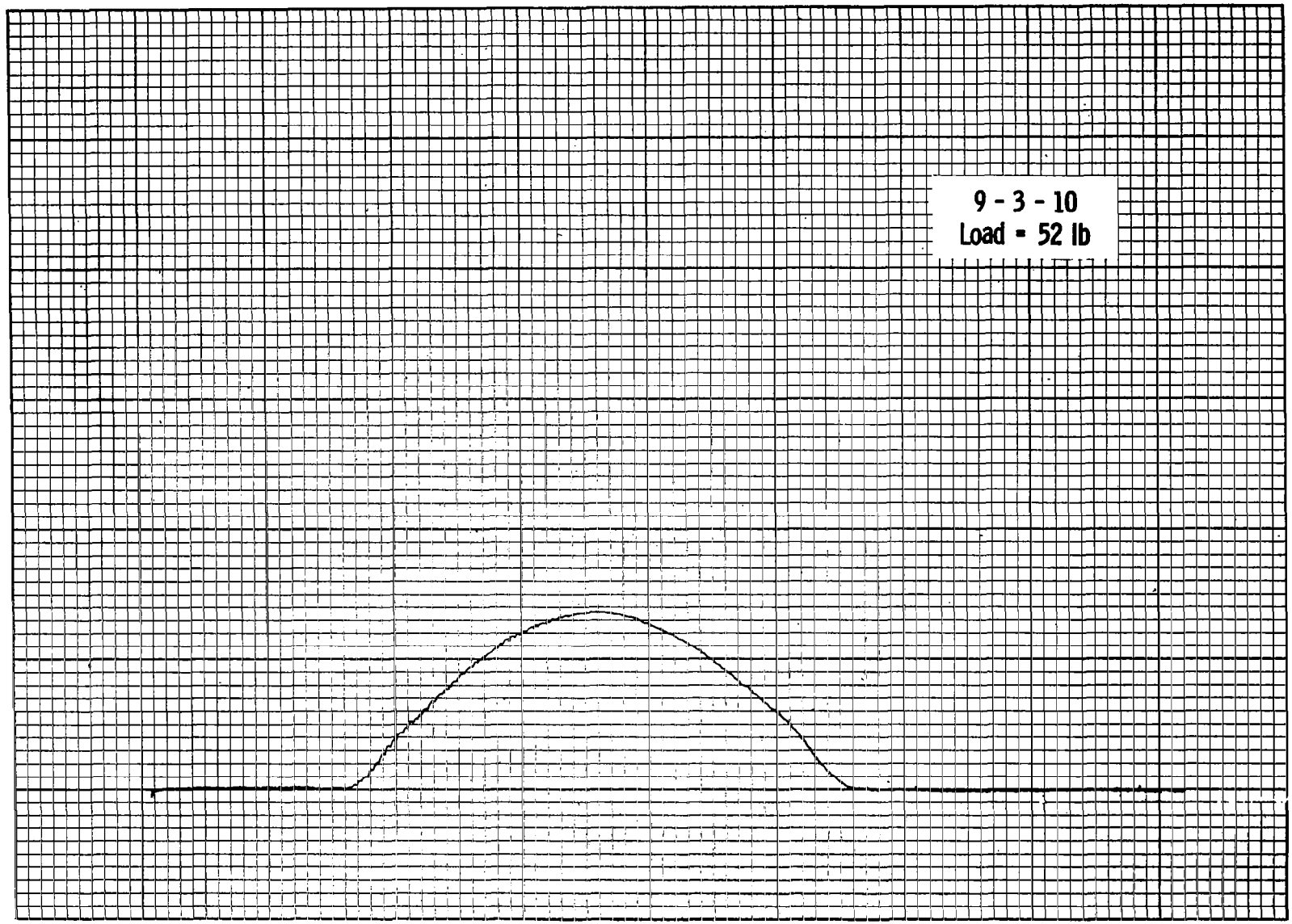
9 - 3 - 10
Load = 52 lb

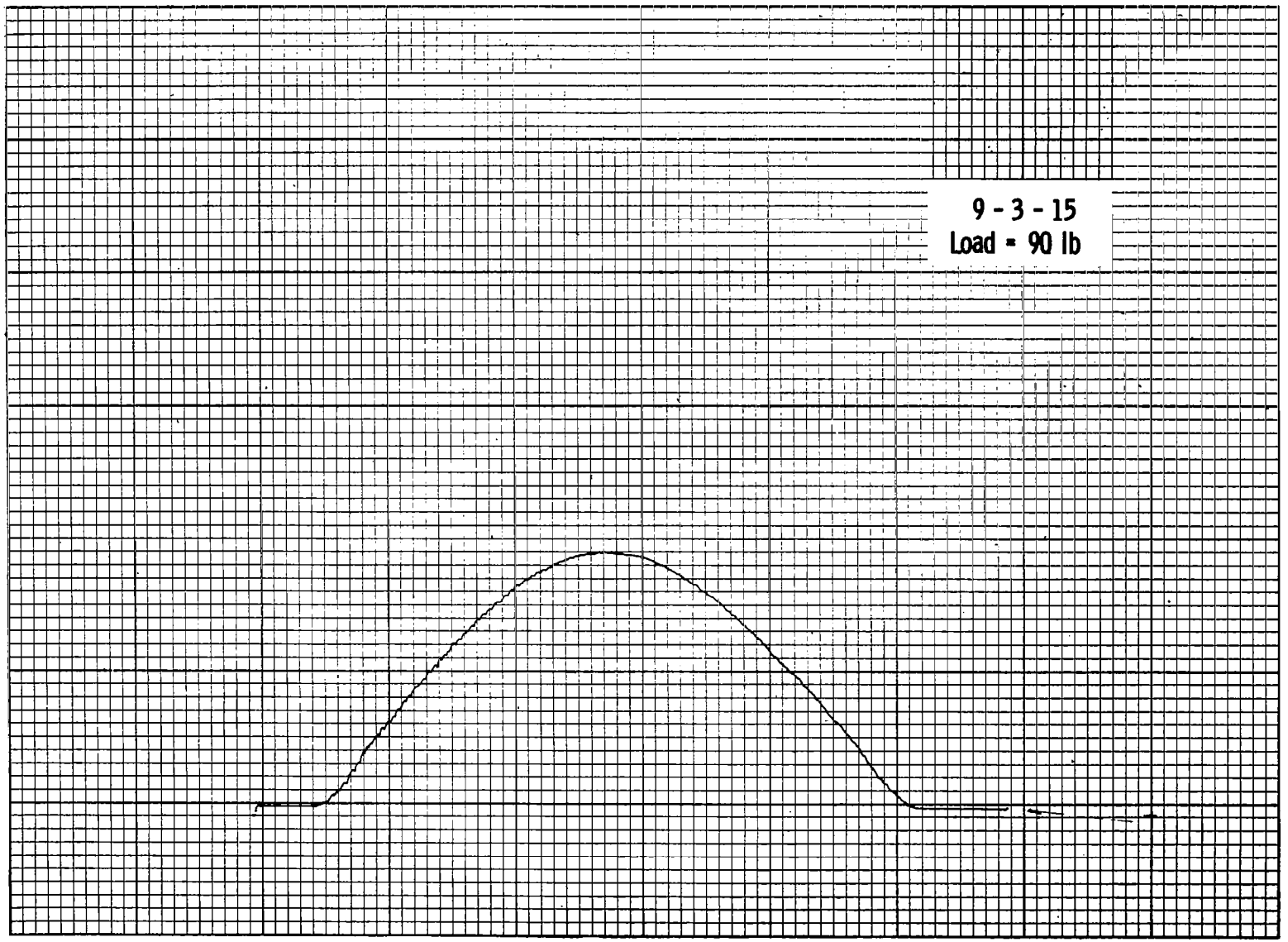
9 - 3 - 15
Load = 90 lb

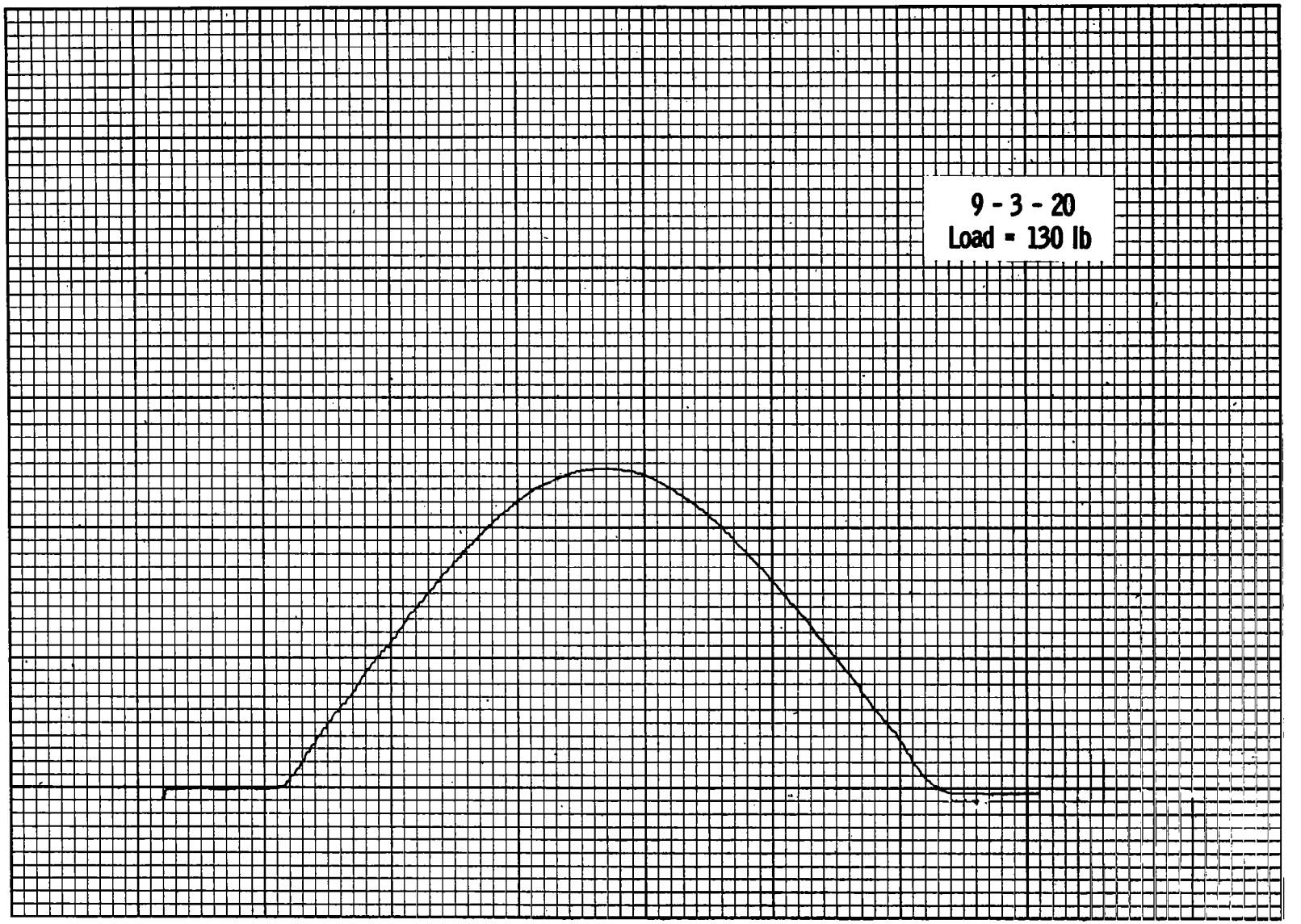
9 - 3 - 20
Load = 130 lb

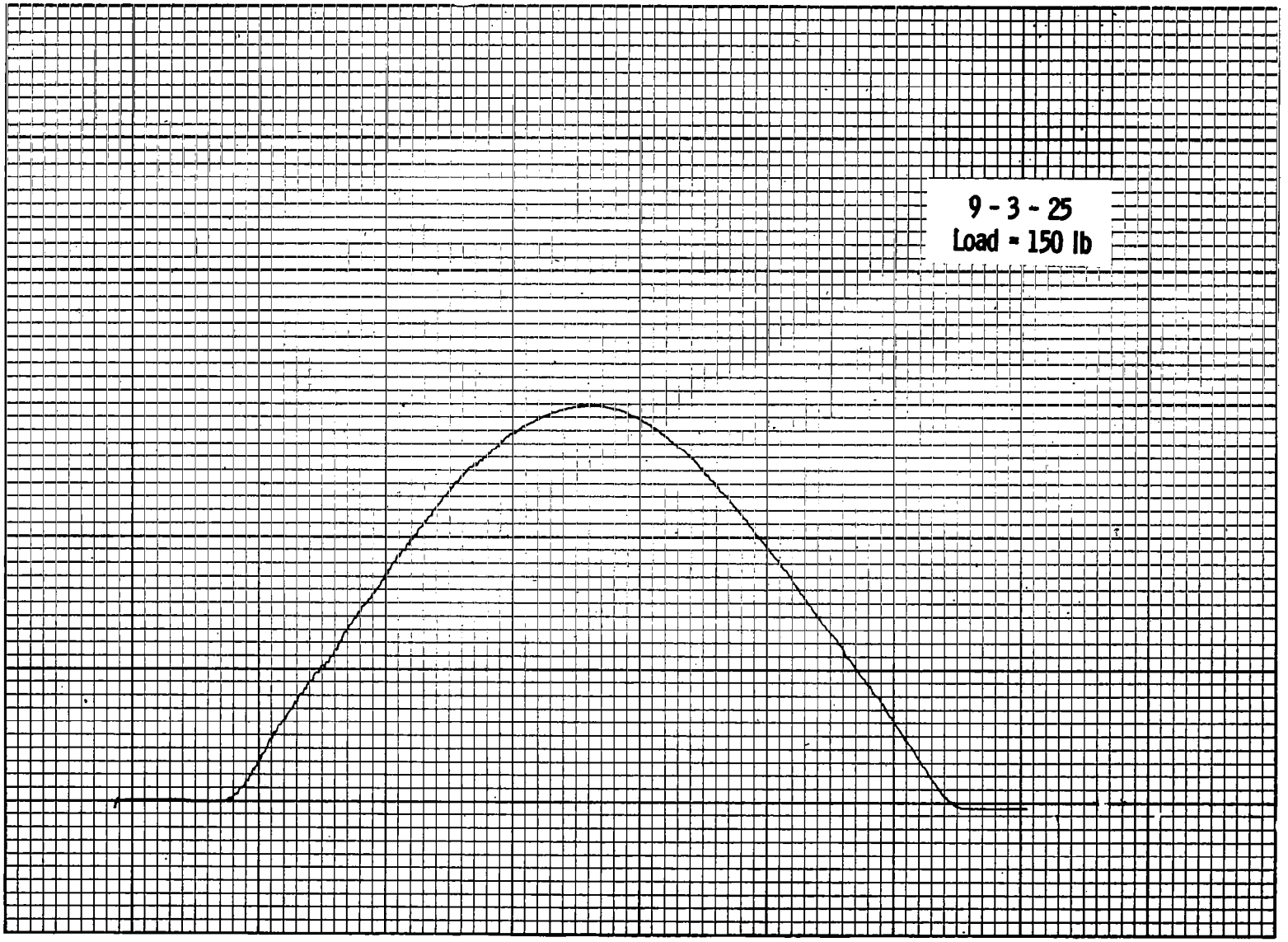
9 - 3 - 25
Load = 150 lb

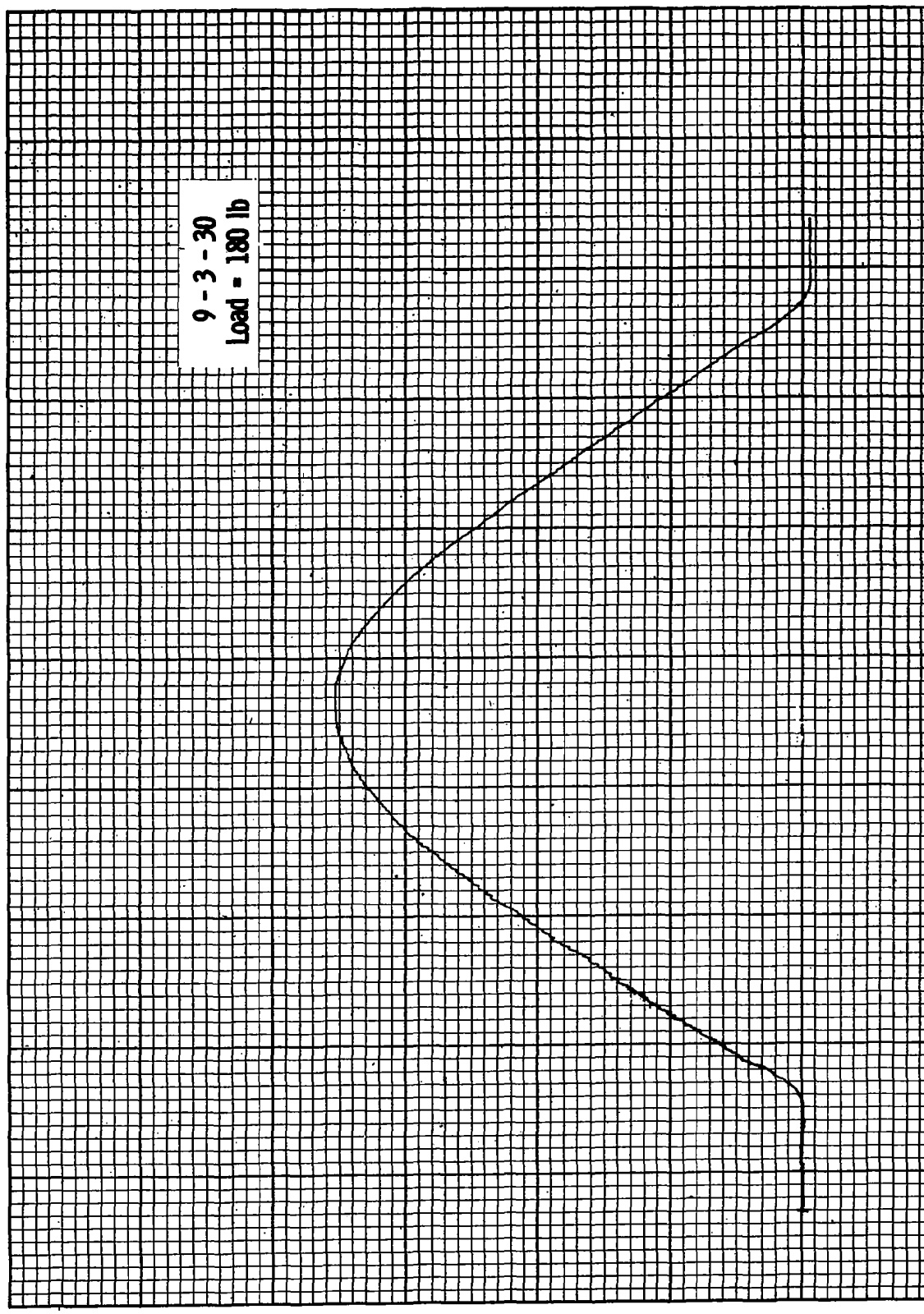
9 - 3 - 30
Load = 180 lb